INAUGURAL-DISSERTATION

zur Erlangung der Doktorwürde

der

Naturwissenschaftlich-Mathematischen Gesamtfakultät

der

Ruprecht-Karls-Universität

Heidelberg

vorgelegt von

Apotheker Sebastian Hausmann

geboren in Northeim

Tag der mündlichen Prüfung:

Antisense studies on base excision repair genes and their effects on cellular sensitivity to ionizing radiation

Referees: PD Dr. Odilia Popanda

Prof. Dr. Gert Fricker

To my family

Division: Epigenomics and Cancer Risk Factors

Head of the division: Prof. Dr. Christoph Plass

German Cancer Research Center (DKFZ), Heidelberg

Declarations according to § 8 (3) b) and c) of the doctoral degree regulations:

I hereby declare that I have written the submitted dissertation myself and in this process have used no other sources or materials than those expressly indicated,

I hereby declare that I have not applied to be examined at any other institution, nor have I used the dissertation in this or any other form at any other institution as an examination paper, nor submitted it to any other faculty as a dissertation.

Heidelberg, February 15, 2011 Sebastian Hausmann

Table of contents

Summary

Introduction: The base excision repair (BER) pathway is considered to be one of the most important pathways involved in the repair of DNA damage induced by ionizing radiation (IR). The DNA-(apurinic or apyrimidinic site) lyase (APEX1) and the DNA repair enzyme XRCC1 are two of its key players. Inconsistent data exist for the association between *APEX1* and *XRCC1* expression and cellular radiosensitivity. Some investigators have demonstrated a positive association, while others have shown little or no correlation. This study aims to investigate the effects of a decrease in the expression of APEX1 and XRCC1 on (i) growth characteristics, (ii) the survival and the cellular sensitivity to ionizing radiation, and (iii) the radiation-induced DNA damage. Gene expression profiles were determined after silencing and after additional irradiation with 5 Gy to identify possible alternative backup repair pathways and differences in the radiation response between normal and cancer cells. Thus, the study will elucidate whether imbalances in BER are associated with altered radiosensitivity. Such imbalances can be used to predict the radiation response after irradiation in cancer patients and will contribute to the understanding of normal tissue toxicity due to genetic variation in BER genes.

Methods: Gene defects were analyzed in two different cell types, the breast adenocarcinoma cell line MCF7 and a healthy counterpart, the human mammary epithelial cells HMEpC. The *APEX1* and/or the *XRCC1* gene were silenced in both cell types by applying the RNAi knockdown technique. Clonogenic assay and Sulforhodamine B assay were performed to assess growth characteristics and sensitivity to radiation. DNA damage after irradiation was evaluated with the DNA single-strand break-specific alkaline comet assay and the γH2AX assay, which uses an antibody specific for the phosphorylated form of the variant histone H2AX (γH2AX) at DNA double-strand breaks. Gene expression profiles were determined on Illumina Human Sentrix-8 BeadChip arrays.

Results: At the time of irradiation, *APEX1* and *XRCC1* mRNA amounts were decreased by more than 80 % in silenced cells, which led to reduced protein levels of up to 90 % in MCF7 cells, and up to 86 % in HMEpC. The silencing did not affect the IR-induced p53 response measured by quantification of *CDKN1A* mRNA levels. In MCF7, a reduced plating efficiency and growth capability was determined in *XRCC1* knockdown cells. Silencing of *APEX1* also resulted in a reduced growth compared to controls. No difference was observed in DNA repair rates. However, *APEX1*-silenced cells showed a trend towards

lower initial single-strand breaks after irradiation, whereas *XRCC1*-silenced cells showed a trend towards a higher damage. In HMEpC, the silencing did not affect growth or the initial damage induction. The functional consequences caused by the simultaneous knockdown of *APEX1* and *XRCC1* were comparable to the controls in both cell types. Further, the irradiation of *APEX1*- and/or *XRCC1*-silenced cells and controls showed no significant differences regarding radiation sensitivity in both cell types. However, these observations are accompanied by a cell type-specific deregulation of DNA repair genes and genes involved in the cell cycle, the cellular growth, and the proliferation. In particular, genes from the nucleotide excision repair (NER) and mismatch repair (MMR) pathway were induced in silenced cells after irradiation.

Conclusions: We have established a cell model to study the effect of a deficiency in BER on cellular radiosensitivity. After silencing *APEX1* and/or *XRCC1,* we did not observe an altered radiosensitivity compared to controls. The response to radiation and the efficiency of BER depend on all BER components and their multiple interactions within the cell. An imbalance in one of the enzymes may be compensated by other components. Based on our results, we assume that i) the *APEX1*-independent pathway and a possible *XRCC1*-independent pathway are used in situations with reduced availability of one of the proteins, and ii) other pathways such as NER and MMR are able to serve as a backup repair mechanism to repair radiation-induced DNA damage in double knockdown cells. This study suggests that *APEX1* and *XRCC1* are useful targets to modulate cellular responses to DNA damaging agents including IR. Our dataset offers several scientific directions for future studies with the aim to further investigate the mechanisms responsible for the different functions of *APEX1* and *XRCC1* in BER in primary and cancer cells.

Zusammenfassung

Einführung: Die Basen-Exzisions-Reparatur (BER) ist einer der wichtigsten Mechanismen zur Reparatur von DNA-Schäden, die durch die Einwirkung von ionisierender Strahlung entstehen. Das Enzym Apurinische Endonuklease 1 (APEX1) und das DNA-Reparaturenzym XRCC1 spielen eine Schlüsselrolle bei der BER. Es liegen nur widersprüchliche Daten vor, die einen Zusammenhang zwischen der Expression von *APEX1* und *XRCC1* hinsichtlich der zellulären Strahlenempfindlichkeit erkennen lassen. Einige Studien haben eine positive Assoziation nachgewiesen, andere hingegen fanden nur eine geringe oder gar keine Assoziation. Diese Arbeit untersucht die Auswirkungen einer verminderten Expression von *APEX1* und/oder *XRCC1* auf (i) das Wachstumsverhalten, (ii) das Überleben und die zelluläre Strahlenempfindlichkeit und (iii) die Induktion und die Reparatur strahleninduzierter DNA-Schäden. Des Weiteren wurden Genexpressionsprofile von Zellen mit herunter reguliertem *APEX1* und/oder *XRCC1* und nach zusätzlicher Behandlung mit ionisierender Strahlung (5 Gy) erstellt, um alternative Reparaturmöglichkeiten und Unterschiede in der Strahlenantwort zwischen primären Zellen und Krebszellen zu erfassen. Auf diese Weise soll mit der vorliegenden Arbeit untersucht werden, ob ein Ungleichgewicht in der BER mit einer veränderten Strahlenempfindlichkeit assoziiert ist. Ein solches Ungleichgewicht könnte zur Vorhersage der Strahlenantwort in Krebspatienten, die eine Bestrahlung erhalten haben, genutzt werden. Des Weiteren werden die Daten zum Verständnis der Strahlentoxizität aufgrund genetischer Unterschiede in BER Genen beitragen.

Methoden: Die Gendefekte wurden in zwei unterschiedlichen Zelltypen untersucht, zum einen in der Brustadenokarzinom-Zelllinie MCF7, zum anderen in Brustepithelzellen einer gesunden Spenderin, HMEpC. Um die Expression der Gene *APEX1* und/oder *XRCC1* zu vermindern, wurde die Technik der RNA-Interferenz angewendet. Die Wachstumseigenschaften und die Strahlenempfindlichkeit wurden mit dem Clonogenic Assay und dem Sulforhodamin B Assay bestimmt. Einzelstrangbrüche nach Bestrahlung wurden spezifisch mit dem alkalischen Comet Assay, Doppelstrangbrüche (DSB) mit dem γH2AX Assay gemessen. Dazu wurde ein Antikörper verwendet, der spezifisch an die phosphorylierte Form des Histons H2AX (γH2AX) bindet, da jeder DSB einen γH2AX-Fokus verursacht. Die Genexpressionsprofile wurden auf Illumina Human Sentrix-8 BeadChips Arrays bestimmt.

Ergebnisse: Zum Zeitpunkt der Bestrahlung waren sowohl die *APEX1* als auch die *XRCC1* mRNA um mehr als 80 % verringert. Die Proteinmengen waren um bis zu 90 % in den

MCF7-Zellen und um bis zu 86 % in den primären Zellen reduziert. Diese Verminderung hatte jedoch keinen Einfluss auf die strahleninduzierte p53-Antwort, welche durch Quantifizierung der *CDKN1A* mRNA gemessen wurde. In MCF7-Zellen führte die Reduktion von *XRCC1* zu einer geringeren Anheftungseffizienz und einem vermindertem Wachstum. Letzteres wurde auch in Zellen mit reduzierter *APEX1*-Expression beobachtet. Hinsichtlich der DNA-Reparaturraten wurde kein Unterschied festgestellt. Jedoch tendierten *APEX1*-verminderte Zellen direkt nach Bestrahlung zu weniger Einzelstrangbrüchen, *XRCC1*-verminderte Zellen dagegen zu vermehrten Einzelstrangbrüchen. In HMEpC hatte die Reduktion von *APEX1* und/oder *XRCC1* keine Auswirkungen auf das Wachstum oder die initialen DNA-Schäden nach Bestrahlung. Die gleichzeitige Verminderung von *APEX1* und *XRCC1* hatte, verglichen mit den Kontrollen, keine Auswirkungen in beiden Zelltypen. Darüber hinaus zeigten *APEX1*- und/oder *XRCC1*-verminderte Zellen keine signifikanten Unterschiede bei der Strahlenempfindlichkeit. Dennoch gehen diese Beobachtungen mit zelltypspezifischen Deregulierungen von DNA Reparaturgenen und Genen, die in der Zellzykluskontrolle, im Zellwachstum und der Proliferation eine Rolle spielen, einher. Insbesondere waren Gene aus dem Nukleotid-Exzisions-Reparaturweg (NER) und dem Mismatch-Reparaturweg (MMR) nach Bestrahlung der *APEX1*- und *XRCC1*-verminderten Zellen verstärkt exprimiert.

Schlussfolgerungen: Wir haben ein Zellmodell etabliert, mit dem die Auswirkungen einer unzureichenden BER auf die zelluläre Strahlenempfindlichkeit untersucht werden konnten. Nach Reduktion von *APEX1* und/oder *XRCC1* konnten zwar Veränderungen im Wachstum aber nicht in der Strahlenempfindlichkeit im Vergleich zu den Kontrollen beobachtet werden. Die zellulären Reaktionen nach Bestrahlung und die Effizienz der BER hängen von allen Komponenten der BER und ihren vielfältigen Interaktionen ab. Ein gestörtes Gleichgewicht in einem der Enzyme vermag durch ein anderes ausgeglichen werden. Auf der Basis unserer Ergebnisse zur Genexpression nehmen wir an, dass (i) der *APEX1*-unabhängige und ein möglicher *XRCC1*-unabhängiger Reparaturweg in Situationen mit verminderter Verfügbarkeit in einem der beiden Proteine genutzt wird, und (ii) andere Reparaturwege, wie NER und MMR, als alternative Reparaturwege strahleninduzierte DNA-Schäden reparieren können. Unsere Arbeit legt nahe, dass *APEX1* und *XRCC1* wertvolle Ziele sind, um die zellulären Reaktionen hinsichtlich DNA-schädigender Agenzien, einschließlich ionisierender Strahlung, zu modifizieren. Unsere Daten eröffnen zahlreiche Richtungen für zukünftige Studien mit dem Ziel, die Mechanismen, die für die verschiedenen Funktionen von *APEX1* und *XRCC1* in der BER in primären Zellen und Krebszellen verantwortlich sind, weiter zu untersuchen.

Abbreviations

Ab	Antibody
ACTB	Actin, cytoplasmic 1
APEX1	DNA-(apurinic or apyrimidinic site) lyase
AP	Apurinic/apyrimidinic or abasic
ATM	Ataxia telangiectasia mutated
BER	Base excision repair
bFGF	Basic fibroblast growth factor
BPE	Bovine pituitary extract
BSA	Bovine serum albumin
BRCA1/2	Breast cancer 1/2, early onset
CDKN1A	Cyclin-dependent kinase inhibitor 1A (p21, Cip1)
cDNA	Complementary deoxyribonucleic acid
CLTC	Clathrin, heavy chain (Hc)
C_p values	Crossing point
DDR	DNA damage response
DKO	Double knockdown
DMSO	Dimethylsulfoxide
DNA	Desoxyribonucleic acid
DNA-PKc	Protein kinase, DNA-activated, catalytic polypeptide
DSB	Double strand break
dsDNA	Double-stranded DNA
dsRNA	Double-stranded RNA
dNTP	2-Desoxynucleotide-5'-triphosphate
DTT	Dithiothreitol
EDTA	Ethylenediaminetetraacetic acid
ELISA	Enzyme immunosorbant assay
EtOH	Ethanol
FACS	Fluorescence activated cell sorter
FCS	Fetal calf serum
FSC	Forward scatter
g	gravitational acceleration (9.80665 m/s^2)
GAPDH	Glyceraldehyde 3-phosphate dehydrogenase
Gy	Gray, absorbed radiation dose of ionizing radiation (1 Gy = 1 J/kg)
γH2AX	Gamma histone variant H2AX
h	Hour(s)
H_2DCFDA	2',7'-dichlorodihydrofluorescein diacetate
HPRT	Hypoxanthine phosphoribosyltransferase
HR	Homologous recombination
HRP	Horseradish peroxidase
IC_{50}	Inhibitory concentration 50
IR	Ionizing radiation
J	Joule
kDa	Kilodalton
L	Liter(s)
LOH	Loss of heterozyygosity
µL	Microliter(s)
mg	Milligramm(s)
µg	Mikrogramm(s)
min	Minute(s)
mL	Milliliter(s)
mm	Millimeter(s)
MMR	Mismatch repair
mRNA	Messenger ribonucleic acid
NER	Nucleotide excision repair
ng	Nanogramm
NHEJ	Non-homologous end joining
PARP1	Poly (ADP-ribose) polymerase 1
PBS	Phosphate buffered saline
PCR	Polymerase chain reaction
PI	Propidium iodide
PVDF	Polyvinylidenfluoride
qRT-PCR	quantitative real-time PCR
r	Correlation coefficient
RNA	Ribonucleic acid
RNAi	RNA interference
RNAse	Ribonuclease
ROS	Reactive oxygen species
rpm	Rotations per minute
RT	Room temperature
SEM	Standard error of the mean
SD	Standard deviation
SDS-PAGE	Sodium dodecyl sulfate polyacrylamide gel electrophoresis
siRNA	small interfering RNA
SNP	Single nucleotide polymorphism
SSB	Single-strand break
SSC	Side scatter
ssRNA	Single stranded RNA
TBE	Tris/borate/EDTA
TBP	TATA box binding protein
TBS	Tris-buffered saline
TBST	TBS containing Tween 20
TCA	Trichloroacetic acid
TMZ	Temozolomide
TP53	Tumor protein 53
U	Unit
UV	Ultraviolet
V	Volt
XRCC1	X-ray repair complementing defective repair in Chinese hamster cells 1

1 Introduction

1.1 Breast cancer

Breast cancer is the most common form of cancer in women and represents the major cause of cancer death among women (1). Around 58.000 women in Germany are diagnosed with breast cancer every year, which accounts for over a quarter (29 %) of all cancers. Around 17.600 cancer-related deaths occur from breast tumors. The average age at onset is 64 year. The relative 5-year survival rates of female breast cancer patients in Germany currently lie between 83 % and 87 % (1). At the end of 2006, about 242.000 women in Germany had been diagnosed with breast cancer within the previous five years (5-year prevalence).

1.1.1 Breast cancer risk factors

Several risk factors have been found to be associated with an increased breast cancer risk. First, early age at menarche increases risk of contracting cancer probably due to a prolonged exposure of breast epithelium to estrogens (2). Likewise, a delayed menopause represents a risk factor (3). Early age at first and second pregnancy, in contrast, has been shown to be protective as well as a prolonged lactation (4-6). Additionally, hormone-replacement therapy during and after the menopause increases the breast cancer risk and so does the use of ovulation inhibitors (oral contraceptiva), even up to ten years after the end of the use (7). Obesity, weight gain, consumption of alcohol and a folate deficiency are serious risk factors for breast cancer (8-11), whereas physical activity and the intake of fruits and vegetables containing antioxidants and other compounds in the human diet, such as omega-3 unsaturated fatty acids, seem to have a protective effect (12-14). Furthermore, the family history of breast cancer is a major risk factor for the development of the disease (15;16).

In the large German case-control study MARIE (Mammakarzinom-Risikofaktoren-Erhebung), the effects of menopausal hormone therapy by type, regimen, timing and progestagenic constituent on postmenopausal breast cancer risk were investigated (17). Based on this population, one recently published paper showed an association of polymorphisms in genes of the thioredoxin system, *CYBA*, and *MT2A* with postmenopausal breast cancer risk (18).

Mutations in *BRCA1* and *BRCA2*, two of the most common breast-cancer related genes, are associated with a significant increase in hereditary breast cancer. *BRCA1* is a tumor suppressor gene whose main function is maintaining genomic integrity. The protein plays a role in transcription, DNA repair of double-stranded breaks, and recombination (19). Mutations in this gene are responsible for approximately 40 % of inherited breast cancers and more than 80 % of inherited breast and ovarian cancers (20;21). *BRCA2* shares several functions with *BRCA1*, but it is specifically involved in the homologous recombination pathway for double-strand DNA repair. Mutations in *BRCA2* are linked with 76 % of breast cancer families. Loss of heterozygosity in both genes is observed in hereditary breast cancer (22). p53, the most commonly mutated gene in all human cancers, was the first tumor suppressor gene linked to hereditary breast cancer (23). Mutations in the phosphatase and tensin homolog-mutated in multiple advanced cancers 1 (*PTEN*) gene, a gene from the p53 repair pathway, the ataxia telangiectasia mutated (*ATM*) gene, the human epidermal growth factor receptor (*HER-2*) gene and the partner and localizer of BRCA2 (*PALB2*) gene are further related to breast cancer (24;25).
Polymorphisms in breast cancer-susceptible genes also contribute to the development of breast cancer, primarily in combination with endogenous and exogenous factors. Polymorphisms in members of the Cytochrome P450 family proteins (CYP450), the Glutathione S-transferase (GST), the Alcohol Dehydrogenase (ADH), or the Methylenetetrahydrofolate reductase (MTHFR) affect or may modulate breast cancer risk (26;27). DNA repair genes represent another group of genes in which polymorphisms modify protein functions and the capacity to repair DNA damage (28;29). Also epigenetic inactivation due to aberrant hypermethylation of microRNAs is involved in breast cancer development (30).

1.2 Treatment of cancer

The cure of cancer depends on several factors such as the size and position of the tumor in the body, the origin of the tissue which it has grown from, and the presence of metastatic spread. An early detection and an immediate treatment of the cancer are main factors influencing the benefit for the patient. Surgery, chemotherapy and radiotherapy are the three bastions in cancer treatment.

1.2.1 Surgery

Surgery is a very effective form of treatment, because solid tumors can be resected in their entirety together with all adjacent tissue into which the tumor may have spread. For a long time, radical mastectomy has been used to treat women with breast cancer. Nowadays, if possible, a segmental mastectomy or breast-conserving therapy is used. This treatment aims to maintain a normal breast appearance after the surgery (31).

1.2.2 Chemotherapy

Chemotherapy is the treatment of cells with cytotoxic drugs that have an effect on the cell division. As cancer cells are dividing faster than normal cells, they are more affected by the cytotoxic effect. These drugs are generally classified according to their mechanism of action into antimetabolites (e.g. 5-fluoruracil), DNA damaging agents (e.g. cyclophosphamide), mitosis inhibitors (e.g. taxol) and cancer cell enzyme inactivators (e.g. tyrosine-kinase inhibitors). All effective drugs, however, have side effects (31).

1.2.3 Radiotherapy

The third hallmark of cancer treatment is radiotherapy, whose biggest advantage is that a surgical operation can be avoided. Around 50 % of cancer patients are treated with radiation therapy, which uses X-ray or γ-rays to destroy the tumor (32). The form, dose, and frequency of radiotherapy depend on the cancer type and the health of the patient. The delivery of multiple doses of radiation is intended to kill only the tumor while sparing normal tissue. This is achieved by an accurate planning and delivery technique, which makes it possible to increase the irradiation dose specific to the tumor while limiting the dose to the healthy tissue adjacent to the tumor. However, this is not always possible, and thus damage to the healthy tissue is likely to occur. This kind of damage is the main cause for the occurrence of side effects due to radiotherapy. Ionizing radiation is not only a therapeutic agent, but it is also a carcinogen. In rare cases, the damage introduced to healthy tissue is repaired incorrectly and contribute to the development of a new cancer. Nevertheless, the benefits of radiotherapy are much greater than the risk involved.

1.3 Side effects of radiotherapy

Side effects are classified into early or acute side effects, which occur during or within weeks of treatment (like skin irritations, hair loss in the treatment area, mouth sores, etc.), and late side effect, which occur 6 months or years after the treatment (like thickening of the skin, damage to nerves or organs of the gastrointestinal tract, etc.) (33). The severity of side effects after radiotherapy depends, for example, on the tissue type and the total radiation dose. Severity is graded according to the toxicity and varies among patients. Genetic variations contribute to these inter-individual differences (34-36). It is not clear yet how inherited factors influence the risk of contracting the disease and the response to therapy after radiation treatment. Improvements in the cure and toxicity of the treatment could be achieved by new technologies such as image-guided radiotherapy (37;38) and intensity-modulated radiotherapy (39;40). Although many factors influencing the radiation toxicity are known, more than 80 % of the variation in normal tissue reaction among patients have not been investigated so far or seem to be genetic (41). Normal tissue radiosensitivity depends on the variation in several genes, especially DNA repair genes. The identification of genetic markers may have the potential to predict normal tissue responses after radiotherapy.

1.4 Cellular response to ionizing radiation

If ionizing radiation is applied to a cell or a cell compartiment, it causes two different effects. First, there are direct effects generated by the interaction of the energy with macromolecules, like the DNA or proteins; second there are indirect effects created by the interaction of the energy with water to produce reactive oxygen species (ROS). For IR such as γ-rays, 60 % of damage is caused by indirect effects (42). The effects of ROS generation are rapidly amplified through their interaction with lipids, membranes, and oxygen. They add up to the normal low-level production of ROS within the cells that is generated as a consequence of oxygen metabolism. An excess of ROS results in a state of oxidative stress for the cell that further damage DNA.

IR-induced damage to DNA causes a broad range of base damage, base modifications and strand breaks (43;44). IR is thought to produce about 1000 single-strand breaks (SSBs) and 25-40 double-strand breaks (DSBs) per cell per gray (45). Base modifications and SSBs are efficiently repaired through the BER pathway (46). DSBs can be repaired through

either homologous recombination (HR) or non-homologous end joining (NHEJ). If unrepaired, DSBs can lead to genetic mutations and trigger carcinogenesis (47). The induction of DSBs correlates with the phosphorylation of the variant histone H2AX (γH2AX), which can be detected with a specific antibody (48).

However, most of the damage overlaps with DNA lesions produced by ROS. In general, DNA damage leads to the activation of DNA damage response (DDR) pathways within the cell, for example by activating cell-cycle checkpoints, DNA repair, transcriptional response, chromatin remodeling, and apoptotic programs (49;50). The DDR is activated by the detection of the damage through specific sensors. The ataxia telangiectasia mutated kinase (*ATM*) is a crucial sensor in this context. Autophosphorylation of ATM activates further ATM-dependent signaling (51). ATM phosphorylates downstream targets like p53 and the checkpoint kinases CHK1 and CHK2 (52). p53 is a transcription factor for several genes and activates their expression by binding to p53-response-elements in promoter regions of these genes (e.g. *CDKN1A*). This leads to cell cycle arrest and up-regulation of repair (53-55). p53-dependent cell cycle arrest is primarily mediated by the cyclin-dependent kinase inhibitor p21, which is encoded by the cyclin-dependent kinase inhibitor 1A (*CDKN1A*) gene. p21 binds to and inhibits the activity of cyclin-CDK2 or -CDK4 complexes, which normally allow the cell to undergo G1/S-phase transition. Thus it functions as a regulator of cell cycle progression at G1-phase and as an inhibitor of proliferation. Furthermore, it functions as an inhibitor of p53-dependent apoptosis. It is not entirely clear how a cell chooses between apoptosis and p21-dependent cell cycle arrest after DNA damage and stabilization of p53 (56-58).

1.5 Repair mechanisms

Normal cells are protected by several defense mechanisms against ionizing radiation and subsequent oxidative stress through reactive oxygen species. Enzyme systems scavenging oxidative substances and repairing DNA damage play a central role. For nearly every type of damage, the cell has a more or less specialized repair pathway to promote its survival and to prevent cell death (Figure 1.1). Most of the repair pathways use an excision mechanism to remove the damage on one strand of the DNA double helix and use the other strand to restore or re-synthesize it. Thus, double-strand breaks are more damaging and if unrepaired, contribute to genomic instability. More than 150 genes have been

found to be involved in repair mechanisms (59;60). The DNA repair pathways can be categorized into at least six main multistep pathways: the base excision repair (BER), the nucleotide excision repair (NER), the mismatch repair (MMR), the homologous recombination (HR), the non-homologous end joining (NHEJ) and the translesional synthesis (TLS) (61). Most of them are involved in the repair of radiation-induced DNA damage.

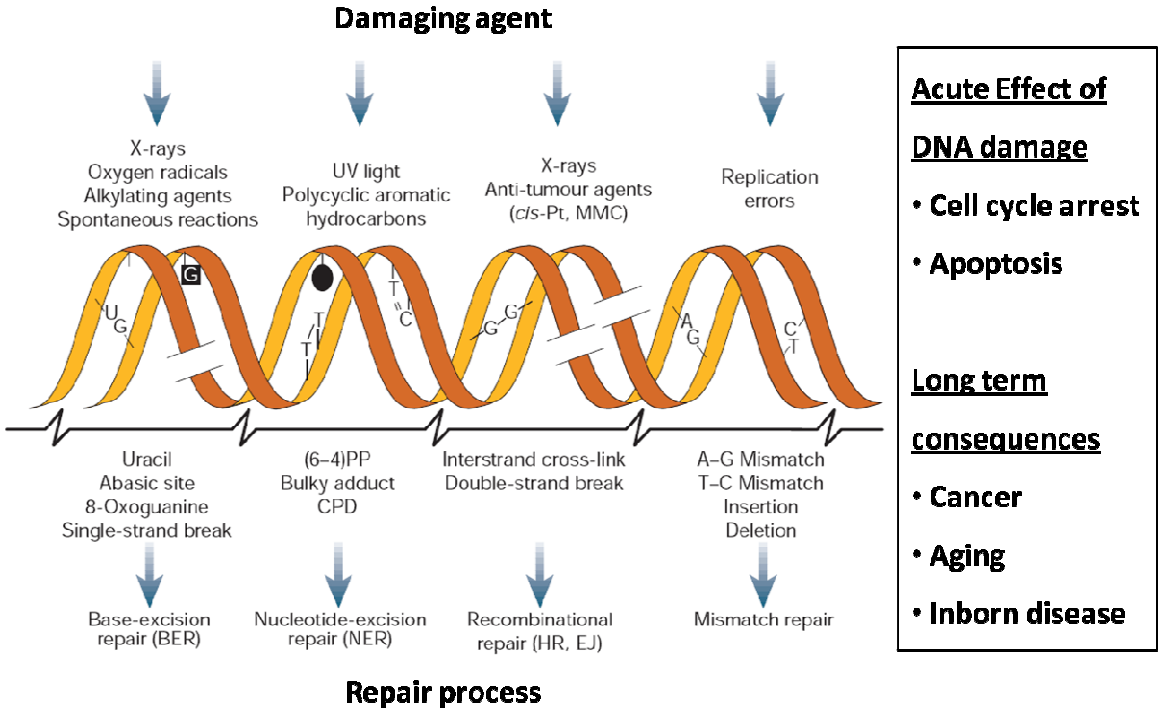

Figure 1.1. DNA damage, repair mechanisms, and consequences (adapted from (62)).

1.5.1 Double-strand break repair

DNA double-strand breaks are considered to be the most severe lesions. They can occur through exogenous DNA-damaging agents such as ionizing radiation or chemicals or endogenously produced by ROS. DSBs can promote genotoxic effects and lead to apoptosis; they also contribute to carcinogenesis through genomic rearrangements (63). Two main interconnected pathways repair DSB: homologous recombination (HR) and non-homologous end-joining (NHEJ). NHEJ allows a fast repair during the entire cell cycle. However, it is very error-prone, because it just joins double stranded DNA ends together. The process of HR is slower and restricted to S and G2 phases of the cell cycle because the

homologous DNA strand is used as a template for repair, therefore it is basically error-free (62;64).

The decision about which repair pathway is used depends on the origin of the damage. Two-ended double strand breaks caused by ionizing radiation appear when the DNA breaks into two parts. This DSB damage can be repaired either by NHEJ or HR. One-ended DSB, which may occur when a replication fork runs into an unrepaired SSB, are processed by HR (Figure 1.2).

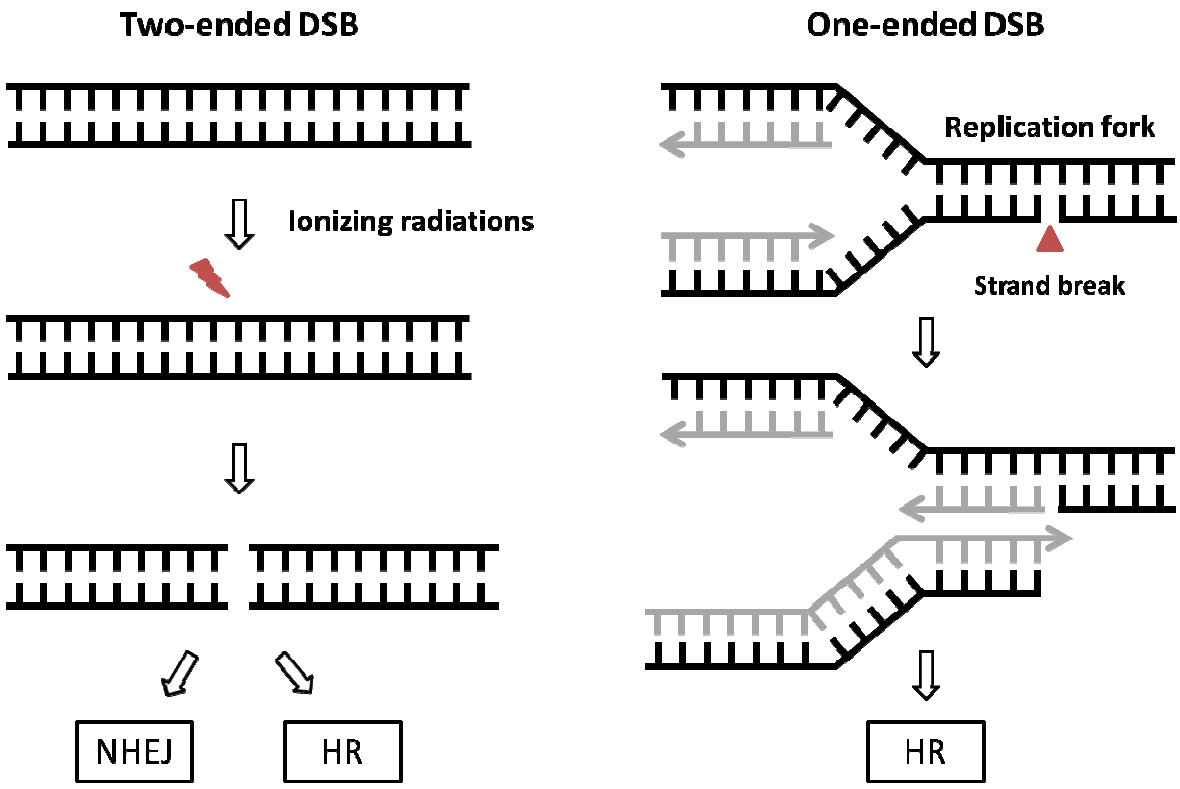

Figure 1.2. DNA double strand breaks formation (according to (65)).

1.5.1.1 Non-homologous end joining

A DSB with two blunt ends is a substrate for NHEJ. Six core components are involved in the repair: Ku70, Ku80, DNA-dependent protein kinase catalytic subunit (DNA-PKcs), DNA ligase IV (LIG4), XRCC4, and XLF. If no end processing is required, the heterodimeric complex Ku70/80 binds to the DNA ends; it recruits and activates DNA-PKcs. The DNA-PKcs undergo autophosphorylation, and the DNA ends become accessible for LIG4, XRCC4, and XLF, which together form the ligase complex and seal the DNA ends. The ligase complex cannot directly religate most of the DSB. First, they have to be processed

by the MRE11-Rad50-NBS1 complex, which has exonuclease and helicase activity and which modifies the DNA for the ligation complex (66).

The joining of DNA ends with 3'- and 5' overhangs, hairpins, flaps, or gaps requires an additional processing of the ends before sealing. This is done by another protein called Artemis, which acts in a complex with DNA-PKcs. Upon phosphorylation, the endonuclease activity of Artemis is activated, and the overhangs are degraded and prepared for sealing (67).

1.5.1.2 Homologous recombination

During homologous recombination, the undamaged sister chromatid is used to repair the DNA damage. The repair is initiated by 5' to 3' nucleolytic resection of the DSB end and by the MRE11-Rad50-NBS1 (MRN) complex to generate 3'-single-stranded DNA tails. The recruitment of the MRN complex is promoted by the binding of NBS1 to yH2AX. After strand resection and protein binding, the resulting complex accesses the complementary sequence of the sister chromatid and catalyzes strand-exchange events which displace one strand as a D-Loop in the end. This process requires the activity of BRCA2 and RAD51. BRCA2 controls the recombinase activity of RAD51 and its loading onto single-stranded DNA. RAD51 is assisted by a number of protein factors including BRCA1, RAD52, RAD54. After D-loop formation, the annealed 3'-end is extended by repair synthesis beyond the original break site to restore the missing sequence information (68;69).

1.5.2 Nucleotide excision repair

The nucleotide excision repair (NER) pathway deals with a wide range of DNA lesions by recognizing abnormal structures of DNA. UV-light induced photolesions like 4-6 photoproducts and cyclobutane pyrimidine dimers, helix-distorting intrastrand cross-links, bulky adducts and minor base damages induced by alkylating and oxidizing agents, are repaired by NER. Additionally, NER is considered to be a backup system for BER to remove oxidative stress induced DNA damage. Several proteins from other repair pathway are involved in the removal of oxidative DNA lesions. XPC acts as a cofactor in BER by stimulating the activity of the DNA glycosylase OGG1 (70), XPG serves as a cofactor for the efficient function of human NTH1 (71) and XPA might have a role in the

repair of oxidized bases (72). In yeast, it was demonstrated that BER acts synergistically with NER to repair endogenously induced oxidative damage (73). Some investigators could show that NER is involved in the repair of 8-oxoG (74;75). It was further shown that NER capacity and the expression of NER related genes may be modulated by oxidative stress (76).

Most NER lesions arise from exogenous sources and more than 30 proteins are involved in the repair. The NER consists of two pathways: the global genomic repair (GG-NER) and the transcription-coupled repair (TC-NER). GG-NER removes lesions from the entire genome whereas the TC-NER repairs polymerase-blocking damage on DNA strands of actively transcribed genes. Both pathways differ in their DNA damage recognition step but share the same mechanism. After the recognition of the damage, a multiprotein complex is assembled at the damaged site. Then the DNA is incised 5' and 3' several nucleotides away from the lesion. The damage containing part is removed, and the resulting gap is filled by a DNA polymerase. The newly synthesized strand is sealed by a DNA ligase (77-79).

1.5.3 Base excision repair

The base excision repair pathway is responsible for repairing most endogenous base lesions (AP sites) and abnormal bases such as 8-oxoguanine (8-oxoG) or formamidopyrimidine (Fapy-G) in the genome (80). BER is also involved in the repair of DNA single-strand breaks (Figure 1.3). Among NHEJ and HR, it is considered to be the most important pathway involved in the repair of radiation-induced DNA damages (62). The majority of damages processed through BER are generated by ROS. However, the functional significance of BER in the prevention of diseases remains unclear. No disease phenotype has been linked to BER deficiency so far.

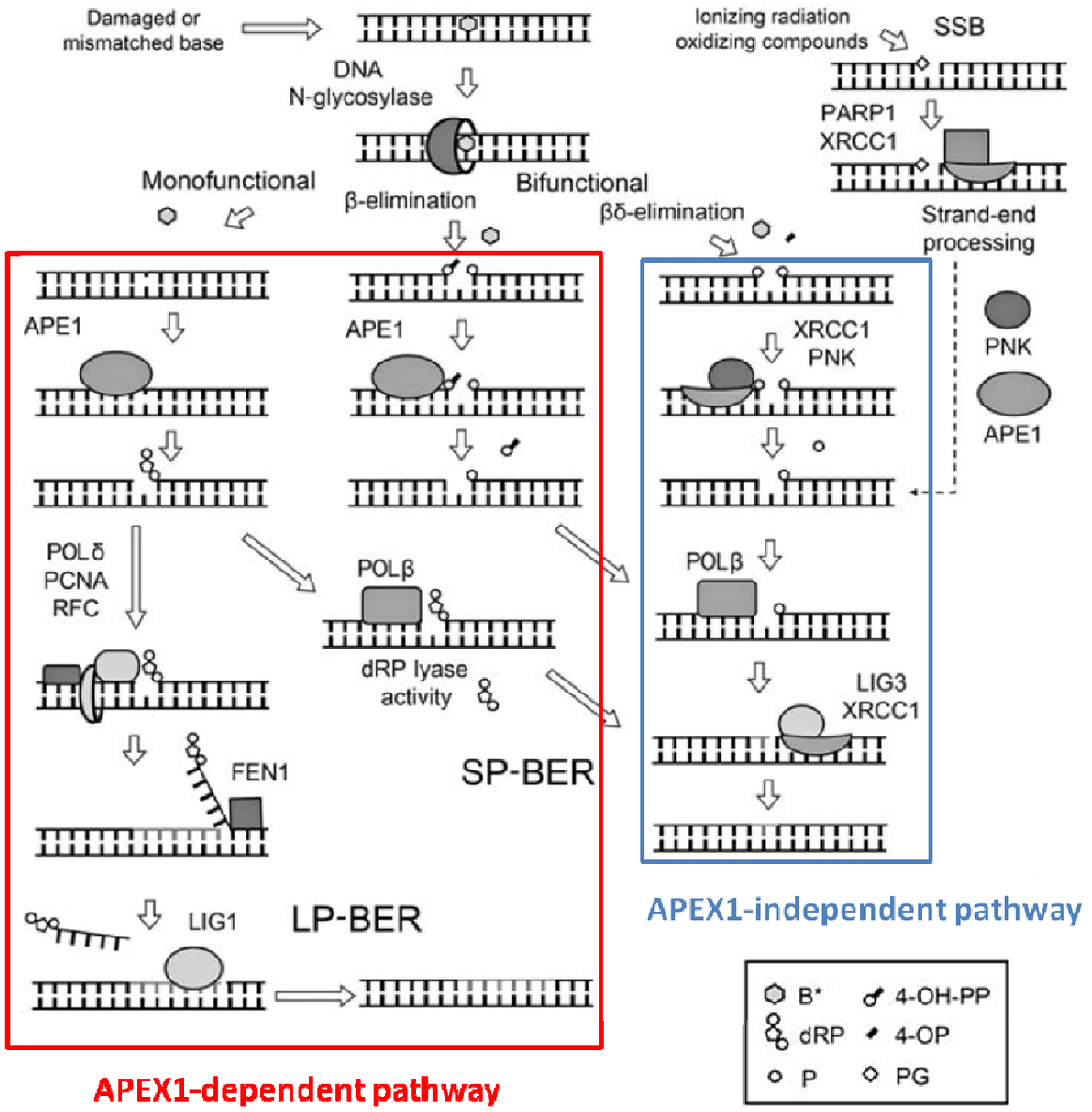

Figure 1.3. Schematic illustration of the BER pathway (adapted from (65)).

BER is initiated by the excision of a damaged base by a DNA glycosylase. Several distinct DNA glycosylases exist in mammalian cells. Each recognizes a limited, partially overlapping number of damaged bases or lesions (Figure 1.4). The glycosylase generates an abasic site (apurinic/apyrimidinic, AP site) due to cleavage of the N-glycosidic bond. An abasic site can also occur spontaneously by hydrolysis. The following steps depend on the activity associated with each DNA glycosylase and can be grouped in APEX1-dependent and APEX1-independent repair. DNA glycosylases can be distinguished in monofunctional and bifunctional glycosylases. The bifunctional glycosylases are specific for oxidized base lesions and have an additional intrinsic AP lyase activity.

In the APEX1-dependent pathway, the monofunctional glycosylases excise the substrate base, leaving an AP site cleaved by APEX1 to generate a 3'-OH and a 5'-deoxyribose phosphate (dRP) terminus. Bifunction glycosylases like NTH1, which prefers oxidized pyrimidines as substrate, and OGG1, which mainly removes 8-oxoG and Fapy-G, catalyze β-elimination of desoxyribose phosphate, leaving a 3'-PUA (3'-phospho-α,β–unsaturated aldehyde) and a 5'-phosphate. The 3'-PUA is removed by the 3'-phosphodiesterase activity of APEX1 to generate a 3'-OH.

In the APEX1-independent pathway, bifunctional glycosylases like NEIL1 and NEIL2 catalyze β,δ-elimination, leaving a 3'-phosphate, a poor substrate for APEX1. Here, the polynucleotide kinase (PNK) with dual 5'-kinase/3'-phosphate activity takes over the cleaning of the 3' end (80).

Then the DNA polymerase can continue the repair. DNA polymerase β (Polβ) initiates short-patch BER (SP-BER) and fills in the single nucleotide gap. The enzyme has an intrinsic dRP lyase activity which cleaves the dRP residue to generate 5'-phosphate. Finally, the ligation step is completed by the LIG3/XRCC1 complex. DNA polymerases Polδ or Polε lack this activity. These enzymes continue the repair via long-patch BER (LP-BER), where the 5'-dRP and 2-10 additional deoxynucleotides, cleaved by flap structure-specific endonuclease 1 (FEN-1), are displaced. LP-BER can be promoted through the stimulation of the strand-displacement activity of POLβ by FEN1 and the flap-cleavage activity of FEN1 by APEX1 (65). The nick is sealed by the DNA ligase LIG1 (81).

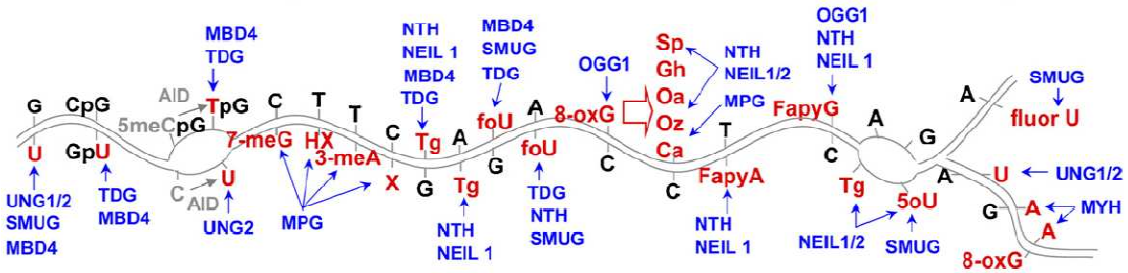

Figure 1.4. Relationship between damaged bases, DNA structure and recognition by DNA glycosylases. DNA glycosylases are shown in blue with arrows to the damaged base(s) recognized. Modified bases shown are in red (according to (82)).

Single-strand breaks are intermediates of the BER process or induced by ionizing radiation and oxidizing compounds. Unrepaired breaks are mutagenic and cytotoxic. Their repair

can be performed through the BER pathway but requires additional activities. The PARP1/XRCC1 complex initially detects the SSBs and the 3'-blocking ends like 3'-phosphate. Further strand processing requires PNK and/or APEX1. PARP1 catalyzes the poly(ADP-ribosyl)ation of several proteins. PARP1 interacts with XRCC1, a scaffold protein, which recruits other associated proteins to the strand break (65).

1.5.3.1 Polymorphisms in BER genes and radiosensitivity

Associations between DNA repair gene polymorphisms and radiosensitivity have been shown by several investigators (83;84). An association between polymorphisms in the BER genes *XRCC1*, *OGG1* and *PARP1* and radiosensitivity was shown in a study of cervical cancer cells (85). In a different study, the association of three polymorphisms in the *XRCC1* gene (Arg194Trp, Arg280His and Arg399Gln) and the possibility of developing an adverse radiotherapy response were examined in 254 breast cancer cases. The 194Trp allele was associated with the risk of developing an adverse response to radiotherapy. Additionally, the combination of the 194Trp and the 399Gln allele of *XRCC1* were found to be more frequent in radiation-sensitive breast cancer patients (86). Furthermore, the *APEX1* Asp148Glu and the *XRCC1* Arg399Gln allele may alter IR sensitivity as measured by prolonged cell cycle G_2 delay in γ-irradiated lymphocytes, particularly in women with a positive family history of breast cancer (87). In a prospective study of female breast cancer patients who received radiotherapy after breast-conserving surgery, Chang-Claude and colleagues evaluated the association of polymorphisms in *XRCC1* (Arg194Trp, Arg280His and Arg399Gln) and *APEX1* (Asp148Glu) with the risk of acute skin reactions after radiotherapy. Even though the development of acute toxicity was not associated with the genetic variants studied, they have shown that the *XRCC1* Arg399Gln and the *APEX1* Asp148Glu alleles may be protective against the development of acute side effects after radiotherapy in normal weight patients (88). A study of 41 patients who received post-mastectomy radiotherapy reported an association of the Arg/Arg genotype in the *XRCC1* codon 399 with an increased risk of radiation-induced subcutaneous fibrosis. The study revealed that the risk of subcutaneous fibrosis correlated with the number of risk alleles in other genes. Patients with few risk alleles exhibited radioresistance (89). Another study examined the association of polymorphisms in *XRCC1* (Arg194Trp, Arg280His, Arg399Gln, Gln632Gln) and *OGG1* (Ser326Cys) with the development of late

radiotherapy reactions. 22 out of 62 women with cervical or endometrial cancer treated with radiotherapy showed late adverse reactions. The 194Trp allele of *XRCC1* showed a significant protective effect. Patients with three or more risk alleles in *XRCC1* had a significantly increased risk of developing normal tissue reactions (90).

Since clear associations between various genetic polymorphisms of DNA repair genes and their phenotypic consequences are not known, correlations concerning functional consequences are of particular interest. Around 30 % of variants of DNA repair proteins are likely to substantially affect the protein function (91). However, there is very limited information on functional consequences of polymorphisms in the DNA repair genes *APEX1* and *XRCC1*. For *APEX1*, one variant allele, Asn148Glu, was associated with a decreased DNA repair rate (91).

No clear relationship was found between the *XRCC1* (exon 10 G → A) Arg399Gln genotype and SSB levels measured by comet assay (92). But the repair rates in DNA were affected by the *XRCC1* Arg399Gln polymorphism, being lower in heterozygous GA and variant AA genotype than in GG wild-type carriers (93). In a later study, Vodicka *et al.* showed again that AA carriers in *XRCC1* Arg399Gln exhibit a significantly decreased DNA repair rate (91). Cornetta *et al.* observed that AA carriers showed lower amounts of SSBs compared to wt or heterozygous subjects, but they did not detected any difference in DNA repair rates (94). In contrast, individuals with the *XRCC1* 399Gln variant allele showed significant increases in tail moment values (95). In sum, the entire information of all available data is very inconsistent. Some reports showed that the *XRCC1* polymorphism in exon 10 resulted in higher residual DNA damage measured by comet assay (96). Other studies concluded that the polymorphism did not influence the DNA damage repair after γ-irradiation (97;98).

The studies discussed above suggest that certain polymorphisms are associated with either increased or decreased radiosensitivity dependent on the type of cancer. Evidently, variants of the *APEX1* and *XRCC1* protein modify the protein's functions. For some polymorphisms in *APEX1* and *XRCC1*, several studies have linked the variant alleles with the risk of side effects and an altered protein function. Thus, *APEX1* and *XRCC1* appear to be good candidates involved in the tissue response to RT. The influence of a lack of those proteins on radiosensitivity should be further investigated.

1.5.3.2 APEX nuclease (multifunctional DNA repair enzyme) 1

The APEX nuclease (multifunctional DNA repair enzyme) 1 (APEX1) is a multifunctional protein. The gene is located on chromosome 14q11.2-12, 2.6 kb in size, and consists of four introns and five exons and encodes a protein of 318 amino acids with a molecular mass of 35kDa (http://www.ncbi.nlm.nih.gov). The protein is abundant (10^4-10^5 copies/cell) and has a relatively long half-life time (ca. 8 h) (cited as unpublished observation in (99)). The N-terminal domain, which contains the nuclear localization sequence (NLS), is essential for the redox activity through Cys65, while the C-terminus is essential for the DNA repair activity of APEX1 (Figure 1.5).

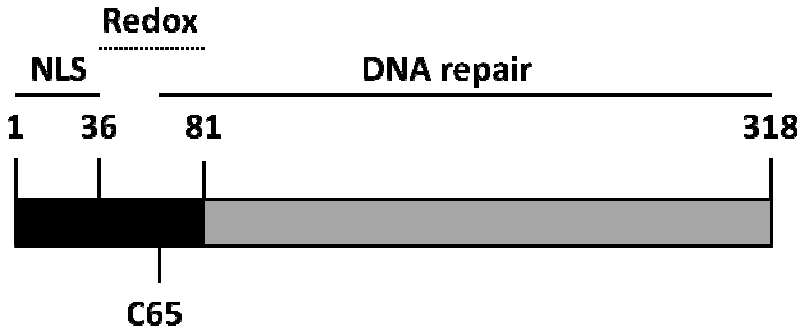

Figure 1.5. Schematic structural features of APEX1. NLS, nuclear localization sequence. C65, Cysteine 65 (adapted and modified from (100)).

APEX1 comprises three important functions: DNA repair activity, redox regulation activity and acetylation-mediated gene regulation. APEX1 is involved in the coordination of BER by interacting directly or indirectly with other BER enzymes (101-103). Furthermore it interacts with proteins involved in ribosomal functions and RNA processing, and with the tumor suppressor p53 (104-106). The redox regulatory function which is only found in mammals is unrelated to the DNA repair function of *APEX1*. This was shown by the observation that a mutation of the Cys65 abolishes the redox function but does not affect the repair function (107). APEX1 can maintain several transcription factors, such as early growth response protein-1 (*Egr-1*), nuclear factor-κB (*NF-κB*), hypoxia inducible factor-1α (*HIF-1α*) and activator protein-1 (*AP-1*) in a reduced activated state through the control of the redox status of Cysteine residues located within the DNA-binding domain of these transcription factors (Figure 1.6) (reviewed in (108)). The third function is associated to the ability of APEX1 to bind indirectly, as a component of a protein complex, to the

negative calcium response elements (nCaRE) of some promoters and thereby acting as a transcriptional repressor (109;110). Bhakat *et al.* showed that the regulation of the parathyroid hormone (*PTH*) gene is regulated by the acetylation of APEX1 through the histone acetyltransferase p300 (111).

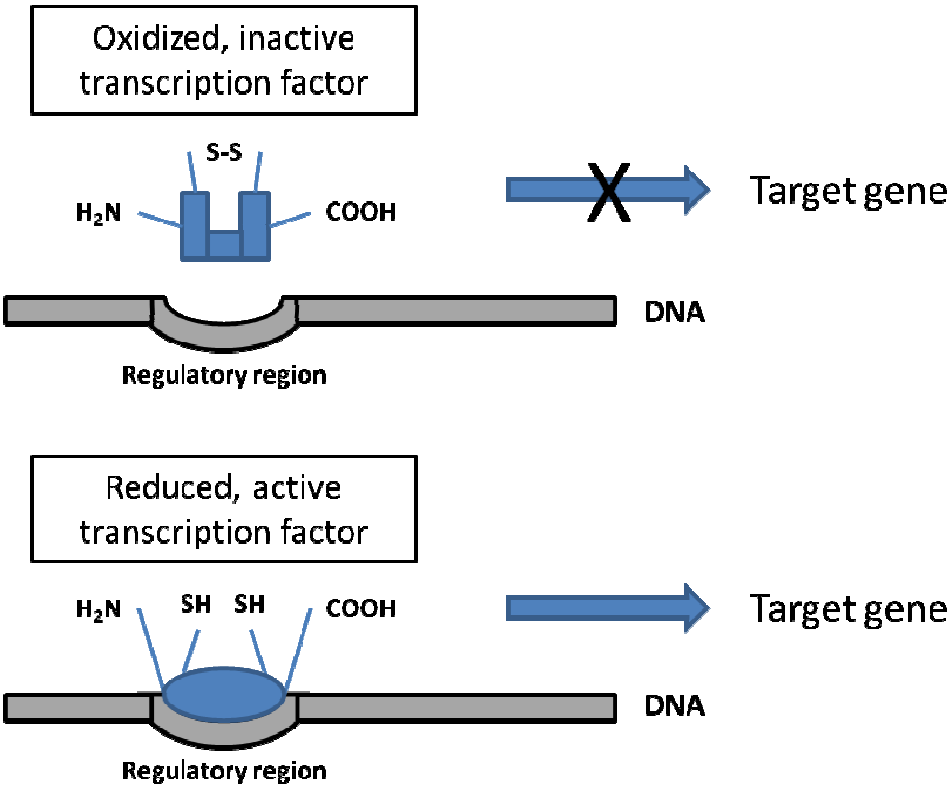

Figure 1.6. Redox activity of APEX1 (according to (112)).

The APEX1 expression in the cell is ubiquitous but differs among tissue types. Some cell types show only nuclear localization, other only cytoplasmic, and some display both (108;112). The nuclear localization is thought to point to its DNA repair function whereas the cytoplasmic localization reflects its role in redox regulation (112).

The APEX1 expression is regulated both at the transcriptional level and at the post-transcriptional level via post-transcriptional modifications. Additionally, the expression can be modified via re-localization of APEX1 from the cytoplasm to the nucleus (99;108;112).

The protein expression is cell cycle dependent, showing the highest expression in early or middle S-phase (113). Tumors often over express the protein and this over expression can be associated with increased levels of p53 which implies a fundamental role of the

protein in preventing cell death and in regulating cell proliferation (114). Several reports demonstrated an anti-apoptotic role and a positive effect on cell proliferation of APEX1 (112;115;116). In contrast, others have shown its role in controlling pro-apoptotic functions through p53-mediated activation of p21 leading to cell cycle arrest (106;117;118). The association of *APEX1* expression on apoptosis has been studied by several investigators, but with conflicting results. Down-regulation of *APEX1* expression was observed with apoptosis in a myeloid leukemia cell line, HL-60 (119). Vascotto and colleagues reported a strong correlation between down-regulation of APEX1 expression and increased apoptosis (120). Another paper showed an activated apoptosis upon down-regulation of *APEX1* in MCF7 (115). In contrast, decreased *APEX1* levels resulted in only a slight increase in apoptosis compared to control treated cells in A2780 and CP70 cell lines (121), in A549 (122) and in LOVO cells (123). Moreover, Fishel and colleagues observed that a reduction in *APEX1* did not coincide with an increase in apoptosis 72 h after transfection with siRNA (124). Similar results were demonstrated for embryonic bodies where a knockdown of *APEX1* expression did not trigger apoptosis (125).

Homologous deletion of *APEX1* in the mouse leads to embryonic lethality which demonstrates that *APEX1* is essential for early embryonic development. The isolation of stable *APEX1* knockout cell lines has been unsuccessful so far, which makes it difficult to explore the importance of each of the three different functions. But the use of specific inhibitors of the DNA repair or the redox regulatory function of *APEX1* offer a good strategy to investigate the biological significance of each function more specifically (126;127).

1.5.3.3 X-ray repair cross complementing group 1

The X-ray repair cross complementing group 1 (*XRCC1*) gene is a major gene involved in BER. It is located on chromosome 19q13.2, spans a genetic distance of 32 kb, comprises 17 exons, and encodes the DNA repair protein XRCC1. This protein contains 633 amino acids and has a molecular weight of 70 kDa (http://www.ncbi.nlm.nih.gov). The protein has no known enzymatic activity, but it interacts with many proteins of the BER. By doing this it functions as a molecular scaffold protein and recruits BER repair factors at the damaged site (128). Interaction partners include the 7,8-dihydro 8-oxo-guanine glycosylase (OGG1), APEX1, PNK and Polβ (129;130). *XRCC1* harbors two BRCT (*BRCA1*,

carboxy-terminal domain) sequence motifs (Figure 1.7). Further, XRCC1 co-localizes and interacts with PCNA (131;132). The BRCT domain is found within many DNA damage repair and cell cycle checkpoint proteins. This domain allows BRCT modules to interact forming homo/hetero BRCT multimers, BRCT-non-BRCT interactions, and interactions within DNA strand breaks. XRCC1 interacts through the BRTC1 domain with PARP1 and limits its poly(ADP-ribosyl)ating activities. Upon activation of PARP1 by SSBs, XRCC1 is recruited to the break by its BRCT1 domain. The BRCT2 domain of XRCC1 binds and stabilizes LIG3 (133-136). However, only a few investigators studied the correlation of XRCC1 expression on apoptosis, cell growth (137;138).

There are a few *XRCC1*-deficient cell lines available. The *XRCC1*-mutant strains of the Chinese hamster ovary (CHO) cells, EM7, EM9, EM-C11 and EM-C12, were isolated from the parental strain, AA8 (138). Null mutant mice showed an early embryonic lethality and an accumulation of endogenous DNA damage. Nevertheless, the isolation of *XRCC1*$^{-/-}$ mouse embryonic fibroblasts was successful (139).

As no human cell line lacking *APEX1* or *XRCC1* has been identified, the RNAi knockdown technique represents a sophisticated model to investigate the effects of a lack or reduced levels of *APEX1* and *XRCC1* on radiosensitivity and the repair of radiation-induced damage.

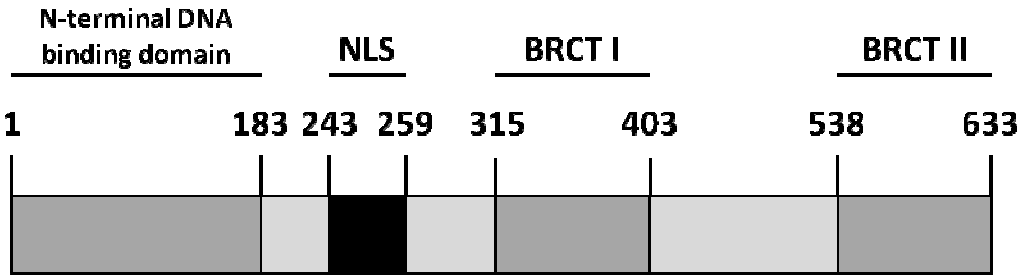

Figure 1.7. Schematic structural features of XRCC1. NLS, nuclear localization sequence. BRCT, BRCA1 carboxy-terminal domain (adapted and modified from (140)).

1.6 Expression of BER enzymes and radiosensitivity

Little has been done to investigate the correlation of *XRCC1* expression and radiosensitivity. *XRCC1* mutant EM9 cells were reported previously to be more radiosensitive than the wild type AA8 cells (141-143). Horton and colleagues identified that *XRCC1*$^{-/-}$ mouse fibroblast were hypersensitive to IR (144). In another study Brem and Hall demonstrated that a reduction in XRCC1 protein levels resulted in a hypersensitivity to ionizing radiation in three human breast cancer cell lines (145).

However, investigations regarding *APEX1* are numerous. Tumors frequently overexpress *APEX1* and are resistant to chemotherapy and ionizing radiation (146). It is not clear yet which cellular mechanism causes the resistance. Inconsistent data exist for the association between *APEX1* expression and cellular radiosensitivity. Some investigators have demonstrated a positive association, while others have found little or no correlation. Down-regulation of *APEX1* enhanced radioresistance in HeLa cells (147) while enhancing sensitivity to radiation in LOVO cells (123), lung carcinoma cells A5186 (148), and three radiation-resistant prostate cancer cell lines, LNCaP-IRR, PC3-IRR, and Du145-IRR (149). Two recently published papers also showed that inhibition of APEX1 made U87, U251, TK6 and HCT116 cells more radiosensitive (150;151). So far the results suggest that there is no clear evidence for a relationship between APEX1 expression and (tumor-) radiosensitivity. These conflicting results are probably due to the different functions of APEX1 in DNA repair and redox regulation. Furthermore, the radiation response or the BER efficiency depends on all BER components within the cell. An alteration in one of the enzymes may be compensated or intensified by a second alteration. This could explain a cell line specific effect. By interfering with the APEX1 expression or another efficient BER inhibition, the resistance of tumors to radiation and chemotherapeutic drugs could be reversed or at least modified. It has already been shown that the APEX1 expression levels and its cellular localization may be used to predict tumor sensitivity towards radio- or chemotherapy (152).

Another strategy would be to combine APEX1 inhibitor with radiotherapy that is applied only to the tumor to reduce normal tissue toxicity. The influence of APEX1 inhibitors has been explored in different cell models with a deregulated APEX1 expression by using knockdown techniques. Counteracting the radioresistance of tumors by targeting these aberrant DNA repair is an effective strategy to sensitize tumors to radiation. One concept

is the approach of “synthetic lethality”, where PARP inhibitors are applied to BRCA-defective tumors. The use of PARP inhibitors forces the cell to use HR as a backup repair pathway because BER is blocked. The lesions that are normally repaired by BER are converted to DSB. Those DSB are usually repaired by HR. HR-proficient cells will survive, whereas tumor cells that are deficient in HR because of the BRCA mutation are selectively killed (153;154). Blocking or inhibiting DNA damage or DNA damage signaling pathways is a good way to take advantage of the differences which exist between tumors and normal tissue.

Based on the present data, it is not possible to distinguish an association between the expression of BER genes and their influence on radiosensitivity. The studies above suggest that both, *APEX1* and *XRCC1*, might have essential functions in the response to radiation treatment and in modulating radiosensitivity. There is a clear need to further elucidate the correlations of a deficiency in BER genes and their influence on radiosensitivity. Based on functional assays, our results will support and extend the finding reported so far regarding the role of *APEX1* and *XRCC1* in BER.

1.7 Background of this thesis

The thesis was part of a project in which risk factors for breast cancer risk and the development of side effects after radiotherapy should be investigated using data from the German case-control study MARIE.

The first part of the project aims to collect clinical data and late side effects of patients from the MARIE study. Further the influence of common SNPs in oxidative stress genes on (i) the breast cancer risk, (ii) the occurrence of late side effects after radiotherapy, and (iii) the prognosis were assessed (18).

The second part of the project aims to investigate the influence of genetic variability in DNA repair genes on breast cancer risk and radiosensitivity. For this, we firstly focused on base excision repair (BER) and the establishment of a cell model where deficiencies in BER pathways were simulated by knockdown of APEX1 and XRCC1. Further the functional consequences due to the silencing and the effects regarding radiosensitivity were investigated.

1.8 Aims of the study

The study aims to investigate the effects of a decrease in the expression of *APEX1* and *XRCC1* on the cellular sensitivity to ionizing radiation. The investigations will not only focus on functional consequences due to the silencing of the single genes, but also on the effects of a simultaneous silencing of both genes. To date this has never been studied and we are the first to report the functional consequences caused by simultaneous silencing of both *APEX1* and *XRCC1*.

Gene defects were analyzed in two different cell types, the breast adenocarcinoma cell line MCF7 and a healthy counterpart, the human mammary epithelial cells HMEpC. The *APEX1* and the *XRCC1* gene were silenced in both cell types by using the RNAi knockdown technique. In order to assess the functional consequences which are caused by mimicking a deficiency in these BER genes, (i) the growth characteristics, (ii) the radiosensitivity and the survival, (iii) the radiation-induced DNA damage, and (iv) the gene expression profiles of silenced cells before and after irradiation were investigated.

The growth characteristics and the survival were determined by using the Sulforhodamine B and the Clonogenic assay. The induction of single-strand breaks and the repair rate were evaluated with the alkaline Comet assay, whereas the induction of double-strand breaks and their rejoining were detected with the γH2AX assay, which uses an antibody specific for the phosphorylated form of the variant histone H2AX (γH2AX). γH2AX is an indicator of double-strand breaks. Gene expression profiles were determined 24 h and 48 h after silencing and after additional irradiation with 5 Gy. They were used to identify possible alternative backup repair pathways and differences in radiation response between normal and cancer cells. In particular, the analysis will focus on expression changes of DNA repair genes. These changes will provide an insight into the regulation of DNA repair in cells with a deficiency in BER.

This study will reveal how imbalances in BER might be associated with altered cellular radiosensitivity. Such imbalances can be used to predict the radiation response in cancer patients, and will expand the understanding of normal tissue toxicity due to genetic variation. The results of this work will be helpful in adjusting radiotherapy protocols for both radiosensitive and –resistant patients.

2 Materials and Methods

2.1 Materials

2.1.1 Cell culture

CO_2-Incubator Jouan IG 150	Astel SA, Chateau Gontier, Frankreich
CO_2 Small-Incubator TECO10	Selutec, Mössingen-Öschingen
Inverse microscope Wilovert	Leica Microsystems AG, Wetzlar
Laboratory microscope Loborlux S	Leica Microsystems AG, Wetzlar
Sterile Werkbank Biogard Hood KL II	Baker, Stanford, USA

2.1.2 Cell culture media and supplements

Fetal calf serum (FCS)	PAA, Pasching, Österreich
Mammary Epithelial Cell Growth Medium	Cellmade, Archamps, France
McCoy's 5A Medium	Invitrogen GmbH, Karlsruhe
PenStrep 10.000 units/mL Penicillin, 10.000 µg/mL Streptomycin	Invitrogen GmbH, Karlsruhe
Roswell Park Memorial Institute Medium (RPMI) 1640	Invitrogen GmbH, Karlsruhe
Supplements (Streptomycin sulfate, Amphotericin B, Insulin, Hydrocortisione, FBS, BPE, bFGF, Heparin, PMA)	Cellmade, Archamps, France
Trypsin-EDTA (1x)	Invitrogen GmbH, Karlsruhe
Trypsin-EDTA Solution	Cellmade, Archamps, France
Trypsin Neutralization Solution	Cellmade, Archamps, France

2.1.3 Cell lines

HMEpC	Cellmade, Archamps, France
MCF7	Human tissue and tumor repository, DKFZ, Germany

2.1.4 Centrifuges

Centrifuge 5402	Eppendorf AG, Hamburg
Centrifuge 5415C	Eppendorf AG, Hamburg
Minifuge T	Heraeus, Hanau

Minifuge Universal	Hettich, Tuttlingen

2.1.5 Electrophoresis

Agagel Midi-Wide	Whatman Biometra GmbH, Göttingen
Agagel Mini	Whatman Biometra GmbH, Göttingen
Elektrophoresis Power Supply EPS 300	Amersham Biotech GmbH, Freiburg
Elektrophoresis Power Supply EPS 3500	Amersham Biotech GmbH, Freiburg
Horizontal Electrophoresis chamber	Renner GmbH, Dannstadt-Schauernheim
Powerpack 25	Whatman Biometra GmbH, Göttingen
X Cell Sure Lock	Invitrogen, Karlsruhe

2.1.6 Enzymes

Benzonase Nuclease	Merck, Darmstadt
Ribonuclease (RNase)	Sigma-Aldrich Chemie GmbH, München
RNasin Ribonuclease Inhibitor 40 units/µL	Promega GmbH, Mannheim
Superscript III Reverse Transcriptase 200 units/µL	Invitrogen GmbH, Karlsruhe
Taq DNA Polymerase 5 units/µL	Qiagen GmbH, Hilden

2.1.7 Materials

24-well plates	Greiner Bio-One GmbH, Frickenhausen
6-well plates	Greiner Bio-One GmbH, Frickenhausen
Blue caps (15 mL, 50 mL)	Greiner Bio-One GmbH, Frickenhausen
CELLCOAT Collagen 6-well plates	Greiner Bio-One GmbH, Frickenhausen
CELLCOAT Collagen 24-well plates	Greiner Bio-One GmbH, Frickenhausen
CELLCOAT Collagen 96-well plates	Greiner Bio-One GmbH, Frickenhausen
Cellstar cell culture flasks 50 mL (T25)	Greiner Bio-One GmbH, Frickenhausen
Cellstar cell culture flasks 250 mL (T75)	Greiner Bio-One GmbH, Frickenhausen
Comet Slides (2 spot, 20 spot)	Trevigen/AMS, Wiesbaden
Cover Slides (24 x 70 mm)	Menzel, Braunschweig
Cryo 1° C Freezing Container	Nalge Europe Ltd., Neerijse, Belgien
Cryo vials (2 mL, 5 mL)	Greiner Bio-One GmbH, Frickenhausen

Cuvettes half-micro	Greiner, Labortechnik
Hematocytometer	Migge, Heidelberg
Hyperfilm	Amersham Biosciences, Little Chalfont, UK
Invitrolon PVDF membranes	Invitrogen GmbH, Karlsruhe
LightCycler 96/384 well plates	Roche Diagnostics GmbH, Mannheim
NuPAGE Novex Bis-Tris gels	Invitrogen GmbH, Karlsruhe
PCR tubes 0.2 mL	Biozym Diagnostik, Oldendorf
PCR tubes (0.5, 1.5, 2.0 mL)	Eppendorf AG, Hamburg
PCR tubes (0.5, 1.5, 2.0 mL)	Greiner Bio.One GmbH, Frickenhausen
Pipette tips, non-sterile (10, 20, 100, 200, 1000 µL)	Eppendorf AG, Hamburg
Pipette filter tips, sterile (10, 20, 100, 200, 1000 µL)	Nerbe Plus GmbH, Winsen/Luhe
Round-Bottom tube 14 mL	Becton Dickinson Labware, Heidelberg
Serological pipettes, sterile (2, 5, 10, 25, 50 mL)	Corning B.V. Life Sciences, Niederlande
Sterile filter (0.2 µm, 0.45 µm)	Millipore, Molsheim
UV-Cuvette micro	Brand GmbH, Wertheim
Wide bore Tips (200 µL)	Stratagene, La Jolla, USA

2.1.8 Nucleic acids

Fluorescein-siRNA	New England Biolabs
GeneRuler 100 bp DNA Ladder	Fermentas GMBH, St. Leon
Magic Mark XP Western Protein Standard	Invitrogen GmbH, Karlsruhe
Oligo $(dT)_{18}$VN Primer	Applied Biosystems, Darmstadt
ON-Target plus siRNA Set of 4, *APEX1*	Dharmacon, Colorado, USA
ON-Target plus siRNA Set of 4, *XRCC1*	Dharmacon, Colorado, USA
ON-Target plus, non-targeting siRNA # 1	Dharmacon, Colorado, USA
pUC19 DNA/MspI (HpaII) Marker, 23	Fermentas GMBH, St. Leon
RNA 6000 ladder	Ambion, Inc. Austin, USA

2.1.9 Other devices

AccuBoy	TecNoMara, Ruhberg
Agfa Curix 60	Agfa, Köln
Agilent 2100 Bioanalyzer	Agilent Technologies, Inc., Palo Alto, USA
Analytic scale A200S	Sartorius AG, Göttingen
Automated Imaging Microscope	Metasystems, Altlußheim
Irradiation device OB 58 (0.575 Gy/min)	Buchler, Braunschweig
Biophotometer	Eppendorf AG, Hamburg
CASY Cell Counter and Analyzer System	innovates AG, Reutlingen
FACS Calibur Becton Dickinson	Labware, Heidelberg
Gammacell 1000 (10.1 Gy/min)	MDS Nordion, Ottawa, Kanada
Hybridizing oven OV2	Whatman Biometra GmbH, Göttingen
Hypercassette	Amersham GE Healthcare, München
Microwave HMT 832C	Robert Bosch GmbH, Stuttgart
pH-Meter pH 211	Hanna Instruments Deutschland GmbH, Kehl
Pipetts (0.1-2.5, 0.5-10, 2-20, 10-100, 20-200, 100-1000 µL)	Eppendorf AG, Hamburg
Scale type 1518	Sartorius AG, Göttingen
Schüttler Duomax 1030	Heidolph Instruments GmbH, Schwabach
Schüttler Minishaker MS2	IKA GmbH, Staufen
Spectramax M5^{e} microplate reader	MDS Molecular devices, USA
Staining chamber	Migge, Heidelberg
Thermomixer Comfort	Eppendorf AG, Hamburg
UV-Densitometer	Herolab, Wiesloch
Vortex Genie 2	Bender & Hobein, Zürich, Schweiz
Watherbath WG	Neolab, Heidelberg

2.1.10 PCR devices

DNA Engine PTC-200	MJ Research, Waltham, USA
LightCycler 480	Roche Diagnostics GmbH, Mannheim
Mastercycler epgradient	Eppendorf AG, Hamburg

2.1.11 Solutions, chemicals, and buffers

Agarose, low melting	Biozym Diagnostics, Hameln
Agarose, PeqGold Universal Agarose	PeqLab, Erlangen
BD FACS Flow	Becton Dickinson Labware, Heidelberg
BD FACS Rinse	Becton Dickinson Labware, Heidelberg
Chloroform	Sigma-Aldrich Chemie GmbH, München
Complete Mini, Protease Inhibitor Cocktail Tablets	Roche Diagnostics GmbH, Mannheim
DharmaFECT 1 Transfection reagent	Dharmacon, Colorado, USA
Diethylpyrocarbonat	Sigma-Aldrich Chemie GmbH, München
Dimethylsulfoxide	Merck, Darmstadt
DL-Dithiothreitol	Sigma-Aldrich Chemie GmbH, München
dNTP Mix (10 mM each)	MBI Fermentas GmbH, St. Leon-Rot
Ethanol absolute	Sigma Aldrich Chemie GmbH, München
Ethidiumbromid (1 mg/mL)	Bio-Rad Laboratories GmbH, München
Ethylendiamine tetraacetic acid-Disodium-solution (EDTA-Na2), 0,5 M	Sigma-Aldrich Chemie GmbH, München
Glycogen	Invitrogen GmbH, Karlsruhe
Isopropanol	Sigma-Aldrich Chemie GmbH, München
Sodium-dihydrogen-phosphat (KH_2PO_4)	Merck, Darmstadt
Loading Dye 6x	Fermentas GMBH, St. Leon
Lysoformin	Lysoform AG, Windisch/Brugg, Schweiz
Magnesium chloride solution	Quiagen GmbH, Hilden
Methanol	Sigma-Aldrich Chemie GmbH, München
Milk powder	Carl Roth GmbH, Karlsruhe
N-Laurylsarcosin-sodium salt	Sigma-Aldrich Chemie GmbH, München
PageRuler Prestained Protein Plus	Fermentas GMBH, St. Leon
Phenylmethylsulfonylfluoride	Sigma-Aldrich Chemie GmbH, München
Phosphate buffered saline	Invitrogen GmbH, Karlsruhe
Propidium Iodide	Sigma-Aldrich Chemie GmbH, München
RNase Away	Sigma-Aldrich Chemie GmbH, München
β-Mercaptoethanol	Sigma-Aldrich Chemie GmbH, München

SeaPlaque agarose	Biozym, Oldendorf, Germany
Sodium chloride	Sigma-Aldrich Chemie GmbH, München
Sodium hydroxide	Sigma-Aldrich Chemie GmbH, München
Sodium dodecylsulfate	Sigma-Aldrich Chemie GmbH, München
SYBR Green I	Molecular Probes, Invitrogen, USA
Tris(hydroxymethyl)aminomethane	Sigma-Aldrich Chemie GmbH, München
Triton X-100	Sigma-Aldrich Chemie GmbH, München
Trizol reagent	Invitrogen GmbH, Karlsruhe
Tween 20	Sigma-Aldrich Chemie GmbH, München
Urea pura	Sigma-Aldrich Chemie GmbH, München
Vectashield	Vector Laboratories, Burlingame, Kanada
Vectashield Hard Set	Vector Laboratories, Burlingame, Kanada
Wasser ultra pure, DNase free, RNase free	Invitrogen GmbH, Karlsruhe

2.1.12 Ready to use kits and solutions

Agilent 6000 Nano LabChip Kit	Agilent Technologies, Inc., Palo Alto, USA
BioRad Protein Assay	Bio-Rad Laboratories, München
NuPAGE Antioxidant	Invitrogen GmbH, Karlsruhe
NuPAGE LDS buffer (4x)	Invitrogen GmbH, Karlsruhe
NuPAGE MOPS SDS Running Buffer (20x)	Invitrogen GmbH, Karlsruhe
NuPAGE Sample Reducing Agent (10x)	Invitrogen GmbH, Karlsruhe
NuPAGE Transfer Buffer (20x)	Invitrogen GmbH, Karlsruhe
QIAquick PCR Purification Kit	Qiagen GmbH, Hilden
QuantiTect SYBR Green PCR Kit	Qiagen GmbH, Hilden
RNeasy Mini Kit	Qiagen GmbH, Hilden
Western Lightning Chemiluminescence Reagent Plus	Perkin Elmer, Life Sciences, Inc., Boston, USA

2.1.13 Antibodies

β-Actin (C-4) mouse monoclonal antibody	Sigma-Aldrich Chemie GmbH, München
Alexa488 mouse Anti-H2AX-phosphorylated (Ser139)	BioLegend, San Diego, USA
Anti-phopho-Histone H2AX (Ser139) mouse monoclonal IgG1 Antibody (clone JBW301)	Millipore, Temecula, CA, USA
Goat Anti-Mouse IgG-Cy3	Jackson ImmunoResearch Ltd., Suffolk, UK
Goat anti-mouse IgG-HRP (sc-2005)	Santa Cruz Biotechnology, Santa Cruz, USA
Goat anti-rabit IgG-HRP (sc-2004)	Santa Cruz Biotechnology, Santa Cruz, USA
p21 (C-19) rabbit polyclonal antibody	Santa Cruz Biotechnology, Santa Cruz, USA
p53 (C-11) mouse monoclonal antibody	Santa Cruz Biotechnology, Santa Cruz, USA
Ref-1 (N-16) goat polyclonal antibody	Santa Cruz Biotechnology, Santa Cruz, USA
XRCC1 (H-300) rabbit polyclonal antibody	Santa Cruz Biotechnology, Santa Cruz, USA

2.1.14 Software and databases

Adobe Photoshop 7.0	Adobe Systems Inc., San Jose, USA
Bead Studio 3.1.3	Illumina Inc., San Diego, USA
Ensembl Genome Browser	http://www.ensembl.org
FlowJo 7.6.1	Tree Star Inc., Ashland, USA
ImageJ 1.41	NIH, USA
Ingenuity Pathway Software Analysis	Ingenuity Systems Inc., Redwood City, USA
Microsoft Office 2007	Microsoft Cooperation, 2008
MultiExperiment Viewer	http://www.tm4.org/
National Center for Biotechnology Information (NCBI)	http://www.ncbi.nlm.nih.gov
Primer Version 0.5	Whitehead Institute for Biomedical Research, Cambridge, USA
Prism 5	GraphPad Software Inc.
Reference Manager 12.0	Thomson Research Soft, Stanford, USA
Sigma Plot 9.0	Systat Software Inc., Point Richmont, USA
Specificity Server	http://informatics-eskitis.griffith.edu.au/
Table Curve 1.0	Jandel Scientific

2.2 Methods

2.2.1 Description of cell lines, their cultivation, and cryoconservation

2.2.1.1 MCF7

This human breast adenocarcinoma cell line was supplied from the human tissue and tumor repository (tumor bank) of the Department of Cellular and Molecular Pathology, DKFZ, Germany. Cells were cultivated in RPMI 1640 media with 10 % fetal calf serum and 1 % antibiotic at 37° C (degree Celsius) in a 5 % CO_2 humidified incubator. Every three to four days, the cells were subcultivated. The media was removed from the adherent growing cells and cells were washed with PBS. Afterwards cells were shortly washed with Trypsin/EDTA and then incubated with 1.5 mL of Trypsin/EDTA for one minute at 37° C. The rounded cells were released from the culture surface by gentle pivoting or rocking of the flask. For inhibiting further tryptic activity, 6 mL of media was added to the cell suspension. Cells were counted with a hemocytometer and inoculated at a density of 20.000 cells/cm^2 for subculturing. For cryoconservation, cells were centrifuged and washed with PBS after trypsinization. Cells were resuspended and frozen in RMPI 1640 with 20 % FBS and 10 % DMSO at a density of $2 \cdot 10^6$ cells/mL.

Cells were controlled for contaminations by multiplex cell contamination test through Genomics and Proteomics Core Facility (GPCF) at DKFZ. Samples were tested before starting any experiments. Multiplex cell contamination test is a high-throughput test and can detect 37 contamination markers for viral contamination, mycoplasma, and cross-contamination by other cell lines in a single PCR reaction.

Further, MCF7 cells were tested for their identity by the German Collection of Microorganisms and Cell Cultures (DSMZ). They created a DNA profile of eight highly polymorphic regions of short tandem repeats (STRs). In addition the cells were tested for the presence of DNA sequences from mouse, rat and hamster.

2.2.1.2 HMEpC

These primary human mammary epithelial cells were purchased from Cellmade, France. The sources of the cells were normal mammary glands of a 29 years old female. Cells were cultivated in Mammary Epithelial Cell Growth Medium which contained antibiotics (Penicillin, Streptomycin sulfate, Amphotericin B), Insulin, Hydrocortisone, FBS, BPE, bFGF, Heparin and PMA. Cells were cultivated in a 37° C, 5 % CO_2 humidified incubator.

Epithelial Cell Growth Medium was changed every 2-3 days. The cells were subcultured when they reached a confluency of 60-80 % (every 3-4 days). Subculturing was performed at RT. The medium was removed from culture flasks by aspiration and the monolayer of cells was washed with HBSS, followed by pipetting of 5 mL of Trypsin/EDTA Solution into the flask. 4 mL of the solution was removed immediately to avoid over trypsinization. The trypsinization progress was monitored under an inverted microscope. After about one minute cells become rounded but still attached to the flask. The rounded cells were released from the culture surface by rocking the flask until most of the cells are detached. 5 mL of Trypsin Neutralizing Solution were added to the flask to inhibit further tryptic activity. Cell suspension was transferred from the flask to a 50 mL sterile conical tube. The conical tube was centrifuged at 220 x g for 5 minutes to pellet the cells. The supernatant was removed and the cells were resuspended in 2 mL of Epithelial Cell Growth Medium by gently pipetting the cells to break up the clumps. Cells were counted with a hemacytometer or cell counter and subcultivated at a cell density of 7.500 cells/cm^2 for rapid growth. For cryoconservation, cells were centrifuged and washed with PBS after trypsinization. Cells were resuspended and frozen in Mammary Epithelial Cell Growth Medium containing 10 % FBS and 10 % DMSO at a density of $1 \cdot 10^6$ cells/mL.

2.2.1.3 Determination of cell viability

The viability of the cells was determined with the trypan blue exclusion assay. Living cells exclude the dye Trypan blue, whereas dead or dying cells with a compromised plasma membrane take up the dye and turn blue. The cells were counted using a hemocytometer or a Cell Counter to estimate the cell concentration and percentage viability.

2.2.1.4 Irradiation of the cells

To assess the consequences of ionizing radiation on the gene expression pattern in cells with silenced genes 24 and 48 h after transfection, several batches of the cells were additionally irradiated with a radiation dose of 5 Gy. The lysis of these cells and the subsequent DNA/RNA isolation was performed after a further incubation step at 37° C for four hours. Changes in gene expression of DNA repair genes were measured via quantitative RT-PCR.

2.2.2 RNA interference

Since its discovery in Caenorhabditis elegans, RNAi has become a widely used method for studying gene function (155). It is a process by which a specific messenger RNA is targeted for degradation by a double-stranded (ds) RNA which is homologous to the corresponding mRNA leading to gene silencing (156).

Briefly, the general mechanism involves the processing of dsRNA into short interfering (si) RNA duplexes of 21-23 nucleotides in length. This process is catalyzed by Dicer, which is a highly conserved endonuclease. The siRNAs are recognized and rearranged by the RNA-induced silencing complexes (RISC), which promotes upon activation the recognition and the cleavage of complementary single-stranded RNAs, such as mRNAs (157-159). RNA silencing is considered to be a defense mechanism of many organisms as a response against RNA viruses and transposable elements (160).

For the silencing of XRCC1 and APEX1, the ON-TARGETplus siRNA from Dharmacon Technologies was used. The product “Set of 4” consists of four individual siRNAs each targeting a different segment of the mRNA of a gene. Three out of four are guaranteed to silence the target gene by 75 % or better. A modification of both strands of the siRNA duplex reduces off-target effects. The sense strand is modified to prevent interaction with RISC and favor antisense strand uptake. Antisense strand seed region is modified to minimize seed-related off-target effects which are primarily driven by antisense strand seed activity. Therefore, sense strand inactivation alone does not decrease the total number of off-target genes (161;162).

2.2.2.1 Optimization of transfection conditions

To obtain the highest transfection efficiency with minimal effects on cell viability the transfection conditions were optimized for each cell line. Cells were plated at three different densities and four DharmaFECT 1 transfection reagent volumes were used as recommended by the manufacturer. Luciferase siRNA, non-coding siRNA and untreated cells were used as negative controls to find conditions that show target mRNA knockdown of > 80 % and > 80 % cell viability. Fluorescein-siRNA was used to estimate transfection efficiency. It facilitates parameter optimization such as cell density and amount of transfection reagent. These optimized conditions were used for all subsequent experiments.

2.2.2.2 Transfection procedure

The transfection was performed according to the manufacturer's general transfection protocol. Each experiment included in triplicate: 1) Untreated cells, 2) Negative control siRNA (Luciferase siRNA or non-targeting siRNA), and 3) the target siRNA (*APEX1*, *XRCC1* siRNA or an equal concentration of both siRNAs). The cells were trypsinized, counted and diluted in antibiotic-free complete medium to obtain the appropriate plating density. For MCF7, a cell plating density of $6.6 \cdot 10^4$ cells per well was used and accordingly for HMEpC $4 \cdot 10^4$ cells per well (24-wells plating format). Cells were then plated in collagen coated cell culture plates and incubated at 37° C with 5 % CO_2 over night. On the next day, in separate tubes, 100 nM of target siRNA and the appropriate volume of DharmaFECT 1 transfection reagent were diluted with serum-free and antibiotic-free medium. For both cell types, 1.33 µL transfection reagent were used per well. The contents were mixed and incubated for 5 minutes at RT. Then, the siRNA solution was added to the Dharmafect solution and the mixture was incubated for 20 minutes at RT to form a complex. Antibiotic-free medium was added to the mix to obtain the desired volume of transfection medium. Cell culture medium from plates was replaced with 500 µL of transfection medium. Cells were incubated at 37° C in 5 % CO_2 for 24-72 h until mRNA and protein analysis (DharmaFECT General transfection protocol, Dharmacon Technologies, 2006).

2.2.3 RNA isolation and analysis

For isolating RNA from cells, the RNeasy Mini Kit (Qiagen) was used. Isolation was performed according the Kit's protocol. The cells grown in a monolayer were lysed directly in the cell culture plate. For this purpose, the cell-culture medium was completely aspired and cells were disrupted by adding 350-600 µL Buffer RLT (10 µL mercaptoethanol (β-ME) was added per 1 mL Buffer RLT before use). The lysate was transferred into a microcentrifuge tube and pipetted to mix. The lysate was homogenized by passing it 5 times through a blunt 20-gauge needle (0.9 mm diameter) fitted to an RNase-free syringe. Then, one volume of 70 % ethanol was added to the homogenized lysate, and mixed well by pipetting. After this step, the sample was transferred to a RNeasy spin column, which was subsequently centrifuged for 15 s at 8000 x g. Next, the spin column was washed once with 700 µL Buffer RW1 and twice with 500 µL Buffer RPE followed by

centrifugation. RNA was eluted with 30-50 µL RNase-free water. The eluted RNA was stored at -80° C.

2.2.3.1 Qualification and quantification of the isolated RNA

The concentration of the isolated RNA was determined using the Nanodrop ND 1000 Spectrophotometer. To characterize the RNA integrity the Agilent 2100 Bioanalyzer was used with the Agilent RNA 6000 Nano Kit according to the manufacturer's protocol. The method is based on a laser induced fluorescence of a RNA-binding Cy3 dye (163). Each chip contains a set of microchannels that is used for separation of nucleic acid fragments based on their size as they are driven through it electrophoretically. During migration of the fragments, the RNA strands are stained with a dye. These complexes are detected by laser-induced fluorescence (Agilent RNA 6000 Nano Kit Guide).

With a ladder that contains RNA fragments of known sizes, a standard curve of migration time versus fragments size is plotted. Besides the quantification, the ratio of the ribosomal RNAs 18s and 28s is determined, giving an indication on the integrity of the RNA sample. Based on an algorithm, a RNA Integrity Number (RIN) is calculated estimating the integrity of total RNA samples based on the entire electrophoretic trace of the RNA sample, including the presence or absence of degradation products. The RIN has a range from 1-10 with 10 representing the best quality and nearly no degradation. The analysis of the results was completed with the 2100 expert software (Agilent 2100 Bioanalyzer Compendium, Agilent Technologies, 2007).

2.2.3.2 First-strand cDNA Synthesis

First-strand cDNA was synthesized using oligo$(dT)_{18}$ primer and Superscript III reverse transcriptase according to the manufacturer's instructions. Briefly, 500 ng of each total RNA sample were diluted with 1 µL of oligo$(dT)_{18}$ (50 µM), 1 µL 10 mM dNTP Mix (10 mM each dATP, dGTP, dCTP and dTTP) and RNAse free water to a volume of 12 µL. This mixture was then heated to 65° C for 5 minutes and incubated on ice for at least 5 minutes. Then, 4 µL of 5x First Strand Buffer, 2 µL 0.1 M DTT, 1 µL RNAse Inhibitor (40 units/µL) and 1 µL Superscript III RT (200 units/µL) was added. Mixture was gently mixed and incubated at 50° C for 50 minutes. The reaction was inactivated by heating at 70° C for 15 minutes. cDNA was diluted 1:10 and stored at -80° C.

2.2.3.3 Verification of the cDNA integrity

To verify the reverse transcription and the accessibility of the cDNA for PCR, a Test-PCR was performed (Table 2.1). In this PCR, a sequence from the 5' and 3' end of the human Clathrin gene (*CLTC*) was amplified. The two products are 570 and 550 bp in length. The mRNA of this gene has a length of 8575 base pairs. If a 5'- and a 3'- product of such a long mRNA transcript can be amplified the integrity of all other cDNAs will be sufficiently good for further accessibility of other target genes with PCR. The amplified PCR products were visualized and checked for their size on a 1.5 % Agarose gel. TBE buffer was used as running buffer. The gel was stained with Ethidium bromide (1.2 mM).

Table 2.1. Reaction composition

Component	Volume/reaction [µL]	Final concentration
10x PCR Buffer	2.5	1x
dNTP mix (10 mM each)	0.5	200 µM
Primer forward (10 µM)	1.25	0.5 µM
Primer reverse (10 µM)	1.25	0.5 µM
Taq DNA Polymerase (5 units/µL)	0.5	2.5 units
Destilled water	18.25	-
Template DNA	2	
Total volume	**26**	

Table 2.2. Thermal cycler conditions

Initial denaturation	3 min	94° C
3 step cycling Denaturation	30 sec	94° C
Annealing	30 sec	56° C
Extension	30 sec	72° C
Number of cycles	30	
Final extension	10 min	72° C

2.2.3.4 Quantitative real-time RT-PCR

For the quantification of the mRNA levels of the candidate and reference genes, the real-time reverse transcription polymerase chain reaction (RT-PCR, qPCR) was used in a LightCycler 480 System.

The real-time RT-PCR is an established technique and the method of choice for the quantification of mRNA (164). The technique uses intercalating dyes such as SYBR Green fluorescent dye that binds to any double-stranded DNA generated during the PCR and emits enhanced fluorescence. The increase in fluorescence is direct proportional to the amount of dsDNA. The intensity of the emitted fluorescence can be detected in real-time during each PCR cycle. Prior to the analysis of mRNA expression, the RNA has to be converted into cDNA by reverse transcription. This cDNA is then used as a template in the RT-PCR. The point at which the fluorescence of the sample rises above the background fluorescence is called the crossing point (C_p-value) (165). The C_p-value is dependent on the amount of cDNA that is present at the beginning of the PCR, but can be used to quantitatively analyze the mRNA expression (166-168). During PCR, the fluorescence in every reaction is plotted over the cycle number and can be monitored.

Most of the primers were already established in the lab. For the design of new gene-specific primer sets, the open source web-based tool Primer 3 was used (169). The source mRNA sequence of each gene was taken from the NCBI database Pubmed (www.ncbi.nlm.nih.gov). The length of each primer was between 18-22 nucleotides with a GC content of 40-60 %. The length of each PCR product was 100-150 bp. The primers were designed intron-spanning. This makes sure that primers will only anneal to cDNA synthesized from correctly spliced mRNAs, but not to genomic DNA. Thus amplification of contaminating DNA is eliminated (QuantiTect SYBR Green PCR Handbook, 2006). The sequences of all primers are listed in the appendix (Supplementary Table 1).

For quantitative real-time PCR the QuantiTect SYBR Green PCR Kit was used. The total reaction volume was 10 µL for the 96-well plate format and 7 µL for the 384-well plate format. The optimum PCR conditions were determined for every gene. The efficiency E of the amplification during the PCR was determined with the following formula (170):

$$E = 10^{-1/slope}$$

The slope of the standard curve describes the kinetics of the PCR amplification and is referred to as the efficiency of the amplification (Roche Applied Science, 2008). Theoretically, a perfect amplification would result in a standard curve with an efficiency of 2, meaning a doubling of the amount of target molecules after each PCR cycle, and can be described by following equation:

$$T_n = T_0 \, x \, 2^n$$

In PCR experiments the efficiency is influenced by many factors and can be more realistically described with:

$$T_n = T_0 \, x \, E^n$$

Here, T_n is the amount of target DNA at cycle n, T_0 is the initial amount of DNA, n is the number of amplification cycles, and E is the efficiency.

The LightCycler 480 Software calculates the efficiency from the slopes obtained from the fluorescence curves. By varying the annealing temperature of the primers, the concentration of input DNA and elongation times, the efficiency was optimized to a value close to 2 for each PCR reaction.

The 2x QuantiTect SYBR Green PCR Mix, template DNA, primers and RNAse free water were thawed and mixed. Then the master mix was prepared according to Table 2.3. In every experiment the samples were analyzed in triplicates and H_2O was used as a negative control. The PCR conditions are shown in Table 2.4.

Table 2.3. Reaction Composition. The components of 2x QuantiTect SYBR Green PCR Mix include HotStarTaq, DNA Polymerase, QuantiTect SYBR Green PCR Buffer, SYBR Green I, and ROX passive reference dye.

Component	Volume/reaction [µL]	Final concentration
2x QuantiTect SYBR Green PCR Mix	5 µL / 3.5 µL	1x
Primer forward (10 µM)	Variable	0.5 µM
Primer reverse (10 µM)	Variable	0.5 µM
Destilled water	Variable	-
Template DNA	2 µL / 1.7 µL	
Total volume	**10 µL / 7 µL**	

Table 2.4. Light Cycler 480 conditions. The annealing temperature was 56° C for *ACTB*, *TBP*, *GAPDH*, *HPRT*, *CDKN1A*, *TP53*, *APEX1*; 61° C for *XRCC1*

Initial denaturation	15 min	95° C
3 step cycling Denaturation	30 sec	94° C
Annealing	30 sec	56° C/61° C*
Extension	30 sec	72° C
Number of cycles	30-40	
Final extension	10 min	72° C

The evaluation of the obtained results (Crossing point values, C_p-values) was performed via relative quantification analysis with efficiency correction (Roche Applied Science, 2008). The analysis is based on the relative expression of a target gene in comparison to a reference gene in the same sample (171). The reference gene is normally a housekeeping gene that is [1] present in all cells, [2] found in constant copy numbers and [3] not affected by different treatments such as transfection of irradiation (172;173). However, no housekeeping gene always shows constant expression levels under all experimental conditions (174). Due to this, several housekeeping genes were tested for their suitability to serve as a reference. TBP was found to be most consistent and used as a housekeeping gene for evaluation.

The LightCycler 480 software uses an algorithm to calculate the efficiency-corrected concentration ratio of the target and the reference (Efficiency Method). This method is based on relative standard curves, which describe the efficiency of the PCR of the target and the reference gene. These relative standard curves were generated by setting up a standard from the cDNA of untreated cells, which was diluted in 5 steps (1:10 dilutions). The obtained standard curves were determined once and stored as external standard curves which were used for each analysis.

$$Ratio\ \frac{target}{reference}\ (Normalized\ ratio) = \frac{concentration\ ratio\ of\ the\ target}{concentration\ ratio\ of\ the\ reference}$$

The gene induction after treatment with IR was calculated by dividing the ratio of the irradiated sample by the ratio of the non-irradiated sample:

$$Induction\ factor = \frac{Normalized\ ratio\ 5\ Gy}{Normalized\ ration\ 0\ Gy}$$

A melting point analysis of the PCR products was performed directly after the relative quantification analysis. The melting temperature of a DNA product can vary depending on its length, its sequence and on the buffer conditions. Melting curve analysis was used to determine the melting temperature of every PCR product. The melting curves were generated by monitoring the fluorescence of the samples while the temperature is increased. At a certain temperature the fluorescence decreases rapidly which indicates the melting point. In case of optimal PCR conditions the same melting peak is expected in every sample of the analysis. Inefficient PCR or the amplification of side products would result in an altered melting point (Roche Applied Science, 2008).

2.2.4 Gene expression analysis on Illumina BeadArrays

Whole-genome expression analysis was carried out by using the Sentrix HumanRef-8 Expression BeadChips from Illumina. Illumina's BeadArray technology uses silica microspheres (beads) as the array elements. Each microsphere of a diameter of 3 µm, is derivatized with a particular oligonucleotide that acts as a probe for the complementary sequence in an assay solution (175). The oligonucleotides synthesized are > 72 bases, consisting of an address code and a 50 base gene-specific sequence (Figure 2.1).

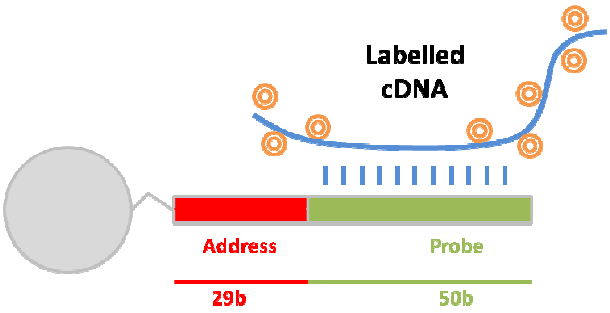

Figure 2.1. Bead design

Each bead carries > $1 \cdot 10^5$ identical > 72mer oligonucleotides. For a 24k gene expression array, 24.000 bead types are prepared, and equal aliquots of each type are pooled. The pool is spread across prefabricated microarrays with defined microwells that fit to the bead size.

The beads are immobilized within the cavities and the 25 base addresses are decoded, to allocate each bead to the respective gene sequence (176). The error rate in decoding is considered low (< $1 \cdot 10^{-4}$). Each bead type has an average 30 fold representation on the

chip – a strategy that provides the statistical accuracy of multiple measurements (Illumina Gene Expression Profiling Technical Bulletin, 2010).

Labeling procedure

1. The total RNA is isolated from the cells.
2. The RNA is turned into a double stranded DNA copy known as a cDNA.
3. The cDNA is allowed to go through in vitro transcription back to RNA. This is done by having uracil bases tagged with the Biotin.
4. The Biotin-labeled cRNA is then added to the array.
5. Anywhere on the array where a RNA fragment and an oligonucleotide on a bead are complimentary, the RNA sticks to the probe on the bead.
6. The array is then washed to remove any RNA that is not stuck to a bead and then stained with the fluorescent molecule that sticks to Biotin.
7. Lastly, the entire array is scanned with a laser and the information is kept in a computer for quantitative analysis of what genes were expressed and at what approximate level (www.dkfz.de/gpcf).

The expression analysis was conducted by the Genomics & Proteomics Core Facility of the DKFZ. Data analysis was performed with Bead Studio Software. For data analysis, the expression patterns of the silenced samples were compared to the control siRNA transfected samples. In case of irradiation, the gene expression changes of irradiated silenced cells were compared to mock irradiated silenced cells.

2.2.5 Protein analysis using Western blot

Cell culture medium was completely aspired and cells were washed with PBS. After trypsinization and determination of cell viability with trypan blue (177), the cells were centrifuged for 5 min at 13.000 x g and 4° C. The supernatant was discarded and the cell pellet was re-suspended in 100 µL of lysis buffer per $1 \cdot 10^6$ cells, vortexed and incubated on ice for 20-30 min (Table 2.5).

Table 2.5. Lysis buffer. Before use 1 mM $MgCl_2$ and 1 mM PMFS was added.

Component	Final concentration
Tris (pH 8.5)	20 mM
Urea	7 M
DTT	100 mM
Triton X-100	1 %

After incubation, the suspension was treated with Benzonase (25 units/100 µL lysis buffer) for 30 min at 37° C to remove all remaining DNA and RNA. Afterwards the mix was centrifuged for 5 min at 13.000 x *g* and 4° C and the supernatant, containing all nuclear and cytoplasmic proteins, was collected. Protein concentration was determined by Bio-Rad Protein Assay according to the manufacturer's protocol (178). Isolated proteins were stored at -80° C.

2.2.5.1 SDS polyacrylamide gel electrophoresis

For gel separation of the proteins, the NuPAGE® Electrophoresis System from Invitrogen was used. The Laemmli system is the most widely used SDS-PAGE method for separating a broad range of proteins according to their size (179). 20-30 µg of proteins were mixed with Sample Buffer (4x), Reducing Agent (10x) and deionized water to obtain a total volume of 30 µL. The samples were heated at 70° C for 10 minutes. Then, the proteins of each sample were separated on a 10 % NuPAGE® Novex Bis-Tris gel using SDS running buffer. PageRuler Prestained Protein Ladder was used to monitor protein migration during electrophoresis and protein transfer onto membranes during Western blotting. MagicMark™ XP Western Protein Standard was used for direct visualization of protein standard bands on the blot. Gels were run at a constant voltage of 200 V for 50-60 minutes.

2.2.5.2 Blotting and immunodetection

The separated proteins in the gel were transferred to the surface of polyvinylidenefluoride - membranes by electroblotting. For this the XCell II™ Blot Module (Invitrogen) was used. The transfer of the proteins was performed at a constant voltage of 30 V for 1 hour at RT according to the manufacturer's protocol.

After transferring the proteins to the PVDF-membrane, the membrane was saturated with 5 % non-fat dry milk in TBST (10 mM Tris pH 8.0, 150 mM NaCl, 0.1 % Tween-20) at room temperature or at 4° C overnight and then incubated with the polyclonal anti-Ref-1 or anti-XRCC1 antibody for 1 h at RT or at 4° C overnight (Table 2.6). After three washes with TBST for 10 minutes, the membranes were incubated for 60 minutes with an anti-rabbit or anti-mouse immunoglobulin coupled to horseradish peroxidase. After incubation the membranes were washed three times with TBST and the blots were developed using enhanced chemiluminescence procedure (Amersham Pharmacia Biotech, Milan, Italy). Normalizations were performed with a polyclonal anti-actin antibody. Exposed hyperfilms were digitalized and signals were quantified using Image J.

Table 2.6. Dilution of antibodies and incubation times

Antibody	Dilution	Incubation time
Anti-Ref-1	1:200	1 h
Anti-XRCC1	1:200	Over night
Anti-p53	1:500	1 h
Anti-β-Actin	1:10.000	1 h
sec. anti-rabbit antibody	1:5000 – 1:10.000	1 h
sec. anti-goat antibody	1:5000	1 h
sec. anti-mouse antibody	1:5000	1 h

In order to evaluate several proteins on the same membrane, the antibodies have to be removed before further protein detection. For this, the membrane was treated with stripping buffer (100 mM Tris pH 6.8, 10 % SDS, 0.08 % β-Mercaptoethanol) for 10-15 minutes at 50° C in a 50 mL bluecap followed by three washes with TBST for 10 minutes.

2.2.6 Single cell gel electrophoresis

The comet assay is a simple and sensitive method for studying DNA strand break induction and repair of DNA in eukaryotic cells (180;181). It has become a useful tool for testing of genotoxic agents, including radiation, chemicals and oxidative stress (182). It is frequently utilized in human biomonitoring (183). The method was firstly described by Singh and colleagues (184) and was performed with the modifications from Popanda *et al.* (185).

Different modifications of the assay have been developed. The most common version applies alkaline electrophoretic conditions in combination with an alkaline pre-treatment of DNA. This leads to the conversion of alkali-labile sites to strand breaks, and increases the spectrum of DNA lesions that can be detected (186).

The principle of the assay is based upon the ability of denatured DNA fragments to migrate out of the cell nucleus under the influence of an electric field. Damaged DNA migrates faster and produces a so-called comet tail whereas undamaged DNA migrates slower and remains within the confines of the nucleus. Evaluation of the DNA comet tail shape and migration pattern allows for assessment of DNA damage (187).

The γ-irradiation of the cells was performed exactly 72 h after transfection. The evening before irradiation, the cells were harvested by trypsinization and viability was determined with Trypan blue. Cell densitiy was adjusted to 50.000 cells per 5 mL medium and cell suspension was pipette onto 2-spot CometSlides, which were placed in Quadriperm cell culture vessels. For every siRNA treatment and for every repair timepoint, a slide was prepared. After attachment of the cells over night, each spot of the slides was covered with 50 µL of low melting agarose (0.7 % SeaPlaque agarose in phosphate-buffered saline (PBS), kept at 42° C) to immobilize the cells. The slides were placed on an ice-cold surface for 10 min to accelerate gelling of the agarose layer. Then, they were irradiated with 5 Gy using a ^{60}Co source (Irradiation device OB 58). One slide was not irradiated and kept separately for the determination of the baseline DNA damage. After treatment with IR, several slides were kept in cell culture medium at 37° C for 5, 10, 15, 20, 30, and 60 minutes to allow for DNA repair. The non-irradiated control slide and the slides with no time for DNA repair were kept on ice and processed directly after the irradiation treatment. All slides were then transferred to pre-cooled lysis solution (2.5 mM NaCl, 10 mM Tris-HCl at pH 10, 100 mM Na_2EDTA, 1 % sodium sarcosinate, 1 % Triton X-100, 10 % DMSO) and incubated over night at 4 ° C. After lysis, slides were washed three times with PBS and then placed into a horizontal electrophoresis chamber filled with alkaline electrophoresis buffer (1 mM Na_2EDTA, 300 mM NaOH, pH 13). After 20 min of DNA unwinding, electrophoresis was performed at 25 V and 300 mA for 20 min. After electrophoresis, the slides were washed three times with PBS, fixed by washing three times with absolute ethanol and subsequently air dried. To prevent additional DNA

damage, all steps after lysis of cells were carried out under red light. For evaluation, each area of the CometSlides was stained with 50 µL SYBR Green solution (10.000x concentrate in DMSO) diluted 1:10.000 in TE buffer (10 mM Tris-HCl, pH 7.5, 1 mM EDTA). SYBR Green is a fluorescent DNA intercalating dye. 51 comets per spot were evaluated by fluorescence microscopy and image analysis software (Version 4.0, Kinetic Imaging Ltd, Liverpool, UK). The extent of DNA damage was measured quantitatively by the tail moment, which is defined as the product of the percentage of DNA in the comet tail and the mean distance of migration in the tail (severity of damage). The median values are presented, because a normal distribution of tail moment values was not observed.

Several experimental parameters were evaluated to characterize cellular radiation effects: (1) baseline DNA damage in non-irradiated cells, (2) initial DNA damage after irradiation (no repair time), (3) DNA damage after 5, 10, 15, and 20 min of time to allow for DNA repair and (4) the DNA repair capacity after 5, 10, 15, and 20 min.

Quantitative and statistical data was generated by analysis of the results using Microsoft Excel.

2.2.7 Clonogenic assay of cells *in vitro*

The clonogenic assay, or colony-formation assay (CFA), was first described by Puck and Marcus and is based on the evaluation of the colony-forming ability of mammalian cells plated in culture dishes or plates (188). Colony-forming ability means the ability of a single cell to grow into a colony. The assay tests every cell for its ability to undergo replication after a specific treatment (189). The clonogenic assay is the method of choice to determine the cellular radiosensitivity after treatment with ionizing radiation (190).

Cells were transfected as described earlier. The evening before irradiation treatment, the cells were trypsinized. Then, the cells were counted with a hemocytometer, diluted into the desired seeding concentration, and seeded into 6-well plates. After attachment of the cells to the plate overnight, the cells were irradiated with increasing doses (1 Gy-5 Gy) 72 h after transfection. Three wells were used per radiation dose. After irradiation, the dishes were placed in an incubator (37° C, 5 % CO_2) and left there for a time equivalent to at least six cell divisions. Cells in the mock-irradiated control plates should form sufficiently large clones.

For fixation and staining, the medium was removed and cells were washed once with PBS. Then 1 mL of a mixture of 6.0 % glutaraldehyde and 0.5 % crystal violet was added to each well. After staining for at least 30 minutes, the staining solution was removed and each plate was rinsed with tap water. The plates were dried at room temperature (20° C).

The colonies were counted using a stereomicroscope. Colonies are considered to represent viable cells if they contain at least 50 cells. Firstly, the number of colonies in control cells, which were not exposed to IR, is determined to calculate the plating efficiency. The surviving fraction of cells after any treatment (IR or transfection with siRNA) is always calculated taking into account the PE of control cells (Formula 2.1).

$$\mathrm{PE} = \frac{\text{no. of colonies formed}}{\text{no. of cells seeded}} \text{ x } 100$$

$$\mathrm{SF} = \frac{\text{no. of colonies formed after treatment}}{\text{no. of cells seeded x PE}}$$

Formula 2.1. Calculations of the plating efficiency (PE) and the surviving fraction (SF).

2.2.8 Sulforhodamine B assay

The sulforhodamine B (SRB) assay measures the cell density which corresponds to the proliferation capability of the cell. The assay is based on the measurement of cellular protein content. The SRB dye binds to protein components of cells that have been fixed to tissue culture plates by tichloroacetic acid. The aminoxanthene dye harbours two sulfonic groups that bind to basic amino-acid residues under acidic conditions, and dissociates under basic conditions. The amount of dye extracted from stained cells is directly proportional to the cell mass. The assay can be used for in vitro drug toxicity screenings and it has been shown to be effective for testing of cancer cell sensitivity to radiation (191;192).

Cells were transfected as described above. The assay started 72 h after transfection. Shortly before that, the cells were harvested by trypsinization, counted and plated in 96-well plates. Optimal seeding densities for each cell line were determined to ensure exponential growth during the assay. MCF7 were seeded at a density of 500 cells per well

and HMEpC at 1000 cells per well. The SRB assay was performed according to the method of Skehan *et al.* with minor modifications (193). The culture medium was aspired prior to fixation. The cells were fixed with 100 µL cold 10 % trichloroacetic acid for 1 h at 4° C followed by five washing steps with deionized water. The cells were then stained for 20 minutes with 100 µL 0.4 % (wt/vol) SRB in 1 % acetic acid and subsequently washed five times with 1 % acetic acid. The plates were left at room temperature to air dry and the protein bound dye was solubilized with 200 µL 10 mM Trisma-Base (tris(hydroxymethyl)aminomethane). The optical density (OD) was measured at 490 and 515 nm using the Spectramax M5^{e} microplate reader. The percentage of cell-growth inhibition was calculated with following formula:

2.2.8.1 Radiation treatment

The radiosensitizing effect was evaluated with the SRB assay. The evening before irradiation, the transfected cells were harvested by trypsinization, counted and plated in 6-well or 96-well plates. After attachment of the cells overnight, the plates were irradiated over the range from 0-5 Gy using a ^{60}Co source exactly 72 h after transfection. Cells were then incubated for at least six cell divisions before determination of the survival by the SRB assay.

2.2.8.2 Temozolomide treatment

The sensitizing effect of temozolomide (TMZ) on cell growth was investigated with the SRB assay. Cells were plated in 96-well plates as described above. 72 h after transfection with the respective siRNA, 8 wells of each sample were treated with different concentrations of temozolomide dissolved in 4 % (vol/vol) DMSO in PBS ranging from 50 to 1.600 µM or with a fixed concentration of 775 µM. Solvent only was used as control. The final concentration of the DMSO was 0.32 % (vol/vol). Assay plates were then incubated at 37° C in a humidified incubator with 5 % CO_2 for 3 days or up to 16 days followed by fixation and staining procedure.

For IC_{50} determination, dose-response curves between the compound concentration and percent growth inhibition was plotted. IC_{50} values were derived from logistic dose response curves using curve-fit transition function (Table Curve).

2.2.9 Measurement of γH2AX

The histone protein H2AX is involved in DNA repair and a central component of signaling pathways in response to DNA double strand breaks. It becomes rapidly phosphorylated on a serine residue when located close to a DSB, for example after exposure to ionizing radiation or ROS (194-196). Within 30 minutes after DSB formation, γH2AX molecules form a focus where DNA repair and chromatin remodeling proteins accumulate (197). These foci can be detected using antibody staining and fluorescence microscopy. Once the break is rejoined and the DSB is repaired, γH2AX foci disappear, either by dephosphorylation of γH2AX or by γH2AX removal from the chromatin (198-202). Immunohistochemistry was used to quantify γH2AX protein followed by further validation with flow cytrometry.

2.2.9.1 Immunofluorescence microscopy

Cells which were grown to 70-90 % confluency were harvested by using trypsinisation and counted with a hemocytometer. They were diluted into to a seeding concentration of 50.000 cells/5 mL and seeded on Assistent Diagnostika 3-spot slides lying in a Quadriperm cell culture vessel. The cells were incubated overnight (37° C, 5 % CO_2). After attachment of the cells to the slides, the cells were transfected with either target siRNA or control siRNA and incubated for 72 h. After 72 h, some slides were mock irradiated or irradiated with a single dose of 5 Gy followed by an incubation step for either 30 minutes or 2 hours with subsequent fixation. For fixation, the slides were incubated in 4 % paraform aldehyde/PBS for 10 minutes. The slides were washed 3 times for 5 minutes with 0.15 % Triton X-100/PBS and 10 minutes with 1 % BSA/0.15 % glycine/PBS. The cells were then incubated with 50 µL/spot of Anti-phospho-Histone H2AX (Ser139) mouse monoclonal IgG1 Antibody (clone JBW301) in a dilution of 1:300 at 4° C overnight. On the next day, the slides were washed once 5 minutes with PBS, 10 minutes with 0.15 % Triton X-100/PBS, 5 minutes with PBS and then 7 minutes with 1 % BSA/0.15 % glycine/PBS. 50 µL of the secondary Antibody (Cy3 Goat Anti-Mouse IgG) (1:300) was applied to each spot of the slide and incubated at RT for 45 minutes in the dark. Next the slides were washed again twice with 0.15 % Triton X-100/PBS for 5 minutes and PBS for 10 minutes, following a nucleus staining step with Hoechst blue (Benzimide-tris-hydrochlorid) for 2 minutes.

2.2.9.2 Measurement of γH2AX and cell cycle analysis after irradiation by flow cytometry

The advantage of the flow cytometry consists of a quick sample processing, quantitative analysis of single cells and multi-parameter analysis. The fixed cells are carried in a sheath stream through a laser beam where fluorescent dyes are excited.

The staining of surface markers or intracellular molecules with fluorescent dyes allows the detection of several transcription factors or phosphoproteins to characterize the sample (203). The emitted fluorescence is amplified and collected using photomultiplier tubes. Besides the fluorescence, light scatter signals are collected. The forward scatter (FCS) characterizes the size of the cell and the side scatter (SSC) the granularity (204;205). By staining of the DNA with propidium iodide, a red-fluorescent nuclear and chromosome counterstain, the DNA content and further the phase of the cell cycle can be determined.

Cells were harvested using trypsinisation and counted with a hemocytometer. They were diluted into the desired seeding concentration (150.000 cells per well) and seed into 6-well plates. After attachment of the cells to the plate overnight, the cells were transfected with target siRNA or control siRNA and incubated for 72 h. After 72 h, the cells were mock irradiated or irradiated with a single dose of 5 Gy followed by immediate fixation or an incubation step for either 30 minutes or 2 hours with subsequent fixation. For fixation, cells were washed with 1 mL of PBS, trypsinized and immediately resuspended in 2 mL ice-cold 5 % AcCOOH/PBS. Fixed cells were incubated for 10 minutes on ice following centrifugation at 140 x g for 5 minutes at 6° C. The cell pellet was resuspended in 3 mL of ice-cold 70 % Ethanol and incubated for 1 hour at 4° C. After centrifugation, the cells were washed 3 times with 3 mL 0.5 % BSA/PBS and then resuspended in RNAse solution (200 µg/mL 0.5 % BSA/PBS). The cells were incubated for 1 hour at 37° C following another centrifugation step. Cells were then resuspended in 100 µL of antibody solution (125 ng Alexa488 mouse Anti-H2AX-phosphorylated (Ser139) AK in 100 µL 0.5 % BSA/PBS) for 1 hour at RT. After antibody binding, cells were mixed with 1 mL PBS and filtered through a with a cell strainer lid. For DNA staining 5 µL propidium iodide solution (1 mg/mL) was added and incubated for 5 minutes.

Cells were analyzed on a Becton-Dickinson Calibur using an Argon laser (excitation 488 nm). For each sample, 25.000 single events were detected and data analysis was performed using FlowJo software.

2.3 Statistical methods

2.3.1 Mean, standard deviation, standard error of the mean, median

As not otherwise specified, the mean is expressed as the arithmetic mean.

The standard deviation (SD) represents the variability from the mean. A low standard deviation indicates that the data points tend to be close to the mean, whereas a high standard deviation indicates that the data are spread out over a large range of values. The standard deviation is expressed in the same units as the data.

The standard error of the mean (SEM) is the standard deviation of the sample means over all possible samples of a given size drawn from the population.

The median is described as the numeric value separating the higher half of a population or distribution, from the lower half. The median of a list of numbers can be found by arranging all the observations from the lowest value to the highest value and picking the middle one. If there is an even number of observations, the median is defined as the mean of the two middle values.

2.3.2 t-statistics

The t-distribution is a continuous probability distribution that arises when estimating the mean of a normally distributed population. The unpaired t-test with Welch's correction was performed. Welch's correction does not assume equal variances. p-values were displayed two-tailed.

2.3.3 Evaluation of Microarrays

To correct for differences in expression level across a chip and between chips, quantile normalization was applied to log2 transformed data. Gene-wise testing was applied using paired t-statistics in order to calculate the induction of differential gene expression in response to the knockdown or irradiation in the different cell groups (knockdown cells/unirradiated, controls/unirradiated, knockdown cells/irradiated, controls/irradiated). Genes were selected as differentially regulated when the adjusted p value was < 0.05 and the estimated fold change was either ≥ 2 or ≤ -2. Selected genes were used to identify the functional pathways or biological functions that were most significant to the dataset by Ingenuity Pathway Analysis (IPA). The p value for the

probability of the association between the genes in the dataset and the pathway due to chance was calculated by Fisher's exact test.

In case of DNA repair genes, a gene was selected as differentially expressed when the adjusted p value was < 0.05 and the estimated fold change was either ≥ 1.2 or ≤ -1.2.

3 Results

3.1 Silencing of the DNA repair genes *APEX1* and *XRCC1*

In order to investigate the consequences caused by mimicking a deficiency in BER genes, the *APEX1* and the *XRCC1* gene were silenced in MCF7 cells and HMEpC using RNAi. The best point of time for functional analyses was selected to be 72 h after transfection, when the mRNA and protein levels of *APEX1* and *XRCC1* are strongly decreased. Then, we expect to reveal the most comprehensive functional consequences of the knockdown regarding growth capability, clonogenic survival, induction of SSBs, formation of DNA-DSB, and DNA repair rates in MCF7 and HMEpC cells (Figure 3.1).

Moreover, to the functional consequences of the silencing, changes in the gene expression patterns after knockdown were determined 24 and 48 h after transfection and after subsequent irradiation.

Figure 3.1 presents a detailed time schedule for the different experiments, and the points of time when the experiments were performed.

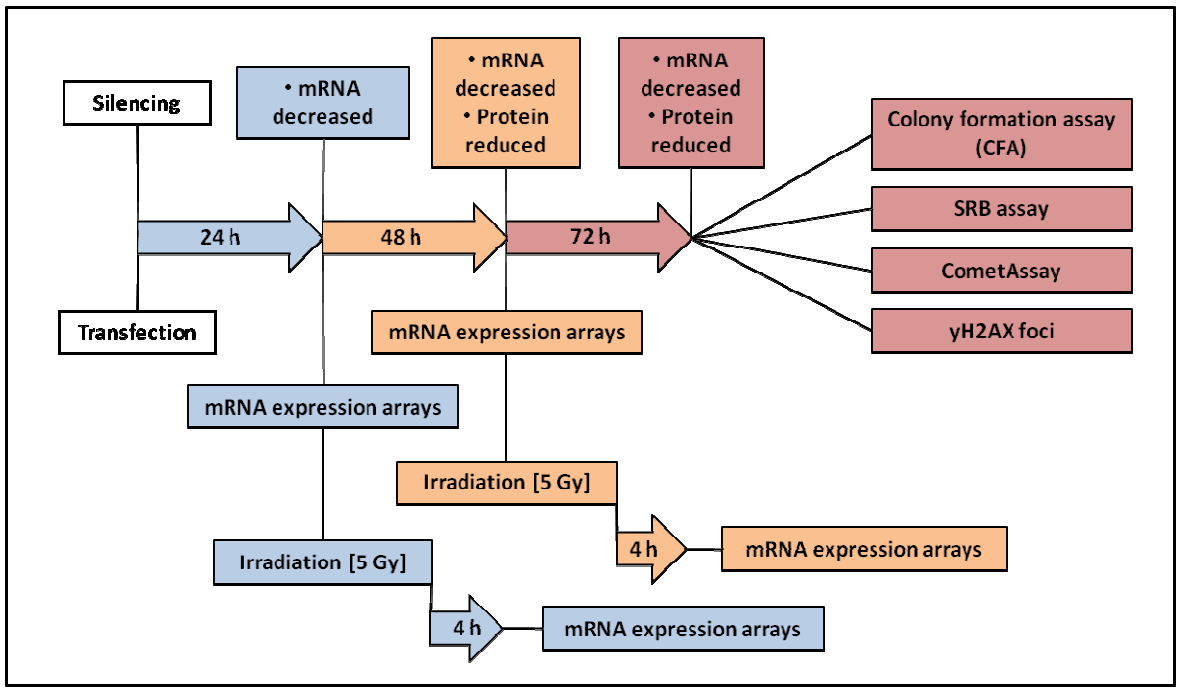

Figure 3.1. Overview of the experimental setup and schedule for MCF7 and HMEpC.

3.1.1 Optimized transfection conditions lead to effective knockdown of *APEX1* mRNA transcripts in MCF7 and HMEpC cells

The *APEX1* and *XRCC1* genes were silenced in MCF7 and HMEpC cells using ON-TARGETplus set of 4 siRNA. Luciferase or non-targeting siRNA were used as a negative control. The Luciferase siRNA has no target mRNA in human cells. The non-targeting siRNA is a random sequence of nucleotides and has also no target mRNA in human cells. The negative controls were applied to detect any unspecific effects. Transfection reagent treated cells and completely untreated cells (NTC) were included as experimental controls. Further, every single siRNA duplex was tested with the *in silico* method "Specificity Server", which can be used to look for potential off-target effects caused by the siRNA down-regulating another gene in a sequence-specific manner. The software found some genes which showed sequence homology, but the scoring which ranks the potential matches according to likelihood was never higher than 73 (out of 100). Most of the siRNA duplexes showed no relevant findings. A score of 73 was found, for instance for the *RIB3IP* gene, and indicated at least three mismatches by comparing the sequence of the second duplex of the *APEX1* siRNA to the *RIB3IP* mRNA.

For MCF7, transfection with 100 nM was recommended together with the appropriate conditions supplied by the manufacturer. As the set of 4 was used, the concentration of each individual duplex was 25 nM. These transfection conditions were confirmed in an experimental setting.

The transfection medium influenced the attachment of the cells to the plate. The cells rounded up and became detached. The transfection is a stress factor and can cause rounding and detachment of cells, even though the cells show a good growth rate in general. Thus, collagen coated cell culture plates were used. These plates have a positive charge on their surface and provide an improved cell adhesion.

The knockdown was 74 % relative to untreated cells as measured by reduction of *APEX1* mRNA transcripts with qRT-PCR (Figure 3.2). Transfection reagent alone showed no toxicity. The viability of the cells was ≥ 85 % in the siRNA transfected sample and in the transfected controls (data not shown). The ratio of DharmaFECT 1 transfection reagent [µL] to siRNA [µg] was 2:1. The effective knockdown of *APEX1* with the given protocol was confirmed and showed that the recommended ratio is optimal for the adherent MCF7 cells.

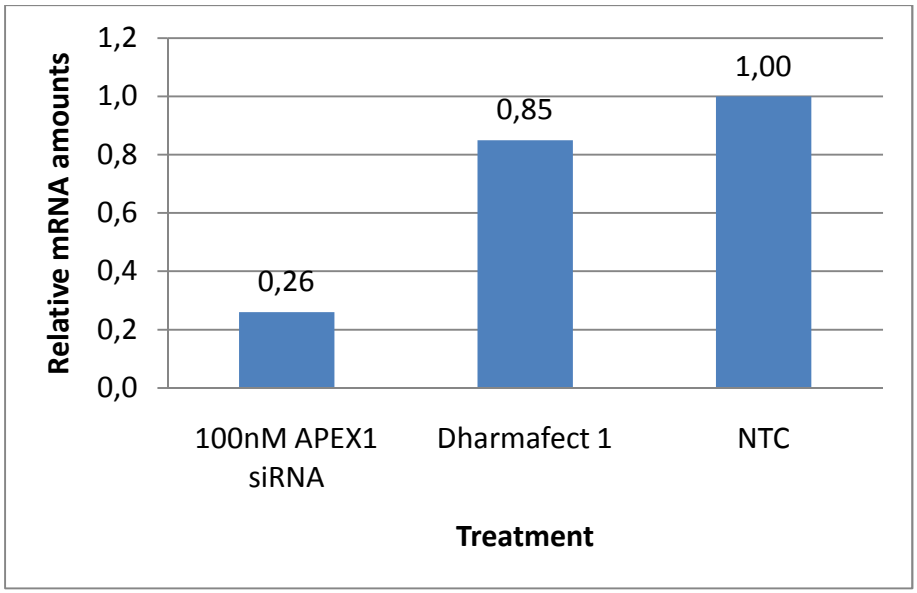

Figure 3.2. Verification of transfection conditions in MCF7. Relative quantification of *APEX1* mRNA levels 24 h after transfection. TBP was used as a reference. Results are shown relative to *APEX1* mRNA expression in untreated cells (NTC).

For HMEpC, the transfection conditions had to be established. Thus, the primary cells were plated at three different plating densities, $2{\cdot}10^4$, $4{\cdot}10^4$ and $6{\cdot}10^4$ cells per well, on a 24-well plate. The concentration of the target siRNA was kept constant at 100 nM. Four different volumes of Dharmafect 1 were used, each representing a different ratio of the volume of transfection reagent to the mass of siRNA. The transfection efficiency was estimated by using Fluorescein-labeled siRNA.

The two higher plating densities provided enough RNA to determine *APEX1* mRNA transcripts. A knockdown of *APEX1* mRNA transcripts by ≥ 90 % was achieved with a transfection reagent to siRNA ratio of 2.24:1 and with a starting plating density of $4{\cdot}10^4$ cells per well (Figure 3.3.B). The viability of the silenced cells and controls was ≥ 85 % (data not shown). In order to use the lowest amount of transfection reagent with the highest transfection efficiency, a ratio of 2:1 was considered to be optimal.

The transfection efficiency was greater than 90 % as measured by fluorescence after transfection of the cells with Fluorescein-siRNA (Figure 3.3.A).

These results demonstrate that a plating density of $4{\cdot}10^4$cells per well, a siRNA concentration of 100 nM, and a ratio of the transfection reagent [µL] to siRNA [µg] of 2:1 represent the optimal transfection conditions. For all further experiments, these optimized transfection conditions were applied.

A.

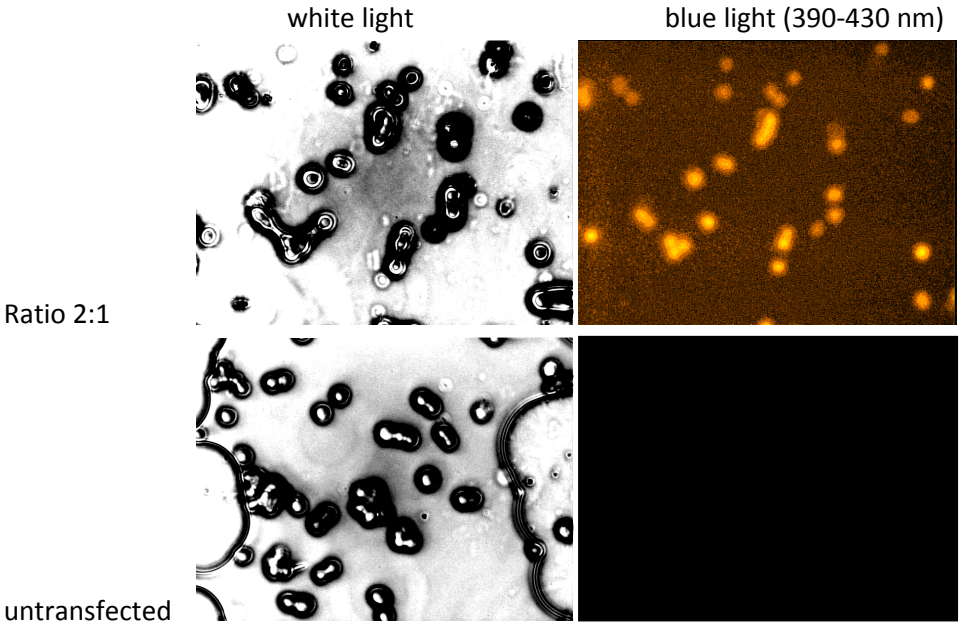

B.

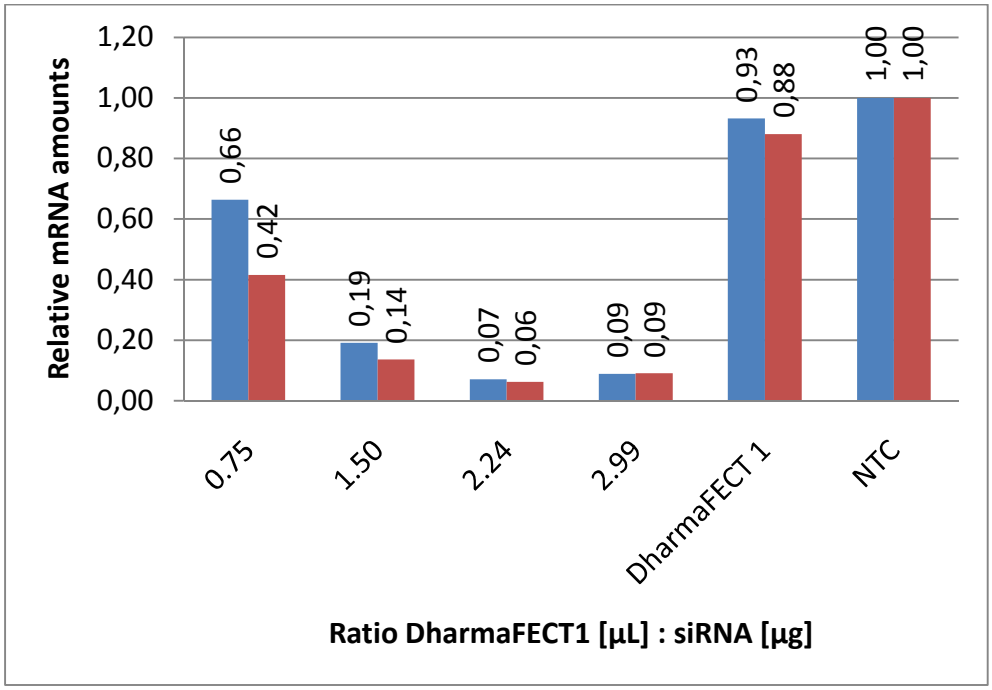

Figure 3.3. Optimization of the transfection conditions for HMEpC. A. Cells observed under fluorescence microscope in blue (wavelength 390-490 nm) and white light six hours after transfection with 15 nM Fluorescein-siRNA (Ratio DharmaFECT 1 to siRNA 2:1). **B.** Relative quantification of *APEX1* mRNA levels 24 h after transfection. TBP was used as a reference. Results are relative to *APEX1* expression in untreated cells (NTC). Blue bars represent a cell density of $4 \cdot 10^4$ per well and red bars $6 \cdot 10^4$ cells per well.

3.1.2 Verification of RNA quality

In order to qualify the isolated RNA from the samples, the Agilent 2100 Bioanalyzer with the Agilent RNA 6000 Nano Kit was used. In Figure 3.4, the 18S and 28S bands of the ribosomal RNA of different samples are shown on the gel and in the electropherogram. These bands are used by the software to make a statement about the quality of the RNA. If both appear as a sharp peak, the quality of the total input RNA is good (Figure 3.4. sample 1-12). All RNA samples showing degradation or appearing with a RIN of ≤ 8.5, which indicates insufficient quality, were excluded from the analyses.

A. **B.**

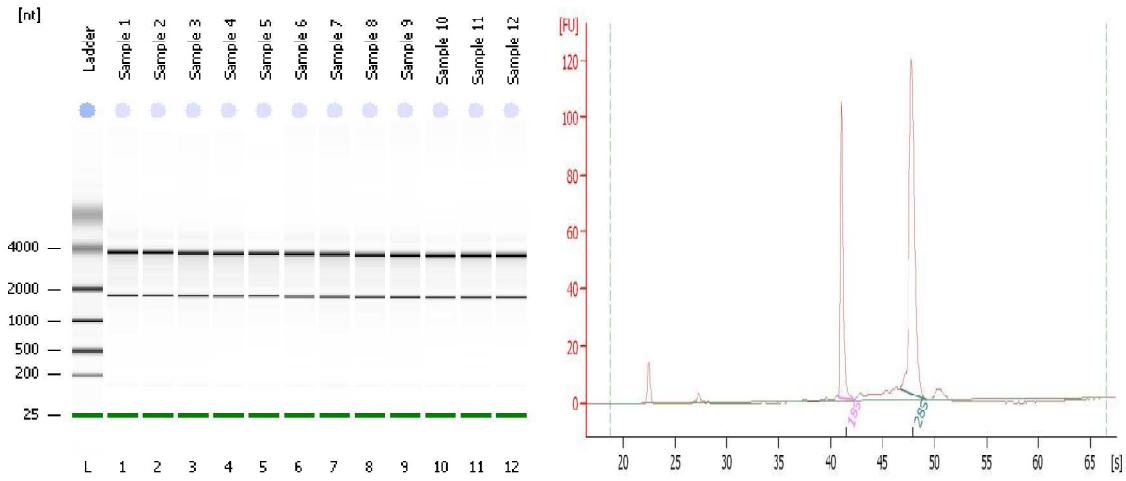

Figure 3.4. RNA quantification and qualification with the Agilent 2100 Bioanalyzer. A. Gel **B.** Electropherogram (of Sample 1).

3.1.3 Verification of cDNA integrity after first-strand synthesis

The quality and accessibility of the synthesized cDNA after reverse transcription (RT) was measured by amplification of the 5'- and the 3'-end of the human Clathrin (CLTR) gene. If both products appear with the same intensity on the gel, the quality of the RT is satisfactory (Figure 3.5). If one PCR-product was missing, the reverse transcription of the input RNA was incomplete. In this casem the RT was repeated for the respective sample.

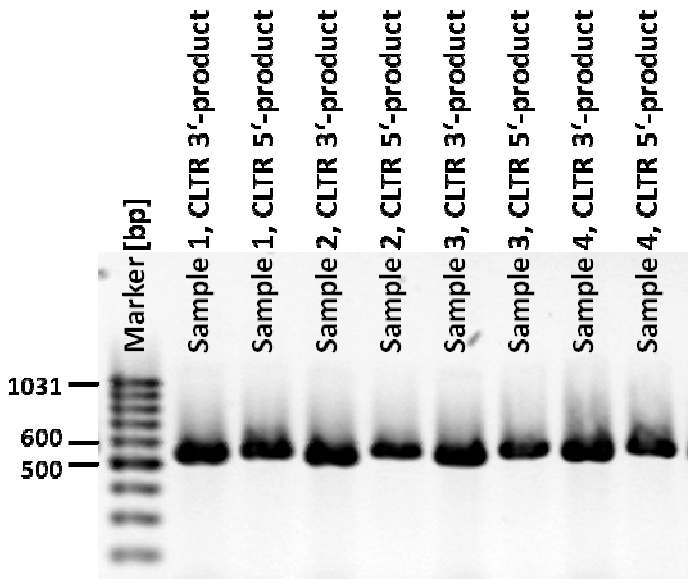

Figure 3.5. Visualization of the CLTR 3'-product (550 bp) and the CLTR 5'-product (570 bp) for selected samples after RT on a 1.5 % agarose gel and after staining with ethidium bromide.

3.2 Investigations in MCF7 cells

3.2.1 Effective knockdown of *APEX1* 72 h after treatment with siRNA

The *APEX1* gene was silenced in exponentially growing MCF7 cells using the transfection conditions described. Luciferase siRNA was used as a negative control. To analyze the knockdown, the expression of the *APEX1* gene was checked both on mRNA and on protein level 24, 48, and 72 h after transfection. The experiment was performed with three replicates for each treatment.

As shown in Figure 3.6, the expression of *APEX1* was reduced by 88 % 24 h after transfection with 100nM *APEX1* siRNA and by 91 % after 48 h. The reduction of the gene expression remained for at least 72 h. On the protein level, a decrease up to 63 % was observed 24 h after transfection and up to 30 % after 48 h. However, the strongest down-regulation of the protein was determined 72 h after treatment (Figure 3.6.B).

These results demonstrate that the treatment of MCF7 with 100 nM *APEX1* siRNA effectively silenced the *APEX1* gene and its protein at least for up to 72 h. On the protein level, we detected the strongest effect after 72 h.

A.

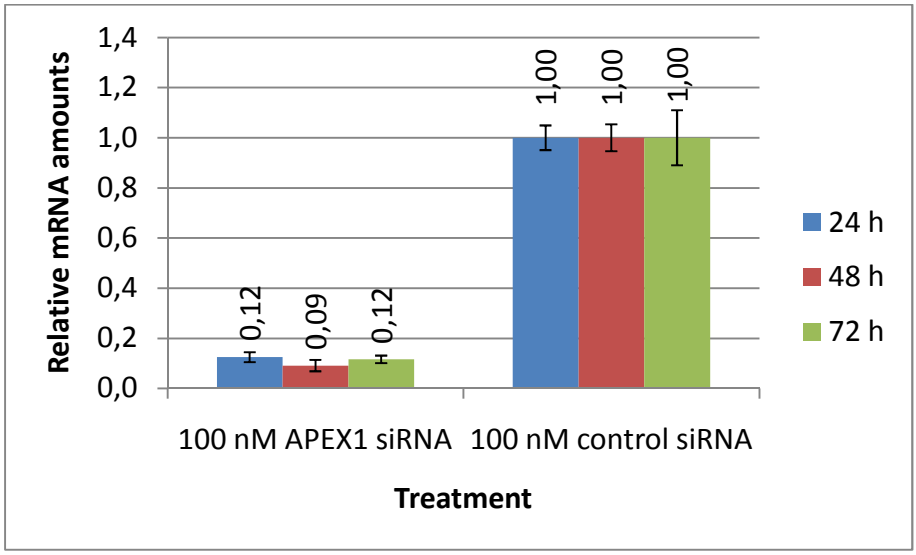

B.

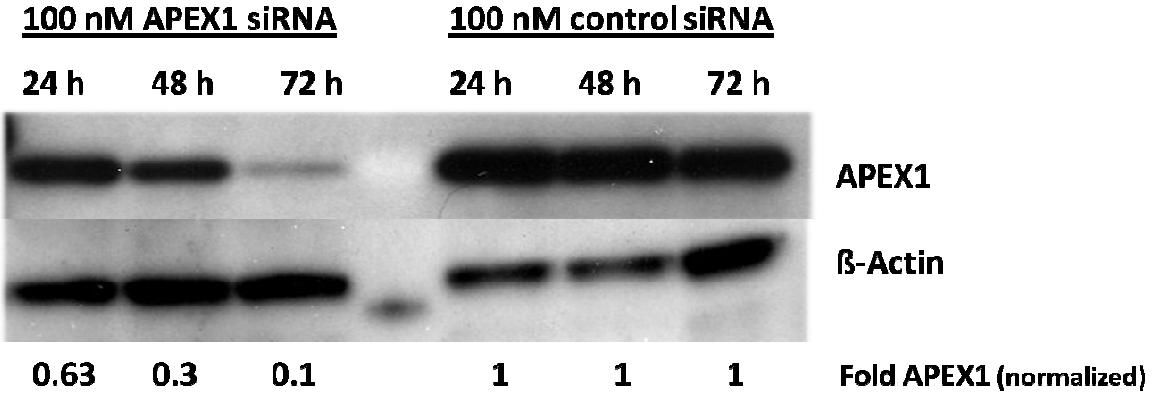

Figure 3.6. *APEX1* knockdown in MCF7 cells 24, 48, and 72 h after transfection with siRNA. A. Relative quantification of *APEX1* expression at mRNA level by real time PCR on LightCycler 480 after reverse transcription. TBP was used as a reference. Results are shown relative to control. Means and standard errors are given for three independent treatments. **B.** Representative western blots which demonstrate the APEX1 protein levels in silenced and control samples. Quantitative analysis of the protein reduction in silenced cells [fold change to controls].

3.2.2 *XRCC1* expression in MCF7 is down-regulated after transfection with 100 nM *XRCC1* siRNA

In a second series of experiments, the *XRCC1* gene was silenced in MCF7 cells. Luciferase siRNA was used as a negative control. To confirm the knockdown of *XRCC1*, the expression of the gene was verified both at mRNA and protein level 24, 48, and 72 h after transfection.

The expression of *XRCC1* was decreased by 83 % 24 h after transfection. This effect was persistent for at least 72 h (Figure 3.7.A). The protein was effectively reduced to 31 % 72 h after transfection (Figure 3.7.B).

A.

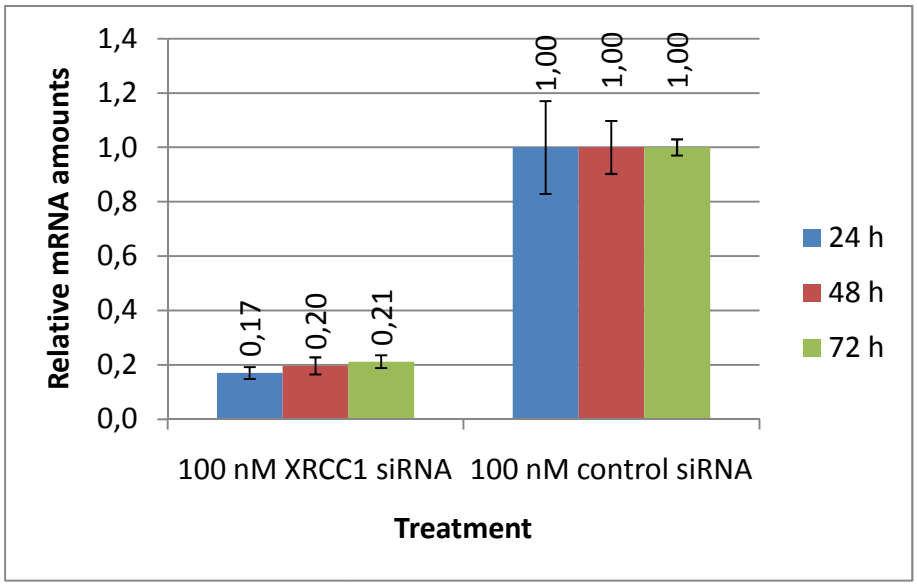

B.

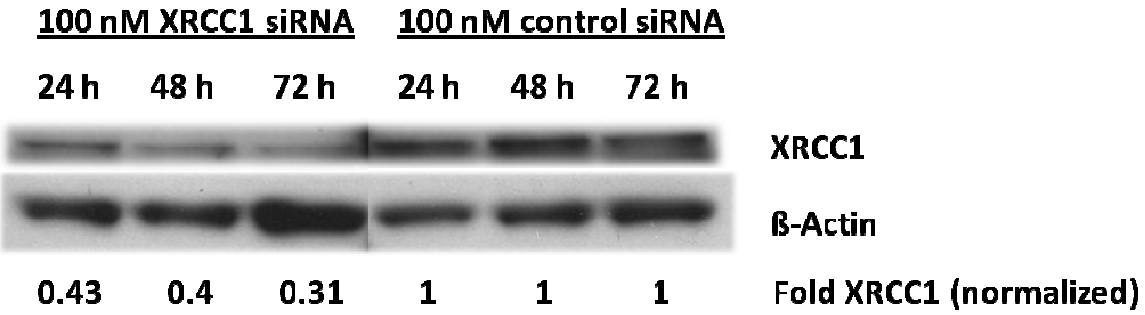

Figure 3.7. *XRCC1* expression in MCF7 cells after transfection with 100 nM *XRCC1* siRNA. A. Relative quantification of *XRCC1* mRNA expression by real time PCR on LightCycler 480 after reverse transcription. TBP was used as a reference. Results are shown relative to controls. Means and standard errors are given for three independent treatments. **B.** Western blot analysis of XRCC1 protein levels in lysates of MCF7 cells transfected with 100 nM *XRCC1* siRNA for 72 h. Quantitative analysis of the protein reduction [fold change to controls].

3.2.3 Decreased mRNA and protein levels after simultaneous silencing of both *APEX1* and *XRCC1*

In a third experiment, both the *APEX1* and the *XRCC1* gene were simultaneously silenced in exponentially growing MCF7 cells. In order to keep the total siRNA concentration and the amount of transfection reagent constant, 50 nM of each set of 4 target siRNA was used to obtain a final concentration of 100 nM. This was essential to avoid toxicity due to an increased amount of applied transfection reagent. Non-targeting siRNA was used as a negative control. To compare the down-regulation of both genes, the expression of the

mRNA and the protein level were analyzed 24, 48, and 72 h after transfection. The experiment was performed with three replicates for each treatment.

Both genes were strongly reduced in their mRNA expression (Figure 3.8.A). The decrease in mRNA levels was detectable at least 72 h. The APEX1 protein was reduced to 23 % and the XRCC1 protein to 12 % compared to controls after 72 h (Figure 3.8.B).

A.

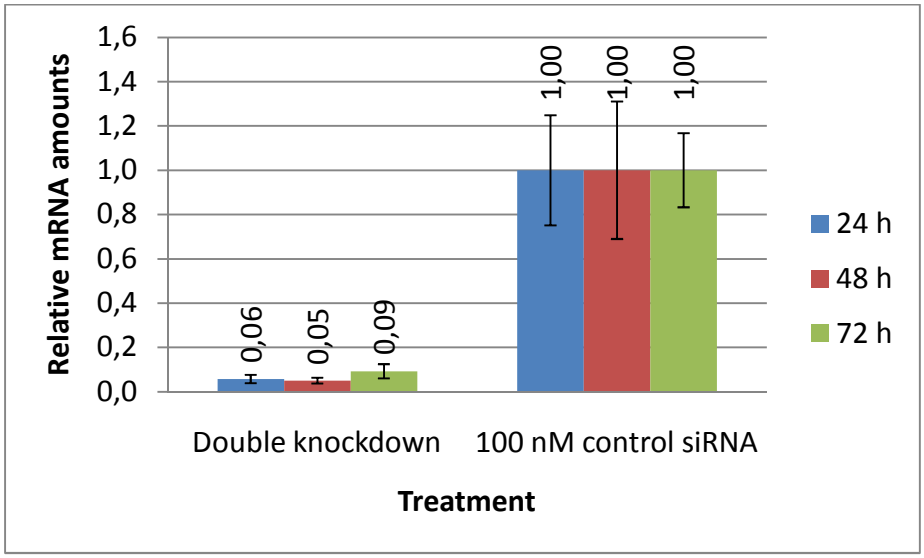

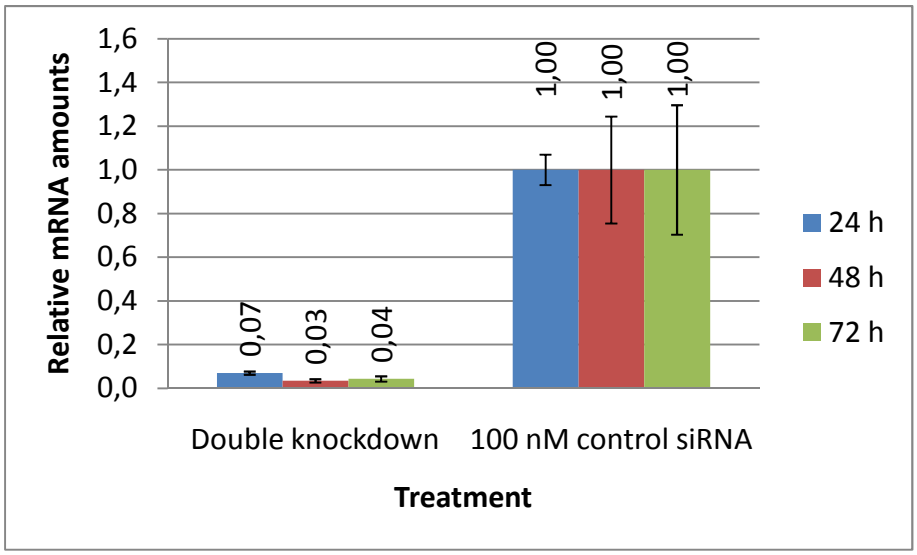

B.

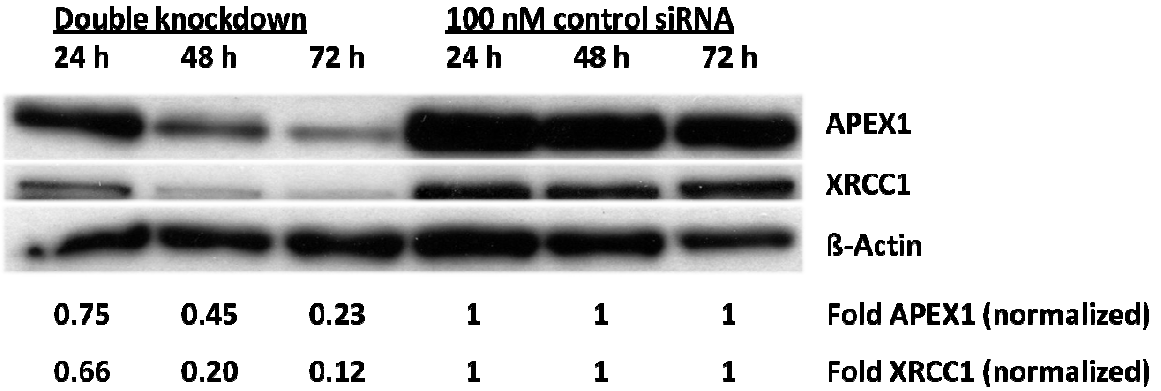

Figure 3.8. Double knockdown of *APEX1* and *XRCC1* in MCF7 cells 24, 48, and 72 h after transfection with siRNA. A. Quantitative real-time RT-PCR analysis of *APEX1* and *XRCC1* mRNA for the indicated length of time. TBP was used as a reference. Results are shown relative to control. Means and standard errors are given for three independent treatments. **B.** APEX1 and XRCC1 protein levels in silenced cells and controls analyzed by western blot. Quantitative analysis of the protein in silenced cells [fold change to controls].

Taken together, these results demonstrate that both the simultaneous and separate transient transfection with *APEX1* and *XRCC1* siRNA leads to a strong decrease of mRNA levels and protein amounts. On mRNA level, a strong reduction was already detected after 24 h and this reduction lasted for at least 72 h. On the protein level, the lowest amount of the proteins was always detected 72 h after transfection. Therefore, the functional assays were performed after 72 h, mRNA expression analysis after 24 and 48 h.

3.2.4 Growth characteristics after knockdown of APEX1, XRCC1, and DKO

To investigate the effect of the silencing of *APEX1*, *XRCC1*, and both genes on cell growth, the ability of siRNA transfected cells to form a colony was explored with the colony-formation assay (CFA). To further verify the results of the CFA assay, the Sulforhodamine B (SRB) assay was used to determine the growth kinetics of silenced cells for up to ten days after transfection. Non-targeting siRNA was used as negative control. The relative mRNA levels of the silenced genes were monitored to confirm the knockdown.

Figure 3.9.B shows that the transfection with siRNA decreased the mRNA expression of the respective genes by more than 90 %.

The plating efficiency which represents the capability of the cell to replicate was significantly decreased to 8.5 % ± 1.1 % in *XRCC1*-silenced cells compared to

controls (Figure 3.9.A). The successive down-regulation of both genes eliminated the effect observed after the *XRCC1* knockdown alone. The plating efficiency for the DKO cells was 16.57 % ± 5.19 % and for the controls 16.51 % ± 2.32 %. *APEX1*-silenced cells showed no difference in their plating efficiency compared to controls (26.46 % ± 12.03 %).

In the SRB assay, silencing of cells with *APEX1* and *XRCC1* siRNA showed a significant inhibition of cell growth compared to controls 10 days after transfection (Figure 3.9.C). Growth inhibition was greatest in *XRCC1*-silenced cells. Again, the silencing of both genes abolished the reduced growth effect determined after knockdown of the single genes.

The results demonstrate that silencing the *XRCC1* gene strongly affects the growth capability of MCF7 cells, whereas the DKO cells behave like the controls.

A.

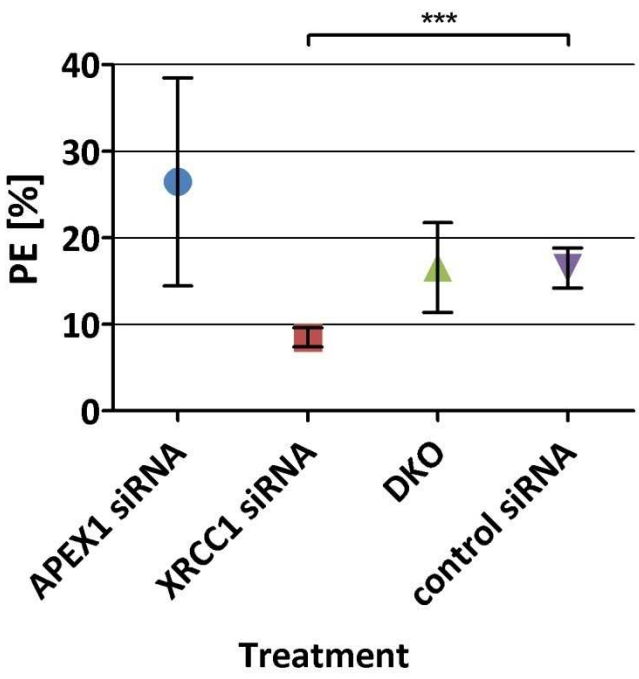

B.

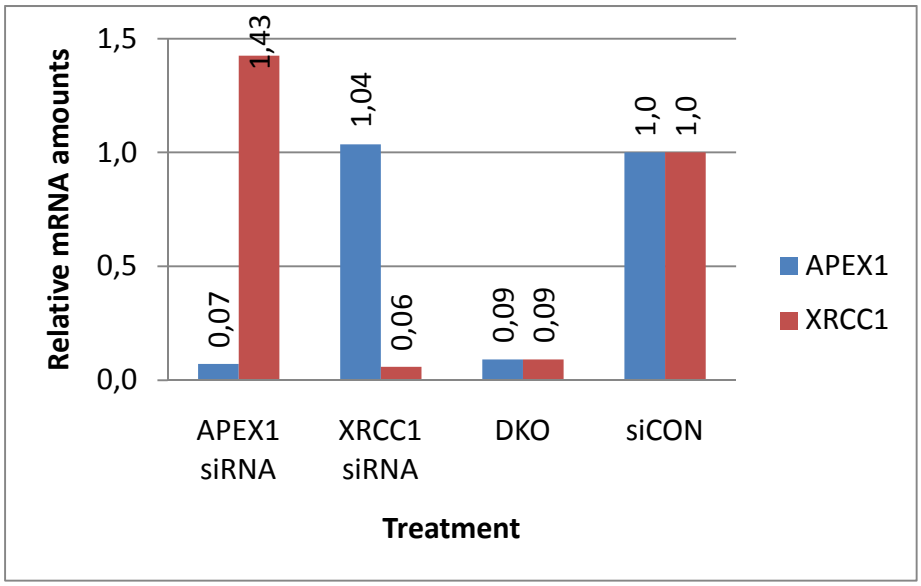

C.

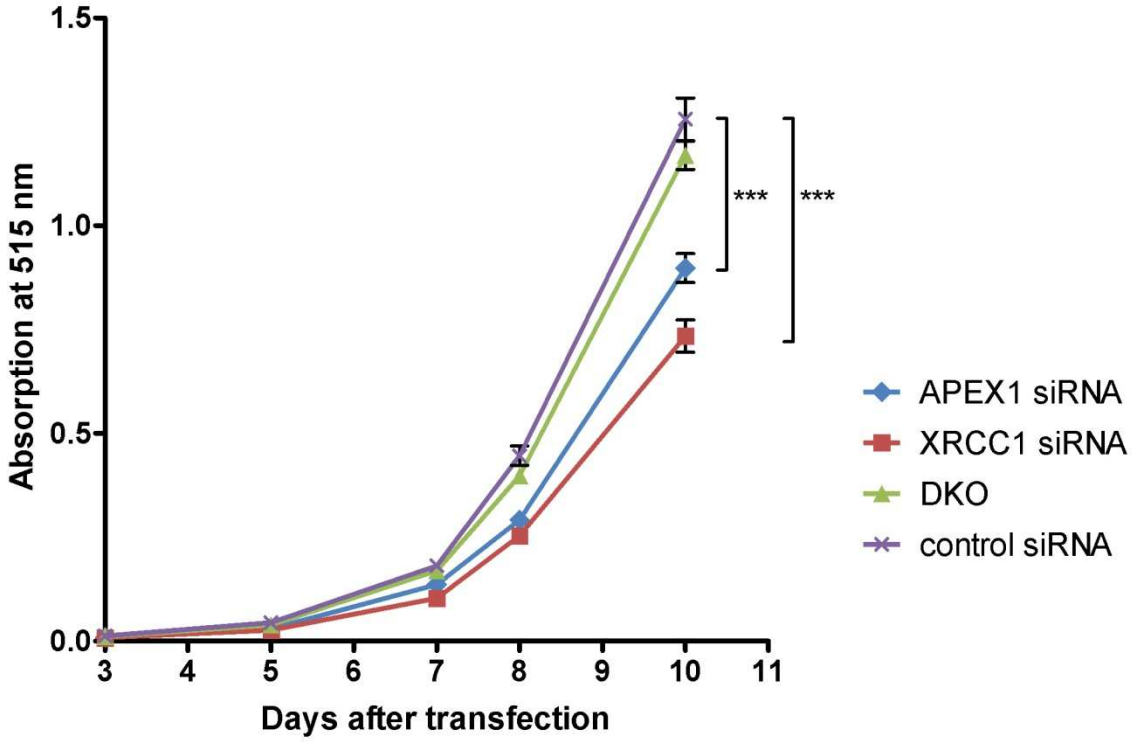

Figure 3.9. Growth capability after transfection with *APEX1* and *XRCC1* siRNA. A. Plating efficiency of MCF7 cells determined with the clonogenic assay. Assay was performed in six well plates after transfection with the respective siRNA. Means and standard errors are from three replicates. Results are shown for three independent experiments. **B.** Relative quantification of *APEX1* and *XRCC1* mRNA expression by real time PCR 24 h after transfection. **C.** Growth curves were obtained with the SRB assay. The results are expressed as mean ± SEM from two experiments with 20 replicates. Statistical analysis was done using t-test. ***$p < 0.001$.

3.2.5 Analysis of gene expression profiles

To identify genes which show expression changes as a consequence of the silencing of *APEX1* or *XRCC1* or both, the gene expression patterns of silenced cells and controls were compared 24 h and 48 h after transfection by using the Sentrix HumanRef-8 Expression BeadChips from Illumina. Before the silenced samples were analyzed for their gene expression pattern changes, the successful knockdown of target genes was verified by qRT-PCR (see Figure 3.6.A, 3.7.A, and 3.8.A).

3.2.5.1 Pathway analysis 24 h after silencing of *APEX1*, *XRCC1*, and DKO

In order to get more insights into the pathways which are affected after knockdown of *APEX1* and *XRCC1*, the Ingenuity Pathway Analysis (IPA) software was used to explore the entire set of differentially expressed genes. The software was applied to interpret the obtained data sets in the context of deregulated pathways, biological processes, and molecular networks. A gene was considered to be differentially expressed when the expression fold change was ≥ 2 or ≤ -2.

In *APEX1*-silenced cells, the knockdown was highly specific for the *APEX1* gene (Table 3.1).

In *XRCC1*-silenced cells, 38 genes showed a differential expression. The oxidative phosphorylation, the ubiquinone biosynthesis, and the mitochondrial dysfunction were the three significant pathways in which *NDUFA3* and *NDUFA13* were down-regulated (Figure 3.10.A).

Again, in double knockdown cells, the silencing was specific for *APEX1* and *XRCC1*. Here, several pathways involved in the cellular immune response were up-regulated in their expression (Figure 3.10.B).

Table 3.1. Genes with expression changes ≥ 2 fold caused by silencing of the respective gene in MCF7 after 24 h.

Regulatory effect of silencing (compared to controls)	Number of regulated genes (up-/down-regulated)	Fold change (min-max)
APEX1	1 (0/1)	0.13
XRCC1	38 (3/35)	0.28-2.13
DKO	9 (7/2)	0.11-4.01

A.

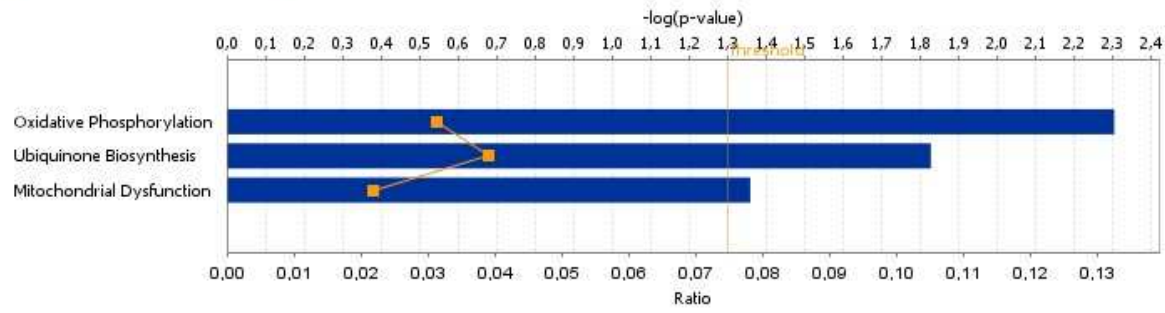

B.

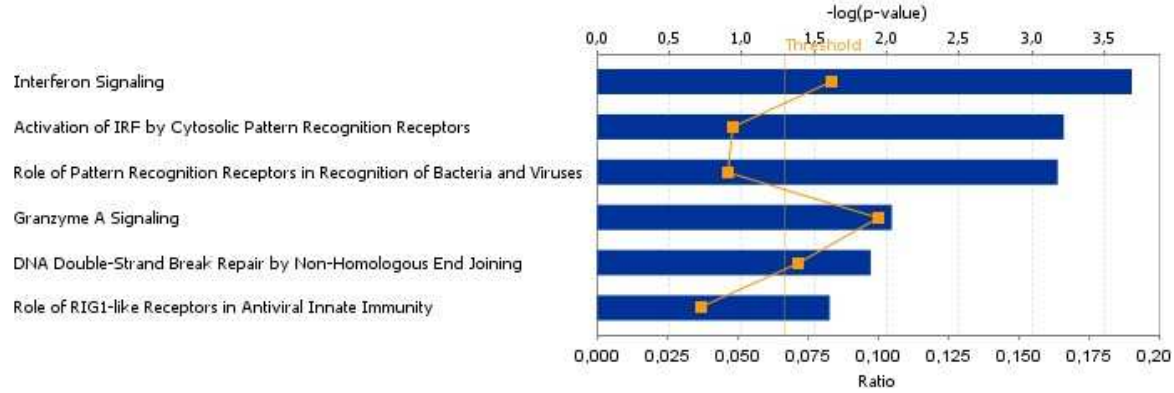

Figure 3.10. Pathway analysis of silencing-induced gene regulation in MCF7 cells. The significance of the association between the dataset and the identified pathway is represented by the ratio (yellow line with data points) and the p-value (blue bars). The ratio is calculated as the number of molecules in a given pathway that meet cutoff criteria divided by the total number of molecules that make up that pathway. The p-value is calculated by Fisher's exact test to determine the probability of the association between the genes in the dataset and the pathway due to chance. The threshold indicates a significance of $p < 0.05$. **A.** *XRCC1* knockdown **B.** DKO.

3.2.5.2 Pathway analysis 48 h after transfection

The knockdown of *APEX1* was still highly specific in *APEX1*-silenced cells. *ERBB3* was the only up-regulated gene (Table 3.2).

In *XRCC1*-silenced cells, a contrary pattern was observed with reference to the pattern after 24 h. More genes were up-regulated than down-regulated in their expression. These genes could not be assigned to common pathways with sufficient probability, but they have multiple functions in regulating gene expression, DNA replication and repair, and cell cycle (Figure 3.11).

In DKO cells, the silencing was highly specific. No specific pathways or functions were altered as only four genes were changed.

Table 3.2. Genes with expression changes ≥ 2 fold caused by silencing of the respective gene in MCF7 after 48 h.

Regulatory effect of silencing (compared to controls)	Number of regulated genes (up-/down-regulated)	Fold change (min-max)
APEX1	2 (1/1)	0.09-2.05
XRCC1	22 (17/5)	0.22-3.47
DKO	4 (2/2)	0.13-2.22

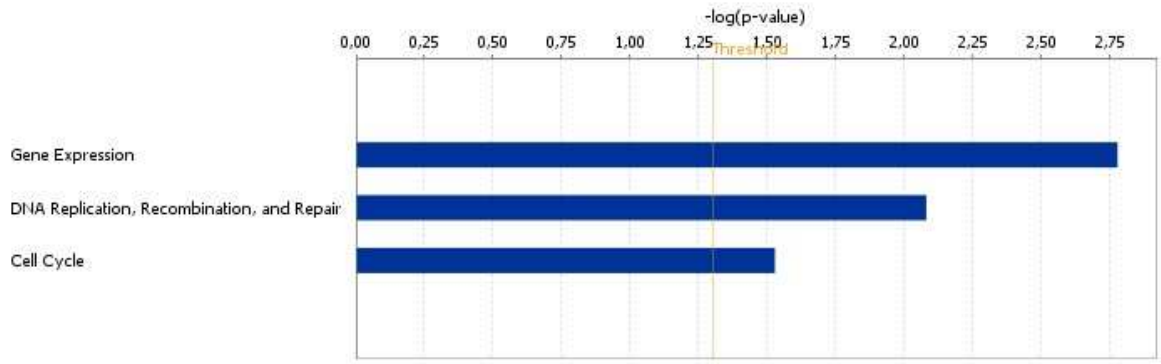

Figure 3.11. Analysis of biological functions and processes which are affected after silencing of *XRCC1*. The blue bars represent the p-value. The yellow line designates the threshold with $p < 0.05$.

In order to verify that the "Specificity Server" predicted genes which showed a sequence homology to some siRNA duplexes were not affected by the knockdown, the expression values of the genes were compared. A differential expression was not detected for any of the predicted genes, neither 24 h nor 48 h after silencing (data not shown). This result shows that the expression profiles are not influenced by off-target effects.

3.2.6 Changes of DNA repair pathways

The evaluation of the gene expression patterns focused on genes involved in DNA repair pathway because, there, major changes were expected due to the disruption of the BER pathway. The expression lists were sorted for a total of 150 genes involved in DNA repair. For a detailed list of repair genes see (60). Genes were ranked according to their expression fold change compared to the reference, which was the control siRNA transfected sample in all cases. But here, more stringent parameters were used than for the analysis of differentially expressed DNA repair genes. In general, a gene was

considered to be differentially expressed in silenced cells when the p-value was less than 0.05, the fold change was ≥ 1.2 or ≤ -1.2, and the mean average expression intensity was greater than 100 in either sample.

3.2.6.1 Deregulation of DNA repair pathways 24 h after silencing

The silencing of the target gene *APEX1* was already confirmed with the genome-wide approach. The expression of *APEX1* was reduced to 13 % of the reference. Besides *APEX1*, *ALKBH2* was reduced in its expression. *HUS1*, *MSH3* (MMR), *ERCC3* (NER), *POLE,* and the polymerase subunit *POLD1* were found to be up-regulated after silencing of *APEX1*.

The most changes in the gene expression pattern were observed for the *XRCC1*-silenced cells. Here, seven genes mainly involved in BER and NER became co-down-regulated. These were besides the target gene *XRCC1*, *NEIL2* and *NTHL1* (BER), *SHFM1* and *XRCC2* (HR), *GTF2H5* and *RPA3* (NER). Twelve genes were up-regulated in their expression, among them *APEX1* and *FEN1*, *EME1* and *RAD54B* (HR), and *ERCC3* and *GTF2H4* (NER). Further, the IR-inducible genes *CDKN1A* and *GADD45A* showed a higher expression level compared to controls. Together with *XPC,* which is also up-regulated after irradiation, the silencing of *XRCC1* causes an over-expression of p53 response genes involved in DNA repair.

In DKO cells, besides the reduced expression of *APEX1* and *XRCC1*, which confirmed the successful silencing, *PARP1* was down-regulated from the BER pathway. Moreover *CCNH* (NER) was less expressed compared to controls. Up-regulated genes were *ERCC2* (NER), *XRCC5* (NHEJ), and the two DNA polymerases *POLG* and *REV1L* (Figure 3.12). It is notable that in nearly all cases where a gene is changed in its expression in the single silenced cells, the effect is abrogated in the DKO cells.

The changes in the gene expression profile of silenced cells clearly demonstrate that the silencing of *APEX1*, *XRCC1*, or both affects the expression pattern of genes involved in DNA repair pathway. Silencing of *XRCC1* affects the cell to a greater extent than the *APEX1* knockdown or the simultaneous silencing of both genes, especially regarding survival and growth.

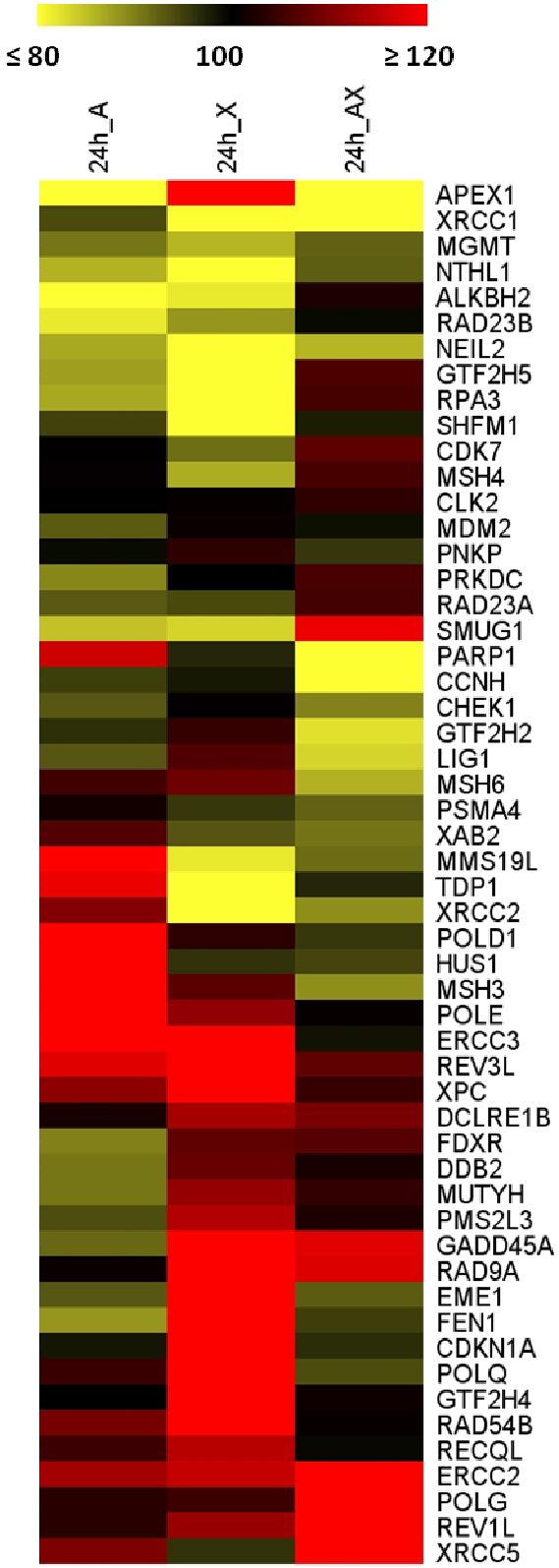

Figure 3.12. Gene expression changes in silenced cells 24 h after transfection. All DNA repair genes which showed a reduction in the gene expression by ≤ 80 % (bright yellow) or an increase ≥ 120 % (bright red) compared to controls in either one of the treatments are displayed. Control siRNA transfected genes were used as a reference. The gene names are indicated. **24h_A.** *APEX1* knockdown cells. **24h_X.** *XRCC1*. knockdown cells. **24h_AX.** DKO cells.

3.2.6.2 Gene expression is still altered 48 h after knockdown

In *APEX1*-silenced cells, the down-regulation of *APEX1* was also confirmed after 48 h. *PARP1*, another gene from the BER pathway which is involved in repair of SSB, showed a reduced expression. The DNA damage response gene *TP53*, the HR gene *DMC1*, and the three NER genes *RAD23A*, *RAD23B*, and *RPA3* were down-regulated. Only *GTF2H5* was up-regulated.

Several genes were observed to be down-regulated with *XRCC1* 48 h after knockdown. These were *NTHL1*, *ALKBH2*, *CHEK2*, *PSMA4*, *XRCC3*, *RAD23A*, *POLG* and *GADD45A*. Here, *PARP1* was up-regulated. Also genes from HR (*MUS81*), NER (*ERCC3*, *ERCC6*) and the repair of cross links (*TDP1*) seemed to be activated upon *XRCC1* knockdown.

After silencing of *APEX1* and *XRCC1*, the expression pattern revealed a down-regulation of several genes. *MBD4* and *PARP1*, which are involved in BER, were down-regulated. Further, *CDK7* (NER), *DMC1* (HR), and *XRCC5* (NHEJ) were reduced in their expression. Two genes, *GTF2H1* and *ERCC6*, showed an increased expression (Figure 3.13).

Taken together, 48 h after transfection most of the siRNA treated cells showed a pattern of co-silenced genes. Only a few genes were up-regulated in their expression.

3.2.6.3 Comparison of differentially expressed DNA repair genes

In *APEX1*-silenced cells, only *APEX1* remained down-regulated after 48 h. In *XRCC1* silenced cells, the *XRCC1* and the *NTHL1* genes still showed a reduced expression, whereas *ERCC3* and *REV3L* were still over-expressed. *TDP1* was the only gene which showed an inverse expression. It was reduced after 24 h and became over-expressed after 48 h. In DKO, *APEX1*, *XRCC1*, and *PARP1* showed an ongoing reduced expression after 48 h. Moreover, *REV1L* was still up-regulated. Here, the *XRCC5* gene was up-regulated after 24 h and demonstrated a reduced expression after 48 h.

All other patterns of differentially expressed genes which were observed after 24 h were not detectable any more after 48 h or replaced by new patterns (see above).

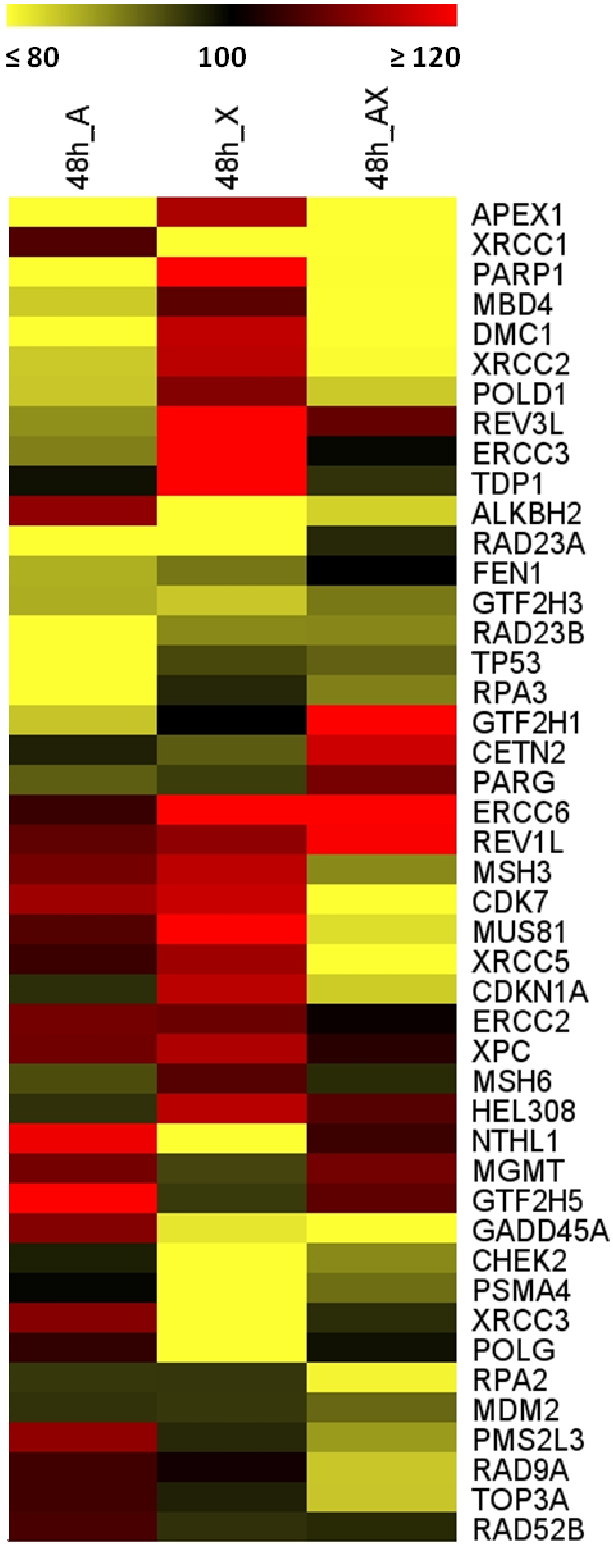

Figure 3.13. Gene expression changes in silenced cells 48 h after transfection. All DNA repair genes which showed a reduction in the gene expression by ≤ 80 % (bright yellow) or an increase ≥ 120 % (bright red) compared to controls in either one of the treatments are displayed. Control siRNA transfected cells were used as a reference. The gene names are indicated. **48h_A.** *APEX1* knockdown cells. **48h_X.** *XRCC1*. knockdown cells. **48h_AX.** DKO cells.

3.2.7 General conditions for the irradiation treatment

For the analysis of the functional impact of the silencing, cells were irradiated 72 h after knockdown when mRNA and protein levels were strongly reduced. Gene expression patterns were obtained from silenced cells 24 and 48 h after transfection and an additional treatment with IR followed by a further incubation step at 37° C for four hours. For a detailed experimental overview, see Figure 3.1. The mRNA expression levels of silenced cells in the corresponding functional experiment at the time point of irradiation are summarized in Table 3.3.

Table 3.3. Relative mRNA amounts of *APEX1* and *XRCC1* in silenced cells obtained in the functional assays at the time of irradiation. Values are normalized to the control.

	APEX1 mRNA (*APEX1*-silenced cells)	XRCC1 mRNA (*XRCC1*-silenced cells)	*APEX1*/*XRCC1* mRNA (DKO cells)
CFA/SRB assay	0.06	0.03	0.09/0.04
Comet assay	0.07	0.08	0.10/0.09
γH2AX assay	0.09	0.07	0.19/0.13

3.2.8 Irradiation of silenced and control cells showed no difference of radiation sensitivity

In order to investigate the effect of the knockdown of *APEX1* and *XRCC1* on radiosensitivity, silenced MCF7 cells were irradiated with increasing doses of ionizing radiation (0-5 Gy). The radiation dose-survival curves were determined with the CFA and the SRB assay. The treatment with ionizing radiation affected the colony-forming ability of the silenced cells in a dose-dependent manner. Considering the standard deviations, the inhibition of expression of *XRCC1* or *APEX1* or both did not influence the radiosensitivity of the cells as determined with the colony-formation assay and the SRB assay (Figure 3.14.A+B).

A.

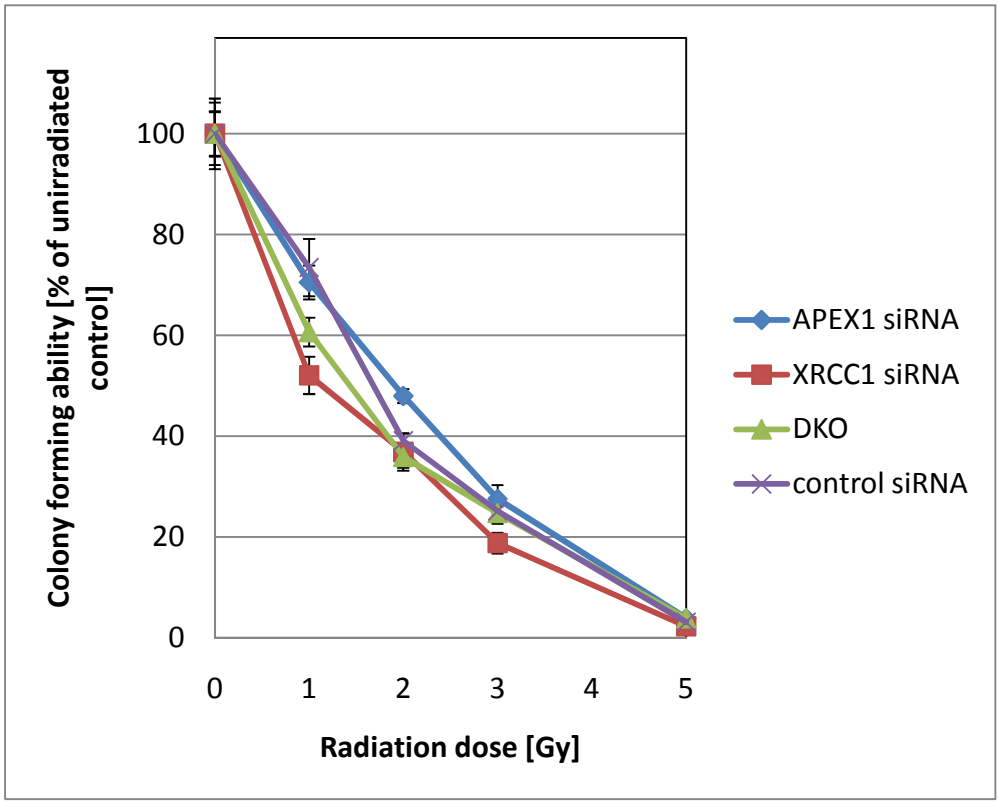

B.

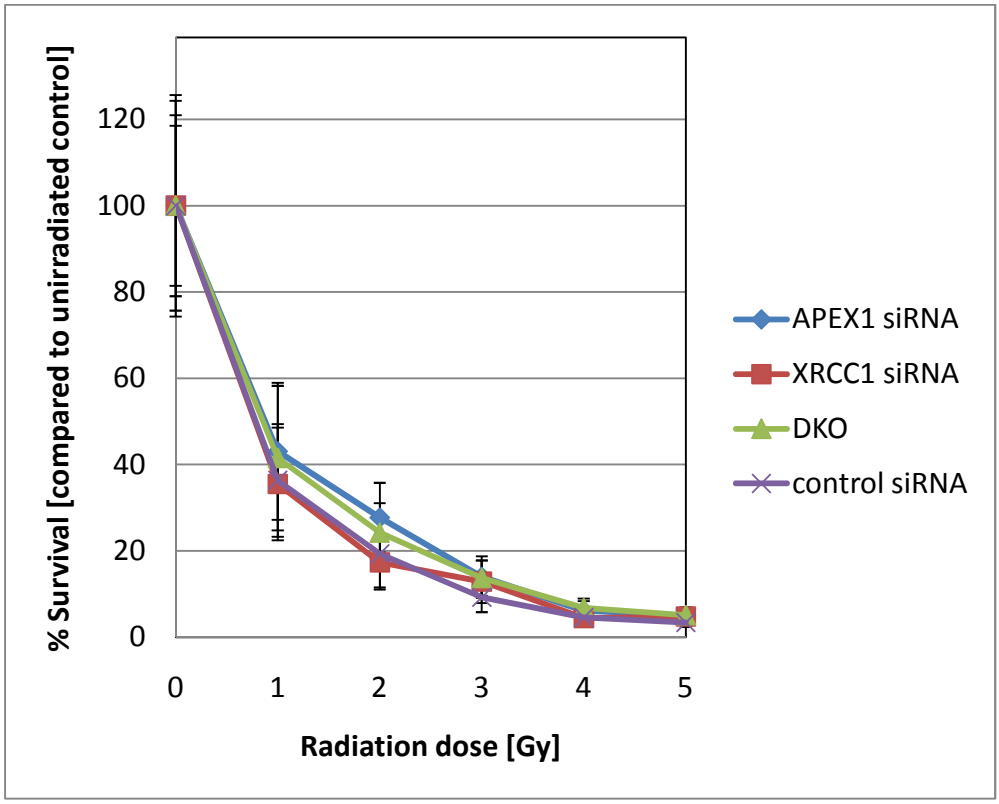

Figure 3.14. Effect of silencing on radiosensitivity and on response to IR. A. Colony-forming ability of silenced and control cells after treatment with IR. Means ± SD are for three independent experiments. **B.** Radiation dose-survival curves determined with the SRB assay. Means ± SD are from sixteen replicates.

Another way of determining the cell's answer to ionizing radiation is to measure the activation of the p53 signal cascade. p53 itself is not regulated upon irradiation, but it activates the expression of several genes such as *CDKN1A*. Consequently, increased expression levels of *CDKN1A* confirm the treatment with IR and the cell's response to it.

As shown in Figure 3.15, treatment with IR caused a strong p53 response measured by *CDKN1A* mRNA induction. However, the silencing of *APEX1* and *XRCC1* did not change the p53 response compared to controls.

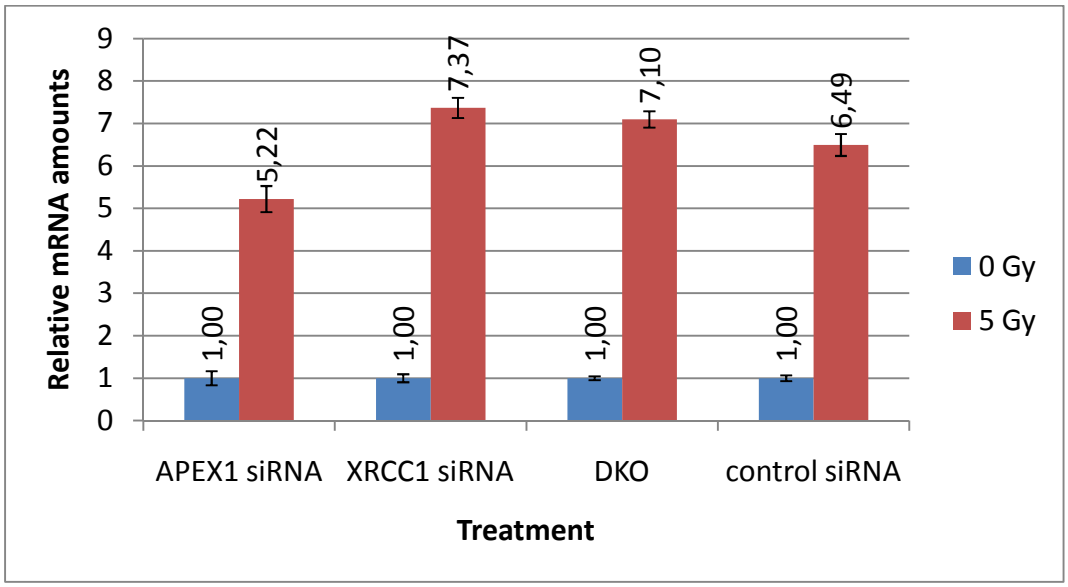

Figure 3.15. p53 response after irradiation. Cells were mock-irradiated or irradiated with 5 Gy 24 h after transfection. *CDKN1A* expression was measured four hours after irradiation. Normalized values are expressed as mean ± SD from three replicates.

3.2.9 Initial DNA damage induction is affected after irradiation of silenced cells as measured by the Comet Assay

To investigate the influence of a deficiency in the BER pathway on radiation-induced DNA damage, the expression of *APEX1* and *XRCC1* was inhibited by transfecting siRNA into exponentially growing MCF7 cells. Then, the cells were irradiated with 5 Gy 72 h after transfection and assayed for their DNA damage by using the alkaline comet assay. Non-targeting siRNA was used as negative control.

No difference was observed between silenced cells and controls in comparison to the residual damage. In all treatments, the DNA repair rates were comparable and within the

variability of the experiment. Nevertheless, a trend regarding the initial damage induction was observed. *APEX1*-silenced cells showed a trend for a lower initial damage induction whereas *XRCC1*-silenced cells showed a trend for a higher initial damage induction (Figure 3.16). For *APEX1*, this was shown in three independent experiments; for *XRCC1*, it was shown in two independent experiments.

In sum, a difference between the silencing of *APEX1* and *XRCC1* can be detected in their response to rejoin DNA single-strand breaks and alkali-labile sites immediately after irradiation. The initial amount of SSB in *XRCC1*-silenced cells is 1/3 higher than in controls. This clearly shows a deficiency in the processing of SSB at a very early stage after damage induction. *APEX1*-silenced cells show a lower tailmoment compared to controls which indicates a lower amount of IR-induced SSB immediately after irradiation.

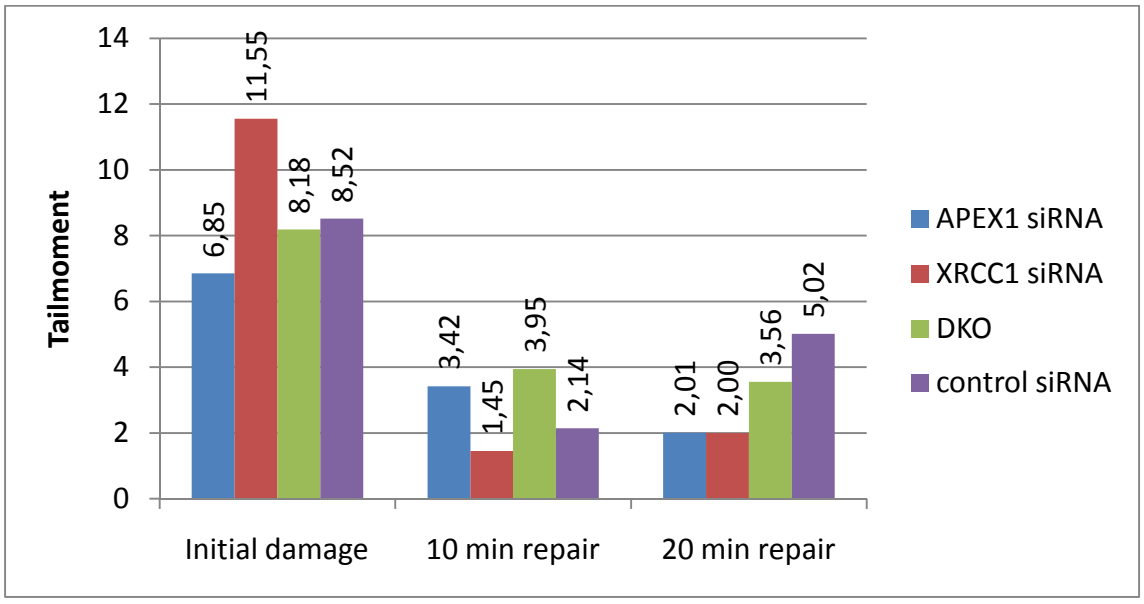

Figure 3.16. Radiation induced DNA damage. *APEX1* and *XRCC1* siRNA treated cells were irradiated with 5 Gy, and alkaline comet assay was carried out. Tailmoment distributions were determined by the scoring of at least 102 cells per sample. Distributions were determined for mock-irradiated cell, and irradiated cells directly, 10 minutes and 20 minutes after irradiation. Absolute values of the mock-irradiated cells were subtracted from values of the irradiated cells. Results are expressed as the median.

3.2.10 Formation of DNA double strand breaks is not affected after silencing of *APEX1* and *XRCC1*

In addition to the analysis of SSB and their repair with the comet assay, we examined the effect of a reduced expression of *APEX1* and *XRCC1* on the repair of IR-induced DNA-DSBs. The induction of DNA double-strand breaks (DSBs) correlates with the phosphorylation of the variant histone H2AX (γH2AX), which can be detected with a specific antibody. Cells were analyzed for their number of γH2AX foci before and after irradiation. To further validate the results, the changes in total γH2AX signal intensity were investigated in *APEX1*-silenced cells by flow cytometry. The total γH2AX signal intensity was assessed either for the whole cell population or according to the individual cell cycle stages.

No difference was observed between the knockdown and the absolute numbers of foci 30 minutes after irradiation the. Two hours after irradiation, the rejoining of DSB was more efficient in *APEX1*-silenced cells than in controls, ranging from 44 foci to 13 foci, and less efficient in *XRCC1*-silenced cells (Figure 3.17.A).

Investigating the total γH2AX signal intensity, no alterations were detected after the transfection with *APEX1* siRNA or control siRNA (Figure 3.17.B). Moreover, the γH2AX signal intensity was not dependent on the cell cycle (data not shown).

In sum, the different siRNA treatments caused no difference in the formation of DSBs 0.5 h after irradiation. Therefore, DSBs do not contribute to the observed results in the comet assay.

A.

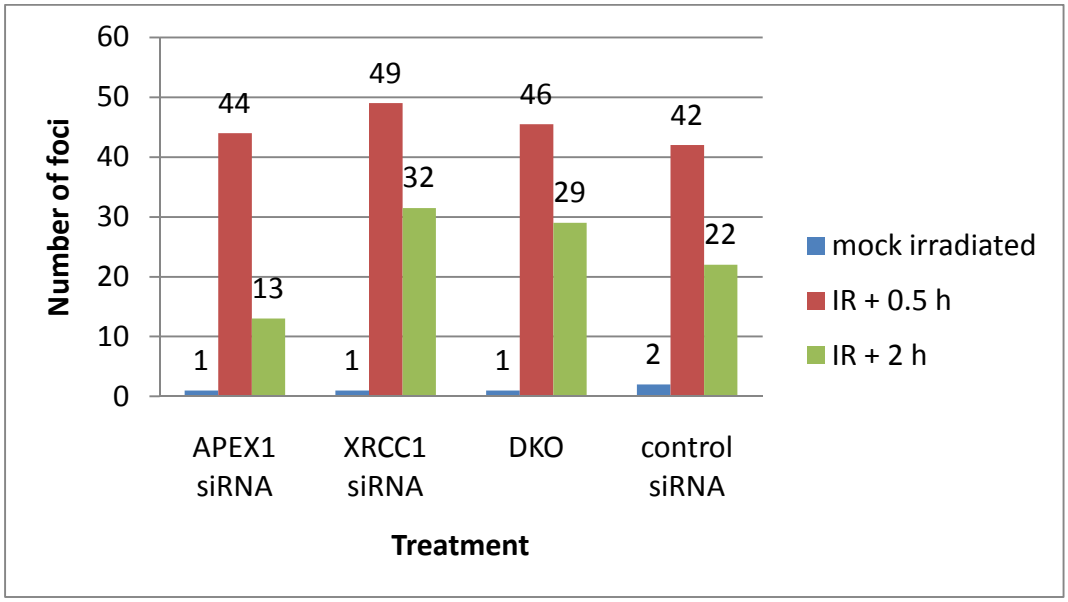

B.

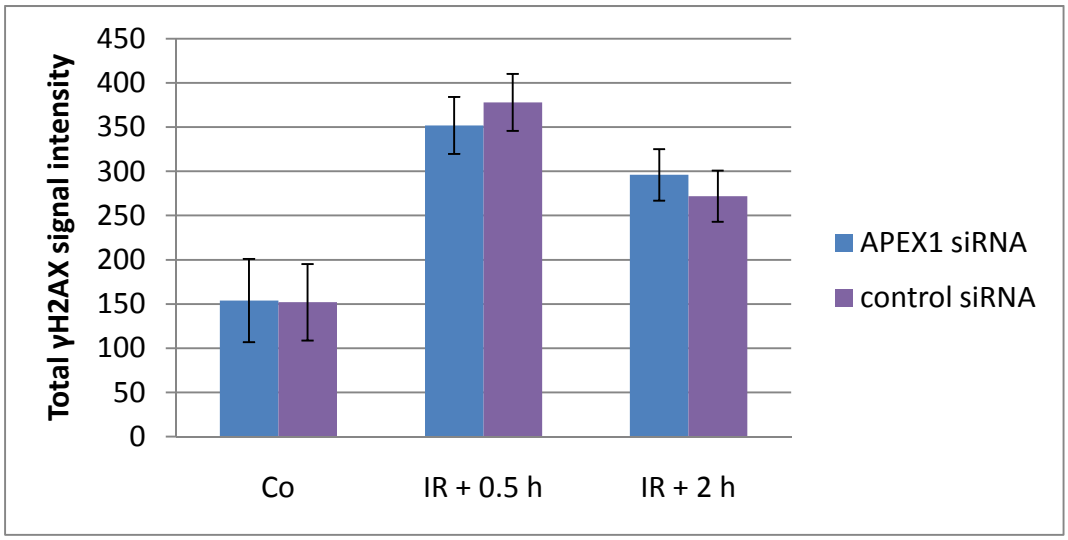

Figure 3.17. Inhibiting the expression of *APEX1* and *XRCC1* by siRNA has no influence on the repair of DSBs. A. Cells were mock-irradiated or irradiated with 5 Gy 72 h after transfection. Cells were fixed 0.5 and two hours after irradiation and stained for γH2AX foci and DNA. At least 250 nuclei were evaluated for each treatment. Results are expressed as the median. **B.** Total signal intensity of γH2AX in mock-irradiated and irradiated cells. Values are displayed as the median. The asterisks indicate robust CV.

3.2.11 Cell cycle distribution of cells is affected after transfection with *APEX1* siRNA but not after additional treatment with ionizing radiation

As irradiation affects the cell cycle and radiosensitivity depends on cell cycle position and progression, *APEX1*-silenced cells were analyzed for cell cycle by flow cytometry. Silenced cells were either mock-irradiated or irradiated with 5 Gy followed by 30 and 120 minutes of incubation to allow for repair.

72 h after transfection, the *APEX1* knockdown cells showed 33 % of cells in the G2-M stage whereas in controls, only 10 % of cells were in G2-M. However, most of the treated cells were in the G1 stage (Figure 3.18.A). Further, a reduction in *APEX1* did not coincide with an increase in apoptosis as detected by sub-G1 fraction (0.2 % versus 0.8 %).

After treatment of the cells with IR, neither a difference in the cell cycle profile of silenced cells and controls nor an increase in apoptosis was detected (Figure 3.18.B+C).

A.

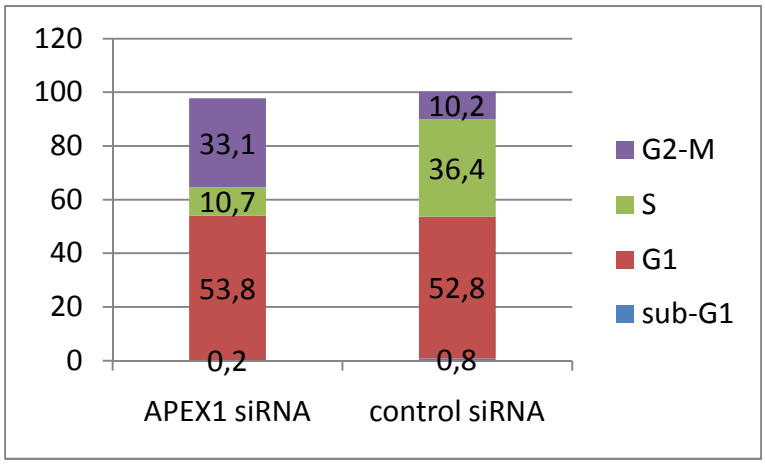

B.

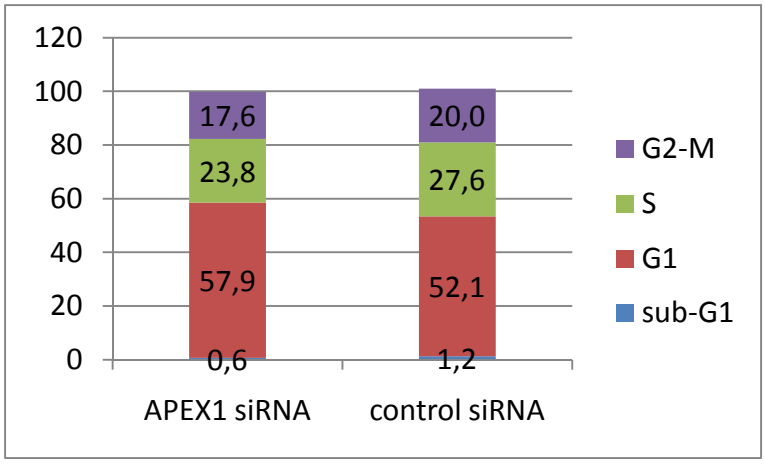

C.

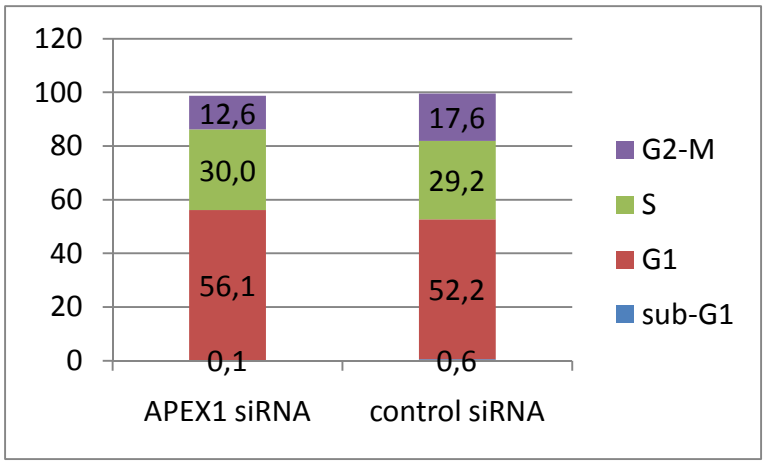

Figure 3.18. Cell cycle profiles of silenced cells before and after irradiation 72 h after transfection, cells were either mock-irradiated or irradiated with 5 Gy. After fixation and DNA staining with propidium iodide, cells were analyzed for their cell cycle stages by flow cytometry. For each sample 25.000 single events were detected. Values are expressed in percent. **A.** Mock-irradiated cells. **B.** Irradiated cells followed by 30 minutes of rejoining time. **C.** Irradiated cells followed by 120 minutes of rejoining.

3.2.12 The irradiation of silenced cells results in changes in the gene expression patterns

Ionizing radiation causes multiple DNA damage and a complex damage response signaling within the cell. To investigate the effect of ionizing radiation on the gene expression pattern of silenced cells, exponentially growing MCF7 cells were transfected with either *APEX1* or *XRCC1* siRNA or both. Cells were mock-irradiated or irradiated with 5 Gy 24 or 48 h after knockdown. Gene expression changes were analyzed on a genome-wide scale on Sentrix HumanRef-8 Expression BeadChips four hours after irradiation.

As shown in Figure 3.19.A+B, the BER-deficient cells remain silenced in their target mRNA levels four hours after irradiation and prior to expression profiling.

A.

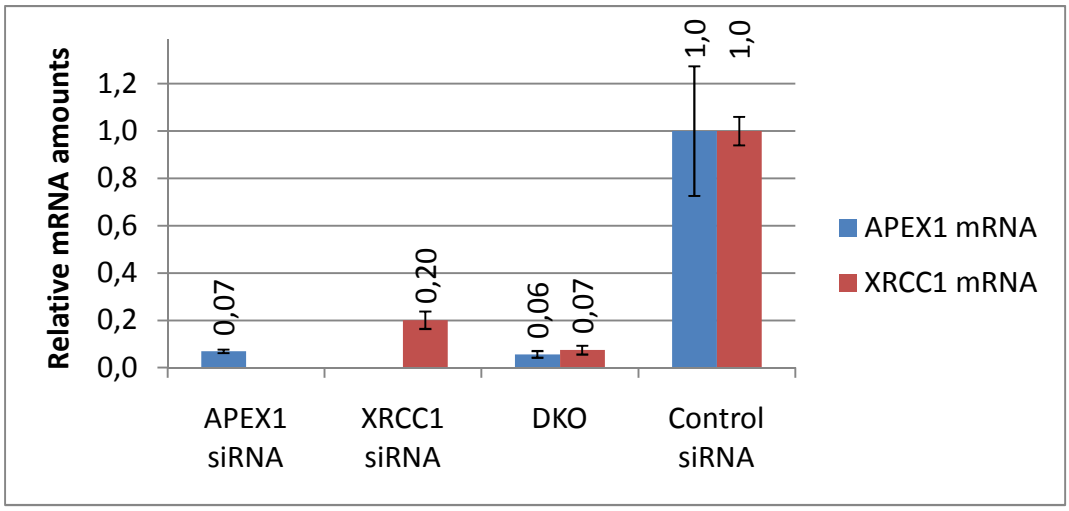

B.

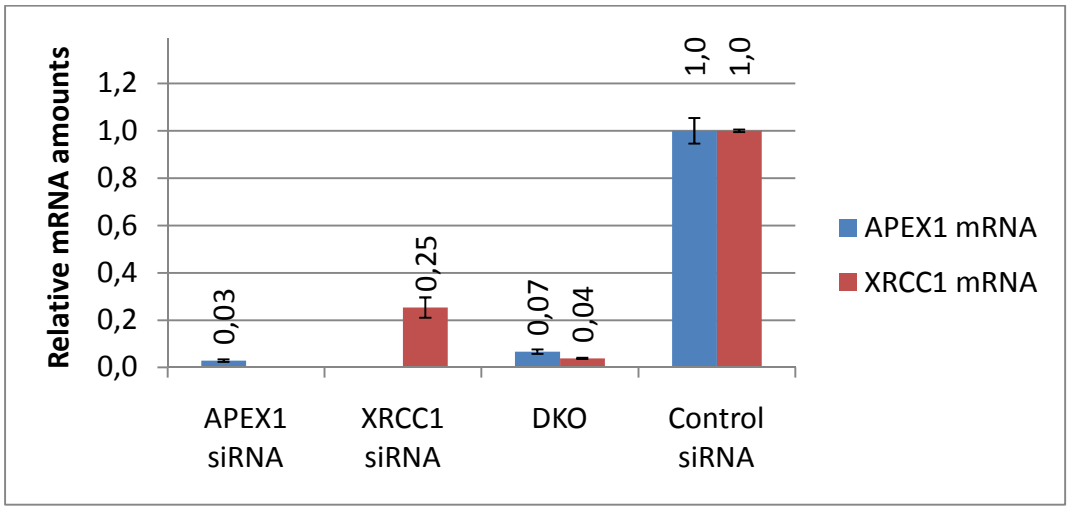

Figure 3.19. Knockdown is still effective after irradiation. Relative quantification of *APEX1* and *XRCC1* mRNA expression by real time PCR four hours after irradiation. **A.** 24 h after transfection. **B.** 48 h after transfection.

3.2.12.1 Pathway analysis of radiation-induced gene regulation in MCF7 cells 24 h after silencing of *APEX1* and *XRCC1*

In *APEX1* knockdown cells, 21 genes regulating 35 canonical pathways were differentially expressed (Table 3.4). These included pathways known to be involved in radiation response such as p53 signaling, ATM signaling and the cell cycle regulation (Figure 3.20.A). Furthermore, *CYP1A1* and *CYP1B1* were highly over-expressed, which activated metabolizing pathways such as the aryl hydrocarbon receptor signaling pathway.

XRCC1-silenced cells showed the largest pattern of differentially expressed genes, which caused an enrichment of eight different pathways. Among them, the oxidative phosphorylation, the ubiquinone biosynthesis, and the metabolizing cytochrome P450 system were most affected (Figure 3.20.B). Again, *CYP1A1* and *CYP1B1* were highly expressed

The effect of irradiation in DKO cells was smaller than in the single knockdowns. However, 27 pathways were affected due to the additional treatment with IR. Radiation response pathways were determined among the top hits besides several cell cycle regulating pathways (Figure 3.20.C).

The irradiated controls showed a large overlap in differentially expressed genes compared to the DKO sample. Seven out of twelve up-regulated genes were identical. For that reason, in the controls similar pathways became deregulated compared to the DKO (Figure 3.20.D). A detailed overview of regulated genes is presented in Table 3.4.

Moreover, seven genes were up-regulated in all four siRNA treatments: *ACTA2*, *BTG2*, *CDKN1A*, *GDF15*, *GRIN2C*, *PHLDA3*, and *SESN1*. Consequently, all treatments showed similar patterns of functions which were deregulated due to the treatment with IR ($p < 0.05$). The genes share functions in regulating the cell cycle, the cellular growth and proliferation, and influencing the cell morphology and cell death.

Table 3.4. Genes with expression changes ≥ 2 fold induced by silencing the respective gene and additional irradiation in MCF7 after 24 h.

Regulatory effect of irradiation on cells with a silenced background (compared to mock-irradiated silenced cells)	Number of regulated genes (up-/down-regulated)	Fold change (min-max)
APEX1	21 (18/3)	0.46-10.54
XRCC1	67 (65/2)	0.46-10.15
DKO	10 (9/1)	0.45-4.85
Control siRNA	12 (12/0)	2.01-3.78

A.

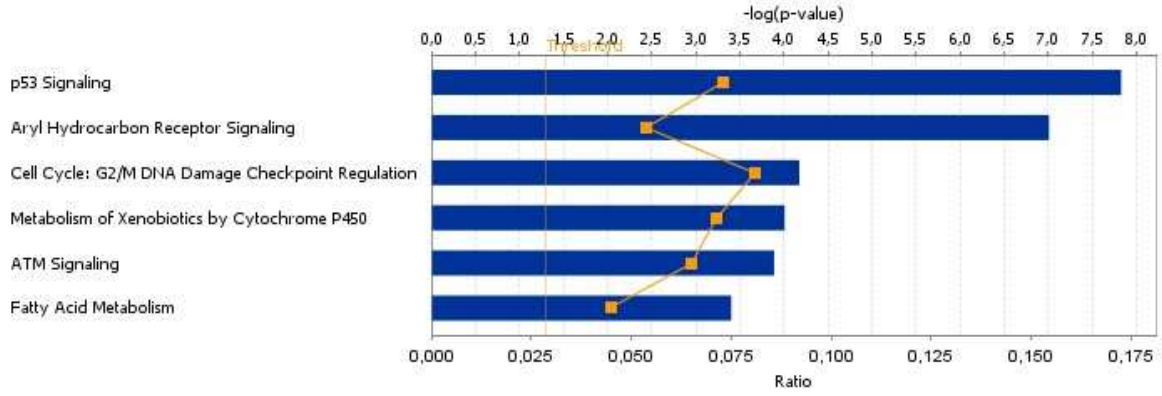

B.

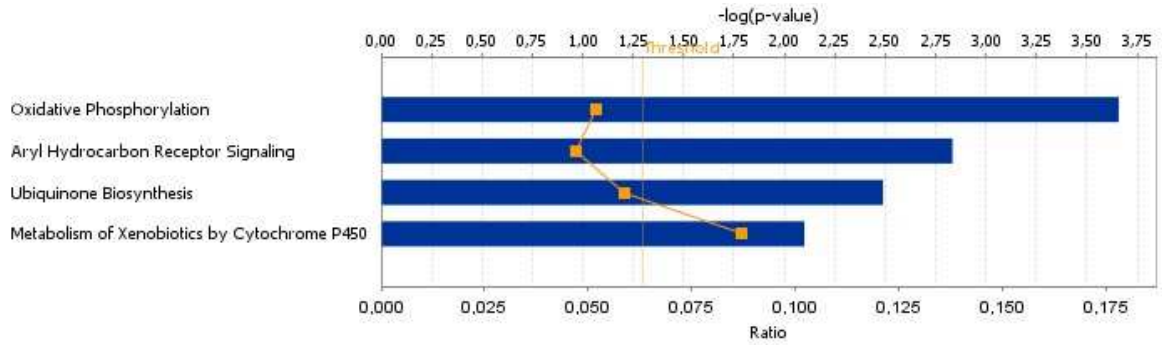

C.

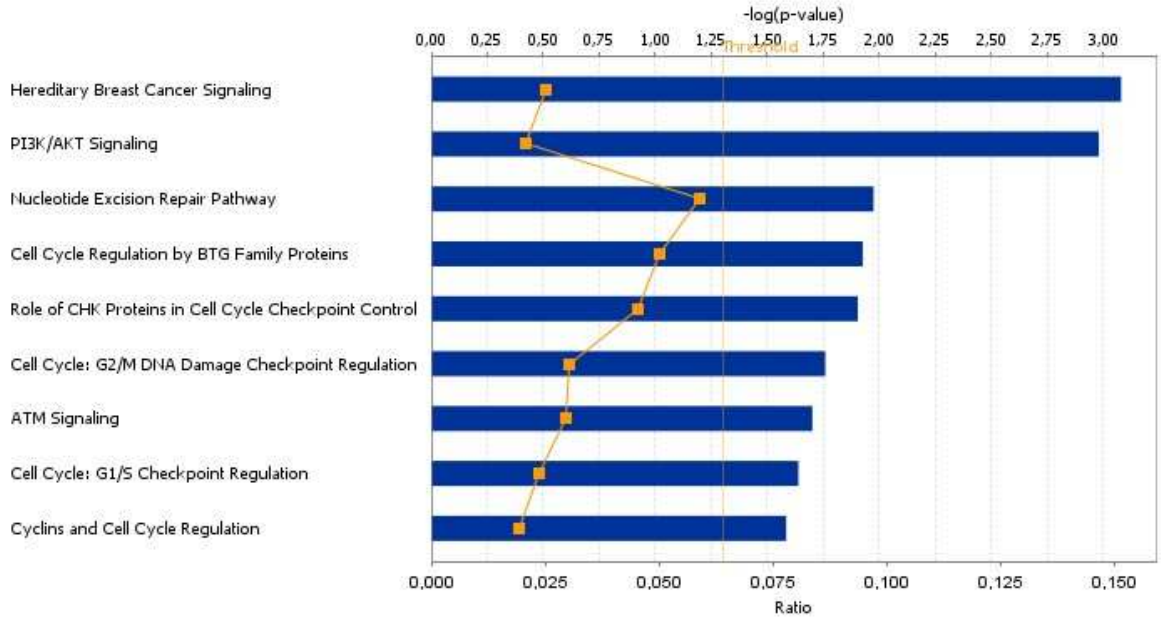

D.

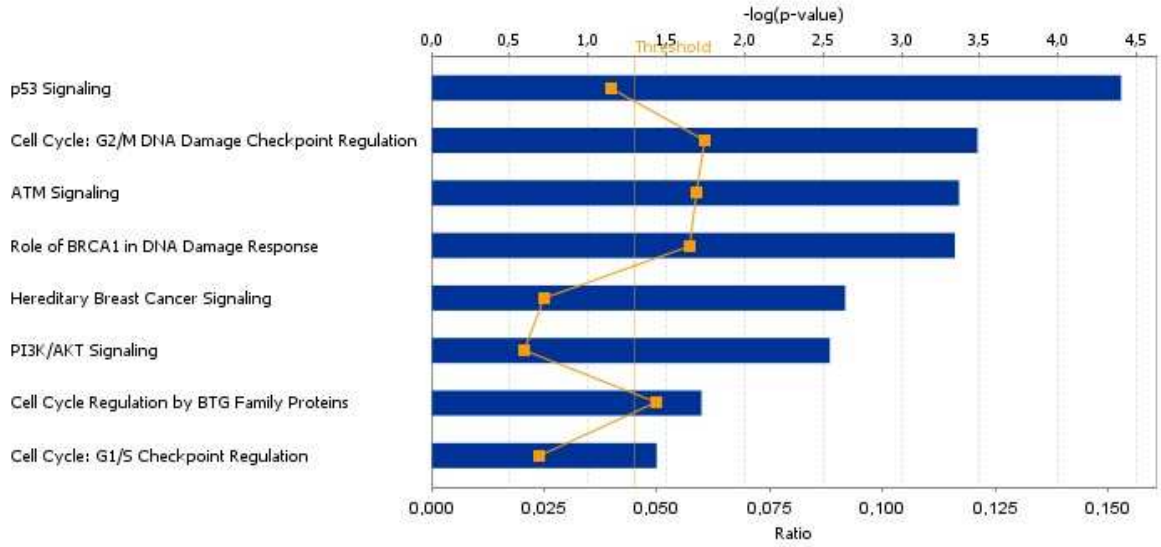

Figure 3.20. Top affected pathways after irradiation. The significance of the association between the dataset and the identified pathway is represented by the ratio (yellow line with data points) and the p-value (blue bars). The ratio is calculated as the number of molecules in a given pathway that meet cutoff criteria divided by the total number of molecules that make up that pathway. The p-value is calculated by Fisher's exact test to determine the probability of the association between the genes in the dataset and the pathway due to chance. The threshold indicates a significance of $p < 0.05$. **A.** *APEX1* knockdown cells **B**. *XRCC1*-silenced cells **C.** DKO cells **D.** controls

3.2.12.2 Pathway analysis 48 h after silencing and additional irradiation

Irradiation caused less expression changes 48 h after transfection. Mainly up-regulated genes were determined except for the gene *CCDC58*, which was down-regulated in the controls (Table 3.5).

Nevertheless, a common pattern of differentially expressed genes was observed in all four treatments. The genes *ACTA2*, *CDKN1A*, *GDF15*, *SESN1*, and *TNFRSF10B* were all up-regulated to a similar extent. Consequently, the identical canonical pathways were activated in all treatments, namely the radiation response pathways such as p53-signaling, ATM-signaling, and cell cycle regulating pathway.

These genes share common functions in regulating the cell cycle, the cellular growth and proliferation, and cell death and in influencing cell morphology. A similar pattern had been determined after 24 h.

Additionally, in *APEX1*-silenced cells, the interferon signaling was affected (Figure 3.21.A). *XRCC1*-silenced cells, again, showed an activation of the cytochrome P450 system after irradiation by a strong increase in the expression of the *CYP1A1* and *CYP1B1* genes (Figure 3.21.B).

Table 3.5. Genes with expression changes ≥ 2 fold induced by silencing of the respective gene in MCF7.

Regulatory effect of irradiation on cells with a silenced background (compared to mock-irradiated silenced cells)	Number of regulated genes (up-/down-regulated)	Fold change (min-max)
APEX1	10 (10/0)	2.01-4.59
XRCC1	15 (15/0)	2.01-7.40
DKO	5 (5/0)	2.24-4.76
Control siRNA	7 (6/1)	0.49-4.47

A.

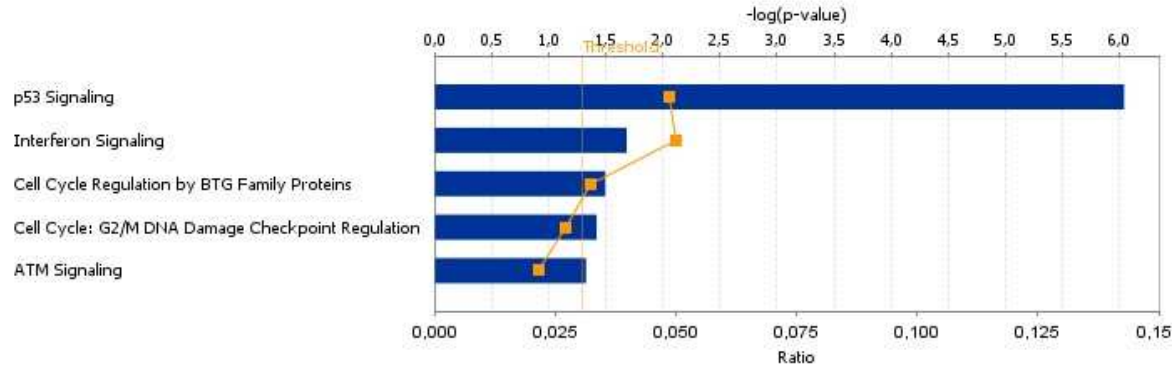

B.

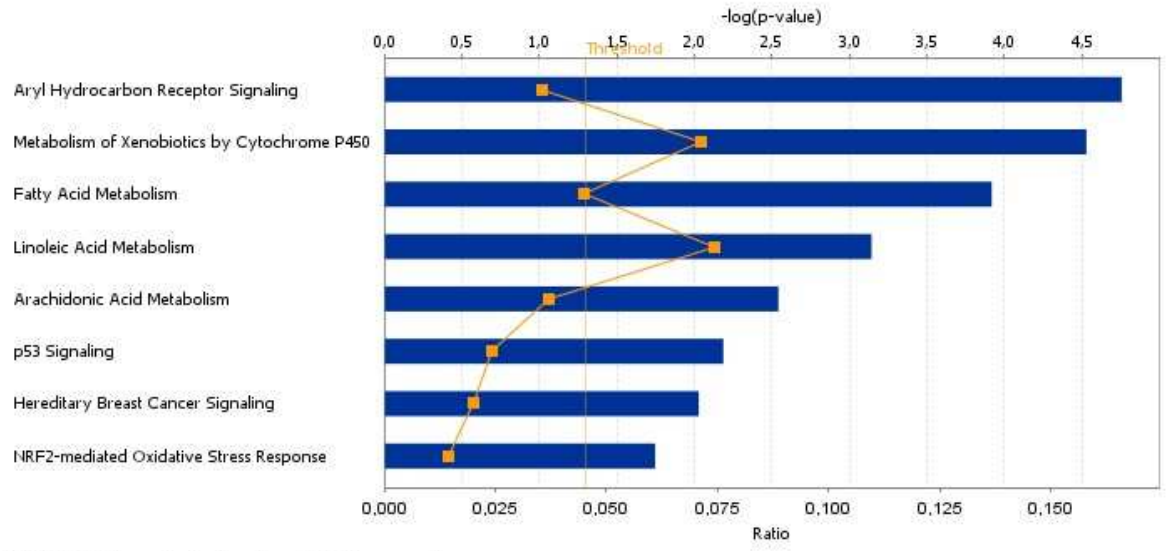

Figure 3.21. Top affected pathways after irradiation in A. *APEX1* knockdown cells **B**. *XRCC1*-silenced cells (for explanations see Figure 3.20).

3.2.13 Changes in DNA repair and DNA damage response pathways after irradiation

In general, after silencing and additional irradiation, more DNA repair genes were altered in their expression compared to the mock-irradiated silenced cells. The expression of IR-inducible genes like *CDKN1A*, *XPC*, *GADD45A*, and *MDM2* was up-regulated by at least 20 % after irradiation (Figure 3.22). Further changes in the profile of DNA repair genes were dependent on the treatment of the cell with the respective siRNA. First, the observed expression patterns in the irradiated controls will be described. The second part will focus on the differentially expressed genes regulated only in the knockdown cells.

3.2.13.1 Gene expression profiles 24 h after transfection and subsequent irradiation with 5 Gy

The irradiation of controls induced the expression of *RAD23A* and *CDK7* (NER), *DDB2* (NER-related) and *REV3L*. Other genes like *ALKBH2*, *GTF2H2*, *CHEK1* (DNA damage response), *POLD1*, and *MSH6* were down-regulated (Figure 3.22).

After irradiation of *APEX1* siRNA treated cells, *MUTYH* (BER), *CLK2* and *RAD9A* (DNA damage response), *PRKDC* (NHEJ), and *ERCC3* and *MMS19L* (NER) became down-regulated. Interestingly, three DNA polymerases (*POLG*, *POLQ*, and *POLE*) were less expressed compared to the mock-irradiated silenced sample. Further, *FDXR*, *PSMA4*, *RAD23B* and *ALKBH2* were up-regulated in their expression.

XRCC1-silenced cells showed a unique pattern of up-regulated genes, in particular, *SMUG1* and *NEIL2* (BER), *XRCC2* and *SHFM1* (HR), *MSH3* and *MSH4* (MMR), and *RPA3* and *GTF2H5* (NER). In addition to the activation of classic repair genes, the *MGMT* and the *XAB2* (NER-related) gene showed an increased expression.

In DKO cells, only a few changes in the gene expression pattern were detectable. Besides *PNKP* (BER), *LIG1* and *CCNH* (NER), which were up-regulated upon irradiation, only *ALKBH2* was reduced in its expression profile compared to mock-irradiated silenced cells. After irradiation, the DKO cells showed a gene expression profile which is totally different compared to the single knockdowns, except for the IR-inducible genes.

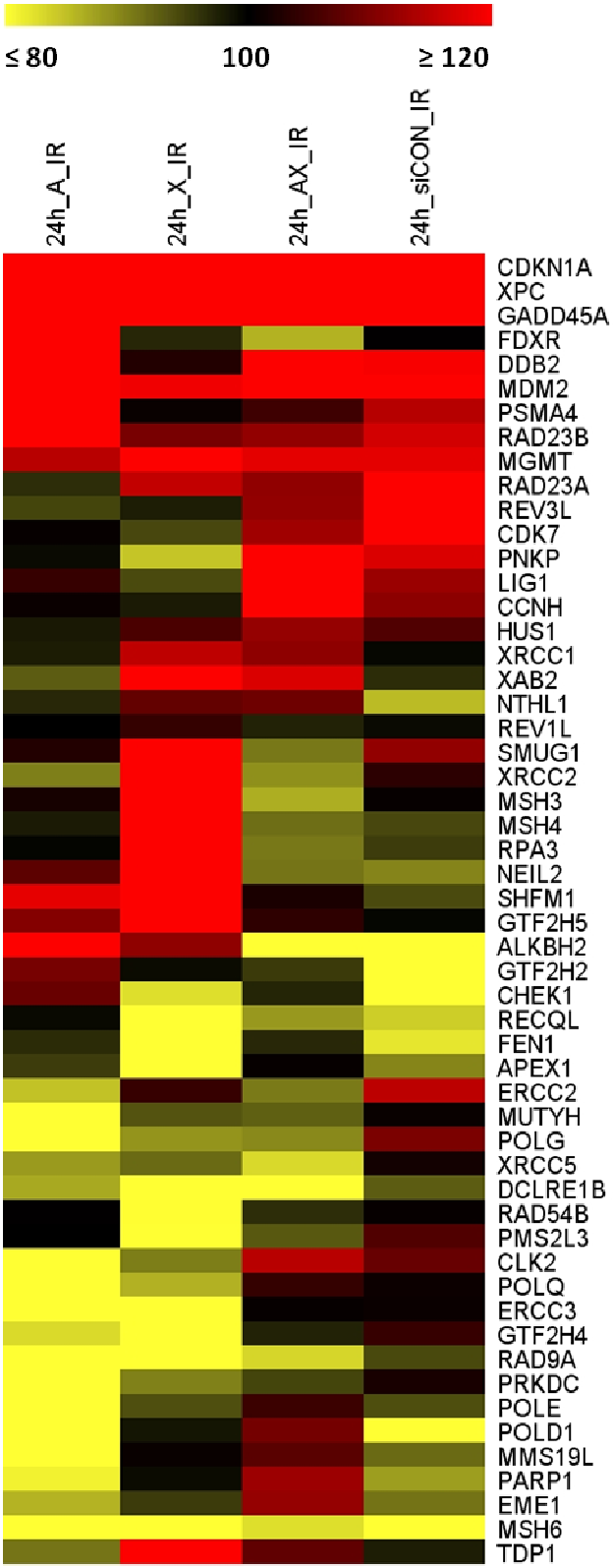

Figure 3.22. Gene expression changes in silenced cells 24 h after transfection and additional treatment with ionizing radiation. All DNA repair genes which showed a reduction in the gene expression by ≤ 80 % (bright yellow) or an increase ≥ 120 % (bright red) compared to mock-irradiated silenced cells (here controls) in either one of the treatments are displayed. Mock-irradiated silenced cells were used as a reference sample. Gene names are indicated. **24h_A_IR.** *APEX1* siRNA transfected cells. **24h_X_IR.** *XRCC1* siRNA transfected cells. **24h_AX_IR.** DKO cells. **24h_control_IR.** Control siRNA transfected cells.

3.2.13.2 Small changes in the gene expression patterns of silenced cells 48 h after transfection and irradiation with 5 Gy

48 h after transfection, the treatment with ionizing radiation caused fewer changes in the expression of DNA repair genes as compared to the pattern obtained after 24 h. For all three knockdown treatments, the detected pattern was comparable with only minor differences.

Again, the treatment with IR caused the induction of the expression of IR-inducible genes: *CDKN1A*, *GADD45A*, and *XPC* in all four treatments. In contrast, the MMR gene *MSH6* was down-regulated in all four siRNA treatments. *MSH3* was down-regulated in DKO cells and controls, *PMS2L3* only in *XRCC1*-silenced cells (Figure 3.23).

The irradiated controls showed the most deregulated pattern of differentially expressed genes. Here, several genes showed a decrease in expression compared to the other treatments. *FEN1*, *MBD4* (BER), *RPA2* (NER), *XRCC2* and *XRCC3* (HR), *RAD9A*, *RAD52B*, and *TOP3A* were decreased in their expression. *ERCC2* (NER) showed an increased expression level compared to mock-irradiated cells.

In *APEX1*-silenced cells, treatment with IR led to the induction of the NER genes *CETN2* and *RAD23A,* the DNA polymerase *REV3L*, and *PARG*. A down-regulation was observed for the HR genes *DMC1* and *MUS81*. Moreover, the DNA polymerase *REV1L* was reduced in its expression.

In *XRCC1*-silenced cells, again, HR (*DMC1*, *MUS81*), BER (*MBD4*), *RAD9A*, and *POLD1* were observed to be down-regulated, whereas two NER genes (*GTF2H3* and *RAD23B*) became up-regulated in their expression. Also *MDM2* and *REV3L* were up-regulated after irradiation compared to the mock-irradiated sample.

In DKO cells, only a few genes were differentially expressed 48 h after transfection and additional irradiation. These were besides the IR-inducible and MMR genes, *CDK7* (NER), *PSMA4*, *MGMT*. All of them were up-regulated, whereas *ALKBH2* (direct reversal) showed a reduced expression.

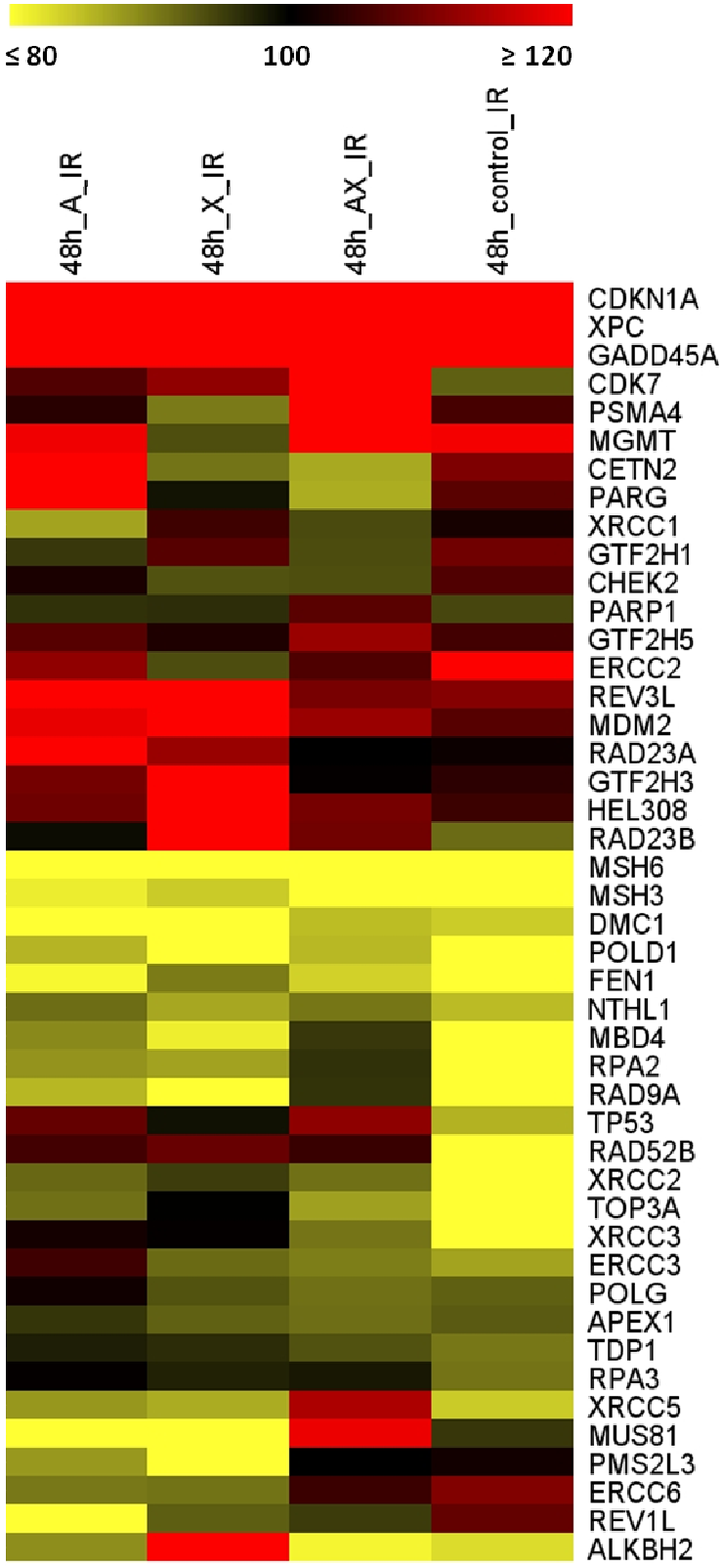

Figure 3.23. Gene expression changes in silenced cells 48 h after transfection and additional treatment with ionizing radiation. All DNA repair genes which showed a reduction in the gene expression by ≤ 80 % (bright yellow) or an increase ≥ 120 % (bright red) compared to to mock-irradiated silenced cells (here controls) in either one of the treatments are displayed. Mock-irradiated silenced cells were used as a reference sample. Gene names are indicated. **48h_A_IR.** *APEX1* siRNA transfected cells. **48h_X_IR.** *XRCC1*. siRNA transfected cells. **48h_AX_IR.** DKO cells. **48h_control_IR.** Control siRNA transfected cells.

3.2.13.3 Comparison of DNA repair pathways obtained 24 and 48 h of silencing

In all four different samples, the IR-inducible genes *CDKN1A*, *XPC*, and *GADD45A* were up-regulated after 24 h and after 48 h. In contrast, several other down-regulated genes were not altered in their expression pattern after 48 h. In *APEX1*-silenced cells, it was *MSH6*. In *XRCC1* knockdown cell, *PMS2L3*, *RAD9A*, and *MSH6* were still silenced. DKO cells revealed *ALKB2H* as a gene which is still down-regulated after 48 h. In the controls, *POLD1* and *MSH6* showed a reduced expression even after 48 h.

3.2.14 Challenging BER with temozolomide leads to growth inhibition in *XRCC1* deficient cells

Ionizing radiation of cells causes a heterogeneous pattern of DNA damage which is not necessarily or only partly processed by BER. As it was seen in the gene expression patterns of silenced cells, several other pathways can be up-regulated after DNA damage induction through irradiation. These pathways may repair lesions which are normally thought to be repaired via BER.

In order to induce more specifically DNA lesions to be repaired via BER, *APEX1* and *XRCC1*-silenced cells were treated with temozolomide (TMZ) and analyzed for their dose-response curves.

Temozolomide is a potent DNA methylating agent. In cells, the drug is rapidly converted to the highly reactive methyldiazonium ion. This ion causes methylation of bases with three major products: N^7-methylguanine (65-80 %), O^6-methylguanine (8 %), and N^3-methyladenine (9 %). N^7-methylguanine accounts for most of the lesions, but it is less toxic than O^6-methylguanine, which is responsible for the cytotoxic effect of TMZ. O^6-methylguanine incorrectly pairs with thymine during replication, which leads to cell death or C:G to T:A transitions. Moreover, TMZ can induce G2/M arrest and apoptosis. The most important DNA repair systems to repair the lesions caused by TMZ are the MMR, O^6-methylguanine-DNA-methyltransferase (*MGMT*), and BER (206;207).

First, dose-response curves were determined for the individually silenced cells. As shown in Figure 3.24, increasing concentrations of temozolomide inhibit silenced cell in a dose-dependent manner. IC_{50}-values were estimated and are shown in Table 3.6. *APEX1*- and

XRCC1-silenced cells appeared to be more sensitive, but as the standard deviations of the particular data points overlap, the difference was not considered to be significant.

Table 3.6. IC_{50} values calculated from dose-response curves

	APEX1 siRNA	*XRCC1* siRNA	DKO	Control siRNA
IC_{50} [µM/L]	668	775	822	795

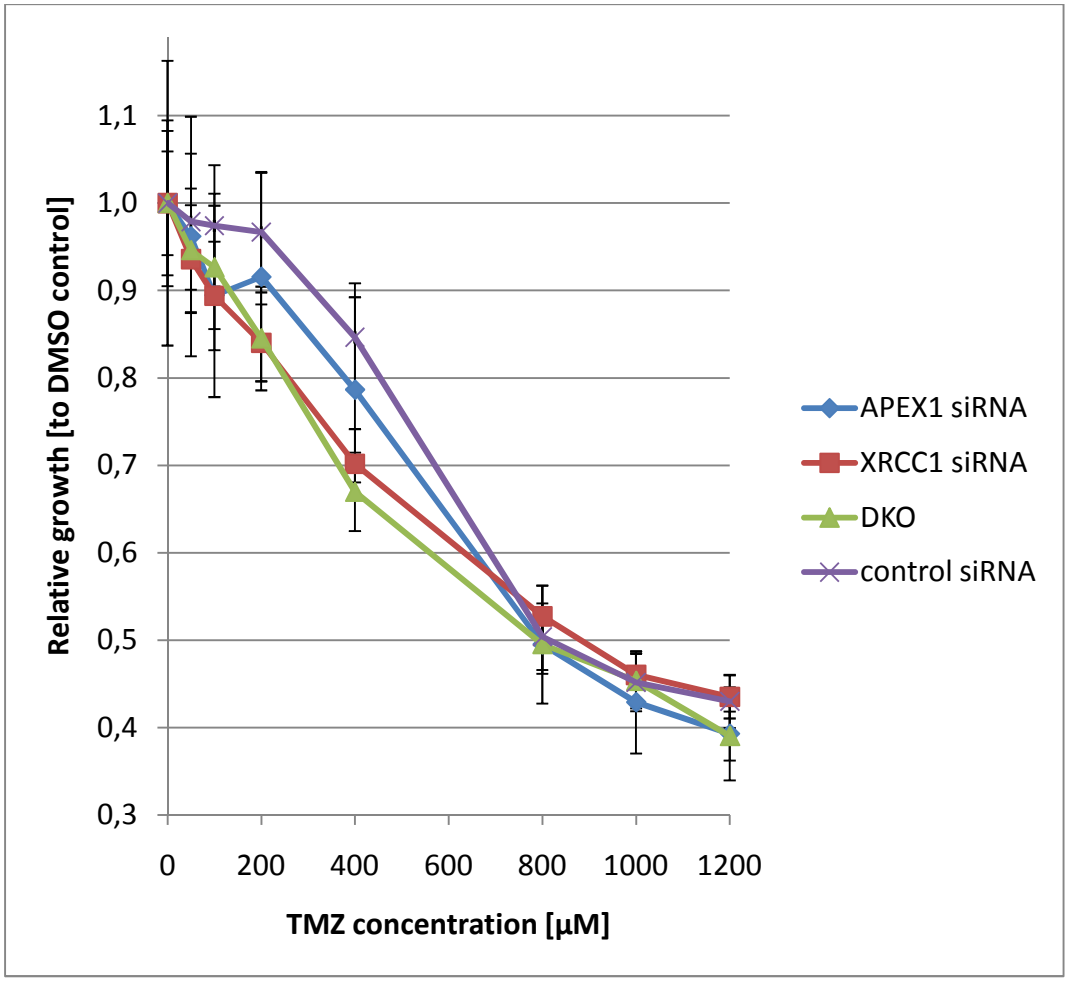

Figure 3.24. Silenced cells showed no difference in their growth behavior 72 h after temozolomide treatment. Growth curves were determined with the SRB assay in a 96-well format. Three days after transfection cells were treated with varying concentrations of temozolomide for 72 h subsequent to fixation. Results are shown as mean ± SD from two independent experiments with eight replicates each.

To further elucidate the effect of the knockdown and the temozolomide treatment on cell growth, silenced cells were treated with a temozolomide concentration of 775 µM, and cell growth was monitored over 16 days. The concentration represents the average of the IC_{50}-values calculated in Table 3.6.

The *XRCC1* knockdown showed a strong inhibition of cell growth, whereas the *APEX1* siRNA transfected cells showed no inhibition compared to controls. Silencing both genes caused a growth inhibition comparable with the *XRCC1* knockdown alone (Figure 3.25). The differences in growth capability after knockdown and temozolomide treatment were not visible before day ten after transfection.

To conclude, in the first part of the experiment, the cells were fixed and stained six days after transfection, but at least ten days are necessary to detect any difference regarding growth inhibition after tranfection of the cells with the siRNAs and after an additional treatment with TMZ. Between days ten and sixteen, the growth curves of the individually transfected cells clearly showed a separation. The *XRCC1* siRNA treated cells showed a significantly reduced growth capability compared to controls. The growth inhibition was similar for the DKO cells. *APEX1*-silenced cells displayed no growth inhibition compared to controls.

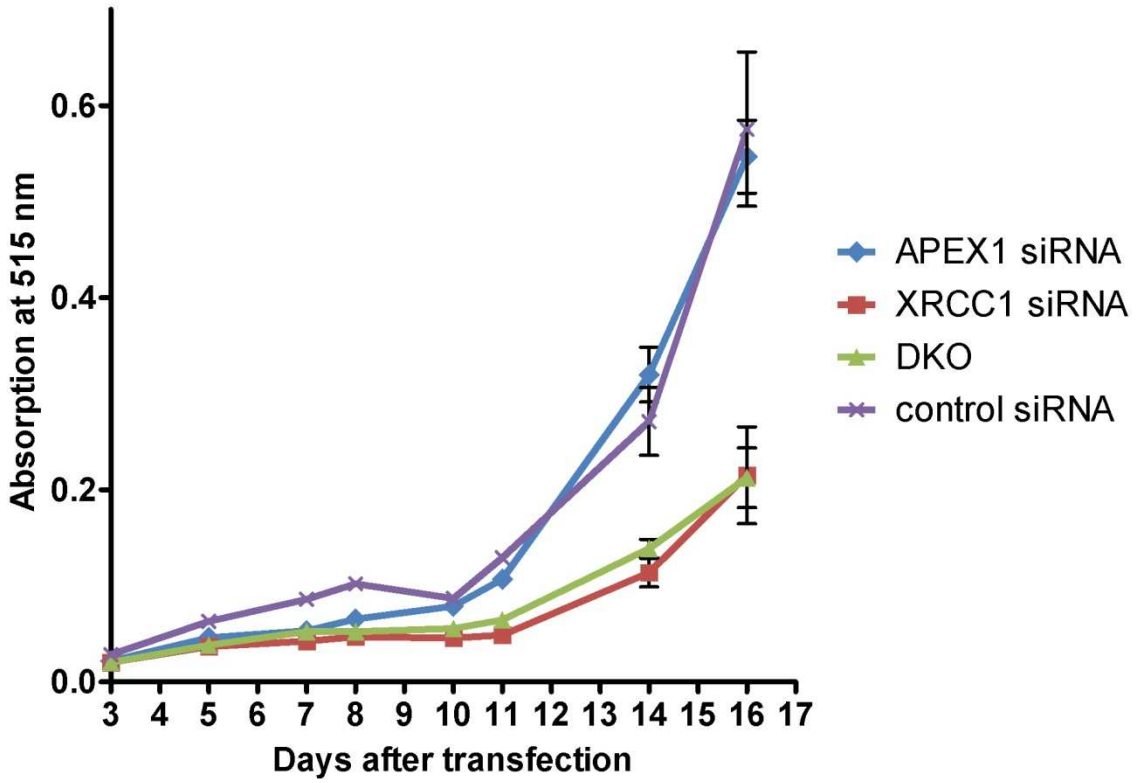

Figure 3.25. *XRCC1* deficient cells showed an inhibition in cell growth after temozolomide treatment. Growth curves were determined with the SRB assay in a 96-well format. Three days after transfection, cells were treated with 775 µM temozolomide for 72 h following media replacement. Cells were cultivated up to 16 days after transfection. Media was replaced every four days. Results are shown as mean ± SEM from eight replicates.

3.3 Investigations in HMEpC

3.3.1 Strong inhibition of *APEX1* after transfection with 100 nM *APEX1* siRNA

The optimized transfection conditions were applied to the HMEpC to reduce the expression of *APEX1* on mRNA and protein level. Luciferase was used as the negative control. In order to verify the efficient silencing 24, 48, and 72 h after *APEX1* siRNA treatment, the expression of *APEX1* was determined by using qRT-PCR.

The expression of *APEX1* on mRNA level was strongly reduced to 5 % compared to control values 24 h after transfection. The efficient silencing was still detectable after 48 h (11 %) and after 72 h (7 %) (Figure 3.26.A).

On protein levels, only a minor decrease was determined 24 h after transfection. The greatest silencing of the protein was found after 72 h with a reduction of 43 % (Figure 3.26.B).

A.

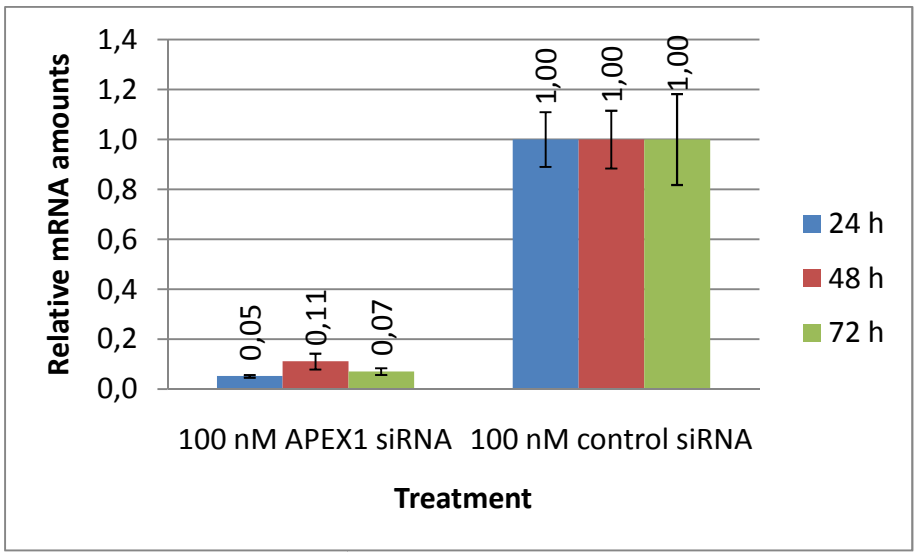

B.

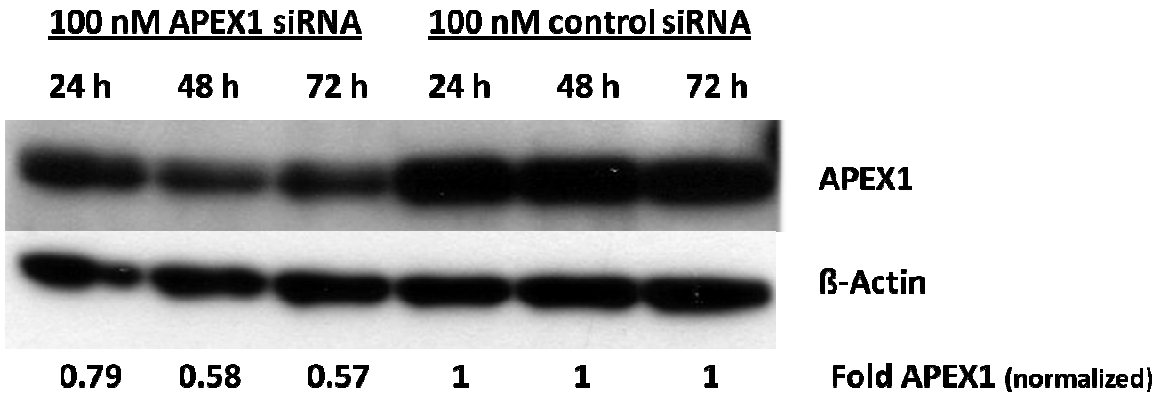

Figure 3.26. *APEX1* knockdown in MCF7 cells 24, 48, and 72 h after transfection with siRNA. A. Relative quantification of *APEX1* mRNA expression by real time PCR on LightCycler 480 after reverse transcription. TBP was used as a reference. Results are shown relative to controls. Means and standard errors are given for three independent treatments. **B.** Representative western blots which demonstrate the APEX1 protein levels in silenced and control samples. β-Actin was used as a reference. Quantitative analysis of the protein reduction after *APEX1* silencing [fold change to controls].

3.3.2 *XRCC1* mRNA is strongly reduced in its expression after silencing of the gene

The *XRCC1* gene was down-regulated in exponentially growing HMEpC to analyze the knockdown of the *XRCC1* gene on both the mRNA and protein level 24, 48, and 72 h after transfection. Luciferase siRNA was used as the negative control.

As shown in Figure 3.27.A, the expression of *XRCC1* was reduced by 80 % 24 h after transfection with 100nM *XRCC1* siRNA and by 82 % after 48 h. The reduction in the gene expression remained for at least 72 h.

On the protein level, a decrease up to 48 % was observed 24 h after transfection and to 41 % after 48 h. Here, the strongest decrease in protein amounts was found. However, 72 h after treatment, the protein expression slightly increased up to 47 % of control amounts (Figure 3.27.B).

A.

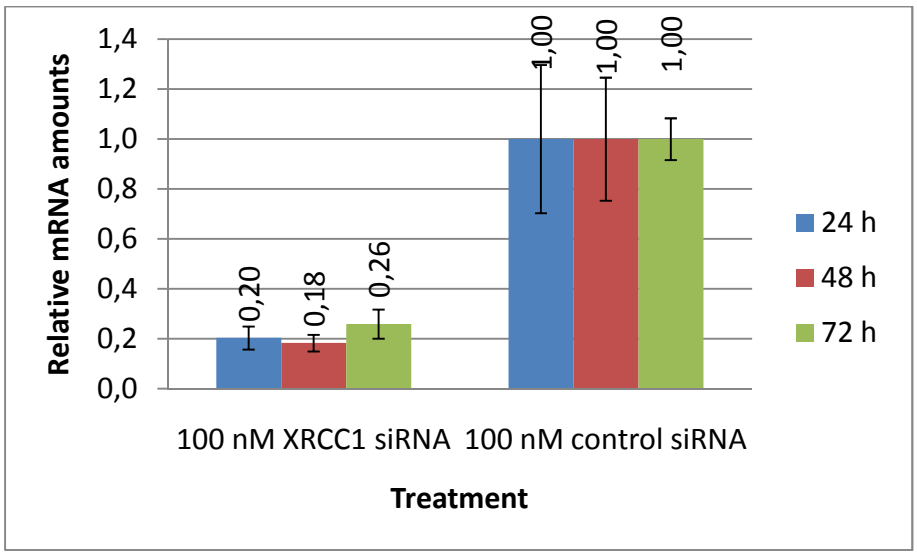

B.

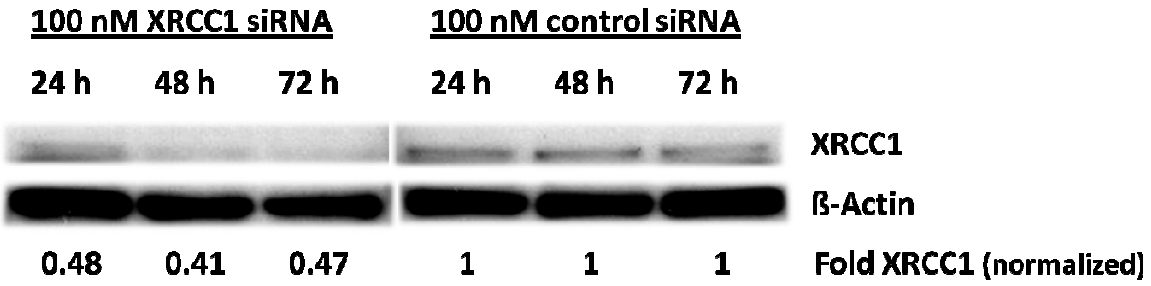

Figure 3.27. *XRCC1* expression in MCF7 cells after transfection with 100 nM *XRCC1* siRNA. A. Relative quantification of *XRCC1* mRNA expression by real time PCR after reverse transcription. TBP was used as a reference. Results are shown relative to controls. Means and standard errors are given for three independent treatments. **B.** Western blot analysis of XRCC1 protein levels in lysates of MCF7 cells transfected with 100 nM *XRCC1* siRNA for 72 h. β-Actin was used as a reference. Quantitative analysis of the protein reduction after *XRCC1* silencing [fold change to controls].

3.3.3 Double knockdown of *APEX1* and *XRCC1* leads to reduced mRNA and protein levels of both genes

In the next experiment, the silencing of the two genes at the same time was elucidated in a time-dependent manner. To confirm the knockdown of *APEX1* and *XRCC1*, the expression of the gene was verified both at mRNA and protein level 24, 48, and 72 h after transfection.

Again each gene was targeted with a concentration of 50 nM of the set of four siRNA. The concentration of every single siRNA duplex was 12.5 nM respectively. Non-targeting siRNA was used as control.

Both genes were highly reduced in their mRNA expression (Figure 3.28.A). The decrease in mRNA levels was detectable at least 72 h. At various times after transfection, the cultures were sampled to assay for APEX1 and XRCC1 expression by immunoblotting. After 72 h, the APEX1 protein was reduced to 14 % and the XRCC1 protein to 48 % (Figure 3.28.B).

A.

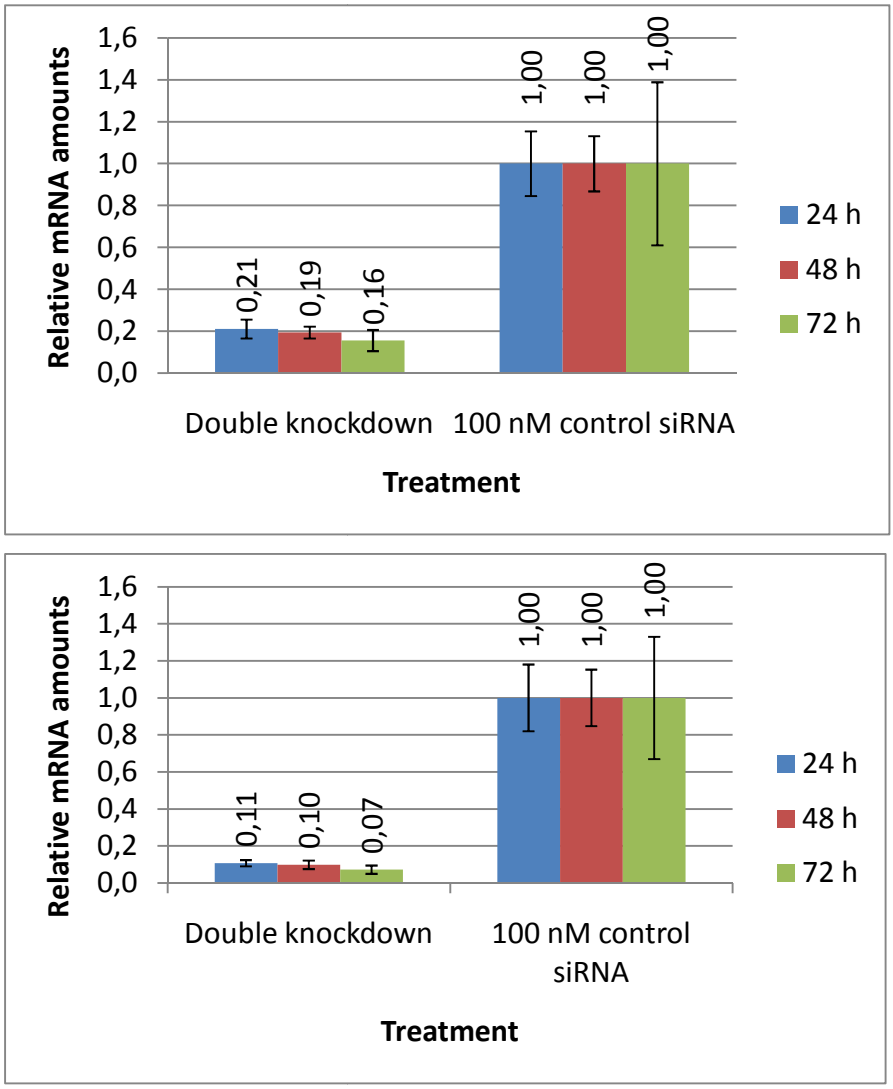

B.

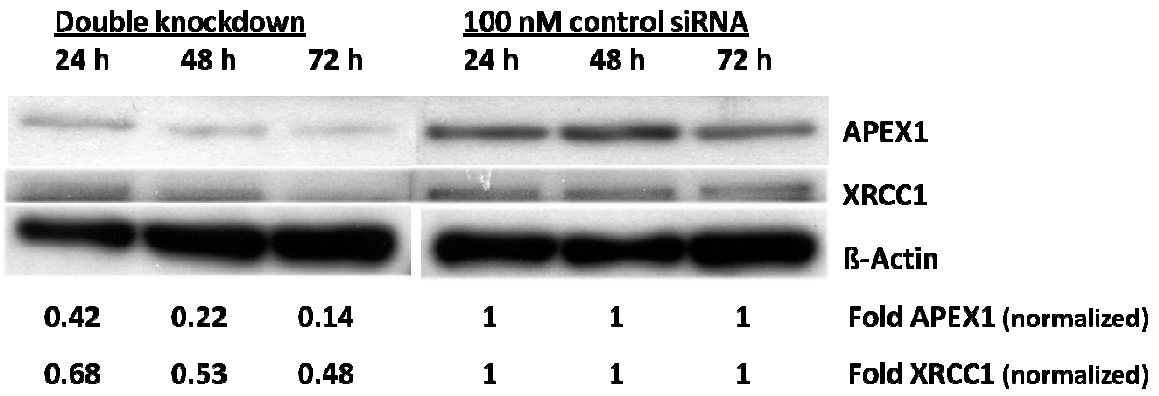

Figure 3.28. Double knockdown in MCF7 cells 24, 48, and 72 h after transfection with siRNA. A. Quantitative real-time RT-PCR analysis of *APEX1* and *XRCC1* mRNA levels in total RNA of MCF7 cells transfected with 100 nM siRNA (50 nM *APEX1* siRNA and 50 nM *XRCC1* siRNA) for the indicated period of time. TBP was used as a reference. Results are shown relative to control. Means and standard errors are given for three independent treatments. **B.** APEX1 and XRCC1 protein levels in silenced cells and controls analyzed by western blot. β-Actin was used as the reference. Reduction of the protein after silencing [fold change to controls].

These results show that the transfection with siRNA which targets either *APEX1* or *XRCC1* or both causes a transient but efficient reduction of the mRNA amount. Already 24 h after transfection, the knockdown was determined to be very high. The decrease of the mRNAs was consistent for at least 72 h.

On protein levels the silencing was not as effective as it was on mRNA levels. In cells where either *APEX1* or *XRCC1* was silenced, the protein amounts were only decreased to around 50 % compared to controls after 72 h. In cells where both genes were silenced simultaneously, the APEX1 protein was strongly reduced by more than 86 %. In contrast, the XRCC1 protein was reduced by only 52 %.

3.3.4 Growth characteristics are not influenced after silencing

To determine whether the silencing of *APEX1* and *XRCC1* influences the growth of HMEpC, a time course of the growth characteristics of silenced cells was measured with the SRB assay.

The plating efficiency was not evaluated due to the special growth characteristics of the primary cells. These cells do not form proper colonies and show a more or less loose and scattered cell assembly pattern during cultivation as compared to MCF7 cells (Figure 3.29). Consequently, growth characteristics were detected with the SRB assay as a powerful technique to determine growth characteristics of cells as validated for MCF7 (see 3.2.4).

A. **B.**

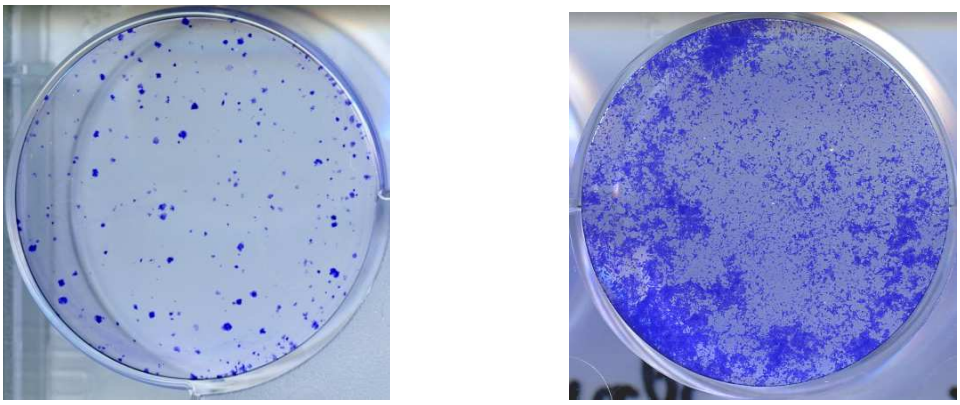

Figure 3.29. Colony-forming ability. Cells were seeded in 96-well plates with a density of 1000 cells/well and incubated for 6 population doubling times. Cells were fixed and stained with crystal violet. **A.** MCF7 **B.** HMEpC.

In the SRB assay, treatment of the cells with *APEX1* and/or *XRCC1* siRNA showed no significant inhibition of cell growth compared to controls between days 3 and 10 after transfection (Figure 3.30.B). The silencing of the genes after transfection was verified on mRNA levels and showed a strong reduction of target mRNA amounts (Figure 3.30.A).

These results demonstrate that the down-regulation of *APEX1* and *XRCC1* does not influence the growth and proliferation capability of HMEpC cells.

A.

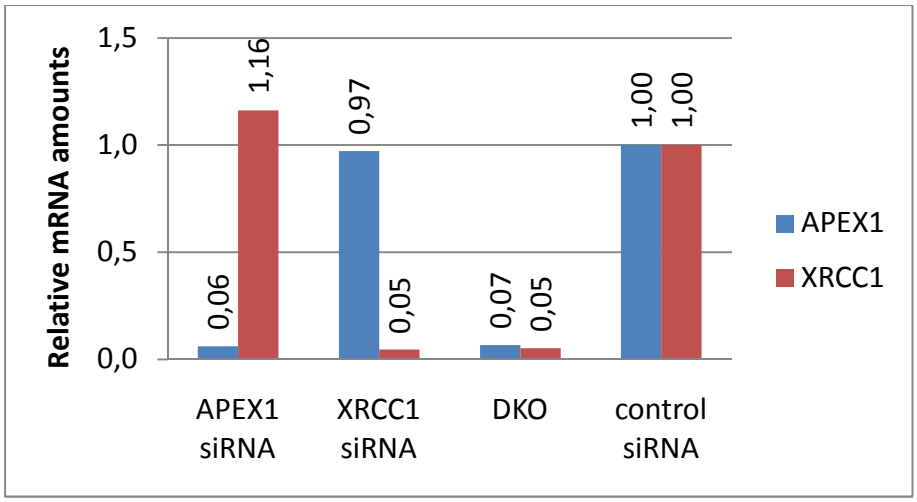

B.

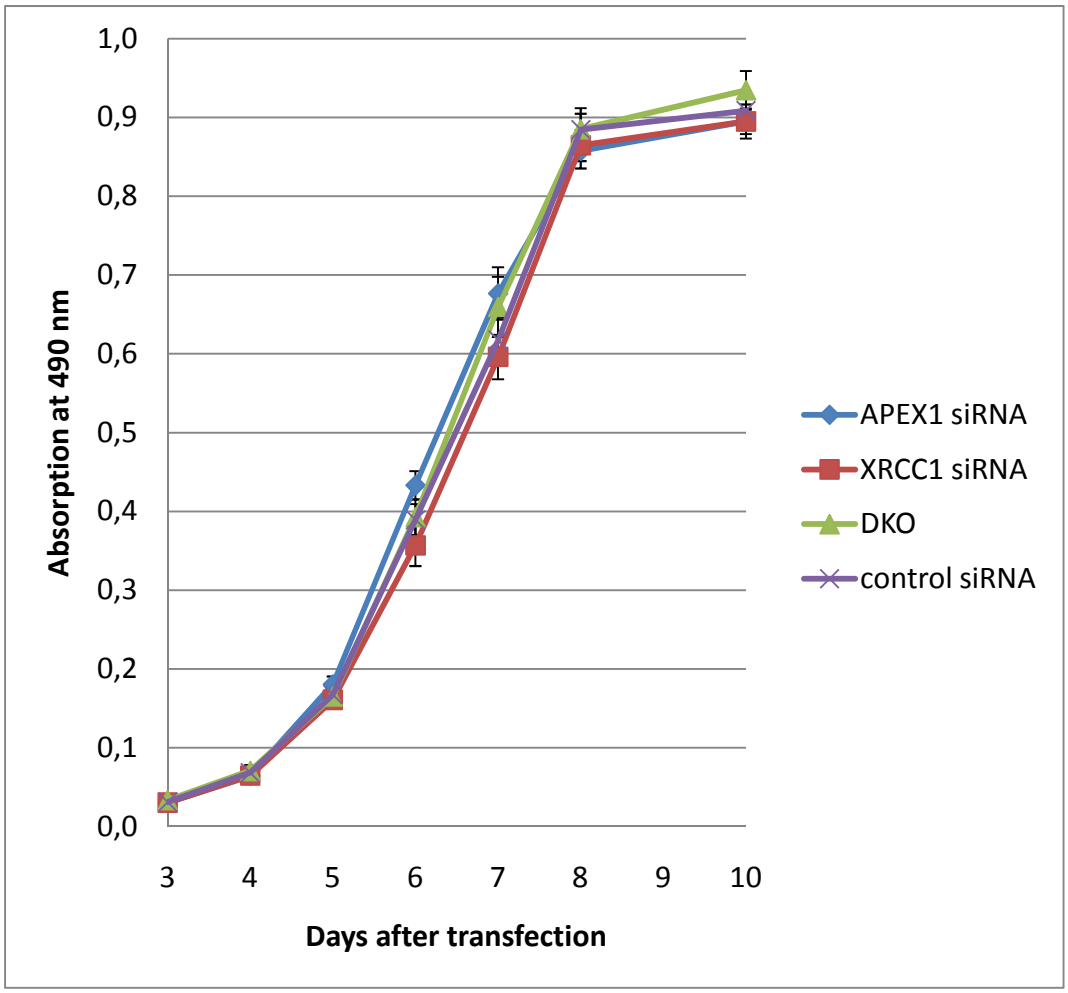

Figure 3.30. No alteration of growth characteristics after transfection with *APEX1* or *XRCC1* siRNA. A. Relative quantification of *APEX1* and *XRCC1* expression at mRNA level by real time PCR 72 h after transfection. **B.** Growth curves were obtained with the SRB assay. The results are expressed as mean ± SD from two experiments with 16 replicates each.

3.3.5 Investigations of gene expression patterns after silencing

To identify genes which show expression changes as a consequence of the silencing of *APEX1* or *XRCC1* or both, the gene expression patterns of silenced cells and controls were compared 24 h and 48 h after transfection by using the Sentrix HumanRef-8 Expression BeadChips.

The gene lists were analyzed for differentially expressed genes which share common functions or which show a common involvement in different pathways. For this analysis the Ingenuity Pathway Analysis Software was used. Here, again, a gene was considered to be differentially expressed when the expression fold change was greater than 2.

To determine the knockdown of the target genes *APEX1* and *XRCC1* 24 h and 48 h after transfection, the mRNA amounts were measured with qRT-PCR. The mRNA levels of the genes were highly decreased 24 h and 48 h after transfection (Figure 3.26.A, 3.27.A, and 3.28.A).

3.3.5.1 Pathway analysis 24 h after silencing of *APEX1*, *XRCC1* and DKO

The silencing of *APEX1* in HMEpC cells caused an induction of immune response pathways. Further, several functions seemed to be deregulated in following categories: DNA replication, recombination and repair, cell death, cellular growth and proliferation; and cell cycle (Figure 3.31).

Only four genes were differentially expressed in *XRCC1*-silenced cells (Table 3.7). The *IFI6* gene, which is induced by interferon, was up-regulated. This indicates the activation of an immune response in the cell.

In DKO cells, the silencing was specific for *APEX1* and *XRCC1*. Only *MX1* was co-down-regulated.

Table 3.7. Genes with expression changes ≥ 2 fold after silencing of *APEX1*, *XRCC1*, and DKO in HMEpC.

Regulatory effect of silencing (compared to controls)	Number of regulated genes (up-/down-regulated)	Fold change (min-max)
APEX1	10 (1/9)	0.10-2.20
XRCC1	4 (2/2)	0.45-2.63
DKO	3 (0/3)	0.31-0.48

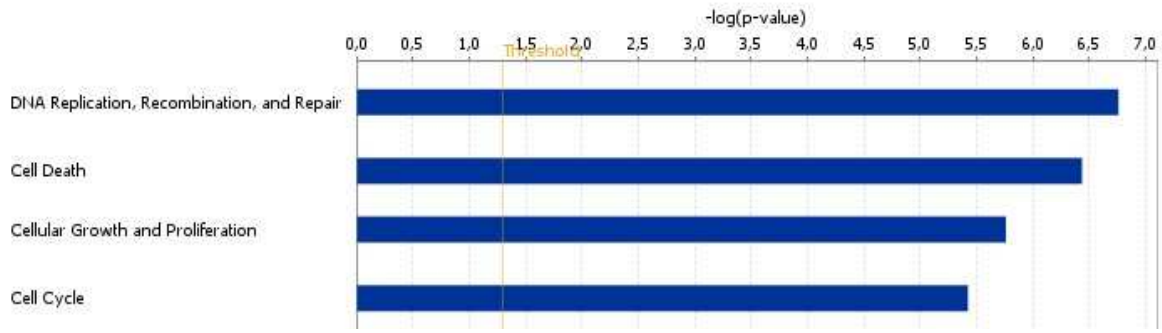

Figure 3.31. Biological functions affected after silencing of *XRCC1*. The blue bars represent the p-value. The yellow line designates the threshold with $p < 0.05$.

3.3.5.2 Pathway analysis 48 h after silencing of *APEX1*, *XRCC1,* and DKO

In *APEX1*-silenced cells, a down-regulation of 17 genes which are involved in several pathways of the immune response was determined (Figure 3.32.A).

The silencing of *XRCC1* resulted in a large amount of differentially expressed genes in 24 different pathways. Pathways with a significant p-value are shown in Figure 3.32.B. The genes of the pathway mismatch repair in eukaryotes were up-regulated, whereas the genes of the other pathway were down-regulated. Several amino acid metabolizing pathways were affected after silencing of *XRCC1*. The large amount of genes led to a manifold deregulation of biological processes (Figure 3.33).

In DKO cells, the silencing was specific for *APEX1.* The fold change of *XRCC1* was 0.59. However, the reduced expression of *XRCC1* was confirmed with qRT-PCR. The *ZNF91* gene was up-regulated (Table. 3.8).

Table 3.8. Genes with expression changes ≥ 2 fold induced 48 h after silencing.

Regulatory effect of silencing (compared to controls)	Number of regulated genes (up-/down-regulated)	Fold change (min-max)
APEX1	17 (0/17)	0.12-0.50
XRCC1	111 (61/50)	0.29-8.29
DKO	2 (1/1)	0.28-2.22

A.

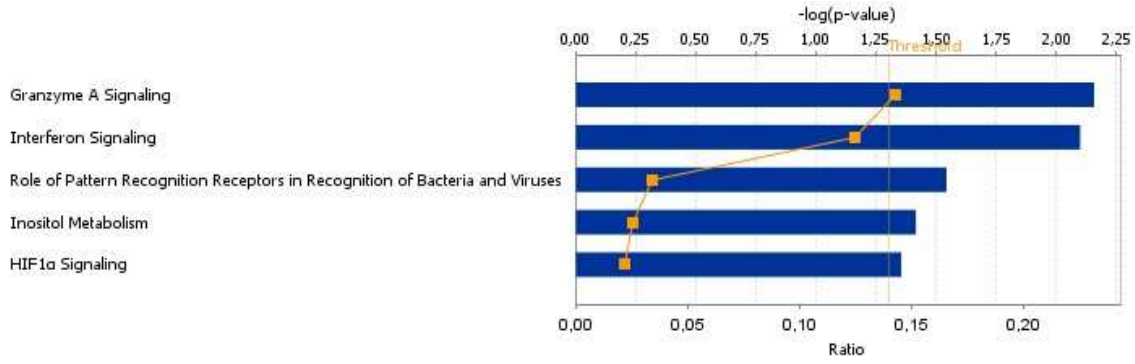

B.

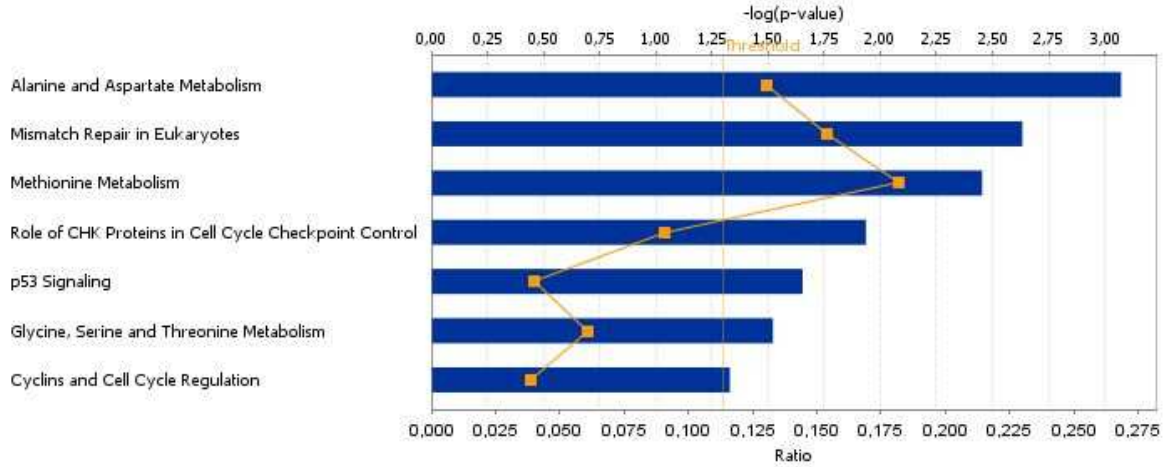

Figure 3.32. Pathway analysis of gene regulation in silenced cells 48 h after transfection. The significance of the association between the dataset and the identified pathway is represented by the ratio (yellow line with data points) and the p-value (blue bars). The ratio is calculated as the number of molecules in a given pathway that meet cutoff criteria, divided by the total number of molecules that make up that pathway. The p-value is calculated by Fisher's exact test to determine the probability of the association between the genes in the dataset and the pathway due to chance. The threshold indicates a significance of $p < 0.05$. **A.** *APEX1*-silenced cells. **B.** *XRCC1*-silenced cells.

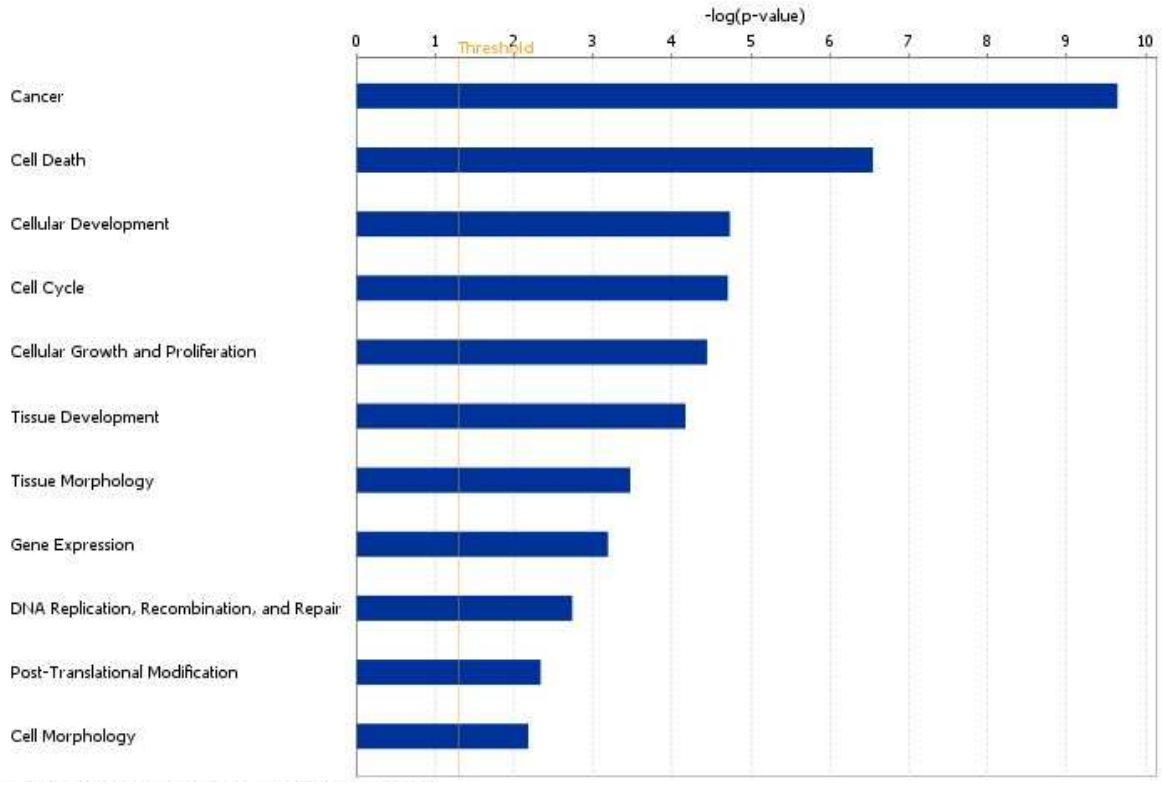

Figure 3.33. Biological functions affected 48 h after silencing of *XRCC1*. The blue bars represent the p-value. The yellow line designates the threshold with $p < 0.05$.

3.3.6 Gene expression changes of DNA repair genes

This part of the results focuses on changes in the gene expression pattern of DNA repair genes as it was done for the MCF7 cells. Gene lists were sorted according to Wood *et al.* (60). A gene was considered to be differentially expressed when the p-value was less than 0.05, the fold change was ≥ 1.2 or ≤ -1.2, and the mean average expression intensity was greater than 100 in either sample.

3.3.6.1 *XRCC1*-silenced cells show multiple changes in their gene expression pattern 24 h after transfection

APEX1 siRNA treated cells showed a highly specific silencing of the *APEX1* gene by 10 fold compared to control. The *GADD45A* gene was co-down-regulated. The DNA polymerase *REV1L* was up-regulated in its expression (Figure 3.34).

In *XRCC1* siRNA treated cells, a large number of differentially expressed genes was detected. Next to *XRCC1*, mainly NER-related (*CDK7*, *CETN2*, *CCNH*, and *GTF2H5*) and MMR genes (*PMS2L3* and *MSH6*) were co-silenced. The polymerase subunit *POLD1*, *RAD23A*, *MGMT*, *SALL3*, and *XAB2* showed an increased expression compared to controls.

In DKO cells, the silencing of *APEX1* and *XRCC1* was accompanied by *POLD1*, *CDK7* (NER) and *EME2* (HR). The genes *MSH3* (HR) and *TDP1* were up-regulated.

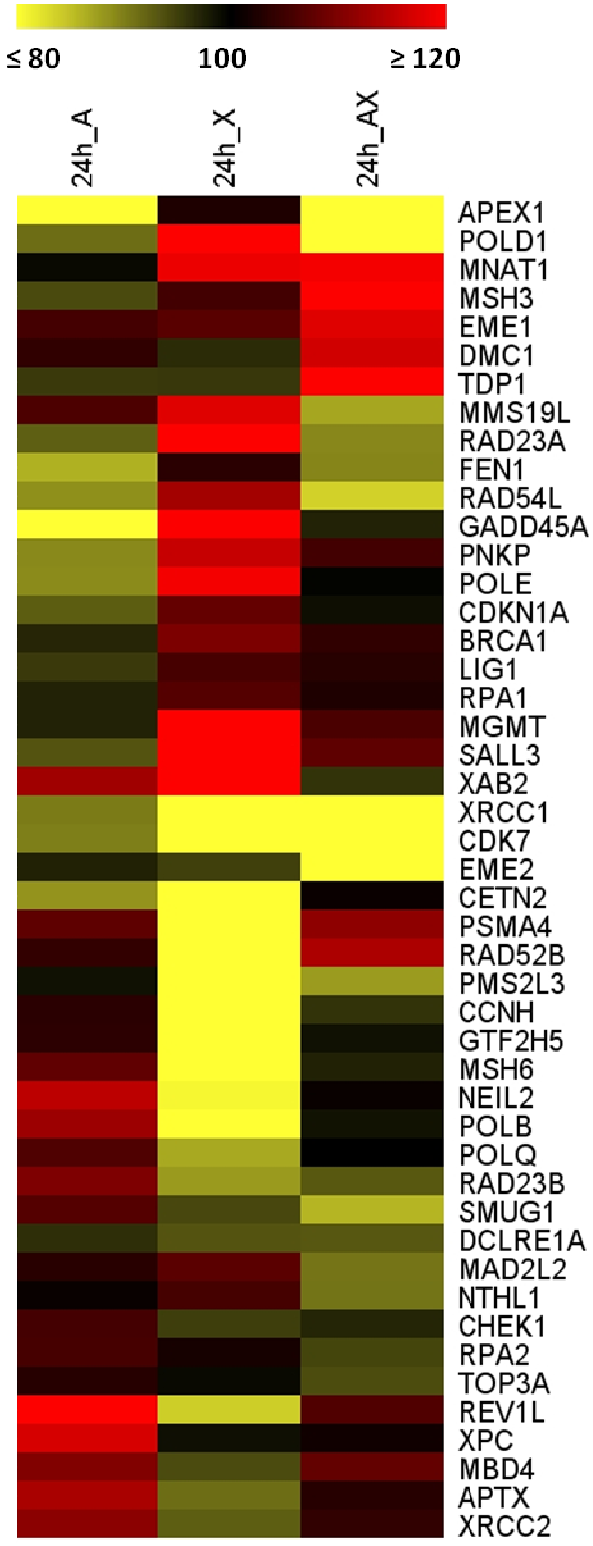

Figure 3.34. Gene expression changes in silenced cells 24 h after transfection All DNA repair genes which showed a reduction in the gene expression by ≤ 80 % (bright yellow) or an increase ≥ 120 % (bright red) compared to controls in either one of the treatments are displayed. Control siRNA transfected cells were used as a reference. The gene names are indicated. **24h_A.** *APEX1* siRNA transfected cells. **24h_X.** *XRCC1*. siRNA transfected cells. **24h_AX.** DKO cells.

3.3.6.2 Several genes are differentially expressed 48 h after transfection

In *APEX1*-silenced cells, the knockdown affected HR where three genes (*MUS81*, *DMC1*, and *XRCC2*) were co-down-regulated. Interestingly, three other BER genes were enhanced in their expression. These were *XRCC1*, *NTHL1*, and *SMUG1*. Further, *GTF2H*, *MNAT1* (NER), X*AB2* (NER-related), *POLD1, POLM*, *RAD9*, and *BRCA1* (HR) were up-regulated.

Treatment with *XRCC1* siRNA resulted in a strong decrease of *XRCC1.* Moreover, silencing *XRCC1* resulted in a co-silencing of several other DNA repair genes. HR was affected with four genes (*DMC1*, *RAD54L*, *SHFM1*, and *XRCC3*), NER with six genes (*LIG1*, *RPA3*, *RPA2*, *GTF2H5*, *CETN2*, and *RPA1*) and three DNA damage response genes (RAD9A, CHEK1, and UBE2N). In addition, PCNA and several DNA polymerases such as *POLQ*, *POLG*, and *POLE* were decreased in their expression levels. In contrast, *APEX1* and *NEIL2* (both BER), MUS81 (HR), CCNH (NER), and ALKBH3 showed a higher expression pattern compared to the reference. Additionally, the normally IR-inducible genes *GADD45A*, *CDKN1A*, and *XPC* showed a higher expression level.

The DKO cells showed only little changes in their gene expression levels of DNA repair genes. The silencing of *APEX1* and *XRCC1* initiated a down-regulation of *RAD54L* (HR), *FEN1*, *RAD1*, *RECQL*, and *POLQ*. *SALL3* and *EME2* (HR) were over-expressed (Figure 3.35).

3.3.6.3 Comparison of changes in the DNA repair pathways 24 h and 48 h after knockdown

More DNA repair genes were differentially expressed 48 h after silencing compared to the 24 h point of time.

In *XRCC1*-silenced cells, *GADD45A* was still up-regulated after 48 h. *CETN2*, *GTF2H5*, and *MSH6* remained silenced after 48 h. But some genes showed a different expression pattern. *POLD1* and *POLE* were up-regulated after 24 h showed a reduced expression after 48 h. In contrast, *CCNH* and *NEIL2* silenced after 24 h were up-regulated after 48 h.

In DKO, *EME2* were reduced in its expression after 24 h and became up-regulated after 48 h.

Besides these results, each silencing caused a distinctive pattern of deregulated DNA repair pathway. This pattern changed after 48 h.

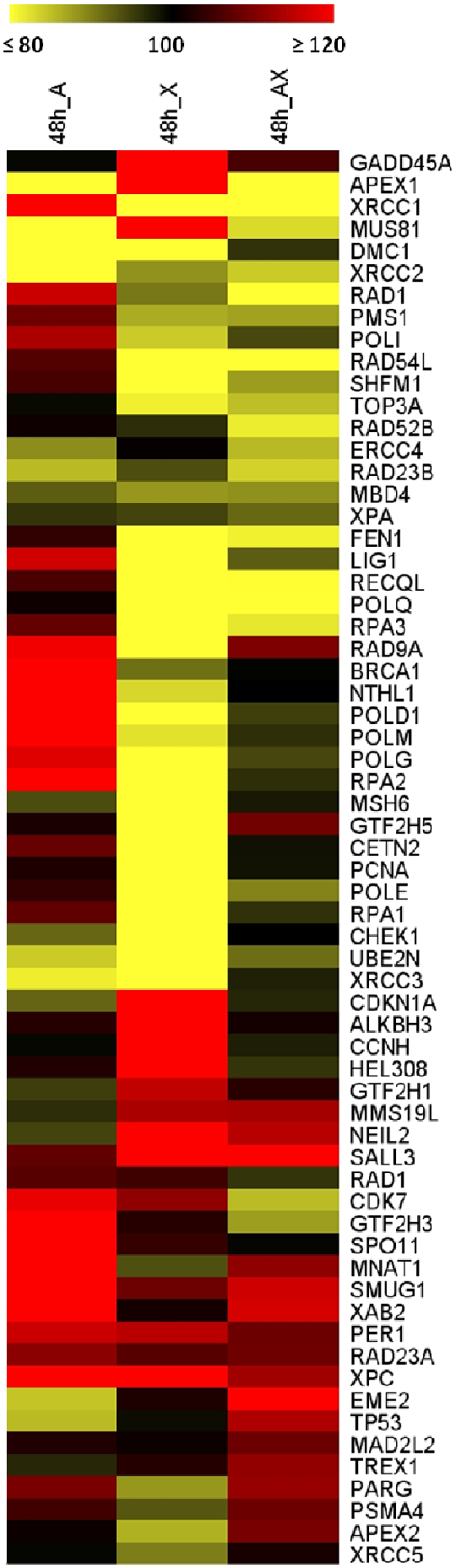

Figure 3.35. Gene expression changes in silenced cells 48 h after transfection All DNA repair genes which showed a reduction in the gene expression by ≤ 80 % (bright yellow) or an increase ≥ 120 % (bright red) compared to controls in either one of the treatments are displayed. Control siRNA transfected cells were used as a reference. The gene names are indicated. **48h_A.** *APEX1* siRNA transfected cells. **48h_X.** *XRCC1*. siRNA transfected cells. **48h_AX.** DKO cells.

3.3.7 Expression levels of *APEX1* and *XRCC1* are strongly reduced at the time of irradiation in the functional assays

To determine the impact of the knockdown on radiosensitivity, the irradiation treatment and the functional investigations were performed 72 h after transfection when mRNA and protein levels were strongly reduced. Global gene expression patterns were determined in silenced cells 24 and 48 h after transfection and after additional treatment with IR. Quantitative RT-PCR showed that the mRNA levels of *APEX1* and *XRCC1* were strongly reduced as compared to controls at the time of irradiation.

Table 3.9 summarizes the mRNA expression levels of silenced cells in the corresponding functional experiment at the time of irradiation.

Table 3.9. Relative mRNA levels of APEX1 and XRCC1 in silenced cells obtained in functional analyses at the time of irradiation. Values are normalized to the control.

	APEX1 mRNA (*APEX1*-silenced cells)	*XRCC1* mRNA (*XRCC1*-silenced cells)	*APEX1*/*XRCC1* mRNA (DKO cells)
CFA/SRB assay	0.05	0.03	0.06/0.05
Comet assay	0.06	0.05	0.07/0.05
γH2AX assay	0.10	0.17	0.16/0.15
Expression profiling 24 h	0.06	0.14	0.17/0.12
Expression profiling 48 h	0.09	0.17	0.19/0.11

3.3.8 Radiosensitivity of cells is not affected after silencing of *APEX1* and *XRCC1* and subsequent treatment with varying doses of IR

In order to investigate the effect of the knockdown of *APEX1* and *XRCC1* on radiosensitivity, silenced cells were irradiated with increasing doses of ionizing radiation. The survival curves were determined with the SRB assay, which was shown to be as useful as the CFA assay for the research on radiotherapy interactions in cell lines (191). In our experiments with MCF7 cells, the results of both assays were comparable (see 3.2.8).

Irradiation of the cells affected the survival in a dose-dependent manner. Higher irradiation doses caused less survival. The inhibition of expression of *XRCC1* or *APEX1* or both did not affect the radiosensitivity of the cells compared to controls as determined with the SRB assay (Figure 3.36).

A.

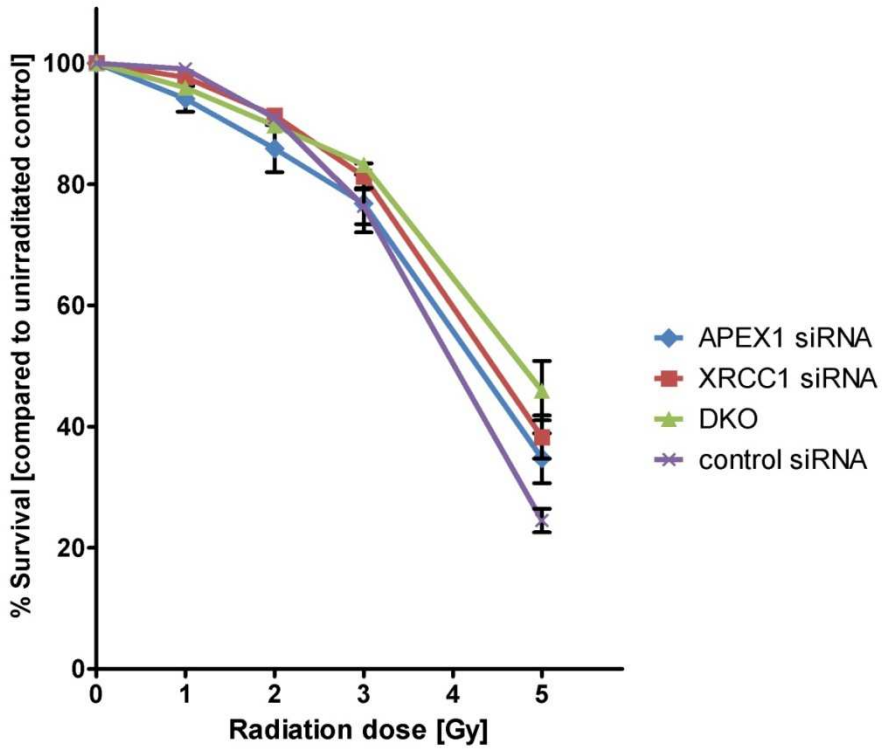

Figure 3.36. Effect of the silencing on radiosensitivity and on response to IR. A. Radiation dose-survival curves were determined with the SRB assay. Means ± SD are from sixteen replicates.

Ionizing radiation caused an induction of p53 response genes as measured by the induction of *CDKN1A* mRNA expression levels. Silencing of *APEX1* and *XRCC1* did not alter the p53 response (Figure 3.37). However, the response was not as strong as seen in MCF7 cells.

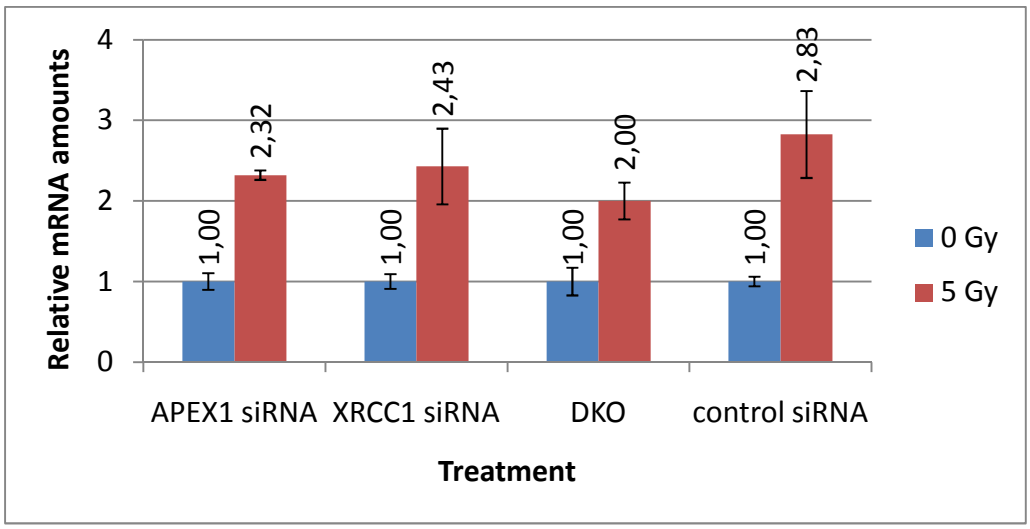

Figure 3.37. p53 response after irradiation. Cells were mock-irradiated or irradiated with 5 Gy 24 h after transfection. *CDKN1A* expression was measured four hours after irradiation. Normalized values are shown as mean ± SD from three replicates.

3.3.9 Reduced protein levels of APEX1 and XRCC1 do not influence the initial damage induction

To investigate whether a reduced BER capacity caused by down-regulation of *APEX1* and/or *XRCC1* results in a difference in the initial amount of DNA damage, silenced cells were assayed for their DNA repair ability after irradiation with 5 Gy by the comet assay. Non-targeting siRNA was used as negative control. The irradiation of silenced cells caused a large amount of SSBs immediately after irradiation. Almost all SSBs were repaired within the first ten minutes.

No difference was observed in the initial damage induction and in repair rates between silenced cells and controls (Figure 3.38).

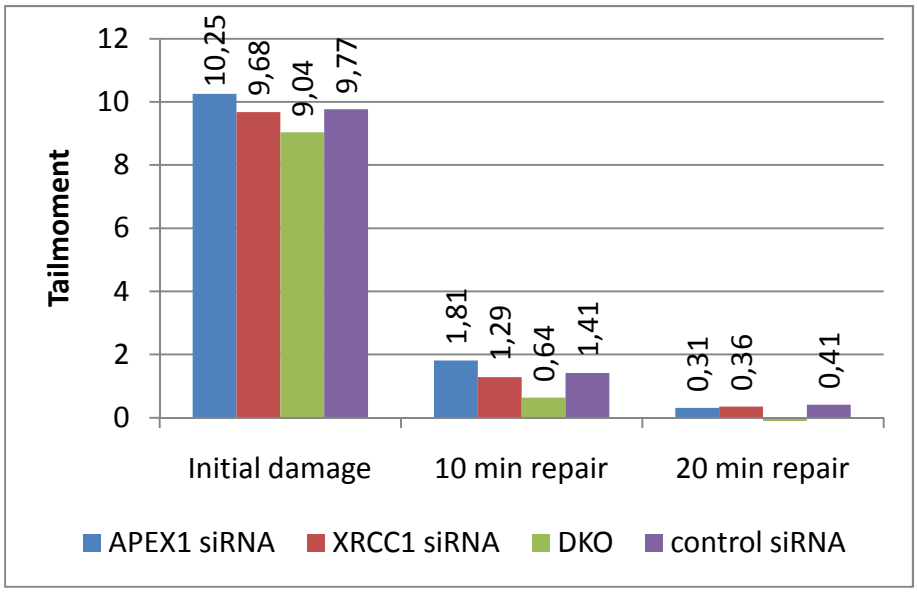

Figure 3.38. Residual damage after irradiation. A. Relative quantification of *APEX1* and *XRCC1* expression at mRNA level by real time PCR at the time of irradiation. **B.** *APEX1* and *XRCC1* siRNA treated cells were irradiated with 5 Gy, and alkaline comet assay was carried out. Tailmoment distributions were determined by scoring at least 102 cells per sample. Distributions were determined for non-irradiated cell, and irradiated cells directly, 10 minutes and 20 minutes after irradiation. Values of the non-irradiated cells are subtracted from values of the irradiated cells. Values are expressed as the median.

3.3.10 Formation of γH2AX foci is not affected after knockdown of *APEX1* and *XRCC1*

To determine the induction of DSBs after treatment with IR, the formation of γH2AX foci was detected in silenced cells by using a specific antibody which binds to the phosphorylation site of the H2AX variant.

The irradiation of silenced cells caused a strong induction of DSBs. Silencing *APEX1* and/or *XRCC1* did not significantly affect the amount of DSBs determined 30 minutes after irradiation. No difference was observed comparing the repair rates determined after zwo hours in silenced cells. (Figure 3.39).

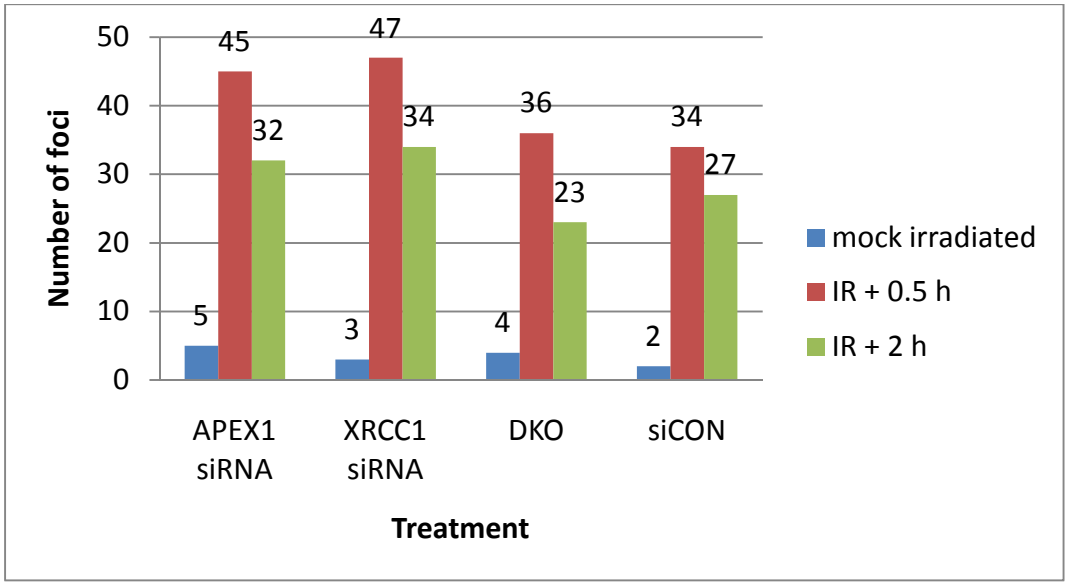

Figure 3.39. Inhibiting the expression of *APEX1* and *XRCC1* by siRNA has no influence on the repair of DSB. Cells were mock-irradiated or irradiated with a single dose of 5 Gy 72 h after transfection. Cells were fixed 0.5 and two hours after irradiation and stained for γH2AX foci and DNA. At least 150 nuclei were evaluated for each treatment. Results are expressed as the median.

3.3.11 Gene expression patterns after transfection and additional irradiation

In order to investigate the effect of ionizing radiation on the gene expression pattern of silenced cells, exponentially growing MCF7 cells were transfected with either *APEX1* or *XRCC1* siRNA or both. Cells were mock-irradiated or irradiated with 5 Gy 72 h after transfection and further incubated for four hours.

As shown in Table 3.9, silenced cells showed a strong reduction in target gene mRNA levels four hours after irradiation.

3.3.11.1 Pathway analysis 24 h after transfection and additional irradiation

The radiation response genes, which normally show an increased expression after treatment with IR, were not among the hit lists after the sorting. This was due to the minor increase in gene expression after irradiation. None of the radiation response genes had an increase in their expression level ≥ 2 fold. This was also observed in the global gene expression levels 48 h after silencing.

However, in *APEX1*-silenced cells, only the two genes *CDC14B* and *GDF15* were induced in their expression. They could not be assigned to any pathway, but *CDC14B* is involved in cell cycle control and regulates the function of p53. *GDF15* is a member of the transforming growth factor-beta superfamily. These are multifunctional proteins that regulate proliferation, differentiation, adhesion, migration, and other functions in many cell types.

In *XRCC1*-silenced cells, 20 genes were differentially expressed. Two immune response pathways, the Granzyme A Signaling and the IL-8 Signaling, were affected after irradiation. Moreover, the metabolism of xenobiotics became deregulated by the strong induction of *CYP1B1* (Figure 3.40). Eighteen genes which have function in several biological processes like cell cycle, DNA replication, and cell growth and proliferation were down-regulated (Figure 3.41).

In DKO cells, four genes were differentially expressed. *KPNA2, NOLA1*, and *CDC14B* were down-regulated, whereas the *TP53INP1* gene was induced upon irradiation treatment.

Irradiation of controls resulted in an over-expression of *GDF15* and *TP53INP1*.

Table 3.10. Genes with expression changes ≥ 2 fold after irradiation.

Regulatory effect of silencing (compared to controls)	Number of regulated genes (up-/down-regulated)	Fold change (min-max)
APEX1	2 (2/0)	2.05-2.61
XRCC1	20 (2/18)	0.39-2.90
DKO	4 (1/3)	0.35-2.11
Control siRNA	2 (2/0)	2.09-2.19

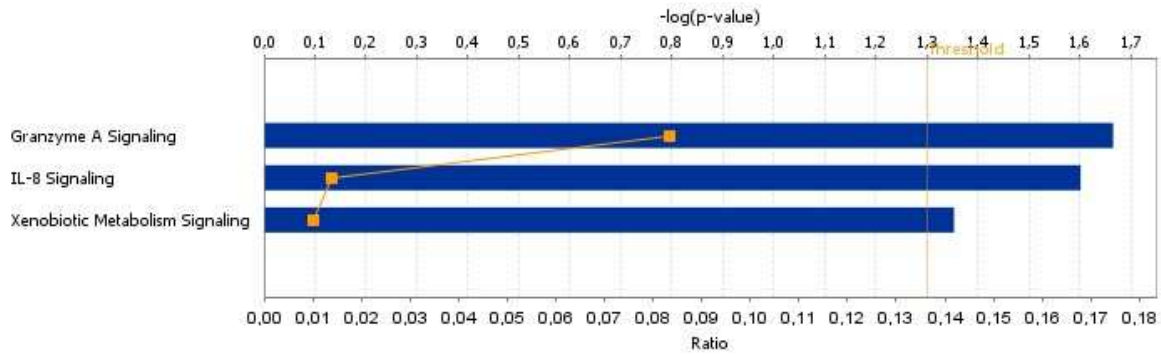

Figure 3.40. Pathway analysis of radiation-induced gene regulation in *XRCC1*-silenced HMEpC. The significance of the association between the dataset and the identified pathway is represented by the ratio (yellow line with data points) and the p-value (blue bars). The ratio is calculated as the number of molecules in a given pathway that meet cutoff criteria, divided by the total number of molecules that make up that pathway. The p-value is calculated by Fisher's exact test to determine the probability of the association between the genes in the dataset and the pathway due to chance. The threshold indicates a significance of $p < 0.05$.

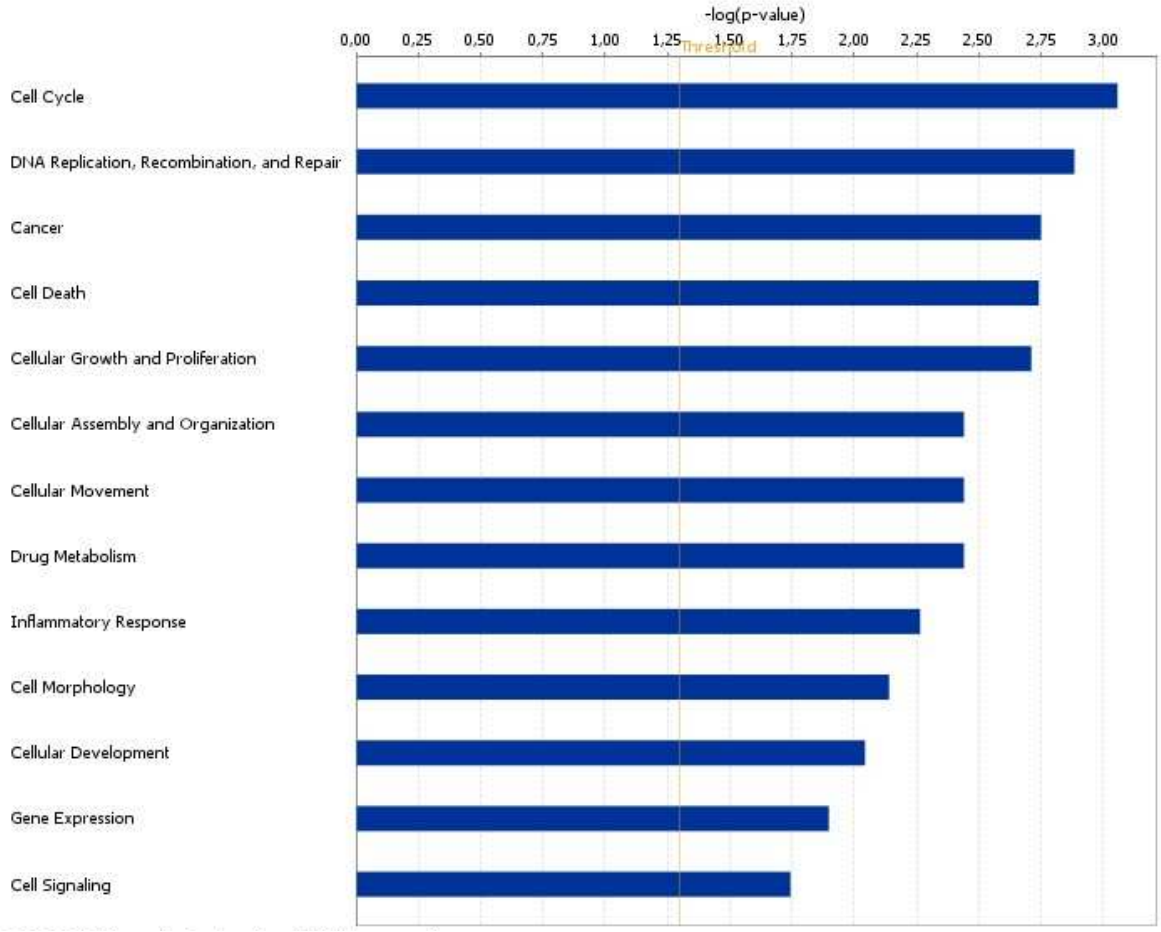

Figure 3.41. Analysis of biological functions in *XRCC1*-silenced cells four hours after irradiation. Blue bars represent the p-value. The yellow line designates the threshold with $p < 0.05$.

3.3.11.2 Pathway analysis 48 h after transfection and additional irradiation

In *APEX1*-silenced cells, four genes got differentially expressed after irradiation treatment. These were *GDF15*, *IFI6*, *IFI27*, and *MX1*, which suggested a deregulation of immune response pathways. The functions of *GDF15* have already been explained (see 3.3.11.1).

Irradiation of *XRCC1*-silenced cells resulted in a large amount of regulated genes. 202 genes were differentially expressed in more than 19 different canonical pathways. Most of them indicated a down-regulation of the IL-8-signaling pathways, but also the p53- and the ATM-signaling were affected (Figure 3.42). These genes have implications in around 60 biological processes. Cancer, cell death, cell cycle, and cellular growth and proliferation were among the most significant processes (Figure 3.43.A).

In DKO cells, irradiation caused an enrichment of seven genes involved in immune response signaling. Several processes were affected, among them cellular movement, cell morphology, and cell signaling (Figure 3.43.B).

The controls showed exactly the same pattern of up-regulated genes as the DKO. This resulted in the same deregulation pattern of pathways and functions. Two genes were down-regulated after irradiation, *BUB1* and *ANGPTL4*.

Table 3.11. Genes with expression fold changes ≥ 2 determined 48 h after silencing and additional treatment with IR.

Regulatory effect of silencing (compared to controls)	Number of regulated genes (up-/down-regulated)	Fold change (min-max)
APEX1	4 (4/0)	2.07-3.88
XRCC1	202 (73/129)	0.06-3.30
DKO	7 (7/0)	2.01-3.79
Control siRNA	8 (6/2)	0.45-4.35

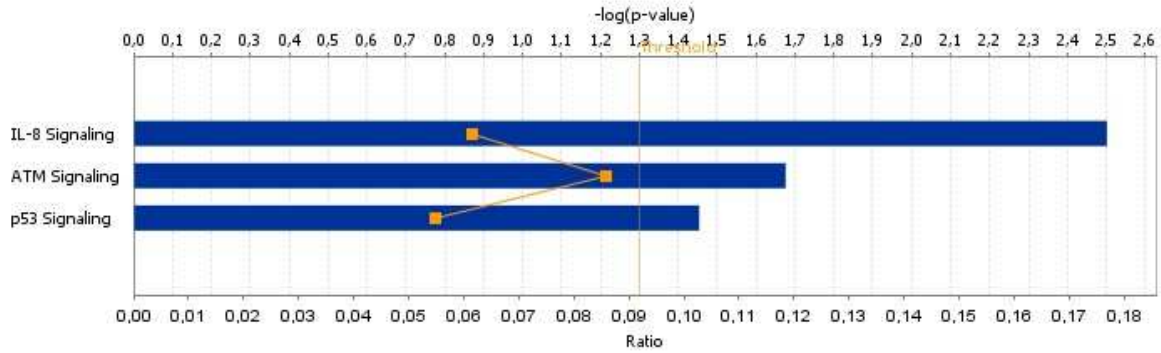

Figure 3.42. Pathway analysis of radiation-induced gene regulation in *XRCC1*-silenced HMEpC cells 48 h after transfection. (see Figure 3.41 for figure legend).

A.

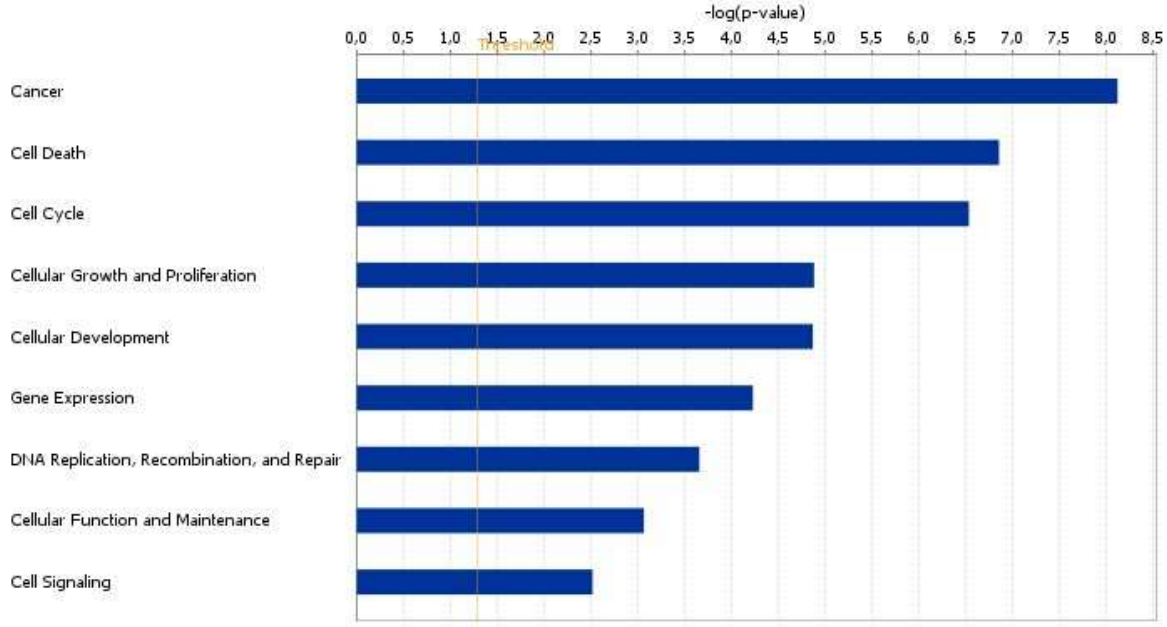

B.

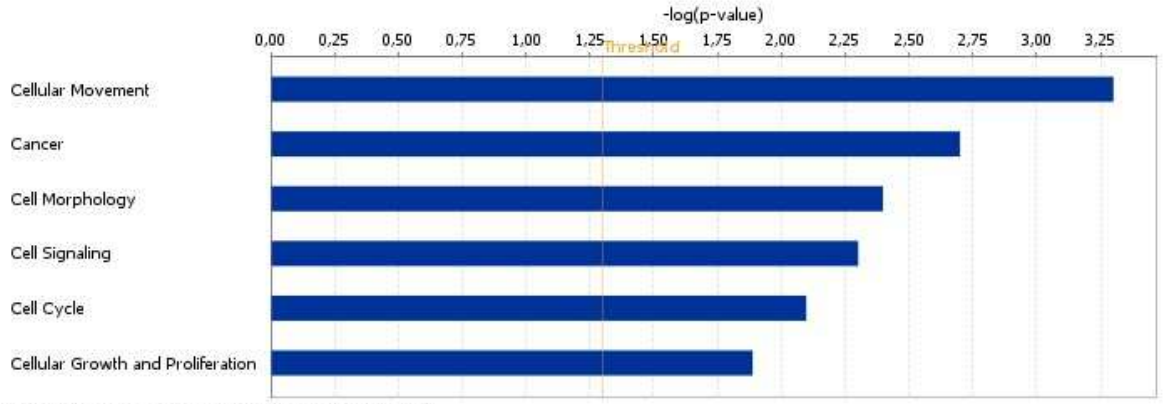

Figure 3.43. Deregulated functions in HMEpC 48 h after transfection and irradiation treatment. **A.** *XRCC1*-silenced cells. **B.** DKO cells.

3.3.12 Changes in DNA repair pathways

3.3.12.1 Silencing of target genes in HMEpC and additional treatment with IR causes large changes in the gene expression pattern of DNA repair genes

The irradiation increased the expression of IR-inducible genes like *CDKN1A*, *GADD45A*, and *XPC* (NER) in *APEX1*-silenced cells and controls. In *XRCC1*-silenced cells, *CDKN1A* and *GADD45A* were induced after irradiation. In DKO cells, only *XPC* was up-regulated (Figure 3.44).

Changes of DNA repair genes in the control sample were evaluated first. The evaluation of the BER-deficient samples focused only on the differences compared to the controls.

The examination of the expression patterns in irradiated controls showed that the NER gene, *RAD23B*, was up-regulated whereas three NER genes (*CCNH*, *RPA1*, and *RPA2*) showed a reduced expression. Moreover, *EME2*, *DMC1*, and *RAD54L* (HR), *SMUG1* (BER), *MSH6* (MMR), and *TOP3A* showed a reduced expression.

In *APEX1* down-regulated cells, the BER gene *PNKP* and the NER genes *MNAT1* and *LIG1* were co-up-regulated. *NEIL2* (BER) showed a decreased expression.

The most deregulated gene expression pattern was detected in *XRCC1*-silenced cells. *APTX*, *RAD52B PSMA4* and the NER genes *CETN2* and *CCNH* were up-regulated after treatment with IR. 16 genes were reduced in their expression. These genes are involved in several DNA repair pathways: *XRCC2* and *BRCA1* (HR); *RAD23A* (NER); *MSH3* and *MSH6* (MMR); and *MBD4* (BER). Also, three DNA Polymerases were found to be decreased in their expression: *POLE*, *MAD2L2*, and *POLQ*.

Cells transfected with *APEX1* and *XRCC1* siRNA showed a strong up-regulation of NER and NER-related genes after irradiation: *LIG1* and *CDK7* (NER), *XAB2* and *MMS19L* (NER-related). In contrast, the HR gene *EME1*, the *DCLRE1A* gene, the MMR gene *MSH3*, and the BER gene *NTHL1* were expressed to a lesser extent.

In sum, these results demonstrate that *XRCC1* siRNA treatment shows the strongest effect both after knockdown and after additional treatment with IR. In *XRCC1*-silenced cells, the gene expression pattern of DNA repair genes becomes strongly deregulated.

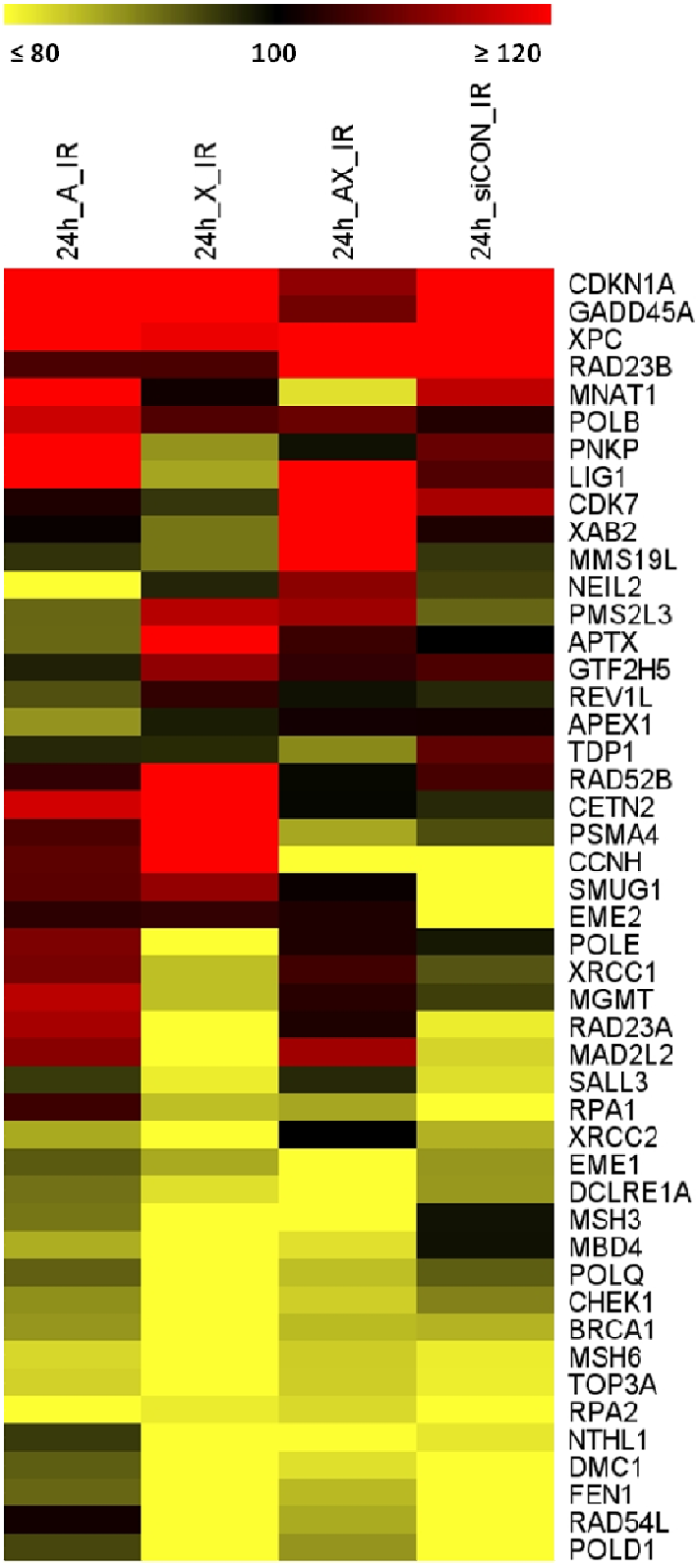

Figure 3.44. Gene expression changes in silenced cells 24 h after transfection and additional treatment with ionizing radiation. All DNA repair genes which showed a reduction in the gene expression by ≤ 80 % (bright yellow) or an increase ≥ 120 % (bright red) compared to mock-irradiated silenced cells (here controls) in either one of the treatments are displayed. Mock-irradiated silenced cells were used as a reference sample. Gene names are indicated. **24h_A_IR.** *APEX1* siRNA transfected cells. **24h_X_IR.** *XRCC1* siRNA transfected cells. **24h_AX_IR.** DKO cells. **24h_control_IR.** Control siRNA transfected cells.

3.3.12.2 Irradiation of silenced cells leads to a deregulation of genes of several DNA repair pathways 48 h after transfection

The irradiation of siRNA treated cells affected again the p53 response genes which were increased in their expression after treatment with ionizing radiation. The genes *CDKN1A* and *XPC* were induced in *APEX1* siRNA, DKO, and control siRNA samples. In *XRCC1*-silenced cells, only *CDKN1A* was up-regulated in its expression. Furthermore, *GADD45A* was induced in the controls (Figure 3.45).

Little changes were observed in the irradiated controls. *PER1* (DNA damage response) and *POLE* showed a reduced expression, whereas *PARG*, *XAB2* (NER), and *SMUG*1 (BER) were decreased in their expression compared to the mock-irradiated sample.

The irradiation of *APEX1*-silenced cells caused an up-regulation of *UBE2N* (RAD6 pathway), *DMC1,* and *XRCC2* (HR) and a strong up-regulation of genes involved in NER (*RAD23B*, *GTF2H3*, *ERCC4*, *XPA*, and *GTF2H1*). Two BER genes (*XRCC1* and *NTHL1*), *MNAT1* (NER), and three DNA polymerases (*POLD1*, *POLM*, and *POLI*) showed a reduced expression.

In *XRCC1* siRNA treated cells, most genes were up-regulated. These perform functions in multiple DNA repair pathways like BER (*NTHL1*, *APEX2*, and *MBD4*), NER (*RPA2*, *GTF2H5*, *LIG1*, *RAD23B*, *RPA1*, and *CCNH*), HR (*XRCC2*, *SHFM1*), MMR (*MSH6* and *PMS1*), and NHEJ (*XRCC5*). Other up-regulated genes were *UBE2N*, *FEN1*, *RAD9A*, *TREX1*, *PSMA4*, *RAD1*, *RECQL*, *TOP3A,* and *PCNA*. Some NER genes (*XPC*, *CDK7*, *RAD23A*, and *MMS19L*), *TP53,* and *GADD45A* showed a reduced expression compared to the mock-irradiated silenced sample.

In DKO cells, again, an up-regulation of NER genes was observed as it had been for the *XRCC1*-silenced cells. These were *RAD23B*, *GTF2H3*, *ERCC4*, *CDK7*, and *CCNH*. Further, *RAD52B*, *HEL308*, and *RAD1* were increased in their expression. Two BER genes, *APEX2* and *NEIL2*, were found to be down-regulated.

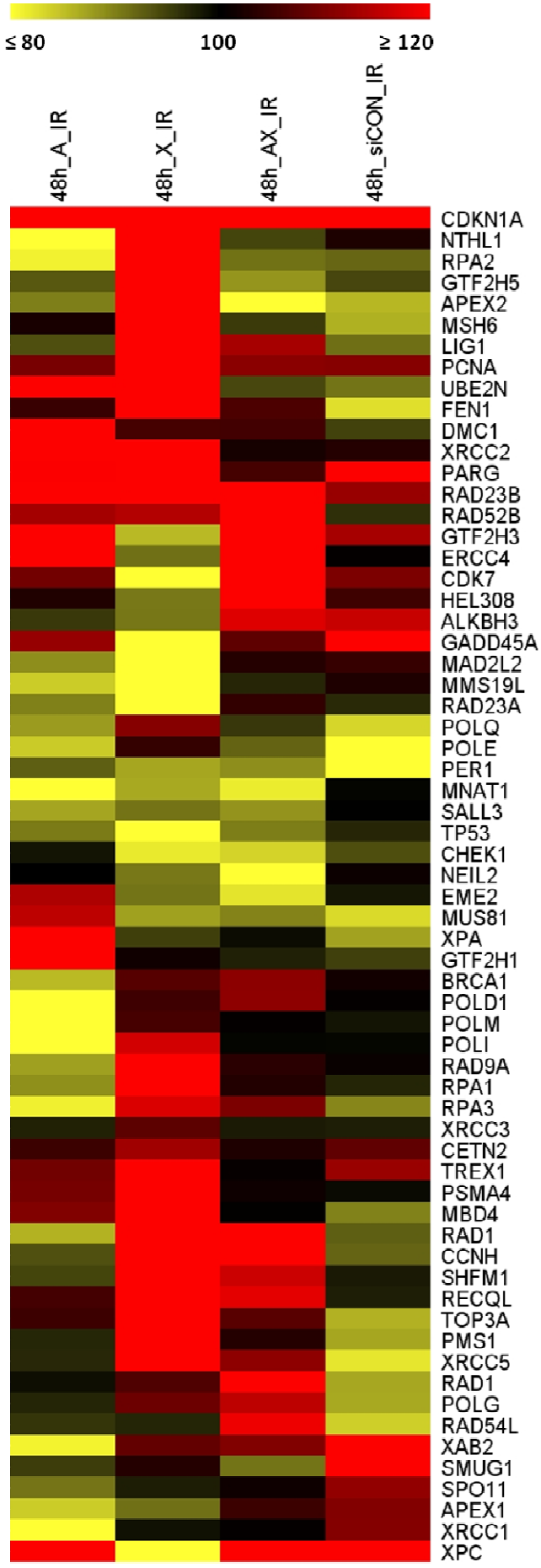

Figure 3.45. Gene expression changes in silenced cells 48 h after transfection and additional treatment with ionizing radiation. All DNA repair genes which showed a reduction in the gene expression by ≤ 80 % (bright yellow) or an increase ≥ 120 % (bright red) compared to to mock-irradiated silenced cells (here controls) in either one of the treatments are displayed. Mock-irradiated silenced cells were used as a reference sample. Gene names are indicated. **48h_A_IR.** *APEX1* siRNA transfected cells. **48h_X_IR.** *XRCC1* siRNA transfected cells. **48h_AX_IR.** DKO cells. **48h_control_IR.** Control siRNA transfected cells.

3.3.12.3 Comparison of DNA repair pathways obtained 24 and 48 h after transfection and additional treatment with IR.

The expression patterns of the IR-inducible genes were the same after 24 h and after 48 h with only one exception. In *XRCC1*-silenced cells, the *GADD45A* genes induced after 24 h showed a decreased expression after 48 h.

Further, in *XRCC1*-silenced cells, *PSMA4*, *CCNH* (both increased), *RAD23A*, and *MAD2L2* (both decreased) showed the same expression pattern. A contrary expression pattern was determined for *XRCC2*, *MBD4*, *MSH6*, *TOP3A*, *NTHL1*, and for *FEN1*, which were down-regulated after 24 h and became up-regulated after 48 h.

Such genes were also found in the other treatments. In DKO cells, *CCNH*, and in the controls, *SMUG1* showed a similar pattern.

4 Discussion

In this research project, we investigated the impact of a reduced *APEX1* and/or *XRCC1* expression on cell growth, cellular radiosensitivity and survival, DNA damage induction, and on the global and DNA repair gene expression before and after irradiation. Gene defects were analyzed in two different cell types - the breast adenocarcinoma cell line MCF7 as well as a healthy counterpart, the human mammary epithelial cells HMEpC - in order to differentiate between cancer specific effects and effects unique to healthy cells.

We were the first to investigate the effects of a deficiency in BER in primary healthy cells. Further, we explored the effects of a simultaneous silencing of *APEX1* and *XRCC1* on radiosensitivity. In this study, siRNA treatment effectively reduced *APEX1* and *XRCC1* mRNA by ≥ 80 %.

APEX1 is a multifunctional protein involved in DNA repair and in the activation of transcription factors. Both functions are independent in their actions and are essential for mammalian cells. Through its redox regulatory function *APEX1* can activate transcription factors which modulate gene expression of genes involved in cell cycle arrest, apoptosis, and cell growth. APEX1 is an abundant protein and it is ubiquitously expressed in every tell type. Many tumors over-express the APEX1 protein (108;112).

XRCC1 is a major gene involved in BER. It is a scaffold protein and interacts with many proteins of the BER pathway. Moreover, *XRCC1* has been shown to participate in the repair of SSBs and might modulate the repair of DSBs.

4.1 MCF7

4.1.1 Effects of the knockdown on growth characteristics

In MCF7, reduced levels of *XRCC1* resulted in a significantly reduced plating efficiency compared to controls. *APEX1*-silenced MCF7 showed no difference in plating efficiency. Silencing of both genes resulted in a plating efficiency similar to controls. Moreover, *APEX1* and *XRCC1*-silenced cells showed a significant growth inhibition 10 days after transfection. Again, the DKO had no effect on the growth capability compared to controls. The slower growth induced by silencing of *APEX1* is not a result of the induction of cell death by apoptosis, as flow cytometry revealed an accumulation of cells in G2-M phase of the cell cycle than an increase in apoptotic sub-G1.

The viability of the cells due to reduced levels of *APEX1* or *XRCC1* was not affected for up to 72 h. This result verifies the observation of Lee *et al.* who also showed that the viability of *APEX1* shRNA-treated HaCaT cells is not affected (208).

Several authors have demonstrated an inhibition of cell growth after reduction of the *APEX1* expression (115;124). When it comes to comparing growth characteristics of *APEX1*-silenced cells, our results are consistent with Fishel's and Fung's findings (115;124). However, it is not sure whether the reduced growth in *APEX1*-silenced cells results from the inhibition of the DNA repair function or its redox regulatory function. We did not measure the redox activity of *APEX1*. With regards to the cell's ability to replicate and to form a colony, our result shows no difference in *APEX1*-silenced cells whereas Vascotto *et al.* measured a strong inhibition with the CFA (120).

APEX1 is an important redox activator which induces the DNA binding activity of several transcription factors, such as AP-1, NF-κB, Egr-1, NF-Y, p53, and HIF1α (117;209-213). Many of their target genes are unknown, which makes it difficult to estimate the consequences of the knockdown for global gene expression and the biological relevance in controlling differentiation, proliferation, and apoptosis of cells. Egr-1 is regulated by growth factors and may play a role in growth and differentiation (214). NF-Y interacts with cell cycle genes including cyclin A, *CDC25C*, and *CDK1* and represses the expression of cytochrome p450-dependent monooxygenases (215).

APEX1 was shown to be a modulator of the cell cycle and is, along with other components of BER, physically associated with cell cycle regulatory proteins, cyclin A, and DNA replication proteins (216). The expression of *CDC25B* is regulated by redox signaling. Moreover, *APEX1* is known to regulate cell cycle status in hematopoietic progenitors and G1-S transition in embryonic bodies (125). It is possible that APEX1 regulates *CDC25B* by its redox function and thereby modulates the G2-M transition of MCF7 cells. This would support our findings of an accumulation of cells in the G2-M phase after silencing of *APEX1*.

Analyzing the gene expression patterns of *APEX1*-silenced cells, we could observe a highly specific down-regulation of *APEX1*. Further, the expression of *HUS1* was up-regulated, which is involved in the activation of cell cycle checkpoints and in the modulation of cell cycle arrest. After 48 h of silencing, we detected a reduced expression of *TP53,* which is a master regulator of the cell cycle. Its activation can induce cell cycle arrest or apoptosis

(217). The increased expression of *HUS1* and the delayed down-regulation of *TP53* in *APEX1*-knockdown cells may result in a delayed cell cycle or arrest. We observed a reduced growth capability; this observation is not accompanied with changes in apoptosis.

There are conflicting results regarding the correlation between a reduced *APEX1* expression and its impact on apoptosis. On the one hand, some investigators have shown apoptosis as a consequence of APEX1 protein reduction; on the other, several reports have shown no or only a slight increase (151). In one study, Fung *et al.* already showed an activation of apoptosis upon down-regulation of *APEX1* in MCF7. We did not measure an increase in apoptosis in the absence of DNA damage in *APEX1*-silenced MCF7 cells, which is in contrast to former observations. However, our results were not able to solve the overall contradictory situation found in previous studies. One reason for this may be that in all studies different cellular systems were used. Different cell types may have individual signaling pathways to regulate apoptosis. Another reason may be that the diversity of the results is a reflection of the variety of experimental methods which were used to measure apoptosis after knockdown.

The silencing of *XRCC1* has been shown once to have no effect on the cell proliferation in MCF7 cells (137). We found a significant decrease of the plating efficiency in the CFA and of growth in the SRB assay after *XRCC1* knockdown. Our result deviates from Kwok *et al.*, who investigated a combined treatment of *XRCC1* siRNA and cisplatin (137). We measured the consequences of the *XRCC1* silencing alone for cell growth. *XRCC1* interacts with many cell cycle checkpoint proteins via its BRCT domain. Thus, it may regulate the cell cycle and affect growth.

Moreover, we found an increased expression of at least 12 genes involved in multiple DNA repair pathways in the expression profiles of *XRCC1*-silenced cells. These up-regulated genes included *CDKN1A*, *GADD45A,* and *RAD9A*. Both, *CDKN1A* and *GADD45A* are major regulators of the cell cycle, and their activation induces cell cycle arrest. p21/CDKN1A binds to and inhibits the activity of cyclin-CDK2 or -CDK4 complexes, which normally allow the cell to undergo G1-S-phase transition. Furthermore, it acts as an inhibitor of p53-dependent apoptosis (57;58). Thus, it functions as a regulator of cell cycle progression at G1-phase and as an inhibitor of proliferation. *GADD45A* is an interaction

partner of p21. It negatively influences the activity of *CDK1* and inhibits G2-M transition (218). Finally, *RAD9A* is involved in the regulation of the cell cycle, and its over-expression supports the findings of a cell cycle delay (219).

It was shown that XRCC1 physically interacts with APEX1 and stimulates its enzymatic activity (136). In the expression profiles, we could identify *APEX1* as one of the up-regulated repair genes 24 h after silencing of *XRCC1*. This result is in agreement with observations in *XRCC1* mutant cells, where up-regulated *APEX1* levels were measured (136). The activation of *APEX1* confirms the physical interaction of XRCC1 and APEX1 and can explain how a deficiency in *XRCC1* results in reduced cell growth and an altered replication capability through the redox regulatory functions of APEX1. Further, in *XRCC1* knockdown cells, several DNA repair genes showed a differential expression. The co-silencing of *NTHL1* and *NEIL2* may restrict the use of BER as the major repair pathway in the cell, while other pathways such as NER and HR become up-regulated.

We also determined a down-regulation of genes such as *NDUFA3* and *NDUFA13*, which are involved in the mitochondria dysfunction pathway 24 h after silencing of *XRCC1*. This suggests a reduced energy metabolism in the cell, which may prevent additional formation of reactive oxygen species produced by the consumption of oxygen in mitochondria. We assume that the cells may prevent a situation of oxidative stress which could cause an excess of oxidative DNA damage. Oxidative DNA damage is principally repaired via BER, which is deficient in *XRCC1*-silenced cells. This confirms the essential functions of *XRCC1* in BER as a major player and interaction partner. Angell *et al.* already showed that the *NDUFA13* protein alters the viability of MCF7 cells (220).

An increased expression of genes which have functions in controlling gene expression, DNA repair and cell cycle was determined 48 h after silencing. In contrast, *CHEK2* was reduced in its expression. *CHEK2* is a cell cycle checkpoint regulator and gets activated in response to DNA damage. The protein is known to inhibit CDC25C phosphatase, which prevents the entry into mitosis; it has been shown to stabilize the tumor suppressor protein p53, which leads to cell cycle arrest in G1. p53 may also trigger G2-M arrest (221). Additionally, it interacts with BRCA1, thus, allowing *BRCA1* to restore survival after DNA damage. In sum, the changes in the gene expression levels are an additional rationale to explain the effects of the *XRCC1* knockdown in the functional analyses causing a delay or arrest in the cell cycle.

For DKO cells, we have assumed that the silencing of both genes has a greater impact on cell growth than the single knockdowns. In contrast to the observation for the single knockdowns, no difference in growth capability and in the plating efficiency was found compared to controls. We are the first to describe these findings after a simultaneous silencing of *APEX1* and *XRCC1*.

Analysis of gene expression patterns showed an activation of immune response pathways, which is already known to occur after transfection of cells with siRNA. Apart from that, the silencing was highly specific for *APEX1* and *XRCC1,* and no other deregulated pathways were found. We do not exactly know why the simultaneous silencing of two important BER enzymes has no effects on the cell growth compared to controls.

Consequently, it was not surprising that only minor expression changes of DNA repair genes occurred. Analysis of differentially expressed DNA repair genes revealed that *CCNH* and *CDK7* were silenced after transfection. Both are regulators of the cell cycle and are important genes during the G2 phase of the cell cycle and the G2-M transition. Many DNA repair genes were down-regulated 48 h after silencing including *GADD45A.* These changes did not affect the cell growth or the ability to replicate. Further analysis is required to reveal the underlying mechanism.

4.1.2 Effects of the knockdown on radiosensitivity

Repair of DNA damage is vital for maintaining genomic stability and for cell survival. Reducing the DNA repair capability of cancer cells could enhance cytotoxicity of radiotherapy. In contrast, the increased expression of DNA repair enzymes in tumor cells may enhance resistance to radiotherapy because cells can repair the DNA and evade the cytotoxic effects of the treatment.

A correlation of the expression of *APEX1* and *XRCC1* and radiosensitivity has previously been investigated but with opposing results. Some studies have demonstrated that the down-regulation of *APEX1* causes radiosensitivity, but others have found little or no correlation. In one study a radioresistance after knockdown of *APEX1* was reported. In our study, the knockdown of *APEX1* or *XRCC1* or both did not affect the radiosensitivity of the cells as determined with the clonogenic and the SRB assay.

The result for *APEX1*-silenced cells overlaps with reports which showed no correlation between an APEX1 activity and radiosensitivity. A clear association between *APEX1* expression and cellular radiosensitivity remains to be demonstrated and is may be explained by existence of an *APEX1*-independent DNA repair pathway in the cell which can be used in a situation where *APEX1* is depleted or deficient (see Chapter 1.5.3 and Figure 1.3). BER is the most important pathway involved in the repair of radiation-induced DNA damage. Incomplete repair would cause cell cycle arrest or apoptosis. Consequently, it is comprehensible that cells have an alternative BER sub-pathway in situations when the other pathway cannot be used, or one major player of the pathway fails.

Another reason which favors the *APEX1*-independent pathway might be the type of damage produced after IR. The *APEX1*-independent pathway is initiated by bifunctional glycosylases with β,δ-elemination activity. The bifunctional glycosylases repair specifically oxidized base lesions. Treatment with ionizing radiation mainly causes DNA damage through the interaction of DNA with ROS and results in an increased occurrence of oxidized base modifications. We assume that the *APEX1*-independent pathway is mainly used to repair damage caused by IR. This hypothesis is supported by the finding that radiosensitivity is not altered in *APEX1* knockdown cells after treatment with IR.

An abnormal distribution of *APEX1*-silenced cells throughout the cell cycle might influence radiosensitivity. Cells in G1 stage of the cell cycle are more radioresistant (147) and are more radiosensitive in the G2-M stage (150). Indeed, we measured an accumulation of *APEX1*-silenced cells in G2-M stage of the cell cycle prior to irradiation. Unexpectedly, the accumulation of APEX1-silenced cells in G2-M did not alter the radiosensitivity investigated with the colonogenic assay. In conclusion, these findings favor the possibility that *APEX1* knockdown cells process IR-induced DNA damage via the postulated *APEX1*-independent DNA repair pathway. The cell cycle distribution of silenced cells is not affected.

Looking at the gene expression profiles, we determined a regulation of pathways involved in radiation response such as the p53-signaling, ATM-signaling, and cell cycle regulation. In detail, these genes were *CDKN1A*, *GADD45A*, *XPC*, and *MDM2*, which is an inhibitor of p53. Further, we observed a deregulation of genes involved in BER, NER, MMR, and NHEJ. This indicates that *APEX1*-silenced cells modify several other DNA repair pathways in their activity to deal with the IR-induced DNA damage. This is corroborated by investigations

that showed that NER and MMR can serve as a backup repair system to repair oxidative base lesions (see below). The down-regulation of DNA polymerases after *APEX1* knockdown and treatment with IR and the up-regulation of *GDF15* might be an indication for cell cycle arrest (222). The *GDF15* protein decreases the viability of MCF7 cells, but as it is induced in all treatments, it causes no difference regarding survival in knockdown cells and controls. Again, an increase in apoptosis was not observed in *APEX1*-silenced after irradiation. This is in contrast to the induction of the *TNFRSF10B* gene after irradiation, which was shown to increase apoptosis in MCF7 cells (223). It remains to be seen whether *XRCC1* knockdown and DKO cells show an increase in apoptosis compared to controls. We further observed a strong induction of the cytochrome p450-dependent monooxygenases *CYP1A1* and *CYP1B1* in *APEX1*-silenced cells. Clearly, this is due to the interaction of *APEX1* with *NF-Y* which modulates the expression of the metabolizing enzymes.

Mutant mice or CHO cells with no functional *XRCC1* were hypersensitive to ionizing radiation (142;143). For *XRCC1*-silenced cells, our result is in disagreement with the studies mentioned above. The reason for this might be that we explored the *XRCC1* deficiency in human cells, whereas the majority of studies investigated radiosensitivity in rodent cells. A species-specific association is possible. One report, however, demonstrated an increased sensitivity to IR after *XRCC1* knockdown in three human breast cancer cell lines (145). Here, the difference in the reduction of the *XRCC1* levels might reflect the difference in radiosensitivity. We were able to decrease the XRCC1 protein levels up to 31 % compared to controls, whereas Brem *et al.* achieved a reduction up to 16 %. The cell might be able to cope with a deficiency in XRCC1 levels up to a defined threshold. If XRCC1 protein levels fall below that threshold, the cells fate might be influenced, and cell cycle arrest and/or apoptosis might be induced.

Another explanation is the identification of a cell type-specific effect. All cancer cells exhibit their individual genetic profile and background of variations. The malignant transformation of a “normal” cell to a cancer cell represents a very complex multistep process in which several factors are thought to alter cell growth regulatory pathways and other signaling cascades. These alterations result in uncontrolled proliferation, which is a characteristic of tumorigenesis.

It has been shown that *XRCC1* interacts with several proteins involved in BER and coordinates the steps of the repair process. Several studies have illustrated the involvement of *XRCC1* in BER. However, we do not know at which stages the protein is essential. Some models leave the possibility of a pathway where *XRCC1* might not be necessary. The LP-BER pathway is a potential candidate to repair DNA damage in situations when *XRCC1* levels are low (80). Further experiments are required, however.

The radiosensitivity of cells due to a simultaneous knockdown of *APEX1* and *XRCC1* has not been investigated to date. The double knockdown offers great potential to investigate its consequences on radiosensitivity because the expression of two important players of the BER pathway is reduced. The *APEX1*-dependent and the *APEX1*-independent pathway where *XRCC1* is important for processing are limited in their efficiency to repair radiation-induced DNA damage. Further, for the double knockdown a strong reduction of APEX1 and XRCC1 protein levels were achieved. Surprisingly, an unexpected outcome was observed in the radiosensitivity assay. We could not detect any difference in radiosensitivity of DKO compared to controls. This is in strong contrast to our assumptions.

The explanation of this phenomenon may be the existence of backup systems for BER to remove oxidative stress-induced DNA damage. NER was shown to be involved in the repair of oxidative base lesions. In particular, the removal of 8-oxoG, which is one of the most abundant oxidative lesions after oxidative damage induction was carried out by NER (see 1.5.2). Similar directions exist for the mismatch repair pathway, which is involved in repair of 8-oxoG:A mismatches (224-226). Several lines of evidence indicate that also translesional synthesis plays a role in the repair of oxidative DNA damage (227;228). Most of the studies identified the removal of 8-oxoG by these “backup” repair pathways. It remains to be demonstrated that also other oxidative base lesions are repaired via these alternative pathways. Additionally, it needs to be shown if the repair is as efficient as BER. Nevertheless, we assume that in cases where the BER pathway cannot properly process IR-induced damage, due to a deficiency of *APEX1* and *XRCC1*, the cells might be able to repair the damage via alternative pathways.

The DKO cells showed a similar pattern in their gene expression profile as it was observed in *APEX1*-silenced cells. In general, radiation response pathways and DNA repair genes

were deregulated. Moreover, the *GDF15* and the *TNFRSF10B* gene were up-regulated as it has already been shown for the *APEX1*-silenced cells (see above).

Summarizing this part, we showed that the interference with BER leads to multiple effects on the gene expression level. BER-deficient cells appear to show a cell cycle delay or arrest but no increase in apoptosis. Probably they activate alternative DNA repair pathways to process the DNA damage introduced by IR. At one point, they overcome the arrest and continue growing. The differences detected on gene expression level could not be confirmed with the functional assay. Probably, our clonogenic assay, as it was performed, is not sensitive enough to elucidate the effects of the knockdown of *APEX1* and *XRCC1* on the survival. Refinement of the model may enable us to show that the changes in the gene expression profiles of silenced cells have a direct consequence on the survival after radiation treatment.

4.1.3 Effects of the knockdown on DNA damage induction and repair after irradiation

Single-strand breaks are among the most frequent lesions produced by direct interaction of IR with DNA. SSBs can be detected with the alkaline comet assay. Additionally, IR induces base modifications which result in DNA nicks and alkali-labile sites followed by initiation of BER. The repair of IR-induced SSBs is very rapid and occurs within the first 20 minutes.

The knockdown of *APEX1* or *XRCC1* did not affect the repair rate of SSBs after IR-treatment with 5 Gy. This observation is in contrast to irradiated *XRCC1* mutant CHO cells (141;229) and *XRCC1*$^{-/-}$ mouse fibroblasts (144), which showed a reduced rate of repair of SSBs by alkaline comet assay. We do not know why the knockdown of *XRCC1* has no implications on the repair rate of MCF7 cells. XRCC1 has essential functions in the repair of SSBs and the coordination of BER. More importantly, the PARP1/XRCC1 complex initially detects the SSBs and accelerates the repair (81). However, *APEX1* and *XRCC1* knockdown cells demonstrate a considerable capability to repair IR-induced damage even with a deficiency in repair mechanisms in which *APEX1* and *XRCC1* have been implicated. Further, *XRCC1* is important for SSB repair, but not critical. This is supported by Caldecott *et al.*, who proposed a *XRCC1*-independent pathway for the repair of SSBs (135).

A trend towards a lower initial damage was determined in *APEX1*-silenced cells. This result is in disagreement with the functions of *APEX1* in BER. In general, APEX1 processes

an AP site by cleaving the deoxyribose phosphate backbone of the DNA, which generates a 3'-OH and a 5'-deoxyribose phosphate (dRP) terminus. We suggest that in *APEX1*-silenced cells, the AP sites are inefficiently processed compared to normal *APEX1* status and that the AP sites accumulate. We expected to observe an increase of SSB with the comet assay due to an accumulation of AP sites and their conversion to DNA breaks under alkaline conditions. It is not exactly known why the knockdown of *APEX1* causes fewer changes on initial damage induction. The *APEX1*-independent repair pathway can be applied to repair, but then, the control cells should have shown a lower damage compared to *APEX1*-silenced cells. The controls are able to process the initial DNA damage via both pathways, the *APEX1*-dependent and -independent ones. Another explanation is that *APEX1* was reported to suppress SSB-induced *PARP1* activation (230). Cells which show reduced levels of *APEX1* might be more capable to repair SSB via recognition by PARP1/XRCC1 complex.

In contrast, irradiated *XRCC1* mutant CHO cells (141) and *XRCC1*$^{-/-}$ mouse fibroblasts (144) were shown to have a trend for a slightly higher initial DNA damage directly after irradiation. Our result that *XRCC1*-silenced cells showed a trend for a higher initial damage induction is in agreement with the central functions of XRCC1 in the repair of SSBs (see above).

DKO cells showed no difference in their initial damage induction compared to controls. On the basis of the present data, we do not know why a knockdown of two major players of BER did not alter the amount of SSBs induced by IR. One reason might be that the regulation of the repair of SSBs after irradiation is still not well understood. In our experiment, it is very likely that other factors contribute to the repair of SSBs. A complete picture thus requires further investigations of the mechanisms behind the DKO.

We further investigated whether the different trends in the initial damage induction are due to a difference in DSB formation after irradiation. DSBs are a direct result of IR or can be produced when a replication fork runs into a SSB. The BER pathway may also produce DSB during the repair of base damage within multiple damage sites composed of more than one lesion (base damage, base loss or strand break) within one or two helical turns of DNA (231).

We assume that a defect in SSB repair due to *XRCC1* knockdown may result in an increase of DSB through a longer duration of persistent SSB and in the increased possibility that SSBs are created in close proximity to opposite DNA strands. A deficiency in *APEX1* may result in less DSB due to the reduced AP endouclease activity of APEX1 within multiple damage sites.

In addition, *XRCC1* has been shown to participate in DSB repair. Levy *et al.* demonstrated that XRCC1 is phosphorylated by the DNA-dependent protein kinase (DNA-PK), a core component in NHEJ (134). Further, XRCC1 stimulates the activity of PNK during the repair of DSBs (232) and is involved in a complex with LIG3 in a PARP1-dependent backup pathway of NHEJ (233). It was already reported that *XRCC1* deficient EM9 cells show a large number of basal γH2AX foci after radiation treatment (134). Toulany *et al.* could confirm this observation in human A549 and MO59K cells transfected with *XRCC1* siRNA (234). In two other studies, a slower rate of rejoining DSB in *XRCC1* mutant EM9 cells was identified after neutral elution experiments (235;236).

In our analysis, no difference between the siRNA treatment and the absolute numbers of γH2AX foci after irradiation was detected. Interestingly, the knockdown has no effect on the total amount of DSB, which is caused by IR. Consequently, DSBs do not contribute to the differences in the initial damage induction, which were measured by the comet assay.

4.1.4 Effects of the knockdown and additional treatment with temozolomide

The DNA damaging agent temozolomide causes methylation of bases. The repair of these lesions is processed more specifically via BER. We had expected that the treatment of *APEX1* and *XRCC1* deficient cells with temozolomide causes more effects on the growth characteristic than IR treatment. *XRCC1*-silenced cells showed a strong inhibition of cell growth whereas the *APEX1*-silenced cells showed no inhibition compared to controls. Silencing of both genes caused a growth inhibition comparable to the *XRCC1* knockdown alone. Both observations are clearly connected to the deficiency in *XRCC1*. Our results support the findings by Horton *et al.* who showed that *XRCC1* deficient mouse fibroblasts are hypersensitive to temozolomide (144). The hypersensitivity data obtained for TMZ in MCF7 are consistent with the proposal that *XRCC1* plays fundamental role in facilitating BER.

For *APEX1*-silenced cells our results contradict former observations which showed that knockdown of *APEX1* sensitizes cancer cells to alkylating agents such as temozolomide (237-239). The hypersensitivity might be due to an inhibition of the DNA repair activity of *APEX1* (240;241). Again, as an explanation for our results, we have to mention the *APEX1*-independent repair pathway, which can be used to repair alkylated bases in situations when the functions of *APEX1* are deficient.

4.2 HMEpC

We also have to consider that the relationship between a reduced expression of *APEX1* and *XRCC1* on radiosensitivity may be dependent on the cell type. Thus, we explored radiosensitivity after knockdown of *APEX1* and *XRCC1* in a second cell line, healthy HMEpC. Basically, all the mechanisms we discussed for the MCF7 cells after silencing of *APEX1* and *XRCC1* can be applied to the primary cells, too, but they are not necessarily the same because tumor cells often show a resistance to radiation treatment and an enhanced DNA repair.

Consequently, the investigations in HMEpC enable us to explore the differences in radiosensitivity between a cancer cell line and a healthy counterpart. The results might have the potential to shed light onto the hidden mechanisms which determine the success of the radiotherapy. Many patients who receive radiotherapy suffer from side effects due to normal tissue reaction. Additionally, the project can have implications on the prediction of the occurrence of side effects in normal tissue after irradiation treatment, especially if these side effects are accompanied with a deficiency in BER.

4.2.1 Effects of the knockdown on growth characteristics

The silencing of either *APEX1* or *XRCC1* caused no inhibition of cell growth compared to controls 10 days after transfection. This result is in contrast to our findings in MCF7. One explanation for this might be that the knockdown of our target genes on the protein level was much weaker than in MCF7, even though we determined a strong inhibition on mRNA level. This is a very crucial observation that implicates that the effects of the knockdown on growth characteristics are dependent on the quality of the silencing. APEX1 is an abundant protein, and an insufficient knockdown causes no functional consequences because the residual activity of *APEX1* is enough for the cell to undergo

normal cell cycle. A similar association is possible after silencing of *XRCC1*. We achieved a strong reduction of the genes on mRNA levels, but the reduction of the proteins could be more effective after silencing.

The effects of the DKO regarding cell growth are identical to those found in MCF7. The DKO did not influence the growth capability of the cells. Here, the knockdown was more efficient for *APEX1* on the protein level than for *XRCC1*. In HMEpC, it is more realistic to assume that other mechanisms may play a role in regulating the growth than *APEX1* and *XRCC1* where they have been implicated in.

This explanation is supported by the changes in the gene expression profile. In *APEX1*-silenced cell we observed a down-regulation of *GADD45A* and *RAD9,* which are involved in cell cycle regulation and other genes such as *BRCA1*, which affect cellular growth and proliferation.

Looking at the changes in *XRCC1*-silenced cells, we detected a large amount of deregulated genes affecting 24 pathways. They could mainly be assigned to have functions in regulating cell death, cellular growth, cell cycle, gene expression, and DNA replication and repair. The DNA repair genes *CDK7* and *CCNH*, both reduced in their expression, are regulators in G2 phase and influence G2-M transition. Moreover *CHEK1* and *RAD9* were down-regulated. *CHEK1* is a negative regulator of cell proliferation. This indicates that the cell modulates the activity of several genes to maintain normal growth and to prevent cell cycle inhibition or arrest. Evidently, more work has to be done to identify further involvements of XRCC1 in regulating cell growth, cell cycle control, and apoptosis.

4.2.2 Effects of the knockdown on radiosensitivity

We could not detect a difference in radiosensitivity after down-regulation of *APEX1* and/or *XRCC1* compared to controls. The result is identical to the results obtained for MCF7. Again, the reason for this may be that the knockdown on protein levels was not very efficient in the single siRNA treatments. However, in the DKO cells, the APEX1 protein was reduced by 86 % compared to controls.

Nevertheless, the radiation itself affected the survival of the cell in a dose-dependent manner. Comparing the shape of the survival curves of silenced cells after irradiation, we identified a difference between the two cell lines. Interestingly, the survival curves of the

HMEpC showed a significant shoulder. In contrast, in MCF7, the survival curves were more linear or even parabolic in the SRB assay. This raises the probability that the primary cells are more radioresistant than MCF7. We confirmed this observation by calculating the mean IC_{50} value for all curves obtained in the SRB assay for both cell types. For HMEpC, the IC_{50} value was 4.47 Gy, and for MCF7 0.69 Gy (data not shown). This confirms our assumption that the primary cells are probably more radioresistant, even though there is no difference between the individual siRNA treatments.

Looking at the gene expression profiles, we initially determined a moderate induction of radiation response genes, such as *CDKN1A*, *GADD45A,* and *XPC*, 24 h after knockdown. Most of them were still up-regulated after 48 h.

As already stated for MCF7, we suggest that *APEX1*-deficient cells are able to repair radiation-induced DNA damage via the *APEX1*-independent pathway and confirmed that suggestion in a second cell type. *CDC14B*, a regulator of the cell cycle and of p53, and *GDF15* were induced in their expression after irradiation. In addition, HR and four genes of the NER pathway were strongly up-regulated, which indicates that other DNA repair pathways become activated after silencing of *APEX1* and additional irradiation.

The strongest changes in the gene expression pattern were detected in *XRCC1*-silenced cells. Here, 202 genes were enriched in 19 different pathways. These genes mainly have functions in the cell cycle, cellular growth and proliferation, regulation of gene expression, and apoptosis. Strikingly, several other DNA repair genes involved in NER, MMR, and HR were highly up-regulated in their expression. Also *CETN2*, *CCNH*, *RAD1*, and *RAD9A* showed an increased expression. Further, we cannot exclude the existence of an *XRCC1*-independent pathway in the *XRCC1*-silenced cell, but this remains to be demonstrated.

To explain the observation obtained in DKO cells, we once more have to refer to previous studies and the evidence that other pathways such as NER and MMR participate in the repair of radiation-induced DNA damage. Certainly, this is possible for all siRNA treatments. In all the expression profiles of silenced cells, we see a strong activation of other DNA repair pathway, mainly NER and MMR, but also HR, which probably “replace” the BER in processing the damage. Regulators of the cell cycle and growth, such as *CDK7*, *CCNH*, and *RAD1* were also up-regulated as well as *TP53INP1*, which induces the transcriptional activation of p53 target promoters such as those of *CDKN1A*. Over-

expression provokes a G1 cell cycle arrest and apoptosis in vitro, which suggests a tumor suppressor activity (242).

4.2.3 Effects of the knockdown on radiation-induced DNA damage and repair

The investigation of the initial amount of radiation-induced SSBs revealed no difference after silencing of *APEX1* and/or *XRCC1*. Further, the silencing did not affect the initial amount of DSB. The rates to repair SSBs and rejoin DSBs were comparable in all four knockdown cells.

How can we explain the differences in MCF7 and in HMEpC? First of all, we have to consider that we did the experiments with two completely different cell types. MCF7 cells are cancer cells whereas the HMEpC were obtained from a healthy donor. Both harbor their own genetic background. MCF7 cells have overcome several functions which are attributed to being “normal”. We could assume that we observed a cell type-specific effect of the knockdown on radiation-induced DNA damage.

Moreover, Scott *et al.* found that about 40 % of breast cancer patients are radiosensitive in comparison to about 9 % of healthy controls (243). This observation explains why the effects of the knockdown on growth and radiosensitivity were weaker in primary HMEpC compared to MCF7 cells. Additionally, genetic polymorphisms influence the DNA repair ability of cells and their radiosensitivity. A possible explanation for the differences between HMEpC and MCF7 is the fact that we obtained the primary cells from a donor who was already radioresistant. We provided strong evidence for this in the survival curves (see above). The analysis of possible polymorphisms in DNA repair genes in the primary cell and in MCF7 has the potential to further elucidate the results obtained from the functional assays in this study.

4.3 Conclusions

We have established a cell model to study the effects of a decreased expression of *APEX1* and/or *XRCC1* on radiosensitivity. After silencing of *APEX1* and/or *XRCC1* we did not observe an altered radiosensitivity. Our data represent an attempt to gain a detailed view of the functional role of *APEX1* and *XRCC1* on radiosensitivity. We clearly showed that both *APEX1* and *XRCC1* play a central role in different biological processes and provided a basis for explaining their multifunctional biological activity. We suggest the possibility of compensatory mechanisms after the knockdown and the presence of indirect effects responsible for the observed results. The response to radiation and the efficiency of BER depend on all BER components and their multiple interactions within the cell. A deficiency in one of the enzymes may be compensated by other components. Based on our results we assume that i) the *APEX1*-independent pathway and a possible *XRCC1*-independent pathway are used in situations with reduced availability of one of the proteins, and ii) other pathways, such as NER and MMR, are able to serve as a backup repair mechanism to repair radiation-induced DNA damage in double knockdown cells. In the specific case, these assumptions are supported by the finding that both cell lines exhibit a very different gene expression profile. Several DNA repair pathways are deregulated after silencing of *APEX1* and *XRCC1* and an additional treatment with IR.

This work and the related studies discussed above suggest that *APEX1* and *XRCC1* are useful targets to modulate cellular responses to DNA damaging agents including IR. Our dataset offers several scientific directions for future studies with the aim to further investigate the mechanisms responsible for the different functions of *APEX1* and *XRCC1* in BER in primary and cancer cells.

Appendix

Supplementary Table 1: List of primers

Primer name	Accesson Number		Sequence (5'-3')
APEX1	NM_001641.2	for	GCTGCCTGGACTCTCTCATC
		rev	TCATGCTCCTCATCGCCTAT
ACTB	AF582799	for	GGCATCCTCACCCTGAAGTA
		rev	GGGGTGTTGAAGGTCTCAAA
CDKN1A	AF497972	for	GTCCGTCAGAACCCATGC
		rev	AGTGGTGTCTCGGTGACAAA
CLTR, 3'	NM_004859.3	for	GCTCACATGGGAATGTTCAC
		rev	ATGTTGTCAAAGTTGTCATAAG
CLTR, 5'	NM_004859.3	for	GACAGTGCCATCATGAATCC
		rev	TTTGTGCTTCTGGAGGAAAAGAA
HPRT	NM_000194.2	for	GACTGTAGATTTTATCAGACTGA
		rev	TGGATTATACTGCCTGACCAA
TBP	NM_003194.3	for	AGCCAAGAGTGAAGAACAGTCC
		rev	CACAGCTCCCCACCATATTC
TP53	NM_000546.2	for	GCACTGGTGTTTTGTTGTGG
		rev	CCCCTGGTTAAGTACGGTGA
XRCC1	NM_006297.2	for	GTGGGTGCTGGACTGTCAC
		rev	GCTTGGGGGCTTCATCTC

Supplementary Tables 2: Gene lists of differentially expressed genes with an expression fold change ≥ 2 or ≤ -2 obtained 24 h and 48 h after knockdown (values are displayed as fold changes to controls).

MCF7

APEX1-silenced cells_24 h

Symbol	ProbeID	regul.
APEX1	1190647	-7.7

XRCC1-silenced cells_24 h

Symbol	ProbeID	regul.
ATOX1	5560131	-2.1
ATP5I	1580603	-2.7
BOLA2	1740717	-2.3
C14orf102	10551	-2.1
C17orf61	2340521	-2.7
C19orf33	630470	-2.0
C20orf52	5220438	-2.6
C3orf34	1850040	-2.6
CCDC34	7040184	-2.1
CCL5	7570408	-2.4
CNFN	7570494	-2.3
DPM3	7320435	-3.1
HCFC1R1	5420347	-2.1
HIST1H4C	3890349	-2.1
LOC653328	6650564	-2.1
LRAP	1010296	-2.3
LSMD1	6480184	-2.6
MT1A	6200402	-3.0
MT1F	4220672	-2.1
MT1X	6620528	-3.5
MT2A	450615	-2.4
NDUFA3	50240	-2.9
RPS21	2690338	-2.4
RPS26L	4670048	-2.1
RPS28	650349	-2.2
S100A4	5290270	-2.2
S100A6	2810315	-2.4
S100P	1510424	-2.5
TCEB2	4730743	-2.2
TDP1	2060110	-2.8
TFF3	7570484	-2.1
UBL5	6420541	-2.0
UPF2	5390603	-2.1
XRCC1	4590139	-3.5
ZMAT3	6560601	-3.1
DNAJC8	5960706	2.1
HMG20B	5670110	2.0
SERTAD1	4290072	2.0

DKO_24 h

Symbol	ProbeID	regul.
APEX1	6510053	-8.9
XRCC1	4590139	-3.0
ACTG2	4610431	2.1
PRIC285	5960343	2.1
IRF7	6400176	2.5
OAS2	7320561	3.3
SP110	1340491	2.0
ISGF3G	2000022	2.3
IFIT1	2000148	4.0

APEX1-silenced cells_48 h

Symbol	ProbeID	regul.
APEX1	6510053	-11.2
ERBB3	4560288	2.1

XRCC1-silenced cells_48 h

Symbol	ProbeID	regul.
C14orf147	1410050	-2.1
FLJ35767	2680390	-4.5
GPX2	5090278	-2.4
GPX3	5490019	-2.3
XRCC1	4590139	-3.3
ARID5B	1410408	2.0
C1QTNF6	1010446	3.5
C3orf34	1850040	2.0
CDC42SE2	6770161	2.2
DCP2	6960349	2.0
DNAJC8	5960706	3.2
E2F5	6650196	2.5
FGFR3	6520139	2.2
FLJ21749	670671	2.3
PPFIBP2	6900053	2.1
RPL34	2490379	2.7
S100A9	5390220	2.1
SPFH2	5570048	2.0
TDP1	2060110	2.5
TMEM134	5690711	2.1
TMEM8	270129	2.3
ZMAT3	6560601	2.1

DKO_48 h

Symbol	ProbeID	regul.
APEX1	6510053	-7.7
XRCC1	4590139	-2.8
FAM46C	6860347	2.2
KCNF1	4610161	2.0

HMEpC

APEX1-silenced cells_24 h

Symbol	ProbeID	regul.
APEX1	3120309	-9.9
CRYAB	6110079	-2.3
CXCL2	4670390	-2.2
DUSP1	6860377	-2.3
GEM	1170246	-2.0
IL6	4040576	-2.7
KRTAP21-2	2070079	-4.0
SOD2	3420373	-2.1
TNF	2640301	-2.2
RPL34	2490379	2.2

XRCC1-silenced cells_24 h

Symbol	ProbeID	regul.
SCML1	1430152	-2.2
XRCC1	4590139	-2.0
CSNK1G2	1240192	2.6
G1P3	5090215	2.3

DKO cells_24 h

Symbol	ProbeID	regul.
MX1	1690066	-2.5
XRCC1	4590139	-2.1
APEX1	6510053	-3.2

APEX1-silenced cells_48 h

Symbol	ProbeID	regul.
APEX1	6510053	-7.6
CPA4	520682	-2.1
CXCL10	6270553	-5.3
FLJ40504	4880333	-2.1
IFI27	3990170	-2.0
IFI44	2570300	-2.4
IFI44L	3870338	-3.0
IFI6	1010246	-2.1
IFIT1	2000148	-5.1
IFIT2	2600747	-2.9
IFIT3	1500280	-4.6
IFITM1	5360156	-2.9
IRF7	6400176	-2.1
ISG15	2100196	-2.6
MX1	1690066	-8.4
NCBP2	1820025	-2.2
OAS2	7320561	-2.5
STAT1	2570079	-2.3

XRCC1-silenced cells_48 h

Symbol	ProbeID	regul.
ACLY	4200259	-2.4
APAF1	1820324	-2.1
ARHGDIB	1570193	-2.1
ASF1B	2630673	-2.0
B3GNT6	2260220	-2.2
C10orf10	2900747	-2.5
CCNA2	2650608	-2.1
CCNE2	4760154	-2.3
CDC42	5270386	-2.1
CDCA5	130022	-2.3
CKS2	780528	-2.3
DBI	2480338	-2.1
DLG7	240221	-2.3
ENO2	50402	-2.5
FEN1	3370703	-3.0
FLJ20647	1780259	-2.2
FLJ34969	1740685	-2.1
HMGCS1	5270112	-2.7
HMMR	4050400	-2.0
HSPA1A	6380717	-2.7
HSPA1B	3850433	-2.3
IDI1	2640670	-2.4
INSIG1	1820332	-2.1
KCTD14	2940632	-2.1
KDELR3	540129	-2.3
KIFC1	5090095	-2.4
LMNB1	3420593	-2.2
LRP8	4780411	-2.1
LRRC20	6620379	-2.0
MCM2	6770408	-2.1
MCM4	6020170	-2.2
MCM6	5690274	-2.3
MPHOSPH1	5900433	-2.0
MT1X	6620528	-2.1
OSR1	3940500	-2.0
PAQR4	3460132	-2.1
PCNA	6900079	-2.0
PFKFB3	4120053	-2.0
PFKFB4	7400653	-2.6
POLE2	1170326	-2.1
PPFIA4	1740167	-2.2
RNASE4	6590041	-2.2
STC1	2650730	-2.6
STIL	6220050	-2.3

TMEM97	3420541	-2.3
TUBA1A	5340187	-2.2
TUBB3	4050040	-3.4
UBE2C	5310471	-2.0
VRK1	2600739	-2.0
XRCC1	4590139	-2.3
AARS	290603	2.0
ADM2	2970452	3.5
ARTN	6560494	2.4
ASNS	1510296	5.1
ASS	110433	2.1
ATF3	4780128	2.2
C6orf48	7150017	2.3
C9orf150	2600379	2.0
CAMSAP1L1	6280209	2.0
CBS	1230047	2.3
CCL20	4220246	3.2
CCNA1	7400279	3.9
CD55	2340220	2.9
CEBPG	4230431	2.1
CHAC1	1500082	2.1
CHIC2	3130576	2.5
CLDN1	5960296	2.9
DDIT3	830619	4.6
E2F5	6650196	2.7
EIF1	3710544	2.0
FOXA2	4610592	2.4
FST	6020286	2.2
G0S2	6180427	2.3
GADD45B	4920110	2.6
GDF15	5090671	3.3
GPT2	5290148	2.5
H1F0	630278	2.6
HBEGF	1820594	3.6
HSD17B2	6980458	2.1
IFNGR1	2470358	3.5
IFRD1	2340082	2.4
IL1A	1980672	5.6
IL1B	840685	2.9
KIAA1754	2690324	2.7
KLF4	2810059	2.3
KRT23	630152	2.2
LARP6	4830433	2.6
LMO4	7210450	2.2
MAT2A	7150176	2.5
MKKS	3830519	2.4
MTHFD2	6620689	2.0
NTN4	3190021	2.3
PCK2	1780446	3.8
PHACTR3	3440341	2.2
PPP1R15A	1340600	3.3
PRDM1	6220288	2.2
PSAT1	4850674	3.6
PTGS2	1820632	2.2
RPIA	3400482	2.1
RPL34	2490379	2.1
RPS6KA2	5360424	2.6
SESN2	6650630	2.2
SHMT2	10341	2.1
SLC3A2	5420575	2.0
SLC6A9	3190608	2.9
STC2	1170170	8.3
TRIB3	1990630	2.8
TUFT1	5220035	2.3
TXNIP	1240440	2.4
UPP1	7570673	2.6
ZNF419	7320148	2.4

DKO cells_48 h

Symbol	**ProbeID**	**regul.**
APEX1	6510053	-3.5
XRCC1	4590139	-1.7
ZNF91	2640619	2.2

Supplementary Tables 3: Gene lists of differentially expressed genes with an expression fold change ≥ 2 or ≤ -2 obtained 24 h and 48 h after knockdown and additional irradiation (values are displayed as fold changes to mock-irradiated silenced cells).

MCF7

APEX1-silenced cells_24 h_IR

Symbol	ProbeID	regul.
JAG2	1500451	-2.1
KIAA1875	5050524	-2.0
LAMA5	2030102	-2.2
ACTA2	430338	2.5
ALDH1A3	360291	2.1
BTG2	110390	2.7
C12orf5	7050706	2.2
CDKN1A	3140066	3.9
CYP1A1	4900541	10.5
CYP1B1	6760255	5.3
FAS	7610196	2.2
GADD45A	3140239	2.4
GDF15	5260242	4.4
GRIN2C	4760050	2.2
MDM2	2750128	2.1
PHLDA3	4010010	2.6
SESN1	3310377	3.1
SLC30A1	730544	2.1
TIPARP	5720681	2.6
TNFRSF10B	6450767	2.3
WIG1	870397	2.1

XRCC1-silenced cells_24 h_IR

Symbol	ProbeID	regul.
IFIT1	2000148	-2.2
TINF2	1740471	-2.0
ACTA2	6480059	3.2
ALDH1A3	4920148	3.6
ANAPC11	4760288	2.0
ATOX1	5560131	2.1
ATP5I	1580603	3.0
ATP5J2	6590593	2.0
BAX	3520092	2.2
BLOC1S1	1450377	2.0
BOLA2	1740717	2.3
BTG2	1010487	2.6
C10orf116	6290168	2.2
C14orf102	10551	2.5
C17orf61	2340521	2.8
C18orf56	1450682	2.2
C19orf33	630470	2.1
C1orf53	990382	2.1
C20orf52	5220438	3.2
C3orf34	1850040	3.2
C6orf129	1340400	2.0
CCDC34	7040184	2.0
CDKN1A	4230201	3.3
CNFN	7570494	2.5
COMMD6	4260484	2.1
CYP1A1	2940332	10.1
CYP1B1	2120053	5.2
DPM3	7320435	2.5
ECGF1	2350504	2.0
EID2B	2350543	2.0
FAM14A	1940274	2.0
GDF15	5090671	4.5
GRIN2C	1300678	3.2
HIST1H4C	3890349	2.2
HIST2H2AC	6100022	2.2
LOC653328	6650564	2.5
LRAP	1010296	3.1
LSM7	5670315	2.2
LSMD1	6480184	2.1
MGC59937	6450162	2.6
MRPL53	2750309	2.0
MT1A	6200402	2.6
MT1X	6620528	3.0
MT2A	450615	2.1
MTA2	2000204	2.1
NDUFA13	2320367	2.4
NDUFA3	50240	2.9
NDUFC1	1110575	2.2
PAQR7	4150017	2.0
RND1	7570053	2.0
RPS21	2690338	2.3
RPS26L	4670048	2.1
RPS28	650349	2.1
RTN2	5090594	2.1
S100A13	5860148	2.0
S100A6	2810315	2.4
S100P	1510424	2.6
SEMA3E	1580608	2.4
SERF2	1580309	2.4
SESN1	1240553	2.1
TCEB2	4730743	2.3
TDP1	2060110	4.0
TFF3	7570484	2.3
TIPARP	6760546	2.4
TOMM7	6940377	2.1
ZMAT3	6560601	3.5
ZSWIM1	4230286	2.0

DKO_24 h_IR

Symbol	ProbeID	regul.
CCDC58	3610300	-2.2
BTG2	1010487	2.9
SESN1	1240553	2.7
GRIN2C	1300678	2.1
C12orf5	2350762	2.4
PHLDA3	3520743	3.0
CDKN1A	4230201	4.0
GDF15	5090671	4.8
ACTA2	6480059	2.2
XPC	6560441	2.1

control_24 h_IR

Symbol	ProbeID	regul.
BTG2	1010487	3.1
SESN1	1240553	2.5
GRIN2C	1300678	2.4
IFIT1	2000148	2.7
TNFRSF10B	2600463	2.0
PHLDA3	3520743	2.7
CDKN1A	4230201	3.8
GADD45A	4880673	2.0
GDF15	5090671	4.4
IRF7	6400176	2.0
ACTA2	6480059	2.5
OAS2	7320561	2.8

APEX1-silenced cells_48 h_IR

Symbol	ProbeID	regul.
ACTA2	6480059	3.2
BTG2	1010487	2.3
C12orf5	2350762	2.4
CDKN1A	4230201	4.6
FLJ11259	4280482	2.0
GDF15	5090671	4.1
PHLDA3	3520743	2.0
SESN1	1240553	2.1
SPATA18	2490215	2.0
TNFRSF10B	2600463	2.1

XRCC1-silenced cells_48 h_IR

Symbol	ProbeID	regul.
ACTA2	6480059	3.8
ALDH1A3	4920148	4.1
BTG2	1010487	2.6
CDKN1A	4230201	4.7
CYP1A1	2940332	7.4
CYP1B1	2120053	6.4
FHL2	6110025	2.0
GDF15	5090671	4.9
GRIN2C	1300678	2.2
PHLDA3	3520743	2.0
RND1	7570053	2.1
SESN1	1240553	2.2
SPATA18	2490215	2.3
TNFRSF10B	2600463	2.2
XPC	6560441	2.0

DKO_24 h_IR

Symbol	ProbeID	regul.
SESN1	1240553	2.3
TNFRSF10B	2600463	2.2
CDKN1A	4230201	4.8
GDF15	5090671	3.3
ACTA2	6480059	3.6

control_48 h_IR

Symbol	ProbeID	regul.
IFI6	1010246	2.2
SESN1	1240553	2.2
PHLDA3	3520743	2.1
CCDC58	3610300	-2.1
CDKN1A	4230201	4.5
GDF15	5090671	2.3
ACTA2	6480059	3.5

HMEpC

APEX1-silenced cells_24 h_IR

Symbol	ProbeID	regul.
CDC14B	6280504	2.05
GDF15	5090671	2.61

XRCC1-silenced cells_24 h_IR

Symbol	ProbeID	regul.
BRD3	6660626	-2.3
C10orf10	2900747	-2.2
C9orf140	1010470	-2.0
CCNF	3130541	-2.1
CDCA8	4830634	-2.1
CDKN2D	7050326	-2.0
CENPA	2600392	-2.1
CXCL2	4670390	-2.5
DKFZp762E1312	3180367	-2.2
FBXO32	1990079	-2.4
FZD2	5720180	-2.3
G1P3	5090215	-2.1
GRB7	5900243	-2.2
HMGB2	5900482	-2.0
IL8	1340743	-2.4
KIFC1	5090095	-2.6
PSRC1	1070762	-2.2
STIL	6220050	-2.0
CYP1B1	2120053	2.9
FGFBP1	7650441	2.2

DKO cells_24 h_IR

Symbol	ProbeID	regul.
NOLA1	130326	-2.3
LOC643995	4230196	-2.2
CDC14B	6280504	-2.8
TP53INP1	5420538	2.1

controls_24 h_IR

Symbol	ProbeID	regul.
GDF15	5090671	2.2
TP53INP1	5420538	2.1

APEX1-silenced cells_48 h_IR

Symbol	ProbeID	regul.
GDF15	5090671	2.1
IFI6	1010246	3.9
IFI27	3990170	2.3
MX1	1690066	3.3

XRCC1-silenced cells_48 h_IR

Symbol	ProbeID	regul.
AARS	290603	-2.4
ABCG1	5860377	-2.8
ADM2	2970452	-5.7
ALOXE3	990685	-2.3
ALPK1	540390	-2.1
ARG2	5720725	-2.2
ARHGEF2	4120411	-2.6
ARID5B	1410408	-2.8
ARTN	6560494	-2.3
ASNS	1510296	-3.6
ATF3	4780128	-2.0
ATF4	3460309	-2.5
BHLHB2	2640735	-2.2
BIRC3	5080021	-7.4
C1orf106	7100021	-2.1
C20orf100	1400601	-3.3
C3orf40	3940564	-2.1
C6orf48	7150017	-2.3
CBS	1230047	-2.7
CCL20	4220246	-5.4
CCNA1	7400279	-2.0
CCNB1IP1	510114	-2.0
CD55	2340220	-2.0
CEBPB	20446	-2.1
CEBPD	5490408	-2.6
CEBPG	4230431	-2.4
CHAC1	1500082	-2.1
CHIC2	3130576	-3.3
CLDN1	5960296	-4.5
CTDSP2	650681	-2.6
CXCL2	4670390	-3.2
DDIT3	830619	-3.7
DDIT4	3190148	-2.3
DOC1	110307	-2.3
EGFR	1050671	-2.1
EGR1	870338	-4.4
ERRFI1	7100639	-3.5
ETS2	4220605	-2.1
FAM100B	520278	-3.1
FAM113B	4200541	-2.5
FANCE	5720192	-2.3
FBXL20	4900240	-2.1
FBXO32	1990079	-3.2
FLJ20152	6420309	-2.1

FNDC6	3400095	-2.2
FOXA2	4610592	-3.2
GABARAPL1	6420465	-2.1
GADD45B	4920110	-2.1
GDF15	5090671	-2.2
GPT2	5290148	-4.6
GRB7	5900243	-4.0
GTF2IRD1	4200577	-2.3
H1F0	630278	-2.9
HBEGF	1820594	-5.9
HMGB2	5900482	-2.3
HNRPDL	6860678	-2.0
IBRDC2	70630	-2.7
ID1	670386	-2.8
IFNGR2	2570291	-2.3
IL1A	1980672	-2.6
IL8	1340743	-6.4
IRAK2	3930750	-4.0
IRS2	6110736	-2.2
JAG1	1010376	-2.0
JUNB	7550500	-2.6
KIAA0247	3170093	-2.4
KIAA0427	730273	-2.1
KIAA1754	2690324	-2.8
KLF9	3390292	-2.2
LARP6	4830433	-3.9
LIF	2650390	-2.2
LMO4	7210450	-2.5
MAP1LC3B	2490754	-2.4
MGC10992	1660681	-2.2
MKKS	3830519	-2.1
MKNK2	1300347	-2.3
MTHFD2	6620689	-2.2
NAV2	4230195	-2.1
NCOA7	630091	-3.1
NFKBIZ	2470348	-3.0
NUPR1	4040181	-2.5
OGT	1430176	-2.2
PCK2	1780446	-4.4
PHACTR3	3440341	-2.7
PHF21A	6580164	-3.6
PHGDH	240086	-2.2
PIM1	3130301	-2.8
PLAU	5360670	-2.3
PPP1R15A	1340600	-3.0
PRDM1	6220288	-4.4
PRKCH	3290731	-2.0
PSAT1	4850674	-3.7
PSPH	870753	-2.0
RELB	730440	-2.2
RNF39	1980255	-2.4

RPS29	2760452	-2.3
RPS6KA2	5360424	-2.5
SAV1	2070025	-2.3
SCNN1G	6270735	-2.4
SESN2	6650630	-2.2
SH3RF2	5570348	-3.1
SHMT2	10341	-2.0
SIAH1	7570537	-2.1
SIX4	20653	-2.1
SIX5	5810672	-2.8
SLC2A3	3800168	-2.4
SLC6A9	3190608	-3.4
SOCS2	6770673	-2.1
SPIRE1	5690246	-2.6
STC2	1170170	-15.8
TNFAIP3	3360681	-2.7
TP73L	6060131	-2.2
TRIB1	4810520	-2.0
TRIB3	1990630	-5.5
TRIM8	940435	-3.1
TSC22D3	6350446	-4.9
TXNIP	1240440	-2.1
UBE2H	4900746	-2.0
UPP1	7570673	-3.5
VEGFA	2640224	-2.4
WASL	6380138	-2.1
YPEL3	130750	-2.1
ZBTB16	5080450	-2.6
ZC3H12A	2490017	-2.2
ZNF161	510341	-2.3
ZNF218	4890292	-2.0
ZNF277	5870180	-2.1
ZNF419	7320148	-2.2
ZSWIM4	1170072	-2.6
ANKRD38	7610128	2.6
ATF5	1570484	2.0
C21orf127	2570707	2.1
CALM1	1660477	2.0
CD24	610437	2.1
CDKN1A	5290475	2.1
CMKOR1	450424	2.7
CTSC	1510433	2.3
CXCR7	4860114	2.2
CYP1B1	2120053	2.2
DNAJA1	1980632	2.6
DTNA	6350164	2.2
DUSP4	2650041	2.5
DYNLL1	6220086	2.0
ENC1	7150563	2.6
FAM43B	4860743	2.1
FEN1	3370703	2.1

FLJ13149	6650220	2.0
G3BP1	5720300	2.1
GAL	60452	2.2
GPR110	6960367	2.0
HAS3	380504	2.3
HIST1H2BD	6200669	2.6
HIST1H2BK	6110630	2.0
HMFN0839	2060477	2.1
HMGB3	7570050	2.3
HMGCS1	5270112	2.8
HMOX1	6660601	2.2
HPS6	2940301	2.2
HS3ST1	4230332	2.6
HS3ST2	5870435	3.3
HSPA1A	6380717	3.3
HSPA1B	3850433	2.9
HSPA2	6270274	2.6
HSPA8	2650619	2.8
HSPH1	150327	2.3
ID2	1660296	2.1
IDI1	2640670	2.4
IKIP	3170605	2.0
INSIG1	1820332	2.0
KBTBD8	6370523	2.2
KITLG	5090500	2.0
METTL1	1990358	2.2
MGC23985	1450161	2.5
MVD	1440020	2.2
NP	6840075	2.6
NSDHL	4260392	2.1
OSR1	3940500	2.3
PCNA	6900079	2.1
POLR2L	6200017	2.0
POP1	3840397	2.7
PRR5	6130630	2.1
PTHLH	6900414	2.3
RBM12	2850438	2.1
RBM14	6660343	2.8
RIS1	3130220	2.4
RPL29	2450167	2.4
S100A2	2970017	2.2
SACS	7510379	2.6
SDF2L1	3120079	2.0
SIPA1L2	3460053	2.1
SPHK1	2470689	2.1
TMEM20	3460551	2.0
TNFRSF10D	830113	2.3
TRIM21	6560075	2.3
TUBA1	4760474	2.1
TUBB2A	450292	2.1
TUBB2C	2070368	3.0
TUBB3	4050040	2.8
TUBB4Q	1990327	2.2
TUBB6	1570092	2.0
ZC3HAV1	6620750	2.5
ZNF365	4180301	2.3

DKO cells_48 h_IR

Symbol	**ProbeID**	**regul.**
MX1	1690066	3.8
IFIT1	2000148	2.3
IFI44L	3870338	2.8
GDF15	5090671	2.5
IFITM1	5360156	2.0
CXCL10	6270553	3.8
OAS2	7320561	2.1

controls_48 h_IR

Symbol	**ProbeID**	**regul.**
BUB1	2070224	-2.2
ANGPTL4	2450592	-2.2
MX1	1690066	4.3
IFIT1	2000148	2.1
IFI44L	3870338	2.5
GDF15	5090671	2.3
IFITM1	5360156	2.2
OAS2	7320561	2.1

Supplementary Tables 4: Gene lists of differentially expressed DNA repair genes with an expression fold change greater than 20 % obtained 24 h and 48 h after knockdown (values are displayed as fold changes to controls).

MCF7

Symbol	Pathway	24h_A	24h_X	24h_AX
ALKBH2	Direct reversal	74.90	81.80	102.35
APEX1	BER	13.05	123.67	12.09
CCNH	NER	95.09	98.16	75.36
CDK7	NER	100.28	91.30	107.44
CDKN1A	Others	98.40	132.54	96.53
CHEK1	DNA damage response	93.23	100.36	89.68
CLK2	DNA damage response	100.20	100.55	103.56
DCLRE1B	suspected DNA repair	101.89	113.12	109.64
DDB2	NER-related	90.68	108.26	101.99
EME1	HR	93.20	123.25	92.85
ERCC2	NER	112.92	115.61	123.29
ERCC3	NER	133.57	128.55	98.55
FDXR	Others	89.79	107.53	106.75
FEN1	Editing and processing nucleases	88.17	125.68	95.02
GADD45A	Others	91.72	125.71	117.82
GTF2H2	NER	96.36	104.37	82.32
GTF2H4	NER	99.94	122.49	101.14
GTF2H5	NER	87.49	69.59	106.22
HUS1	DNA damage response	121.99	96.04	94.61
LIG1	NER	93.28	106.40	83.37
MDM2	Others	92.94	101.00	98.81
MGMT	Direct reversal	90.70	85.72	92.29
MMS19L	NER-related	121.55	81.77	91.51
MSH3	MMR	122.11	107.24	88.92
MSH4	MMR	100.41	86.45	105.71
MSH6	MMR	105.09	108.68	86.06
MUTYH	BER	90.64	111.85	104.14
NEIL2	BER	86.77	65.84	85.62
NTHL1	BER	85.98	79.57	92.54
PARP1	BER	116.25	97.05	78.16
PMS2L3	MMR	93.94	114.24	102.30
PNKP	BER	99.10	103.60	95.82
POLD1	Polymerases	136.78	103.48	95.65
POLE	Polymerases	124.75	111.46	100.56
POLG	Polymerases	103.37	104.71	120.35
POLQ	Polymerases	104.62	129.47	93.99
PRKDC	NHEJ	89.44	99.89	105.87
PSMA4	Others	101.64	95.61	92.21
RAD23A	NER	93.07	94.14	105.43
RAD23B	NER	81.77	88.22	99.15
RAD54B	HR	109.40	121.46	100.59
RAD9A	DNA damage response	100.98	123.74	117.46
RECQL	suspected DNA repair	104.77	114.54	99.34
REV1L	Polymerases	103.28	112.11	121.46

REV3L	Polymerases	117.63	128.62	107.64
RPA3	NER	86.70	67.12	105.54
SHFM1	HR	94.78	66.12	97.79
SMUG1	BER	84.71	83.36	118.98
TDP1	Repair of DNA-protein crosslinks	118.56	75.75	97.09
XAB2	NER-related	106.55	93.38	90.88
XPC	NER	111.08	127.77	104.51
XRCC1	BER	94.08	28.30	33.35
XRCC2	HR	110.28	75.26	88.88
XRCC5	NHEJ	110.01	96.03	128.23

Symbol	Pathway	48h_A	48h_X	48h_AX
ALKBH2	Direct reversal	111.55	55.29	83.52
APEX1	BER	10.03	113.67	13.17
CDK7	NER	112.67	115.90	76.86
CDKN1A	Others	96.41	114.95	83.94
CETN2	NER	97.36	92.84	116.26
CHEK2	DNA damage response	97.57	79.47	89.22
DMC1	HR	75.77	115.19	74.82
ERCC2	NER	109.32	108.55	100.95
ERCC3	NER	89.93	147.55	99.38
ERCC6	NER-related	104.57	122.65	121.38
FEN1	Editing and processing nucleases	86.29	90.63	100.10
GADD45A	Others	110.50	81.97	77.26
GTF2H1	NER	84.62	99.89	121.61
GTF2H3	NER	86.44	84.37	90.56
GTF2H5	NER	123.00	95.54	107.70
HEL308	suspected DNA repair	96.19	114.81	106.77
MBD4	BER	84.10	107.36	70.97
MDM2	Others	96.07	95.68	91.70
MGMT	Direct reversal	109.30	94.64	109.18
MSH3	MMR	109.29	115.02	89.27
MSH6	MMR	94.01	106.90	96.61
MUS81	HR	106.66	120.28	82.73
NTHL1	BER	118.86	78.84	104.76
PARG	Others	92.62	95.15	109.56
PARP1	BER	75.60	131.50	80.20
PMS2L3	MMR	111.68	96.76	87.81
POLD1	Polymerases	84.33	110.44	84.17
POLG	Polymerases	104.08	79.89	98.64
PSMA4	Others	99.54	79.50	91.32
RAD23A	NER	76.40	75.42	96.86
RAD23B	NER	76.00	89.25	89.49
RAD52B	suspected DNA repair	105.88	96.22	96.65
RAD9A	DNA damage response	105.08	101.66	84.47
REV1L	Polymerases	107.57	111.43	119.73
REV3L	Polymerases	88.72	139.97	108.08
RPA2	NER	95.63	95.83	80.84
RPA3	NER	76.73	96.90	89.93
TDP1	Repair of DNA-protein crosslinks	98.68	145.43	96.01
TOP3A	Others	105.23	97.44	84.50
TP53	DNA damage response	77.23	94.29	92.29
XPC	NER	109.02	114.01	103.28
XRCC1	BER	106.40	30.22	36.06
XRCC2	HR	84.31	114.89	80.28
XRCC3	HR	110.59	75.42	96.53
XRCC5	NHEJ	104.67	112.62	78.96

HMEpC

Symbol	Pathway	24h_A	24h_X	24h_AX
APEX1	BER	10.03	102.54	27.76
APTX	suspected DNA repair	113.42	91.45	103.07
BRCA1	HR	96.94	109.96	103.90
CCNH	NER	103.43	75.01	95.99
CDK7	NER	89.99	79.81	74.42
CDKN1A	Others	92.66	108.03	98.84
CETN2	NER	88.40	74.26	100.97
CHEK1	DNA damage response	105.43	95.13	97.12
DCLRE1A	suspected DNA repair	96.36	93.38	93.16
DMC1	HR	103.87	96.58	116.56
EME1	HR	105.43	106.99	117.71
EME2	HR	97.36	94.92	71.19
FEN1	Editing and processing nucleases	86.13	103.48	89.56
GADD45A	Others	76.51	119.93	97.27
GTF2H5	NER	103.53	79.23	98.63
LIG1	NER	95.45	105.61	103.19
MAD2L2	Polymerases	103.30	107.23	90.80
MBD4	BER	110.31	94.05	107.92
MGMT	Direct reversal	97.27	126.00	105.99
MMS19L	NER-related	106.18	117.69	86.97
MNAT1	NER	99.27	118.81	119.32
MSH3	MMR	94.19	105.29	128.09
MSH6	MMR	107.63	77.26	97.35
NEIL2	BER	114.96	80.62	100.82
NTHL1	BER	100.85	105.50	90.97
PMS2L3	MMR	98.68	78.65	87.83
PNKP	BER	89.22	115.69	105.30
POLB	Polymerases	112.54	76.75	98.54
POLD1	Polymerases	91.39	143.99	71.68
POLE	Polymerases	89.09	119.42	99.73
POLQ	Polymerases	106.33	86.71	100.19
PSMA4	Others	107.57	73.62	111.33
RAD23A	NER	92.51	127.16	89.39
RAD23B	NER	109.96	87.90	93.03
RAD52B	suspected DNA repair	104.14	73.66	113.72
RAD54L	HR	88.73	112.95	83.56
REV1L	Polymerases	122.20	83.82	106.43
RPA1	NER	97.29	106.73	102.50
RPA2	NER	105.68	101.83	94.63
SALL3	Others	93.37	137.07	107.55
SMUG1	BER	106.73	94.39	85.80
TDP1	Repair of DNA-protein crosslinks	95.48	95.64	121.18
TOP3A	Others	103.09	99.24	94.01
XAB2	NER-related	112.74	140.14	95.93
XPC	NER	116.96	98.80	101.37
XRCC1	BER	90.34	48.99	48.49
XRCC2	HR	111.10	92.57	103.99

Symbol	Pathway	48h_A	48h_X	48h_AX
ALKBH3	Direct reversal	103.07	127.32	101.68
APEX1	BER	14.01	121.27	28.49
APEX2	BER	101.06	86.17	109.59
BRCA1	HR	123.21	91.29	99.70
CCNH	NER	99.42	120.90	97.62
CDK7	NER	118.51	111.51	85.33
CDKN1A	Others	92.10	132.39	97.09
CETN2	NER	108.22	79.68	98.63
CHEK1	DNA damage response	91.98	74.20	100.14
DMC1	HR	51.23	74.29	96.04
EME2	HR	84.56	102.35	125.14
ERCC4	NER	88.89	100.62	85.42
FEN1	Editing and processing nucleases	103.99	33.51	81.05
GADD45A	Others	99.43	198.84	105.77
GTF2H1	NER	95.10	115.32	103.26
GTF2H3	NER	121.91	103.08	87.67
GTF2H5	NER	102.21	71.68	109.00
HEL308	suspected DNA repair	102.60	124.44	95.91
LIG1	NER	116.50	53.34	92.76
MAD2L2	Polymerases	102.66	101.09	108.55
MBD4	BER	92.64	88.08	88.69
MMS19L	NER-related	96.40	113.49	113.16
MNAT1	NER	120.61	93.74	111.43
MSH6	MMR	94.01	56.58	98.08
MUS81	HR	74.55	123.60	82.87
NEIL2	BER	94.72	120.94	114.54
NTHL1	BER	124.23	83.13	100.23
PARG	Others	109.57	88.10	112.04
PCNA	Polymerases	102.54	76.28	98.56
PER1	DNA damage response	116.05	114.68	108.61
PMS1	MMR	108.75	86.45	87.28
POLD1	Polymerases	127.47	77.61	95.00
POLE	Polymerases	103.94	67.34	89.71
POLG	Polymerases	117.71	76.92	94.50
POLI	Polymerases	113.67	84.10	94.31
POLM	Polymerases	133.66	82.25	96.37
POLQ	Polymerases	101.19	53.67	77.50
PSMA4	Others	105.19	93.18	108.56
RAD1	DNA damage response	106.92	105.06	95.86
RAD1	DNA damage response	116.03	90.57	76.61
RAD23A	NER	111.07	106.98	108.72
RAD23B	NER	85.39	93.95	83.51
RAD52B	suspected DNA repair	101.32	96.44	81.37
RAD54L	HR	106.52	76.14	79.72
RAD9A	DNA damage response	119.18	61.86	110.01
RECQL	suspected DNA repair	105.79	65.07	80.04
RPA1	NER	107.73	68.52	96.15

RPA2	NER	122.21	70.76	96.33
RPA3	NER	107.93	54.43	81.86
SALL3	Others	107.71	124.54	127.93
SHFM1	HR	105.72	78.75	87.70
SMUG1	BER	121.58	108.65	116.35
SPO11	Editing and processing nucleases	122.18	104.20	99.54
TOP3A	Others	99.28	81.14	85.03
TP53	DNA damage response	85.38	99.03	113.93
TREX1	DNA damage response	96.87	102.92	111.72
UBE2N	Rad6 pathway	84.00	76.47	91.43
XAB2	NER-related	126.07	101.75	116.90
XPA	NER	95.88	94.70	91.87
XPC	NER	120.29	124.19	112.79
XRCC1	BER	142.12	43.75	58.91
XRCC2	HR	70.48	88.56	84.07
XRCC3	HR	81.29	74.36	97.41
XRCC5	NHEJ	99.55	90.16	102.11

Supplementary Tables 5: Gene lists of differentially expressed DNA repair genes with an expression fold change greater than 20 % obtained 24 h and 48 h after knockdown and additional irradiation (values are displayed as fold changes to mock-irradiated silenced cells).

MCF7

Symbol	Pathway	24h_A_IR	24h_X_IR	24h_AX_IR	24h_control_IR
ALKBH2	Direct reversal	120.08	111.41	72.45	77.65
APEX1	BER	95.27	78.88	100.55	89.55
CCNH	NER	100.97	97.95	123.49	111.27
CDK7	NER	100.67	94.32	112.81	123.09
CDKN1A	Others	281.44	223.17	293.21	277.11
CHEK1	DNA damage response	108.34	82.55	97.11	79.47
CLK2	DNA damage response	77.95	90.08	114.67	108.17
DCLRE1B	suspected DNA repair	86.77	79.38	77.36	92.77
DDB2	NER-related	155.20	102.89	131.94	119.71
EME1	HR	85.96	95.30	111.89	90.85
ERCC2	NER	84.74	104.38	90.39	114.93
ERCC3	NER	79.60	79.09	100.58	100.98
FDXR	Others	163.94	96.94	86.03	100.28
FEN1	Editing and processing	96.61	77.89	96.84	81.93
GADD45A	Others	240.18	145.28	147.73	200.03
GTF2H2	NER	109.47	99.13	95.38	76.96
GTF2H4	NER	82.86	70.17	97.32	104.39
GTF2H5	NER	110.51	154.30	103.74	99.58
HUS1	DNA damage response	98.06	106.00	111.85	106.41
LIG1	NER	104.46	94.15	128.64	112.28
MDM2	Others	138.01	119.00	127.06	125.75
MGMT	Direct reversal	114.59	127.56	118.13	118.12
MMS19L	NER-related	79.38	100.85	107.08	91.66
MSH3	MMR	101.91	131.23	86.30	100.62
MSH4	MMR	97.95	121.52	91.32	94.29
MSH6	MMR	61.13	78.29	82.55	65.22
MUTYH	BER	76.98	93.34	92.40	100.84
NEIL2	BER	107.41	144.60	90.78	89.64
NTHL1	BER	96.84	107.90	108.86	85.29
PARP1	BER	80.95	99.07	112.52	87.61
PMS2L3	MMR	100.00	76.84	93.05	106.45
PNKP	BER	99.15	84.51	122.11	117.35
POLD1	Polymerases	68.24	98.33	109.24	77.77
POLE	Polymerases	58.89	93.73	104.71	93.87
POLG	Polymerases	79.37	88.34	89.26	109.80
POLQ	Polymerases	72.11	86.05	104.24	101.15
PRKDC	NHEJ	62.44	89.85	94.60	102.07
PSMA4	Others	125.26	100.84	104.98	114.44
RAD23A	NER	96.45	115.42	111.60	125.01
RAD23B	NER	129.45	109.62	111.76	116.67
RAD54B	HR	100.26	80.07	96.42	100.67

RAD9A	DNA damage response	60.76	77.33	83.15	94.20
RECQL	suspected DNA repair	99.22	74.88	88.01	83.77
REV1L	Polymerases	100.04	104.19	97.28	99.16
REV3L	Polymerases	94.64	97.68	111.67	122.00
RPA3	NER	99.63	142.96	90.57	95.26
SHFM1	HR	118.30	141.49	102.26	94.13
SMUG1	BER	102.78	124.43	90.52	111.68
TDP1	DNA-protein crosslinks	90.79	205.47	107.66	97.71
XAB2	NER-related	92.76	122.90	117.32	96.48
XPC	NER	186.31	169.06	213.89	198.08
XRCC1	BER	97.73	115.18	111.30	99.38
XRCC2	HR	89.97	128.53	88.73	103.56
XRCC5	NHEJ	87.90	91.63	82.91	101.64

Symbol	Pathway	48h_A_IR	48h_X_IR	48h_AX_IR	48h_control_IR
ALKBH2	Direct reversal	88.85	125.21	80.74	82.70
APEX1	BER	95.78	92.37	91.31	92.88
CDK7	NER	106.37	111.51	164.79	92.46
CDKN1A	Others	298.90	302.33	319.89	293.56
CETN2	NER	128.27	90.93	86.71	110.00
CHEK2	DNA damage response	102.27	93.53	93.83	106.40
DMC1	HR	79.82	74.35	85.19	83.97
ERCC2	NER	111.48	93.95	106.25	120.40
ERCC3	NER	104.94	91.68	90.11	87.17
ERCC6	NER-related	90.54	90.98	104.63	110.34
FEN1	Editing and processing	80.47	90.27	83.59	78.09
GADD45A	Others	144.38	182.83	156.49	145.72
GTF2H1	NER	95.65	106.89	94.00	108.90
GTF2H3	NER	109.32	125.17	100.41	103.57
GTF2H5	NER	106.96	102.43	112.18	105.39
HEL308	suspected DNA repair	108.79	121.74	109.35	104.71
MBD4	BER	89.23	81.30	95.65	77.32
MDM2	Others	118.38	125.85	112.38	106.95
MGMT	Direct reversal	119.00	93.83	130.52	119.36
MSH3	MMR	81.35	84.13	69.60	71.05
MSH6	MMR	64.32	75.05	70.21	64.20
MUS81	HR	79.09	78.85	118.81	95.73
NTHL1	BER	91.38	86.83	90.74	85.28
PARG	Others	122.48	98.50	86.38	107.12
PARP1	BER	96.12	96.43	107.11	94.46
PMS2L3	MMR	88.00	78.44	100.22	101.53
POLD1	Polymerases	85.86	78.20	85.52	73.87
POLG	Polymerases	101.45	93.46	91.21	92.44
PSMA4	Others	103.25	90.35	129.61	105.58
RAD23A	NER	120.77	112.19	100.03	101.12
RAD23B	NER	99.01	123.27	109.00	91.57
RAD52B	suspected DNA repair	105.30	108.20	104.59	78.38
RAD9A	DNA damage response	85.59	69.87	95.97	71.00
REV1L	Polymerases	75.37	92.58	95.32	107.86
REV3L	Polymerases	127.34	130.52	109.55	110.62
RPA2	NER	88.41	87.24	96.22	75.94
RPA3	NER	100.42	97.38	98.15	90.84
TDP1	DNA-protein crosslinks	97.62	96.49	93.62	90.59
TOP3A	Others	91.15	99.87	87.42	70.40
TP53	DNA damage response	108.03	98.74	111.35	86.00
XPC	NER	191.97	200.83	196.04	172.01
XRCC1	BER	87.14	105.08	94.16	101.90
XRCC2	HR	91.82	95.27	91.17	66.69
XRCC3	HR	101.73	100.52	90.81	77.16
XRCC5	NHEJ	88.10	86.48	113.68	84.08

HMEpC

Symbol	Pathway	24h_A_IR	24h_X_IR	24h_AX_IR	24h_siCON_IR
APEX1	BER	88.42	97.87	101.68	101.60
APTX	suspected DNA repair	91.81	123.83	104.64	99.99
BRCA1	HR	88.10	72.86	85.34	85.83
CCNH	NER	107.51	124.50	77.39	79.43
CDK7	NER	102.73	95.80	121.43	113.36
CDKN1A	Others	149.87	143.92	111.35	132.52
CETN2	NER	116.64	127.76	99.42	96.77
CHEK1	DNA damage response	88.83	75.29	83.79	89.66
DCLRE1A	suspected DNA repair	91.21	82.45	72.06	88.03
DMC1	HR	92.60	76.00	82.46	75.05
EME1	HR	92.91	86.59	68.86	88.19
EME2	HR	103.46	104.18	102.74	72.46
FEN1	Editing and processing	91.95	66.96	85.44	72.61
GADD45A	Others	124.07	120.81	109.03	126.37
GTF2H5	NER	97.46	111.58	103.79	106.14
LIG1	NER	123.65	87.07	121.38	106.46
MAD2L2	Polymerases	110.95	75.66	112.91	83.36
MBD4	BER	86.40	79.65	82.38	98.59
MGMT	Direct reversal	114.96	85.17	103.24	95.04
MMS19L	NER-related	96.05	90.70	122.05	95.82
MNAT1	NER	120.93	101.41	82.38	115.09
MSH3	MMR	90.66	72.56	68.82	98.51
MSH6	MMR	83.21	75.98	83.97	81.36
NEIL2	BER	79.66	97.10	111.11	94.89
NTHL1	BER	95.56	72.92	78.45	81.83
PMS2L3	MMR	91.86	114.53	112.74	92.03
PNKP	BER	122.35	88.36	98.74	108.17
POLB	Polymerases	116.06	106.40	108.41	102.85
POLD1	Polymerases	94.40	59.30	88.29	62.50
POLE	Polymerases	109.93	74.18	102.64	98.23
POLQ	Polymerases	92.45	79.73	85.14	92.54
PSMA4	Others	106.05	127.14	86.94	93.79
RAD23A	NER	113.22	79.16	102.41	81.35
RAD23B	NER	105.95	105.99	131.81	128.29
RAD52B	suspected DNA repair	103.91	130.95	99.30	105.66
RAD54L	HR	101.62	73.26	86.58	68.42
REV1L	Polymerases	93.61	104.04	98.60	96.96
RPA1	NER	104.97	85.13	87.02	79.05
RPA2	NER	76.53	81.55	83.03	71.76
SALL3	Others	95.60	81.40	96.73	82.64
SMUG1	BER	107.28	111.84	101.00	77.21
TDP1	DNA-protein crosslinks	96.91	96.65	89.30	107.66
TOP3A	Others	83.51	76.94	83.90	81.31
XAB2	NER-related	100.81	90.72	124.78	102.41
XPC	NER	130.54	118.76	126.22	129.16
XRCC1	BER	109.49	85.14	105.20	93.36
XRCC2	HR	86.64	66.35	99.98	86.15

Symbol	Pathway	48h_A_IR	48h_X_IR	48h_AX_IR	48h_siCON_IR
ALKBH3	Direct reversal	95.58	90.64	117.63	115.80
APEX1	BER	83.94	91.20	104.74	110.48
APEX2	BER	90.00	133.74	79.12	85.62
BRCA1	HR	85.40	106.84	111.17	101.53
CCNH	NER	93.66	126.32	134.04	92.09
CDK7	NER	109.14	77.46	130.40	109.90
CDKN1A	Others	157.39	173.49	161.35	143.40
CETN2	NER	104.78	112.82	102.44	107.73
CHEK1	DNA damage response	98.38	81.66	83.41	93.81
DMC1	HR	144.58	105.53	105.26	94.75
EME2	HR	113.80	90.97	82.07	98.25
ERCC4	NER	128.04	91.16	120.92	100.44
FEN1	Editing and processing	104.50	208.78	106.18	82.40
GADD45A	Others	112.00	66.46	107.51	125.45
GTF2H1	NER	121.41	101.44	97.48	94.93
GTF2H3	NER	131.32	85.44	134.49	113.21
GTF2H5	NER	93.09	134.17	88.30	94.50
HEL308	suspected DNA repair	102.70	90.52	124.66	105.06
LIG1	NER	93.78	161.42	113.25	91.25
MAD2L2	Polymerases	88.84	73.68	103.03	104.40
MBD4	BER	110.31	126.24	100.36	89.73
MMS19L	NER-related	83.98	65.22	96.97	102.58
MNAT1	NER	77.19	86.70	81.43	99.68
MSH6	MMR	102.00	144.37	95.43	86.12
MUS81	HR	115.00	87.35	89.70	82.85
NEIL2	BER	100.05	90.57	74.20	101.12
NTHL1	BER	77.19	132.53	94.66	102.40
PARG	Others	119.98	122.36	105.56	125.49
PCNA	Polymerases	109.62	148.42	111.04	110.71
PER1	DNA damage response	92.54	86.93	88.80	76.81
PMS1	MMR	97.04	127.07	102.95	86.91
POLD1	Polymerases	76.63	104.94	111.31	100.41
POLE	Polymerases	84.09	104.16	92.17	75.86
POLG	Polymerases	97.17	108.55	115.03	86.74
POLI	Polymerases	78.17	116.68	99.62	99.49
POLM	Polymerases	72.42	105.67	100.45	98.40
POLQ	Polymerases	87.79	110.69	95.62	83.24
PSMA4	Others	109.37	120.56	101.32	99.22
RAD1	DNA damage response	86.03	120.31	124.17	92.47
RAD1	DNA damage response	98.85	106.33	126.59	86.87
RAD23A	NER	89.87	64.50	104.14	96.76
RAD23B	NER	122.87	121.90	123.51	112.13
RAD52B	suspected DNA repair	113.07	114.26	130.69	96.28
RAD54L	HR	95.78	97.11	118.95	83.73
RAD9A	DNA damage response	87.44	124.43	103.40	100.83
RECQL	suspected DNA repair	105.43	134.77	118.15	97.63
RPA1	NER	88.72	122.20	102.76	97.11

RPA2	NER	80.96	142.25	91.11	91.99
RPA3	NER	81.11	117.28	109.89	89.46
SALL3	Others	87.01	90.89	88.40	99.85
SHFM1	HR	94.59	133.73	116.09	98.03
SMUG1	BER	95.19	103.01	90.95	124.13
SPO11	Editing and processing	90.81	97.67	101.20	111.74
TOP3A	Others	104.81	127.77	107.01	86.08
TP53	DNA damage response	90.30	78.04	90.09	97.01
TREX1	DNA damage response	108.96	125.55	100.59	112.20
UBE2N	Rad6 pathway	143.77	166.77	94.43	90.94
XAB2	NER-related	80.92	107.83	110.33	135.43
XPA	NER	123.46	95.02	99.01	87.28
XPC	NER	126.64	77.43	137.74	153.10
XRCC1	BER	62.92	98.67	100.41	110.53
XRCC2	HR	126.81	128.95	101.93	102.98
XRCC3	HR	97.34	107.44	97.96	97.58
XRCC5	NHEJ	96.79	123.03	111.32	81.91

Reference List

(1) Husmann G, Kaatsch P, Kalinic A, Bertz J. Cancer in Germany 2005/2006 - Incidence and Trends. 7th ed. Robert Koch Institute and the Association of Population-based Cancer Registries in Germany; 2010.

(2) Berkey CS, Frazier AL, Gardner JD, Colditz GA. Adolescence and breast carcinoma risk. Cancer 1999 Jun 1;85(11):2400-9.

(3) Breast cancer and hormonal contraceptives: collaborative reanalysis of individual data on 53 297 women with breast cancer and 100 239 women without breast cancer from 54 epidemiological studies. Collaborative Group on Hormonal Factors in Breast Cancer. Lancet 1996 Jun 22;347(9017):1713-27.

(4) Pathak DR, Osuch JR, He J. Breast carcinoma etiology: current knowledge and new insights into the effects of reproductive and hormonal risk factors in black and white populations. Cancer 2000 Mar 1;88(5 Suppl):1230-8.

(5) McPherson K, Steel CM, Dixon JM. ABC of breast diseases. Breast cancer-epidemiology, risk factors, and genetics. BMJ 2000 Sep 9;321(7261):624-8.

(6) Lipworth L, Bailey LR, Trichopoulos D. History of breast-feeding in relation to breast cancer risk: a review of the epidemiologic literature. J Natl Cancer Inst 2000 Feb 16;92(4):302-12.

(7) Breast cancer and hormonal contraceptives: further results. Collaborative Group on Hormonal Factors in Breast Cancer. Contraception 1996 Sep;54(3 Suppl):1S-106S.

(8) Huang Z, Hankinson SE, Colditz GA, Stampfer MJ, Hunter DJ, Manson JE, et al. Dual effects of weight and weight gain on breast cancer risk. JAMA 1997 Nov 5;278(17):1407-11.

(9) Lahmann PH, Hoffmann K, Allen N, van Gils CH, Khaw KT, Tehard B, et al. Body size and breast cancer risk: findings from the European Prospective Investigation into Cancer And Nutrition (EPIC). Int J Cancer 2004 Sep 20;111(5):762-71.

(10) Singletary KW, Gapstur SM. Alcohol and breast cancer: review of epidemiologic and experimental evidence and potential mechanisms. JAMA 2001 Nov 7;286(17):2143-51.

(11) Duthie SJ. Folic acid deficiency and cancer: mechanisms of DNA instability. Br Med Bull 1999;55(3):578-92.

(12) Lagerros YT, Hsieh SF, Hsieh CC. Physical activity in adolescence and young adulthood and breast cancer risk: a quantitative review. Eur J Cancer Prev 2004 Feb;13(1):5-12.

(13) Van Duyn MA, Pivonka E. Overview of the health benefits of fruit and vegetable consumption for the dietetics professional: selected literature. J Am Diet Assoc 2000 Dec;100(12):1511-21.

(14) Lee IM. Antioxidant vitamins in the prevention of cancer. Proc Assoc Am Physicians 1999 Jan;111(1):10-5.

(15) Lux MP, Fasching PA, Beckmann MW. Hereditary breast and ovarian cancer: review and future perspectives. J Mol Med 2006 Jan;84(1):16-28.

(16) Familial breast cancer: collaborative reanalysis of individual data from 52 epidemiological studies including 58,209 women with breast cancer and 101,986 women without the disease. Lancet 2001 Oct 27;358(9291):1389-99.

(17) Flesch-Janys D, Slanger T, Mutschelknauss E, Kropp S, Obi N, Vettorazzi E, et al. Risk of different histological types of postmenopausal breast cancer by type and regimen of menopausal hormone therapy. Int J Cancer 2008 Aug 15;123(4):933-41.

(18) Seibold P, Hein R, Schmezer P, Hall P, Liu J, Dahmen N, et al. Polymorphisms in oxidative stress-related genes and postmenopausal breast cancer risk. Int J Cancer 2010 Nov 12.

(19) Deng CX, Brodie SG. Roles of BRCA1 and its interacting proteins. Bioessays 2000 Aug;22(8):728-37.

(20) Ford D, Easton DF, Stratton M, Narod S, Goldgar D, Devilee P, et al. Genetic heterogeneity and penetrance analysis of the BRCA1 and BRCA2 genes in breast cancer families. The Breast Cancer Linkage Consortium. Am J Hum Genet 1998 Mar;62(3):676-89.

(21) Linger RJ, Kruk PA. BRCA1 16 years later: risk-associated BRCA1 mutations and their functional implications. FEBS J 2010 Aug;277(15):3086-96.

(22) Osorio A, de la Hoya M, Rodriguez-Lopez R, Martinez-Ramirez A, Cazorla A, Granizo JJ, et al. Loss of heterozygosity analysis at the BRCA loci in tumor samples from patients with familial breast cancer. Int J Cancer 2002 May 10;99(2):305-9.

(23) Malkin D. Germline p53 mutations and heritable cancer. Annu Rev Genet 1994;28:443-65.

(24) de Jong MM, Nolte IM, te Meerman GJ, van der Graaf WT, Oosterwijk JC, Kleibeuker JH, et al. Genes other than BRCA1 and BRCA2 involved in breast cancer susceptibility. J Med Genet 2002 Apr;39(4):225-42.

(25) Simpson S. PALB2-new breast-cancer susceptibility gene. Lancet Oncol 2007 Feb;8(2):105.

(26) Campbell IG, Baxter SW, Eccles DM, Choong DY. Methylenetetrahydrofolate reductase polymorphism and susceptibility to breast cancer. Breast Cancer Res 2002;4(6):R14.

(27) Coutelle C, Hohn B, Benesova M, Oneta CM, Quattrochi P, Roth HJ, et al. Risk factors in alcohol associated breast cancer: alcohol dehydrogenase polymorphism and estrogens. Int J Oncol 2004 Oct;25(4):1127-32.

(28) Goode EL, Ulrich CM, Potter JD. Polymorphisms in DNA repair genes and associations with cancer risk. Cancer Epidemiol Biomarkers Prev 2002 Dec;11(12):1513-30.

(29) Eccles D, Tapper W. The influence of common polymorphisms on breast cancer. Cancer Treat Res 2010;155:15-32.

(30) Lehmann U, Hasemeier B, Christgen M, Muller M, Romermann D, Langer F, et al. Epigenetic inactivation of microRNA gene hsa-mir-9-1 in human breast cancer. J Pathol 2008 Jan;214(1):17-24.

(31) Stephens FO, Aigner KR. Basics of Oncology. Springer; 2009.

(32) World Health Organization. World Cancer Report 2008. International Agency for Research on Cancer (IARC); 2008.

(33) Bentzen SM. Preventing or reducing late side effects of radiation therapy: radiobiology meets molecular pathology. Nat Rev Cancer 2006 Sep;6(9):702-13.

(34) Bentzen SM, Overgaard J. Patient-to-Patient Variability in the Expression of Radiation-Induced Normal Tissue Injury. Semin Radiat Oncol 1994 Apr;4(2):68-80.

(35) Barnett GC, West CM, Dunning AM, Elliott RM, Coles CE, Pharoah PD, et al. Normal tissue reactions to radiotherapy: towards tailoring treatment dose by genotype. Nat Rev Cancer 2009 Feb;9(2):134-42.

(36) Holscher T, Bentzen SM, Baumann M. Influence of connective tissue diseases on the expression of radiation side effects: a systematic review. Radiother Oncol 2006 Feb;78(2):123-30.

(37) Dawson LA, Sharpe MB. Image-guided radiotherapy: rationale, benefits, and limitations. Lancet Oncol 2006 Oct;7(10):848-58.

(38) van HM. Different styles of image-guided radiotherapy. Semin Radiat Oncol 2007 Oct;17(4):258-67.

(39) Glatstein E. Intensity-modulated radiation therapy: the inverse, the converse, and the perverse. Semin Radiat Oncol 2002 Jul;12(3):272-81.

(40) Moran JM, Elshaikh MA, Lawrence TS. Radiotherapy: what can be achieved by technical improvements in dose delivery? Lancet Oncol 2005 Jan;6(1):51-8.

(41) Turesson I, Nyman J, Holmberg E, Oden A. Prognostic factors for acute and late skin reactions in radiotherapy patients. Int J Radiat Oncol Biol Phys 1996 Dec 1;36(5):1065-75.

(42) Barcellos-Hoff MH, Park C, Wright EG. Radiation and the microenvironment - tumorigenesis and therapy. Nat Rev Cancer 2005 Nov;5(11):867-75.

(43) Feinendegen LE, Bond VP, Sondhaus CA, Muehlensiepen H. Radiation effects induced by low doses in complex tissue and their relation to cellular adaptive responses. Mutat Res 1996 Nov 4;358(2):199-205.

(44) Wallace SS. DNA damages processed by base excision repair: biological consequences. Int J Radiat Biol 1994 Nov;66(5):579-89.

(45) Olive PL. The role of DNA single- and double-strand breaks in cell killing by ionizing radiation. Radiat Res 1998 Nov;150(5 Suppl):S42-S51.

(46) Barnes DE, Lindahl T. Repair and genetic consequences of endogenous DNA base damage in mammalian cells. Annu Rev Genet 2004;38:445-76.

(47) Bonner WM, Redon CE, Dickey JS, Nakamura AJ, Sedelnikova OA, Solier S, et al. GammaH2AX and cancer. Nat Rev Cancer 2008 Dec;8(12):957-67.

(48) MacPhail SH, Banath JP, Yu TY, Chu EH, Lambur H, Olive PL. Expression of phosphorylated histone H2AX in cultured cell lines following exposure to X-rays. Int J Radiat Biol 2003 May;79(5):351-8.

(49) Mullenders L, Atkinson M, Paretzke H, Sabatier L, Bouffler S. Assessing cancer risks of low-dose radiation. Nat Rev Cancer 2009 Aug;9(8):596-604.

(50) Jackson SP, Bartek J. The DNA-damage response in human biology and disease. Nature 2009 Oct 22;461(7267):1071-8.

(51) Bakkenist CJ, Kastan MB. DNA damage activates ATM through intermolecular autophosphorylation and dimer dissociation. Nature 2003 Jan 30;421(6922):499-506.

(52) Rouse J, Jackson SP. Interfaces between the detection, signaling, and repair of DNA damage. Science 2002 Jul 26;297(5581):547-51.

(53) el-Deiry WS. Regulation of p53 downstream genes. Semin Cancer Biol 1998;8(5):345-57.

(54) Zhao R, Gish K, Murphy M, Yin Y, Notterman D, Hoffman WH, et al. The transcriptional program following p53 activation. Cold Spring Harb Symp Quant Biol 2000;65:475-82.

(55) Zhao R, Gish K, Murphy M, Yin Y, Notterman D, Hoffman WH, et al. Analysis of p53-regulated gene expression patterns using oligonucleotide arrays. Genes Dev 2000 Apr 15;14(8):981-93.

(56) Bae I, Fan S, Bhatia K, Kohn KW, Fornace AJ, Jr., O'Connor PM. Relationships between G1 arrest and stability of the p53 and p21Cip1/Waf1 proteins following gamma-irradiation of human lymphoma cells. Cancer Res 1995 Jun 1;55(11):2387-93.

(57) Harper JW, Adami GR, Wei N, Keyomarsi K, Elledge SJ. The p21 Cdk-interacting protein Cip1 is a potent inhibitor of G1 cyclin-dependent kinases. Cell 1993 Nov 19;75(4):805-16.

(58) Gartel AL, Tyner AL. The role of the cyclin-dependent kinase inhibitor p21 in apoptosis. Mol Cancer Ther 2002 Jun;1(8):639-49.

(59) Wood RD, Mitchell M, Sgouros J, Lindahl T. Human DNA repair genes. Science 2001 Feb 16;291(5507):1284-9.

(60) Wood RD, Mitchell M, Lindahl T. Human DNA repair genes, 2005. Mutat Res 2005 Sep 4;577(1-2):275-83.

(61) Slupphaug G, Kavli B, Krokan HE. The interacting pathways for prevention and repair of oxidative DNA damage. Mutat Res 2003 Oct 29;531(1-2):231-51.

(62) Hoeijmakers JH. Genome maintenance mechanisms for preventing cancer. Nature 2001 May 17;411(6835):366-74.

(63) Lavelle C, Salles B, Wiesmuller L. DNA repair, damage signaling and carcinogenesis. DNA Repair (Amst) 2008 Apr 2;7(4):670-80.

(64) Featherstone C, Jackson SP. Ku, a DNA repair protein with multiple cellular functions? Mutat Res 1999 May 14;434(1):3-15.

(65) Altieri F, Grillo C, Maceroni M, Chichiarelli S. DNA damage and repair: from molecular mechanisms to health implications. Antioxid Redox Signal 2008 May;10(5):891-937.

(66) Christmann M, Tomicic MT, Roos WP, Kaina B. Mechanisms of human DNA repair: an update. Toxicology 2003 Nov 15;193(1-2):3-34.

(67) Rassool FV. DNA double strand breaks (DSB) and non-homologous end joining (NHEJ) pathways in human leukemia. Cancer Lett 2003 Apr 10;193(1):1-9.

(68) Helleday T, Lo J, van Gent DC, Engelward BP. DNA double-strand break repair: from mechanistic understanding to cancer treatment. DNA Repair (Amst) 2007 Jul 1;6(7):923-35.

(69) Wyman C, Kanaar R. DNA double-strand break repair: all's well that ends well. Annu Rev Genet 2006;40:363-83.

(70) D'Errico M, Parlanti E, Teson M, de Jesus BM, Degan P, Calcagnile A, et al. New functions of XPC in the protection of human skin cells from oxidative damage. EMBO J 2006 Sep 20;25(18):4305-15.

(71) Klungland A, Hoss M, Gunz D, Constantinou A, Clarkson SG, Doetsch PW, et al. Base excision repair of oxidative DNA damage activated by XPG protein. Mol Cell 1999 Jan;3(1):33-42.

(72) Dusinska M, Dzupinkova Z, Wsolova L, Harrington V, Collins AR. Possible involvement of XPA in repair of oxidative DNA damage deduced from analysis of damage, repair and genotype in a human population study. Mutagenesis 2006 May;21(3):205-11.

(73) Gellon L, Barbey R, Auffret vdK, Thomas D, Boiteux S. Synergism between base excision repair, mediated by the DNA glycosylases Ntg1 and Ntg2, and nucleotide excision repair in the removal of oxidatively damaged DNA bases in Saccharomyces cerevisiae. Mol Genet Genomics 2001 Aug;265(6):1087-96.

(74) Reardon JT, Bessho T, Kung HC, Bolton PH, Sancar A. In vitro repair of oxidative DNA damage by human nucleotide excision repair system: possible explanation for neurodegeneration in xeroderma pigmentosum patients. Proc Natl Acad Sci U S A 1997 Aug 19;94(17):9463-8.

(75) Sunesen M, Stevnsner T, Brosh RM, Jr., Dianov GL, Bohr VA. Global genome repair of 8-oxoG in hamster cells requires a functional CSB gene product. Oncogene 2002 May 16;21(22):3571-8.

(76) Langie SA, Knaapen AM, Houben JM, van Kempen FC, de Hoon JP, Gottschalk RW, et al. The role of glutathione in the regulation of nucleotide excision repair during oxidative stress. Toxicol Lett 2007 Feb 5;168(3):302-9.

(77) Batty DP, Wood RD. Damage recognition in nucleotide excision repair of DNA. Gene 2000 Jan 11;241(2):193-204.

(78) Friedberg EC. How nucleotide excision repair protects against cancer. Nat Rev Cancer 2001 Oct;1(1):22-33.

(79) Nouspikel T. DNA repair in mammalian cells : Nucleotide excision repair: variations on versatility. Cell Mol Life Sci 2009 Mar;66(6):994-1009.

(80) Hegde ML, Hazra TK, Mitra S. Early steps in the DNA base excision/single-strand interruption repair pathway in mammalian cells. Cell Res 2008 Jan;18(1):27-47.

(81) Almeida KH, Sobol RW. A unified view of base excision repair: lesion-dependent protein complexes regulated by post-translational modification. DNA Repair (Amst) 2007 Jun 1;6(6):695-711.

(82) Xu G, Herzig M, Rotrekl V, Walter CA. Base excision repair, aging and health span. Mech Ageing Dev 2008 Jul;129(7-8):366-82.

(83) Popanda O, Marquardt JU, Chang-Claude J, Schmezer P. Genetic variation in normal tissue toxicity induced by ionizing radiation. Mutat Res 2009 Jul 10;667(1-2):58-69.

(84) Gossage L, Madhusudan S. Cancer pharmacogenomics: role of DNA repair genetic polymorphisms in individualizing cancer therapy. Mol Diagn Ther 2007;11(6):361-80.

(85) Gurska S, Farkasova T, Gabelova A. Radiosensitivity of cervical cancer cell lines: the impact of polymorphisms in DNA repair genes. Neoplasma 2007;54(3):195-201.

(86) Moullan N, Cox DG, Angele S, Romestaing P, Gerard JP, Hall J. Polymorphisms in the DNA repair gene XRCC1, breast cancer risk, and response to radiotherapy. Cancer Epidemiol Biomarkers Prev 2003 Nov;12(11 Pt 1):1168-74.

(87) Hu JJ, Smith TR, Miller MS, Mohrenweiser HW, Golden A, Case LD. Amino acid substitution variants of APE1 and XRCC1 genes associated with ionizing radiation sensitivity. Carcinogenesis 2001 Jun;22(6):917-22.

(88) Chang-Claude J, Popanda O, Tan XL, Kropp S, Helmbold I, von FD, et al. Association between polymorphisms in the DNA repair genes, XRCC1, APE1, and XPD and acute side effects of radiotherapy in breast cancer patients. Clin Cancer Res 2005 Jul 1;11(13):4802-9.

(89) Andreassen CN, Alsner J, Overgaard M, Overgaard J. Prediction of normal tissue radiosensitivity from polymorphisms in candidate genes. Radiother Oncol 2003 Nov;69(2):127-35.

(90) De RK, Van EM, Claes K, Morthier R, De PA, Vral A, et al. Radiation-induced damage to normal tissues after radiotherapy in patients treated for gynecologic tumors: association with single nucleotide polymorphisms in XRCC1, XRCC3, and OGG1 genes and in vitro chromosomal radiosensitivity in lymphocytes. Int J Radiat Oncol Biol Phys 2005 Jul 15;62(4):1140-9.

(91) Vodicka P, Stetina R, Polakova V, Tulupova E, Naccarati A, Vodickova L, et al. Association of DNA repair polymorphisms with DNA repair functional outcomes in healthy human subjects. Carcinogenesis 2007 Mar;28(3):657-64.

(92) Naccarati A, Soucek P, Stetina R, Haufroid V, Kumar R, Vodickova L, et al. Genetic polymorphisms and possible gene-gene interactions in metabolic and DNA repair genes: effects on DNA damage. Mutat Res 2006 Jan 29;593(1-2):22-31.

(93) Vodicka P, Kumar R, Stetina R, Sanyal S, Soucek P, Haufroid V, et al. Genetic polymorphisms in DNA repair genes and possible links with DNA repair rates, chromosomal aberrations and single-strand breaks in DNA. Carcinogenesis 2004 May;25(5):757-63.

(94) Cornetta T, Festa F, Testa A, Cozzi R. DNA damage repair and genetic polymorphisms: assessment of individual sensitivity and repair capacity. Int J Radiat Oncol Biol Phys 2006 Oct 1;66(2):537-45.

(95) Weng H, Weng Z, Lu Y, Nakayama K, Morimoto K. Effects of cigarette smoking, XRCC1 genetic polymorphisms, and age on basal DNA damage in human blood mononuclear cells. Mutat Res 2009 Sep;679(1-2):59-64.

(96) Aka P, Mateuca R, Buchet JP, Thierens H, Kirsch-Volders M. Are genetic polymorphisms in OGG1, XRCC1 and XRCC3 genes predictive for the DNA strand break repair phenotype and genotoxicity in workers exposed to low dose ionising radiations? Mutat Res 2004 Nov 22;556(1-2):169-81.

(97) Godderis L, Aka P, Mateuca R, Kirsch-Volders M, Lison D, Veulemans H. Dose-dependent influence of genetic polymorphisms on DNA damage induced by styrene oxide, ethylene oxide and gamma-radiation. Toxicology 2006 Feb 15;219(1-3):220-9.

(98) Rzeszowska-Wolny J, Polanska J, Pietrowska M, Palyvoda O, Jaworska J, Butkiewicz D, et al. Influence of polymorphisms in DNA repair genes XPD, XRCC1 and MGMT on DNA damage induced by gamma radiation and its repair in lymphocytes in vitro. Radiat Res 2005 Aug;164(2):132-40.

(99) Tell G, Quadrifoglio F, Tiribelli C, Kelley MR. The many functions of APE1/Ref-1: not only a DNA repair enzyme. Antioxid Redox Signal 2009 Mar;11(3):601-20.

(100) Gorman MA, Morera S, Rothwell DG, de La FE, Mol CD, Tainer JA, et al. The crystal structure of the human DNA repair endonuclease HAP1 suggests the recognition of extra-helical deoxyribose at DNA abasic sites. EMBO J 1997 Nov 3;16(21):6548-58.

(101) Hill JW, Hazra TK, Izumi T, Mitra S. Stimulation of human 8-oxoguanine-DNA glycosylase by AP-endonuclease: potential coordination of the initial steps in base excision repair. Nucleic Acids Res 2001 Jan 15;29(2):430-8.

(102) Bennett RA, Wilson DM, III, Wong D, Demple B. Interaction of human apurinic endonuclease and DNA polymerase beta in the base excision repair pathway. Proc Natl Acad Sci U S A 1997 Jul 8;94(14):7166-9.

(103) Masuda Y, Bennett RA, Demple B. Dynamics of the interaction of human apurinic endonuclease (Ape1) with its substrate and product. J Biol Chem 1998 Nov 13;273(46):30352-9.

(104) Vascotto C, Fantini D, Romanello M, Cesaratto L, Deganuto M, Leonardi A, et al. APE1/Ref-1 interacts with NPM1 within nucleoli and plays a role in the rRNA quality control process. Mol Cell Biol 2009 Apr;29(7):1834-54.

(105) Zhou J, Ahn J, Wilson SH, Prives C. A role for p53 in base excision repair. EMBO J 2001 Feb 15;20(4):914-23.

(106) Hanson S, Kim E, Deppert W. Redox factor 1 (Ref-1) enhances specific DNA binding of p53 by promoting p53 tetramerization. Oncogene 2005 Feb 24;24(9):1641-7.

(107) Luo M, Delaplane S, Jiang A, Reed A, He Y, Fishel M, et al. Role of the Multifunctional DNA Repair and Redox Signaling Protein Ape1/Ref-1 in Cancer and Endothelial Cells: Small-Molecule Inhibition of the Redox Function of Ape1. Antioxid Redox Signal 2008 Jul 16.

(108) Evans AR, Limp-Foster M, Kelley MR. Going APE over ref-1. Mutat Res 2000 Oct 16;461(2):83-108.

(109) Okazaki T, Chung U, Nishishita T, Ebisu S, Usuda S, Mishiro S, et al. A redox factor protein, ref1, is involved in negative gene regulation by extracellular calcium. J Biol Chem 1994 Nov 11;269(45):27855-62.

(110) Fuchs S, Philippe J, Corvol P, Pinet F. Implication of Ref-1 in the repression of renin gene transcription by intracellular calcium. J Hypertens 2003 Feb;21(2):327-35.

(111) Bhakat KK, Izumi T, Yang SH, Hazra TK, Mitra S. Role of acetylated human AP-endonuclease (APE1/Ref-1) in regulation of the parathyroid hormone gene. EMBO J 2003 Dec 1;22(23):6299-309.

(112) Tell G, Damante G, Caldwell D, Kelley MR. The intracellular localization of APE1/Ref-1: more than a passive phenomenon? Antioxid Redox Signal 2005 Mar;7(3-4):367-84.

(113) Fung H, Bennett RA, Demple B. Key role of a downstream specificity protein 1 site in cell cycle-regulated transcription of the AP endonuclease gene APE1/APEX in NIH3T3 cells. J Biol Chem 2001 Nov 9;276(45):42011-7.

(114) Couture C, Raybaud-Diogene H, Tetu B, Bairati I, Murry D, Allard J, et al. p53 and Ki-67 as markers of radioresistance in head and neck carcinoma. Cancer 2002 Feb 1;94(3):713-22.

(115) Fung H, Demple B. A vital role for Ape1/Ref1 protein in repairing spontaneous DNA damage in human cells. Mol Cell 2005 Feb 4;17(3):463-70.

(116) Mitra S, Izumi T, Boldogh I, Bhakat KK, Chattopadhyay R, Szczesny B. Intracellular trafficking and regulation of mammalian AP-endonuclease 1 (APE1), an essential DNA repair protein. DNA Repair (Amst) 2007 Apr 1;6(4):461-9.

(117) Gaiddon C, Moorthy NC, Prives C. Ref-1 regulates the transactivation and pro-apoptotic functions of p53 in vivo. EMBO J 1999 Oct 15;18(20):5609-21.

(118) Jayaraman L, Murthy KG, Zhu C, Curran T, Xanthoudakis S, Prives C. Identification of redox/repair protein Ref-1 as a potent activator of p53. Genes Dev 1997 Mar 1;11(5):558-70.

(119) Robertson KA, Hill DP, Xu Y, Liu L, Van ES, Hockenbery DM, et al. Down-regulation of apurinic/apyrimidinic endonuclease expression is associated with the induction of apoptosis in differentiating myeloid leukemia cells. Cell Growth Differ 1997 Apr;8(4):443-9.

(120) Vascotto C, Cesaratto L, Zeef LA, Deganuto M, D'Ambrosio C, Scaloni A, et al. Genome-wide analysis and proteomic studies reveal APE1/Ref-1 multifunctional role in mammalian cells. Proteomics 2009 Feb;9(4):1058-74.

(121) Zhang Y, Wang J, Xiang D, Wang D, Xin X. Alterations in the expression of the apurinic/apyrimidinic endonuclease-1/redox factor-1 (APE1/Ref-1) in human ovarian cancer and indentification of the therapeutic potential of APE1/Ref-1 inhibitor. Int J Oncol 2009 Nov;35(5):1069-79.

(122) Wang D, Xiang DB, Yang XQ, Chen LS, Li MX, Zhong ZY, et al. APE1 overexpression is associated with cisplatin resistance in non-small cell lung cancer and targeted inhibition of APE1 enhances the activity of cisplatin in A549 cells. Lung Cancer 2009 Dec;66(3):298-304.

(123) Xiang DB, Chen ZT, Wang D, Li MX, Xie JY, Zhang YS, et al. Chimeric adenoviral vector Ad5/F35-mediated APE1 siRNA enhances sensitivity of human colorectal cancer cells to radiotherapy in vitro and in vivo. Cancer Gene Ther 2008 Oct;15(10):625-35.

(124) Fishel ML, He Y, Reed AM, Chin-Sinex H, Hutchins GD, Mendonca MS, et al. Knockdown of the DNA repair and redox signaling protein Ape1/Ref-1 blocks ovarian cancer cell and tumor growth. DNA Repair (Amst) 2008 Feb 1;7(2):177-86.

(125) Zou GM, Luo MH, Reed A, Kelley MR, Yoder MC. Ape1 regulates hematopoietic differentiation of embryonic stem cells through its redox functional domain. Blood 2007 Mar 1;109(5):1917-22.

(126) Bapat A, Fishel ML, Kelley MR. Going ape as an approach to cancer therapeutics. Antioxid Redox Signal 2009 Mar;11(3):651-68.

(127) Fishel ML, Kelley MR. The DNA base excision repair protein Ape1/Ref-1 as a therapeutic and chemopreventive target. Mol Aspects Med 2007 Jun;28(3-4):375-95.

(128) Fan J, Wilson DM, III. Protein-protein interactions and posttranslational modifications in mammalian base excision repair. Free Radic Biol Med 2005 May 1;38(9):1121-38.

(129) Marsin S, Vidal AE, Sossou M, Menissier-de MJ, Le PF, Boiteux S, et al. Role of XRCC1 in the coordination and stimulation of oxidative DNA damage repair initiated by the DNA glycosylase hOGG1. J Biol Chem 2003 Nov 7;278(45):44068-74.

(130) Wong HK, Wilson DM, III. XRCC1 and DNA polymerase beta interaction contributes to cellular alkylating-agent resistance and single-strand break repair. J Cell Biochem 2005 Jul 1;95(4):794-804.

(131) Fan J, Otterlei M, Wong HK, Tomkinson AE, Wilson DM, III. XRCC1 co-localizes and physically interacts with PCNA. Nucleic Acids Res 2004;32(7):2193-201.

(132) Mortusewicz O, Leonhardt H. XRCC1 and PCNA are loading platforms with distinct kinetic properties and different capacities to respond to multiple DNA lesions. BMC Mol Biol 2007;8:81.

(133) Kiran M, Saxena R, Kaur J. Distribution of XRCC1 genotypes in north Indian population. Indian J Med Res 2010 Jan;131:71-5.

(134) Levy N, Martz A, Bresson A, Spenlehauer C, de MG, Menissier-de MJ. XRCC1 is phosphorylated by DNA-dependent protein kinase in response to DNA damage. Nucleic Acids Res 2006;34(1):32-41.

(135) Caldecott KW. XRCC1 and DNA strand break repair. DNA Repair (Amst) 2003 Sep 18;2(9):955-69.

(136) Vidal AE, Boiteux S, Hickson ID, Radicella JP. XRCC1 coordinates the initial and late stages of DNA abasic site repair through protein-protein interactions. EMBO J 2001 Nov 15;20(22):6530-9.

(137) Kwok JM, Peck B, Monteiro LJ, Schwenen HD, Millour J, Coombes RC, et al. FOXM1 confers acquired cisplatin resistance in breast cancer cells. Mol Cancer Res 2010 Jan;8(1):24-34.

(138) Thompson LH, Rubin JS, Cleaver JE, Whitmore GF, Brookman K. A screening method for isolating DNA repair-deficient mutants of CHO cells. Somatic Cell Genet 1980 May;6(3):391-405.

(139) Tebbs RS, Flannery ML, Meneses JJ, Hartmann A, Tucker JD, Thompson LH, et al. Requirement for the Xrcc1 DNA base excision repair gene during early mouse development. Dev Biol 1999 Apr 15;208(2):513-29.

(140) Sterpone S, Cozzi R. Influence of XRCC1 Genetic Polymorphisms on Ionizing Radiation-Induced DNA Damage and Repair. J Nucleic Acids 2010;2010.

(141) Thompson LH, Brookman KW, Jones NJ, Allen SA, Carrano AV. Molecular cloning of the human XRCC1 gene, which corrects defective DNA strand break repair and sister chromatid exchange. Mol Cell Biol 1990 Dec;10(12):6160-71.

(142) Taverna P, Hwang HS, Schupp JE, Radivoyevitch T, Session NN, Reddy G, et al. Inhibition of base excision repair potentiates iododeoxyuridine-induced cytotoxicity and radiosensitization. Cancer Res 2003 Feb 15;63(4):838-46.

(143) Neijenhuis S, Begg AC, Vens C. Radiosensitization by a dominant negative to DNA polymerase beta is DNA polymerase beta-independent and XRCC1-dependent. Radiother Oncol 2005 Aug;76(2):123-8.

(144) Horton JK, Watson M, Stefanick DF, Shaughnessy DT, Taylor JA, Wilson SH. XRCC1 and DNA polymerase beta in cellular protection against cytotoxic DNA single-strand breaks. Cell Res 2008 Jan;18(1):48-63.

(145) Brem R, Hall J. XRCC1 is required for DNA single-strand break repair in human cells. Nucleic Acids Res 2005;33(8):2512-20.

(146) Kakolyris S, Kaklamanis L, Giatromanolaki A, Koukourakis M, Hickson ID, Barzilay G, et al. Expression and subcellular localization of human AP endonuclease 1 (HAP1/Ref-1) protein: a basis for its role in human disease. Histopathology 1998 Dec;33(6):561-9.

(147) Batuello CN, Kelley MR, Dynlacht JR. Role of Ape1 and base excision repair in the radioresponse and heat-radiosensitization of HeLa Cells. Anticancer Res 2009 Apr;29(4):1319-25.

(148) Chen DS, Olkowski ZL. Biological responses of human apurinic endonuclease to radiation-induced DNA damage. Ann N Y Acad Sci 1994 Jul 29;726:306-8.

(149) Skvortsova I, Skvortsov S, Stasyk T, Raju U, Popper BA, Schiestl B, et al. Intracellular signaling pathways regulating radioresistance of human prostate carcinoma cells. Proteomics 2008 Nov;8(21):4521-33.

(150) Naidu MD, Mason JM, Pica RV, Fung H, Pena LA. Radiation resistance in glioma cells determined by DNA damage repair activity of ape1/ref-1. J Radiat Res (Tokyo) 2010;51(4):393-404.

(151) Fung H, Demple B. Distinct roles of Ape1 protein in the repair of DNA damage induced by ionizing radiation or bleomycin. J Biol Chem 2010 Nov 15.

(152) Herring CJ, West CM, Wilks DP, Davidson SE, Hunter RD, Berry P, et al. Levels of the DNA repair enzyme human apurinic/apyrimidinic endonuclease (APE1, APEX, Ref-1) are

associated with the intrinsic radiosensitivity of cervical cancers. Br J Cancer 1998 Nov;78(9):1128-33.

(153) Edwards SL, Brough R, Lord CJ, Natrajan R, Vatcheva R, Levine DA, et al. Resistance to therapy caused by intragenic deletion in BRCA2. Nature 2008 Feb 28;451(7182):1111-5.

(154) Fong PC, Boss DS, Yap TA, Tutt A, Wu P, Mergui-Roelvink M, et al. Inhibition of poly(ADP-ribose) polymerase in tumors from BRCA mutation carriers. N Engl J Med 2009 Jul 9;361(2):123-34.

(155) Fire A, Xu S, Montgomery MK, Kostas SA, Driver SE, Mello CC. Potent and specific genetic interference by double-stranded RNA in Caenorhabditis elegans. Nature 1998 Feb 19;391(6669):806-11.

(156) Hammond SM, Caudy AA, Hannon GJ. Post-transcriptional gene silencing by double-stranded RNA. Nat Rev Genet 2001 Feb;2(2):110-9.

(157) Hannon GJ. RNA interference. Nature 2002 Jul 11;418(6894):244-51.

(158) De PD, Bentley MV, Mahato RI. Hydrophobization and bioconjugation for enhanced siRNA delivery and targeting. RNA 2007 Apr;13(4):431-56.

(159) Elbashir SM, Lendeckel W, Tuschl T. RNA interference is mediated by 21- and 22-nucleotide RNAs. Genes Dev 2001 Jan 15;15(2):188-200.

(160) Meister G, Tuschl T. Mechanisms of gene silencing by double-stranded RNA. Nature 2004 Sep 16;431(7006):343-9.

(161) Jackson AL, Burchard J, Leake D, Reynolds A, Schelter J, Guo J, et al. Position-specific chemical modification of siRNAs reduces "off-target" transcript silencing. RNA 2006 Jul;12(7):1197-205.

(162) Jackson AL, Burchard J, Schelter J, Chau BN, Cleary M, Lim L, et al. Widespread siRNA "off-target" transcript silencing mediated by seed region sequence complementarity. RNA 2006 Jul;12(7):1179-87.

(163) Mueller O, Hahnenberger K, Dittmann M, Yee H, Dubrow R, Nagle R, et al. A microfluidic system for high-speed reproducible DNA sizing and quantitation. Electrophoresis 2000 Jan;21(1):128-34.

(164) Bustin SA, Benes V, Nolan T, Pfaffl MW. Quantitative real-time RT-PCR--a perspective. J Mol Endocrinol 2005 Jun;34(3):597-601.

(165) Higuchi R, Fockler C, Dollinger G, Watson R. Kinetic PCR analysis: real-time monitoring of DNA amplification reactions. Biotechnology (N Y) 1993 Sep;11(9):1026-30.

(166) Bustin SA, Nolan T. Pitfalls of quantitative real-time reverse-transcription polymerase chain reaction. J Biomol Tech 2004 Sep;15(3):155-66.

(167) Bustin SA. Absolute quantification of mRNA using real-time reverse transcription polymerase chain reaction assays. J Mol Endocrinol 2000 Oct;25(2):169-93.

(168) Derveaux S, Vandesompele J, Hellemans J. How to do successful gene expression analysis using real-time PCR. Methods 2010 Apr;50(4):227-30.

(169) Rozen S, Skaletsky H. Primer3 on the WWW for general users and for biologist programmers. Methods Mol Biol 2000;132:365-86.

(170) Rasmussen R. Quantification on the LightCycler. In: Meuer S, Wittwer C, Nakagawara K, editors. Rapid Cycle Real-time PCR, Methods and Applications. 1 ed. Heidelberg: Springer Press; 2001. p. 21-34.

(171) Pfaffl MW. A new mathematical model for relative quantification in real-time RT-PCR. Nucleic Acids Res 2001 May 1;29(9):e45.

(172) Huggett J, Dheda K, Bustin S, Zumla A. Real-time RT-PCR normalisation; strategies and considerations. Genes Immun 2005 Jun;6(4):279-84.

(173) Vandesompele J, De PK, Pattyn F, Poppe B, Van RN, De PA, et al. Accurate normalization of real-time quantitative RT-PCR data by geometric averaging of multiple internal control genes. Genome Biol 2002 Jun 18;3(7):RESEARCH0034.

(174) Janssens N, Janicot M, Perera T, Bakker A. Housekeeping genes as internal standards in cancer research. Mol Diagn 2004;8(2):107-13.

(175) Steinberg G, Stromsborg K, Thomas L, Barker D, Zhao C. Strategies for covalent attachment of DNA to beads. Biopolymers 2004 Apr 5;73(5):597-605.

(176) Gunderson KL, Kruglyak S, Graige MS, Garcia F, Kermani BG, Zhao C, et al. Decoding randomly ordered DNA arrays. Genome Res 2004 May;14(5):870-7.

(177) Toni Lindl, Gerhard Gstraunthaler. Zell- und Gewebekultur : von den Grundlagen zur Laborbank. 6th ed. Heidelberg: Spektrum Akademischer Verlag; 2008.

(178) Bradford MM. A rapid and sensitive method for the quantitation of microgram quantities of protein utilizing the principle of protein-dye binding. Anal Biochem 1976 May 7;72:248-54.

(179) Laemmli UK. Cleavage of structural proteins during the assembly of the head of bacteriophage T4. Nature 1970 Aug 15;227(5259):680-5.

(180) Collins AR. The comet assay for DNA damage and repair: principles, applications, and limitations. Mol Biotechnol 2004 Mar;26(3):249-61.

(181) Olive PL, Banath JP, Durand RE. Heterogeneity in radiation-induced DNA damage and repair in tumor and normal cells measured using the "comet" assay. Radiat Res 1990 Apr;122(1):86-94.

(182) Dusinska M, Collins AR. The comet assay in human biomonitoring: gene-environment interactions. Mutagenesis 2008 May;23(3):191-205.

(183) Wasson GR, McKelvey-Martin VJ, Downes CS. The use of the comet assay in the study of human nutrition and cancer. Mutagenesis 2008 May;23(3):153-62.

(184) Singh NP, McCoy MT, Tice RR, Schneider EL. A simple technique for quantitation of low levels of DNA damage in individual cells. Exp Cell Res 1988 Mar;175(1):184-91.

(185) Popanda O, Ebbeler R, Twardella D, Helmbold I, Gotzes F, Schmezer P, et al. Radiation-induced DNA damage and repair in lymphocytes from breast cancer patients and their

correlation with acute skin reactions to radiotherapy. Int J Radiat Oncol Biol Phys 2003 Apr 1;55(5):1216-25.

(186) Collins AR. Investigating oxidative DNA damage and its repair using the comet assay. Mutat Res 2009 Jan;681(1):24-32.

(187) McKelvey-Martin VJ, Green MH, Schmezer P, Pool-Zobel BL, De Meo MP, Collins A. The single cell gel electrophoresis assay (comet assay): a European review. Mutat Res 1993 Jul;288(1):47-63.

(188) PUCK TT, MARCUS PI. Action of x-rays on mammalian cells. J Exp Med 1956 May 1;103(5):653-66.

(189) Franken NA, Rodermond HM, Stap J, Haveman J, van BC. Clonogenic assay of cells in vitro. Nat Protoc 2006;1(5):2315-9.

(190) Plumb JA. Cell sensitivity assays: clonogenic assay. Methods Mol Med 2004;88:159-64.

(191) Pauwels B, Korst AE, de Pooter CM, Pattyn GG, Lambrechts HA, Baay MF, et al. Comparison of the sulforhodamine B assay and the clonogenic assay for in vitro chemoradiation studies. Cancer Chemother Pharmacol 2003 Mar;51(3):221-6.

(192) Griffon G, Merlin JL, Marchal C. Comparison of sulforhodamine B, tetrazolium and clonogenic assays for in vitro radiosensitivity testing in human ovarian cell lines. Anticancer Drugs 1995 Feb;6(1):115-23.

(193) Skehan P, Storeng R, Scudiero D, Monks A, McMahon J, Vistica D, et al. New colorimetric cytotoxicity assay for anticancer-drug screening. J Natl Cancer Inst 1990 Jul 4;82(13):1107-12.

(194) Rogakou EP, Pilch DR, Orr AH, Ivanova VS, Bonner WM. DNA double-stranded breaks induce histone H2AX phosphorylation on serine 139. J Biol Chem 1998 Mar 6;273(10):5858-68.

(195) Rogakou EP, Boon C, Redon C, Bonner WM. Megabase chromatin domains involved in DNA double-strand breaks in vivo. J Cell Biol 1999 Sep 6;146(5):905-16.

(196) Hagen U. Mechanisms of induction and repair of DNA double-strand breaks by ionizing radiation: some contradictions. Radiat Environ Biophys 1994;33(1):45-61.

(197) Paull TT, Rogakou EP, Yamazaki V, Kirchgessner CU, Gellert M, Bonner WM. A critical role for histone H2AX in recruitment of repair factors to nuclear foci after DNA damage. Curr Biol 2000 Jul 27;10(15):886-95.

(198) Chowdhury D, Keogh MC, Ishii H, Peterson CL, Buratowski S, Lieberman J. gamma-H2AX dephosphorylation by protein phosphatase 2A facilitates DNA double-strand break repair. Mol Cell 2005 Dec 9;20(5):801-9.

(199) Keogh MC, Kim JA, Downey M, Fillingham J, Chowdhury D, Harrison JC, et al. A phosphatase complex that dephosphorylates gammaH2AX regulates DNA damage checkpoint recovery. Nature 2006 Jan 26;439(7075):497-501.

(200) Chowdhury D, Xu X, Zhong X, Ahmed F, Zhong J, Liao J, et al. A PP4-phosphatase complex dephosphorylates gamma-H2AX generated during DNA replication. Mol Cell 2008 Jul 11;31(1):33-46.

(201) Nakada S, Chen GI, Gingras AC, Durocher D. PP4 is a gamma H2AX phosphatase required for recovery from the DNA damage checkpoint. EMBO Rep 2008 Oct;9(10):1019-26.

(202) Downs JA, Allard S, Jobin-Robitaille O, Javaheri A, Auger A, Bouchard N, et al. Binding of chromatin-modifying activities to phosphorylated histone H2A at DNA damage sites. Mol Cell 2004 Dec 22;16(6):979-90.

(203) Nolan JP, Yang L. The flow of cytometry into systems biology. Brief Funct Genomic Proteomic 2007 Jun;6(2):81-90.

(204) Shapiro HM. Practical flow cytometry. 4th ed. New York: Wiley-Liss; 2003.

(205) Tung JW, Parks DR, Moore WA, Herzenberg LA, Herzenberg LA. New approaches to fluorescence compensation and visualization of FACS data. Clin Immunol 2004 Mar;110(3):277-83.

(206) Chalmers AJ, Ruff EM, Martindale C, Lovegrove N, Short SC. Cytotoxic effects of temozolomide and radiation are additive- and schedule-dependent. Int J Radiat Oncol Biol Phys 2009 Dec 1;75(5):1511-9.

(207) Marchesi F, Turriziani M, Tortorelli G, Avvisati G, Torino F, De VL. Triazene compounds: mechanism of action and related DNA repair systems. Pharmacol Res 2007 Oct;56(4):275-87.

(208) Lee HM, Yuk JM, Shin DM, Yang CS, Kim KK, Choi DK, et al. Apurinic/apyrimidinic endonuclease 1 is a key modulator of keratinocyte inflammatory responses. J Immunol 2009 Nov 15;183(10):6839-48.

(209) Xanthoudakis S, Curran T. Identification and characterization of Ref-1, a nuclear protein that facilitates AP-1 DNA-binding activity. EMBO J 1992 Feb;11(2):653-65.

(210) Nishi T, Shimizu N, Hiramoto M, Sato I, Yamaguchi Y, Hasegawa M, et al. Spatial redox regulation of a critical cysteine residue of NF-kappa B in vivo. J Biol Chem 2002 Nov 15;277(46):44548-56.

(211) Huang RP, Adamson ED. Characterization of the DNA-binding properties of the early growth response-1 (Egr-1) transcription factor: evidence for modulation by a redox mechanism. DNA Cell Biol 1993 Apr;12(3):265-73.

(212) Nakshatri H, Bhat-Nakshatri P, Currie RA. Subunit association and DNA binding activity of the heterotrimeric transcription factor NF-Y is regulated by cellular redox. J Biol Chem 1996 Nov 15;271(46):28784-91.

(213) Lando D, Pongratz I, Poellinger L, Whitelaw ML. A redox mechanism controls differential DNA binding activities of hypoxia-inducible factor (HIF) 1alpha and the HIF-like factor. J Biol Chem 2000 Feb 18;275(7):4618-27.

(214) Christy B, Nathans D. DNA binding site of the growth factor-inducible protein Zif268. Proc Natl Acad Sci U S A 1989 Nov;86(22):8737-41.

(215) Poch MT, Al-Kassim L, Smolinski SM, Hines RN. Two distinct classes of CCAAT box elements that bind nuclear factor-Y/alpha-actinin-4: potential role in human CYP1A1 regulation. Toxicol Appl Pharmacol 2004 Sep 15;199(3):239-50.

(216) Parlanti E, Locatelli G, Maga G, Dogliotti E. Human base excision repair complex is physically associated to DNA replication and cell cycle regulatory proteins. Nucleic Acids Res 2007;35(5):1569-77.

(217) Bitomsky N, Hofmann TG. Apoptosis and autophagy: Regulation of apoptosis by DNA damage signalling - roles of p53, p73 and HIPK2. FEBS J 2009 Nov;276(21):6074-83.

(218) Zhan Q. Gadd45a, a p53- and BRCA1-regulated stress protein, in cellular response to DNA damage. Mutat Res 2005 Jan 6;569(1-2):133-43.

(219) Lieberman HB, Bernstock JD, Broustas CG, Hopkins KM, Leloup C, Zhu A. The role of RAD9 in tumorigenesis. J Mol Cell Biol 2011 Feb;3(1):39-43.

(220) Angell JE, Lindner DJ, Shapiro PS, Hofmann ER, Kalvakolanu DV. Identification of GRIM-19, a novel cell death-regulatory gene induced by the interferon-beta and retinoic acid combination, using a genetic approach. J Biol Chem 2000 Oct 27;275(43):33416-26.

(221) Jin S, Levine AJ. The p53 functional circuit. J Cell Sci 2001 Dec;114(Pt 23):4139-40.

(222) Li PX, Wong J, Ayed A, Ngo D, Brade AM, Arrowsmith C, et al. Placental transforming growth factor-beta is a downstream mediator of the growth arrest and apoptotic response of tumor cells to DNA damage and p53 overexpression. J Biol Chem 2000 Jun 30;275(26):20127-35.

(223) Pan G, Ni J, Wei YF, Yu G, Gentz R, Dixit VM. An antagonist decoy receptor and a death domain-containing receptor for TRAIL. Science 1997 Aug 8;277(5327):815-8.

(224) Gu Y, Parker A, Wilson TM, Bai H, Chang DY, Lu AL. Human MutY homolog, a DNA glycosylase involved in base excision repair, physically and functionally interacts with mismatch repair proteins human MutS homolog 2/human MutS homolog 6. J Biol Chem 2002 Mar 29;277(13):11135-42.

(225) Mazurek A, Berardini M, Fishel R. Activation of human MutS homologs by 8-oxo-guanine DNA damage. J Biol Chem 2002 Mar 8;277(10):8260-6.

(226) Colussi C, Parlanti E, Degan P, Aquilina G, Barnes D, Macpherson P, et al. The mammalian mismatch repair pathway removes DNA 8-oxodGMP incorporated from the oxidized dNTP pool. Curr Biol 2002 Jun 4;12(11):912-8.

(227) Haracska L, Yu SL, Johnson RE, Prakash L, Prakash S. Efficient and accurate replication in the presence of 7,8-dihydro-8-oxoguanine by DNA polymerase eta. Nat Genet 2000 Aug;25(4):458-61.

(228) Avkin S, Livneh Z. Efficiency, specificity and DNA polymerase-dependence of translesion replication across the oxidative DNA lesion 8-oxoguanine in human cells. Mutat Res 2002 Dec 29;510(1-2):81-90.

(229) Nocentini S. Rejoining kinetics of DNA single- and double-strand breaks in normal and DNA ligase-deficient cells after exposure to ultraviolet C and gamma radiation: an

evaluation of ligating activities involved in different DNA repair processes. Radiat Res 1999 Apr;151(4):423-32.

(230) Peddi SR, Chattopadhyay R, Naidu CV, Izumi T. The human apurinic/apyrimidinic endonuclease-1 suppresses activation of poly(adp-ribose) polymerase-1 induced by DNA single strand breaks. Toxicology 2006 Jul 5;224(1-2):44-55.

(231) Weinfeld M, Rasouli-Nia A, Chaudhry MA, Britten RA. Response of base excision repair enzymes to complex DNA lesions. Radiat Res 2001 Nov;156(5 Pt 2):584-9.

(232) Chappell C, Hanakahi LA, Karimi-Busheri F, Weinfeld M, West SC. Involvement of human polynucleotide kinase in double-strand break repair by non-homologous end joining. EMBO J 2002 Jun 3;21(11):2827-32.

(233) Audebert M, Salles B, Calsou P. Involvement of poly(ADP-ribose) polymerase-1 and XRCC1/DNA ligase III in an alternative route for DNA double-strand breaks rejoining. J Biol Chem 2004 Dec 31;279(53):55117-26.

(234) Toulany M, Dittmann K, Fehrenbacher B, Schaller M, Baumann M, Rodemann HP. PI3K-Akt signaling regulates basal, but MAP-kinase signaling regulates radiation-induced XRCC1 expression in human tumor cells in vitro. DNA Repair (Amst) 2008 Oct 1;7(10):1746-56.

(235) Schwartz JL, Giovanazzi S, Weichselbaum RR. Recovery from sublethal and potentially lethal damage in an X-ray-sensitive CHO cell. Radiat Res 1987 Jul;111(1):58-67.

(236) vanAnkeren SC, Murray D, Meyn RE. Induction and rejoining of gamma-ray-induced DNA single- and double-strand breaks in Chinese hamster AA8 cells and in two radiosensitive clones. Radiat Res 1988 Dec;116(3):511-25.

(237) Silber JR, Bobola MS, Blank A, Schoeler KD, Haroldson PD, Huynh MB, et al. The apurinic/apyrimidinic endonuclease activity of Ape1/Ref-1 contributes to human glioma cell resistance to alkylating agents and is elevated by oxidative stress. Clin Cancer Res 2002 Sep;8(9):3008-18.

(238) McNeill DR, Wilson DM, III. A dominant-negative form of the major human abasic endonuclease enhances cellular sensitivity to laboratory and clinical DNA-damaging agents. Mol Cancer Res 2007 Jan;5(1):61-70.

(239) McNeill DR, Lam W, DeWeese TL, Cheng YC, Wilson DM, III. Impairment of APE1 function enhances cellular sensitivity to clinically relevant alkylators and antimetabolites. Mol Cancer Res 2009 Jun;7(6):897-906.

(240) Fishel ML, He Y, Smith ML, Kelley MR. Manipulation of base excision repair to sensitize ovarian cancer cells to alkylating agent temozolomide. Clin Cancer Res 2007 Jan 1;13(1):260-7.

(241) Taverna P, Liu L, Hwang HS, Hanson AJ, Kinsella TJ, Gerson SL. Methoxyamine potentiates DNA single strand breaks and double strand breaks induced by temozolomide in colon cancer cells. Mutat Res 2001 May 10;485(4):269-81.

(242) Cano CE, Gommeaux J, Pietri S, Culcasi M, Garcia S, Seux M, et al. Tumor protein 53-induced nuclear protein 1 is a major mediator of p53 antioxidant function. Cancer Res 2009 Jan 1;69(1):219-26.

(243) Scott D, Barber JB, Levine EL, Burrill W, Roberts SA. Radiation-induced micronucleus induction in lymphocytes identifies a high frequency of radiosensitive cases among breast cancer patients: a test for predisposition? Br J Cancer 1998 Feb;77(4):614-20.

Poster presentations

Popanda O., Seibold P., **Hausmann S.**, Flesch-Janys D., Chang-Claude J., Schmezer P. Polymorphisms in base excision repair genes and postmenopausal breast cancer risk in a German case-control study. 11th Biennual DGDR Meeting held by the German Society for Research on DNA Repair, Jena, September 2010.

Hausmann S., Schmezer P., Chang-Claude J., Popanda O. DNA-(apurinic or apyrimidinic site) lyase and its role in the repair of radiation-induced DNA damage. 11th Biennual DGDR Meeting held by the German Society for Research on DNA Repair, Jena, September 2010.

Hausmann S., Popanda O., Schmezer P. APEX1 knockdown affects cellular response to ionizing radiation. DKFZ Poster Presentation, Heidelberg, December 2009.

Kuhmann C., **Hausmann S.**, Schmezer P., Popanda O. Determination of apurinic sites in APEX1-downregulated cells. Gesellschaft für Umwelt-Mutationforschung e.V. (GUM), Würzburg, 2008.

Acknowledgements

I want to thank my supervisors PD Dr. Odilia Popanda and Dr. Peter Schmezer for giving me the opportunity to write my PhD thesis at the DKFZ. Without their encouragement and suggestions, I would have never finished the dissertation. Special thanks go to Odilia for her helpful feedback, particularly during the final phase of my work.

I also want to thank Prof. Dr. Gert Fricker for taking the role of second reader and PD Dr. Heinz Schmeiser for all his scientific input and personal advice. Additionally, I would like to express my gratitude to Prof. Dr. Jürgen Kleinschmidt and Prof. Dr. Christoph Plass.

I am thankful to the Dietmar Hopp Foundation for supporting this project financially.

My special thanks go to the Group DNA Repair and Epigenomics. I thank Reinhard Gliniorz, Peter Waas, and Otto Zelezny for their excellent assistance during my experiments. I would like to thank Jittiporn Chaisaingmongkol, Céline Dutruel, Lea Geiselhart, and Christine Kuhmann for the friendly atmosphere and the great time in and outside the lab. I am thankful for their help and support throughout my entire project.

I want to thank Dr. Christian Maul for all his encouragement, excellent proof-reading skills, and for always believing in me.

Last, but not least, I want to thank my family, Helga, Bernd, Niklas, Benedikt, and Florian Hausmann for all their support and love. I dedicate my work to them.